PROCEEDINGS OF THE JOINT SEMINAR

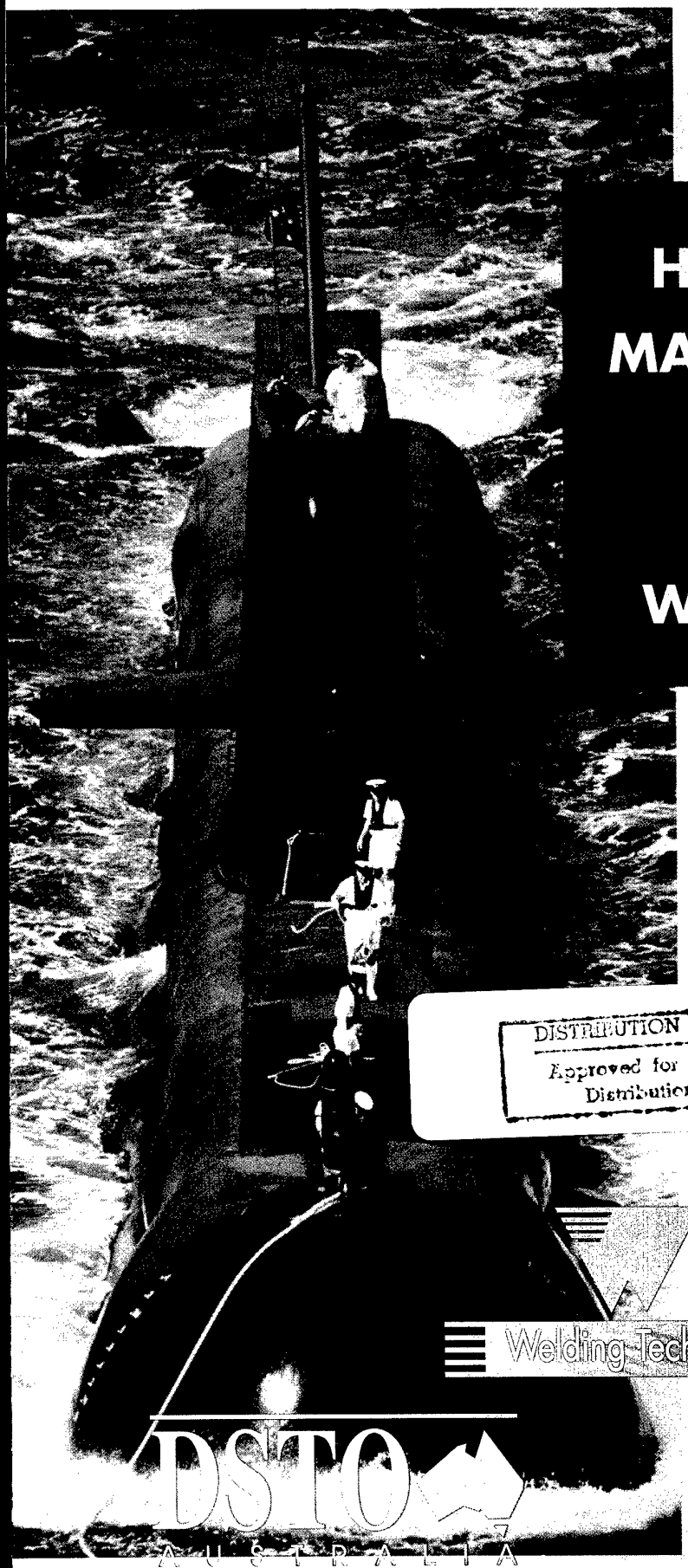

Edited by
J.L.Davidson and D.L.Olson

HYDROGEN MANAGEMENT IN STEEL WELDMENTS

MELBOURNE
23 October 1996

TIA
Welding Technology Institute of Australia

DSTO
AUSTRALIA
DEFENCE SCIENCE AND TECHNOLOGY ORGANISATION

Sponsored by US Army Research Office

HYDROGEN MANAGEMENT IN STEEL WELDMENTS

Joint Seminar

Melbourne, Australia
23rd October 1996
Sponsored by the US Army Research Office

Proceedings of the Seminar

Edited by
J. L. Davidson and D. L. Olson

Published June 1997
by the Organising Committee of the Joint Seminar
on behalf of

DSTO AUSTRALIA
Defence Science and Technology Organisation
and

WTIA
Welding Technology Institute of Australia

ISBN 0 7311 0809 4

This work is related to Department of the Navy Grant N62649-96-1-0008 issues by U.S. FISC YOKOSUKA. The United States Government has a royalty-free license throughout the world in all copyrightable material contained herein.

HYDROGEN MANAGEMENT IN STEEL WELDMENTS

• Table of Contents •

REPORT DOCUMENTATION PAGE

Form Approved
OMB NO. 0704-0188

1. AGENCY USE ONLY *(Leave blank)*	2. REPORT DATE	3. REPORT TYPE AND DATES COVERED
		Reprint

4. TITLE AND SUBTITLE

Title on Reprint

5. FUNDING NUMBERS

DAAH04-94-G-0281

6. AUTHOR(S)

Authors on Reprint

7. PERFORMING ORGANIZATION NAMES(S) AND ADDRESS(ES)

Colorado School of Mines
Golden, CO 80401

8. PERFORMING ORGANIZATION REPORT NUMBER

9. SPONSORING / MONITORING AGENCY NAME(S) AND ADDRESS(ES)

U.S. Army Research Office
P.O. Box 12211
Research Triangle Park, NC 27709-2211

10. SPONSORING / MONITORING AGENCY REPORT NUMBER

ARO 32823.4-MS

11. SUPPLEMENTARY NOTES

The views, opinions and/or findings contained in this report are those of the author(s) and should not be construed as an official Department of the Army position, policy or decision, unless so designated by other documentation.

12a. DISTRIBUTION / AVAILABILITY STATEMENT

Approved for public release; distribution unlimited.

12 b. DISTRIBUTION CODE

13. ABSTRACT *(Maximum 200 words)*

ABSTRACT ON REPRINT

14. SUBJECT TERMS	15. NUMBER IF PAGES
	16. PRICE CODE

17. SECURITY CLASSIFICATION OR REPORT	18. SECURITY CLASSIFICATION OF THIS PAGE	19. SECURITY CLASSIFICATION OF ABSTRACT	20. LIMITATION OF ABSTRACT
UNCLASSIFIED	UNCLASSIFIED	UNCLASSIFIED	UL

PREFACE

This volume contains the proceedings of a one-day seminar, organised as part of a three-day workshop on the topic of hydrogen management in steel weldments. The workshop was held under the auspices of the Technical Co-operation Program (TTCP), an arrangement between the United States, the United Kingdom, Australia, Canada and New Zealand for sharing defence research.

This meeting was part of a project undertaken by TTCP Technical Panel P1, *Metals Technology and Performance*. It was organised jointly by the DSTO Aeronautical and Maritime Research Laboratory and the Welding Technology Institute of Australia, with sponsorship from the US Army Research Office.

These proceedings form a permanent record of loose-leaf papers presented on the day.

J.C. Ritter

INTRODUCTION

Despite 50 years of research into the prevention of hydrogen induced cracking in weldments, this form of cracking is still the most serious problem facing the steel fabrication industry today.

Increased performance for defence platforms requires stronger lighter structures which have largely been obtained using high strength steels. As the strength is increased, so is the risk of hydrogen induced cracking after welding. To address this issue, the management of hydrogen, and the elimination of hydrogen induced cracking during the welding of high strength structural steels, has been made the focus of an international research program between American and Australian defence scientists.

As part of this collaborative program, a public seminar was held at the Carlton Crest Hotel in Melbourne on October 23, 1997. The seminar brought together experts in the field of hydrogen cracking from industry, academia, research institutions and defence agencies, to establish the state-of-the-science, to review the progress of the collaborative research project and to address the feasibility of alternative approaches for hydrogen and preheat management. Seminar papers covered a range of topics from safe hydrogen management practice for today, to the science based development of low-hydrogen consumables for the future. Accordingly, this collection of papers provides a unique opportunity for the reader to become aware of the current directions of hydrogen management in high strength steel weldments.

J.L. Davidson
D.L. Olson

Hydrogen Management in High Strength Steel Weldments

D.L. Olson, I. Maroef, C. Lensing, R.D. Smith, W.W. Wang, S. Liu, T. Wildeman and M. Eberhart

Center for Welding, Joining and Coating Research
Colorado School of Mines
Golden, Colorado 80401-1887
USA

1. INTRODUCTION

Common practice to reduce cold cracking in high strength steel welding is the pre- or post-weld heat treatment. Heat treatment is performed to control the cooling rate and to ensure sufficient removal of hydrogen from the weld metal. Recent scientific approaches supported by FEM calculation have made it possible to determine the heat treatment that provides an appropriate combination of microstructure (hardness), stress intensity factor and diffusible hydrogen content that does not allow susceptibility to hydrogen cracking (1). More often an acceptable selection of welding parameters to avoid hydrogen cracking is achieved by a costly testing program. However, such methodologies that require tight monitoring and control of the temperature as well as welding parameters are frequently found to be impractical and complicated. Therefore, new approaches to hydrogen management in steel welding, based on more fundamental metallurgical understanding and predictions, are being investigated. The CSM approach is to develop consumables based on three independent proposed practices to hydrogen management. They are described here as three steps.

2. STEP 1: PROPER SELECTION OF WELD METAL MARTENSITE START TEMPERATURE.

The hydrogen content in a weldment is dependent on both the hydrogen source and the ability of the weldment to transport hydrogen from the weld metal to the heat affected zone. The transport aspect becomes important because of the higher hydrogen solubility but lower hydrogen diffusion rate in austenite (FCC crystal structure), in contrast to ferrite and martensite that have orders of magnitude higher hydrogen diffusion coefficients than austenite (2). As a result of the different hydrogen diffusivitiy in austenite compared to martensite/ferrite and the different thermal experience, a non-uniform distribution of hydrogen may result across the weldment according to the austenite decomposition behavior of the alloys (3,4). Evidence of this resulting localized hydrogen distribution can be seen in the laser induced breakdown spectroscopy data (5) for hydrogen spectral emission scans across a weldment as shown in Figure 1. The effect of hydrogen damage is magnified when the location of the susceptible microstructures (martensite) overlaps the localized, high hydrogen content.

Proper alloying elements and their contents in the consumable are being determined to insure maximum hydrogen transport away from the weldment (weld metal and HAZ) during the welding thermal cycle. The martensite start temperature is used as an indicator for effective transport of hydrogen. A large difference between the M_s (weld metal) and M_s (base metal) will indicate difficulties in hydrogen transport in the weldment and the tendency for high localization in hydrogen contents. Thus the martensite start temperature is a measure of the microstructure evolution and the ability to have a phase (ferrite/martensite) available for rapid hydrogen transport (3,4).

Granjon (3) introduced a conceptual model that describes how the austenite-ferrite (or austenite-martensite) phase transformation in steel weldments affects the resulting hydrogen distribution. Two cases are illustrated in Figure 2. When the austenite-martensite

transformation in the fusion zone (weld metal) occurs at a higher temperature than the heat affected zone diffusible hydrogen will segregate in the heat affected zone just under the fusion line. This HAZ region is often the location of underbead cracking in high strength steel weldments. On the other hand, when the martensite transformation in the heat affected zone occurs at a higher temperature than in the fusion zone, it is possible that excess hydrogen may accumulate in the weld metal. This situation could promote weld metal hydrogen cracking or micro-fissuring.

CASE 1: WELD METAL WITH LOWER M_S TEMPERATURE THAN THE HAZ.

This case can be described as a situation where the weld metal is overmatched with respect to the base metal with higher alloying content. The weld metal exhibits a higher strength than the base metal and its martensite start temperature is depressed to below that of the base metal. While the austenite in the HAZ has begun transforming, the austenite in the weld metal remains unchanged. After a period of time, the HAZ immediately adjacent to the fusion zone will transport hydrogen at a higher rate than that in the weld metal. If the HAZ martensite start temperature (M_s) is sufficiently high, the hydrogen will be able to transport a significant distance into the parent metal. Especially if the transformation occurs at a moderately elevated temperature, the situation described can potentially reduce the localized hydrogen content in the hard microstructure adjacent to the fusion line, thus reducing the hydrogen cracking susceptibility. However, the hydrogen transport cannot proceed extensively until the weld metal transforms because austenite has the ability of storing high hydrogen contents but can not move it fast enough to the fusion line. If the weld metal M_s temperature is too low, then the hydrogen transport from the weld metal is limited. Very little hydrogen can reach the heat affected zone adjacent to the fusion line that may eventually lead to weld metal cracking.

To demonstrate the effect of martensite start temperature on hydrogen transport, the diffusion process was modeled considering incremental time periods and temperature which decreases according to the welding heat input and cooling rate. The martensite start was allowed to occur in the HAZ and weld metal, but at different times. Simple but reasonable boundary conditions were established for the solution of Fick's 2nd law. Several hydrogen profiles were determined (6) and the dotted traced line in Figure 3 illustrates the diffusible hydrogen distribution. This profile is the case where the HAZ M_s temperature is greater than the weld metal M_s temperature, and for a location indicated in Figure 3. This situation is prone to hydrogen cracking in the weld deposit which also has been observed for some high strength weldments.

CASE 2: HAZ WITH LOWER M_S TEMPERATURE THAN THE WELD METAL.

This case can be described as a situation where the weld metal is undermatched with respect to the base metal. Since the heat affected zone transforms from austenite to ferrite at lower temperatures and at a later time than the weld metal, the HAZ becomes an austenite diffusion barrier for hydrogen transport. A high hydrogen accumulation in the heat affected zone adjacent to the fusion line results. This situation promotes underbead

hydrogen cracking. Figure 3 also plots the hydrogen profile (solid line) obtained in calculations following the procedure outlined in Case 1. Instead of having a high hydrogen concentration in the weld metal, hydrogen peaks are observed in the heat affected zone as shown in Figure 1. This profile supports the hydrogen distribution model as proposed and suggest that the hydrogen cracking being limited to a few grains (austenite) adjacent to the fusion line. Thus, a HAZ with lower M_s temperature may result in underbead hydrogen cracking and localized weld metal cracking along the fusion line.

To evaluate the ability of using the martensite start temperature as a hydrogen cracking index, the diffusible hydrogen content was plotted as a function of the calculated weld metal martensite start temperature for welds made on the same base metal (7). Figure 4 illustrates a demarcation line between the cracked and the uncracked weldments.

From the application of the M_s temperature, it is possible to obtain a ΔM_s expression, and the sign and magnitude of this ΔM_s expression will better describe the hydrogen diffusion behavior:

$$\Delta M_s = M_{s(WM)} - M_{s(BM)}$$

If $\Delta M_s < 0$, hydrogen accumulation will be in the weld metal. If $\Delta M_s > 0$, hydrogen accumulation in the HAZ is possible and underbead cracking may occur.

Some preliminary hydrogen cracking data is plotted with ΔM_s as a function of M_s HAZ in Figure 5. This data indicates some ability to establish a demarcation line between cracking and non-cracking. Further work is necessary to evaluate the correlation between cracking and ΔM_s.

Selection of the alloy additions has to be determined to achieve only a slightly higher martensite start temperature of the weld metal than that of the HAZ, for maximum hydrogen transport to the base metal. In addition, the absolute martensite start temperatures of the weld metal and the HAZ should be high enough to facilitate rapid hydrogen transport in the martensite phase.

3. STEP 2: HYDROGEN ABSORPTION CONTROL BY THERMO-CHEMICAL REACTIONS IN ARC PLASMA

Selected oxides or fluorides are being used as the consumable flux ingredient to minimize hydrogen absorption to the weld pool during arc melting. Hydrogen absorption can be minimized through the formation of water vapor or hydrogen fluoride in a thermo-chemical reaction with oxygen or fluorine gas in the welding plasma. Please notice on attached figures (Fig.6 and Fig. 7) that increasing either oxygen or fluorine will decrease the amount of hydrogen available to enter the weld deposit. These gases shall be generated from the selected fluxes that easily decompose during arc heating. The detrimental effects of excessive amounts of oxygen to the weldment toughness and those effects of fluorine to the working

environment will be considered in the determination of the types and amounts of the flux additions.

Increasing the weld pool oxygen content has been found to reduce the resulting weld metal hydrogen content by perturbing the water reaction (8). A thermodynamic analysis that sequentially follows the oxide (inclusions) formation from solidification to room temperature was performed. This methodology allows for the prediction of total weld metal hydrogen content and has been found to correlate reasonably well with experimental data. The major drawback of using oxygen to control weld metal hydrogen is the resulting oxygen pick up, primarily as inclusions. In excessive amounts, these oxides can alter the mechanical properties detrimentally. This concern requires new research into other weld pool reactions that can also significantly alter the weld metal hydrogen content.

The use of fluorine at small concentration levels to alter the HF reaction, associated with the weld pool and thus reduced the weld metal hydrogen content, is being investigated. Preliminary thermochemical calculations were made and the results illustrated that the use of fluorine holds reasonable promise. Figure 8 illustrates some of the preliminary results where fluorides in the welding flux are used to control hydrogen pick-up during welding of steel with a primer coating (9). It is also known that Teflon® additions have been made by some SMA electrode manufacturers to assist in hydrogen management.

4. STEP 3: DIFFUSIBLE HYDROGEN CONTROL BY HYDROGEN TRAPS

Final suppression of diffusible hydrogen will be achieved by introduction of selected rare earth metal and transition metal additions to the weld metal to serve as hydrogen traps. These traps, in the form of oxides or carbo-nitrides have high binding energies with hydrogen. They are capable of immobilizing hydrogen at temperature ranges much higher than 100 °C, before the risk of cold cracking emerges. With proper trap morphology, number and distribution, it is possible to have a large portion of hydrogen being trapped uniformly throughout the weld metal and leave the remaining diffusible hydrogen in a much smaller content. In this way, transport to and accumulation of hydrogen at potential cracking initiation sites will be kept below the critical value for cold cracking initiation.

In steel, hydrogen is not homogeneously distributed as it would be in a perfect iron crystal. Hydrogen will be found not only in the host lattice, but also segregated to atomic and microstructural imperfections such as vacancies, solute atoms, dislocations, grain boundaries, voids, and second phase particles. In these localized regions, the mean residence time of hydrogen atoms is considerably longer than in normal interstitial lattice sites. In the extreme case, these regions are sinks into which hydrogen atoms fall and remain even during loading. Therefore, the generic term for this behavior is hydrogen trapping.

A prominent effect of trapping is to decrease the apparent hydrogen diffusivity (10). The ability of a trap site to hold hydrogen atoms is associated with the hydrogen-trap binding energy. Consequently, a trapped hydrogen atom must acquire an energy substantially greater than the lattice migration energy to escape the trap and contribute to the measured diffusivity.

Numerous studies on different traps have been reviewed by several authors (11-14). From various reported data, values of hydrogen-trap binding energies in iron were identified and are listed in Table 1. In addition, an electronic structure calculation was also applied in searching for other forms of potential traps that can be introduced in steel welding (15). Several inclusions in steel were investigated and, among them, Ce_2O_3 oxide was found to have the highest binding energy followed by TiC, Y_2O_3, VC, NbC and finally Mo_2C, in the order of decreasing energy. The binding energy of 60 kJ/mol H for a dislocation or a grain boundary is generally regarded as the typical limiting value of a reversible trap. With this energy level, a reversible trap becomes effective in capturing hydrogen around 400 °K but does not reach saturation at room temperature, as shown in Figure 9. A graphical description of this hydrogen distribution was calculated for selected hydrogen traps and is presented in terms of the saturation temperature in Figure 10. The saturation temperature was approximated for 0.9 fraction of trap occupation and was predicted to increase with increasing binding energy. A reversible trap whose binding energy is lower than 60 kJ/mol will not be able to prevent hydrogen cracking. The trapped hydrogen will be picked up by moving dislocations and eventually be delivered to crack initiation sites (16). The preferred traps are then those having binding energies higher than 60 kJ/mol and are termed irreversible traps (17).

A preliminary numerical study of hydrogen trapping during the welding cooling cycle has been conducted as a basis for criteria of trap selection. This study involved the prediction of diffusible hydrogen content, which changes with time due to both the hydrogen removal out of the weld metal and the hydrogen capture by trap sites in the weld metal. A diffusion model of hydrogen in steel containing trap sites, similar to the McNabb and Foster model (18), has been applied. The calculation was done numerically to take account the variation of both the hydrogen diffusion coefficient and the hydrogen capturing rate by trap sites with temperature and the associated microstructure of the diffusing medium. An example of the calculated result is shown in Figure 11a, where the diffusible hydrogen content (HD) of the weld metal containing traps is predicted to be lower than that of the steel without traps.Also shown in Figure 11a is the trapped hydrogen (HT) whose amount increases with time.

An abrupt change of slope can be observed in the diffusible hydrogen content right at the martensite start temperature of the weld metal. Phase transformation from austenite to martensite is accompanied by a large increase in the hydrogen diffusion coefficient which in turn accelerates both the hydrogen capture and the hydrogen removal out of the weld metal. The kinetics of hydrogen capturing can be more clearly explained in Figure 11b which shows the equilibrium trap occupancy (neq), the actual trap occupancy (n) and the rate of hydrogen capture (dn/dt). The hydrogen capture rate depends both on hydrogen diffusivity and the driving force for hydrogen entrapment (neq-n). It can be seen that a sudden increase in the rate of capture always follows the occurrence of martensite phase formation where both capture determining factors are maximized.

The criteria for the use of traps to reduce the susceptibility of HAC should include a proper combination of several factors. These factors are the hydrogen-trap binding energy, the trap density, the martensite start temperature and the cooling rate ($\Delta t_{8/5}$). In this preliminary

investigation, each of the above mentioned variables was varied independently and the resulting amount of diffusible hydrogen at 100 °C as well as at 300 °C are summarized in Figures 12 to 15. The temperature 100 °C has been considered as the temperature where the potential for HAC starts to become a problem.

The first important parameter of a trap is the hydrogen-trap binding energy. In this calculation, four values of binding energies that correspond to different trap sites were used. They are 60 kJ/mol for dislocations, 80 kJ/mol for Al_2O_3 inclusions, 100 kJ/mol for TiC particles, and 120 kJ/mol for rare earth additions. As shown in Figure 12, the amount of diffusible hydrogen content decreases with increasing hydrogen-trap binding energy. The major advantage of traps with high binding energy is that they provide a high driving force for hydrogen capture within high temperature regions. The data at 300 °C shows a better insight to how much faster the hydrogen is captured by high binding energy traps as opposed to those with low binding energy. Should the HAC start to occur at a higher temperature than 100 °C (which may be possible for weld metal with low martensite start temperature) the weld metal containing high binding energy traps may have a better chance to survive.

The diffusivity of hydrogen in the austenite phase is very low, so that the hydrogen cannot be effectively captured or removed out of the weld metal until the martensite temperature is reached. The lower the martensite start temperature is, the longer time hydrogen has to remain in the weld metal lattice sites. It also means that the available temperature range for effective hydrogen diffusivity and trapping in the ferrite phase becomes narrower and the suppression of diffusible hydrogen content by certain traps becomes less effective. The extreme situation is depicted in Figure 13 for the case of weld metal possessing martensite start temperature of 400 °C. The advantage of using a trap with higher binding energy, i.e., higher capture rate, is then obvious in this very narrow temperature range situation. However, the employment of high binding energy traps for a high martensite start temperature weld metal can lead to a situation where the trapping capacity will be wasted at high temperature regions. This behavior can occur even when the hydrogen diffusivity provides a high potential for easy hydrogen removal out of the weld metal. Therefore, the selection of hydrogen traps must consider other factors than just the weld metal or consumable alloying contents.

Conventional hydrogen management usually applies proper heat treatment or sufficiently low cooling rate to provide easy hydrogen removal out of the weld and to form a less susceptible microstructure to HAC. In case of weld metal containing trap sites, a certain rate of cooling is also necessary to allow for enough hydrogen capture time before the temperature reaches 100 °C. In the present calculation, the cooling rate is assumed to occur naturally and relatively fast, so that sufficient hydrogen removal by lattice diffusion alone can not be obtained. The effect of cooling rate, shown in Figure 14, appears to be similar to that of the martensite start temperature. A very fast cooling rate, such as those with $\Delta t_{8/5}$ equal to one second, does not permit enough time for hydrogen to leave the weld metal or jump into the trap sites. On the other hand, in a slightly slower cooling rate, the presence of traps may yield a low diffusible hydrogen content at 100°C and alleviate the tendency for weld metal HAC. This prediction shows the potential usage of traps to substitute for the tight heat-treatment procedure necessary for high strength steel welding.

The number of trap sites translates into the capacity to hold hydrogen atoms. A higher number of trap sites in the weld metal will produce a lower diffusible hydrogen content, which is in agreement with the calculated result shown in Figure 15. There is also an apparent threshold number of trap sites for optimum hydrogen trapping that can be observed in Figure 15. The number of traps used in the present calculation corresponds to a 100 to 500 ppm range of substitutional atom traps in the weld metal. In the case of inclusion traps, which is the most probable form of traps in weld metal, the trap sites on the surface are of the inclusion - matrix interface. Depending on the cooling rate, the number of trap sites used in this calculation may correspond to a relatively high inclusion volume fraction that yields weld metal with intrinsically low toughness. Obviously, the number of trap sites that can be used is limited to an extent in which the toughness is still maintained at an acceptable level. This issue suggests that the success of using hydrogen traps should not be related to significant diffusible hydrogen suppression in the weld metal. Its main function should be to promote a proper distribution of hydrogen in weld metal so that a high local accumulation of hydrogen at crack initiation sites can be prevented. Furthermore, in high strength steel welding, where hydrogen is highly accumulated at crack initiation sites, the presence of trap sites may give a higher tolerance for diffusible hydrogen content. Normally, a low maximum acceptable level of hydrogen content in the weldment is usually required for conventional welding procedures.

5. PROSPECTIVES

Use of these three steps for hydrogen management will reduce susceptibility to hydrogen cracking in welds. With further quantification and correlations, analytical procedures can be developed for designing welding consumables and practices for high strength steel that require a very low diffusible hydrogen content.

6. ACKNOWLEDGMENT

The authors acknowledge and appreciate the research support of the US Army Research Office.

7. REFERENCES :

1 . R.A.J. Karppi, J. Ruusila, M. Toyoda, K. Satoh, and K. Vartiainen, Scandinavian Journal of Metallurgy, Vol. 13, (1984), pp. 66-74.
2. Th. Bollinghaus, H. Hoffmeister, and A. Dangeleit, "A scatter Band for Hydrogen Diffusion Coefficients in Microalloyed and Low Carbon Structural Steels". (IIW Document IX-1767-94, 1994).
3. H. Granjon, "Cold Cracking in Welding of Steels", Intl. Symposium on Cracking and Fracture in Welds, Conf. Proc. Japan Welding Society, (1971), IB, 1.1.
4. B. Gravile, "Hydrogen Cracking Sensitivity of HSLA Steels", The Metallurgy, Welding and Qualification of Microalloyed (HSLA) Steel Weldments, (1990), 127
5. R.D. Smith, Private Communication, Colorado School of Mines, (1996).
6. W. Wang, S. Liu and D.L. Olson, "Consequences of Weld Undermatching and Overmatching: Non-Uniform Hydrogen Distribution", in Intl. Conf. on Offshore Mechanics and Artic Engineering - Materials Enginnering', ASME, Vol. III, , Florence, Italy, (1996), pp. 403-409
7. D.L. Olson, S. Liu, W. Wang, R. Pieters, and S. Ibarra, "Martensite Start Temperature as a Weldability Index", in Conf. Proc. on 'Research Trends in Welding Science and Technology', pp. 615-620, Gatlinburg, Tennessee, (1995), ASM Intl., 1996.
8. S. Liu, D.L. Olson & S. Ibara, "Electrode Formulation to Reduce Weld Metal Hydrogen and Porosity", Intl. Conf. on Offshore Mechanics and Arctic Engineering, ASME-OMAE, (1994), pp. 291-298
9. K. Johnson, Private Communication, Colorado School of Mines, (1996).
10. H.H. Johnson, Metall. Trans., Vol. 19B, (1988), pp. 691-707.
11. J.P. Hirth, Metall. Trans., Vol.11A, (1980), pp. 861-890.
12. I.M. Bernstein and G.M. Pressouyre, in Hydrogen Degradation of Ferrous Alloys, ed. by R.A. Oriani, J.P. Hirth and M. Smialowski, Noyes Pub., (1985), pp 641-685.
13. P. Kedzierzawski, in Hydrogen Degradation of Ferrous Alloys, ed. by R.A. Oriani, J.P. Hirth and M. Smialowski, Noyes Pub., (1985), pp. 271 - 288.
14. R. Gibala and A.J. Kumnick, in Hydrogen Embrittlement and Stress Corrosion Cracking, ed. by R. Gibala and R.F. Hehemann, ASM, Metals Park, Ohio, (1984), pp. 61 - 77.
15. M. Eberhart, Private communication, Colorado Schoool of Mines, (1995).
16. J.K. Tien, A.W. Thompson, I.M. Bernstein, and R.J. Richards, Metall. Trans., Vol.7A, (1976), pp. 821-829.
17. G.M. Pressouyre and I.M. Bernstein, Metall. Trans., Vol. 12A, 1981, pp. 835-844.
18. A. McNabb and P.K. Foster, Trans. of the Metall. Soc. of AIME, Vol. 227, (1963), pp. 618-627.
19. R. Gibala, in Stress Corrosion Cracking and Hydrogen Embrittlement of Iron Base Alloys, ed. by R.W. Staehle, J. Hochmannn, R.D. McCright, and J.E. Slater, NACE-5, NACE, Houston, TX, (1977), pp. 244-268.
20. W.Y. Choo and J.Y. Lee, Metall. Trans., Vol. 13A, (1982), p. 135.
21. A.J. Kummick and H.H. Johnson, Acta Metall., Vol. 28, (1980), pp. 33-40.
22. K. Ono and M. Meshi, Acta Metall., Vol. 40 (6), (1992), pp. 1357-1364

23. T. Asaoka, C. Dagbert, M. Aucouturier, and J. Galland, Scripta Metall., Vol.11, (1977), pp. 467-472.
24. E. Chornet and R.W. Coughlin, J. Catal., Vol.72, (1972), pp. 246-265.
25. D.O. Hayward and B.M.W. Trapnell, in Chemisorption, Butterworths, London, (1964), p.203.
26. J.R. Scully, J.A. Van den Avyle, M.J. Cieslak, A.D. Romig,Jr., and C.R. Hills, Metall. Trans., Vol.22A, (1991), pp. 2429-2445.
27. K.Y. Lee, J.Y. Lee and D.R. Kim, Mater. Sci. Eng., Vol. 67, (1984), p. 213
28. H.H. Podgurski and R.A. Oriani, Metall. Trans., Vol.3, (1972), pp. 2055-2063.
29. J.L. Lee and J.Y. Lee, Metal Sci., Vol. 17, (1983), p. 462.
30. J.L. Lee and J.Y. Lee, Metall. Trans., Vol. 35A, (1987), pp. 2695-2700
31. P. Lacombe, M. Aucouturier, J.P. Laurent, and G. La Passet, in Stress Corrosion Cracking and Hydrogen Embrittlement of Iron Base Alloys, ed. by R.W. Staehle, J. Hochmannn, R.D. McCright, and J.E. Slater, NACE-5, NACE, Houston, TX, (1977), pp. 423-430.
32. H.G. Lee and J.Y. Lee, Acta Metall., Vol.32, (1984), p. 131
33. G.M. Pressouyre and I.M. Bernstein, Metall. Trans., Vol. 9A, (1978), pp. 1571-1580.
34. G.M.Pressouyre, Metall. Trans., Vol. 10A, (1979), pp.1571-1573

Table 1. Hydrogen trapping in Iron. Reference state : H in perfect lattice

Trap Site	Binding Energy (kJ/mol)	Matrix	Assessment Method	Ref.
H-dislocation elastic stress field	0 - 20.2	Iron	calculated	19
H-dislocation core (screw)	20 - 30	Iron	calculated	11
H-dislocation	26	Iron	thermal analysis	20
H-dislocation core (mixed)	59	Iron	permeation	21
H-grain boundary	18 - 20	C-Mn Steel	thermal analysis	20
H-grain boundary	60	Iron	thermal analysis	22
H-grain boundary	59	Iron	permeation	21,23
H-Free surface	70	Iron	permeation	24
H-Free surface	95	Iron	permeation	25
β-NiAl	27	Steel *	permeation	26
H-PdAl interface	34	Steel *	permeation	25
H-Fe-oxide interface	47	C-Mn Steel	thermal analysis	27
H-AlN interface	65	Iron	permeation	28
H-MnS interface	72	C-Mn Steel	thermal analysis	29
H-Al_2O_3 interface	79	C-Mn Steel	thermal analysis	30
H-Fe_3C interface	84	C-Mn Steel	permeation	23,31
H-TiC interface	87	Iron	thermal analysis	32
H-TiC interface	95	C-Mn Steel	permeation	33
H-Nd	129	Iron	calculated	34

* Matrix element is precipitation hardened martensitic stainless steel.

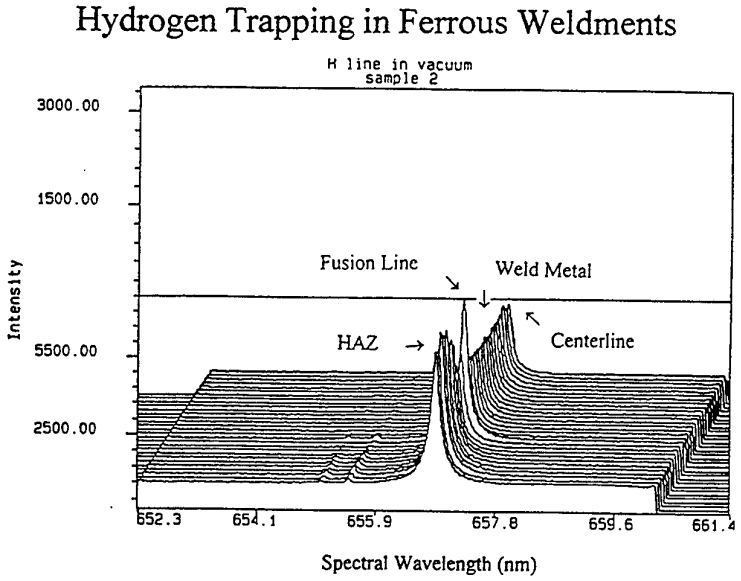

Figure 1. Non-uniform distribution of hydrogen across the center line of a weldment. Intensities of the hydrogen spectral emission are proportional to the hydrogen concentration.

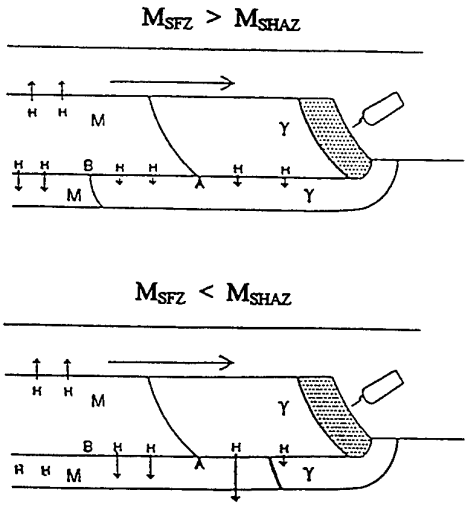

Figure 2. Illustration of hydrogen diffusion at different martensite start temperature for weldment and base metal (3)

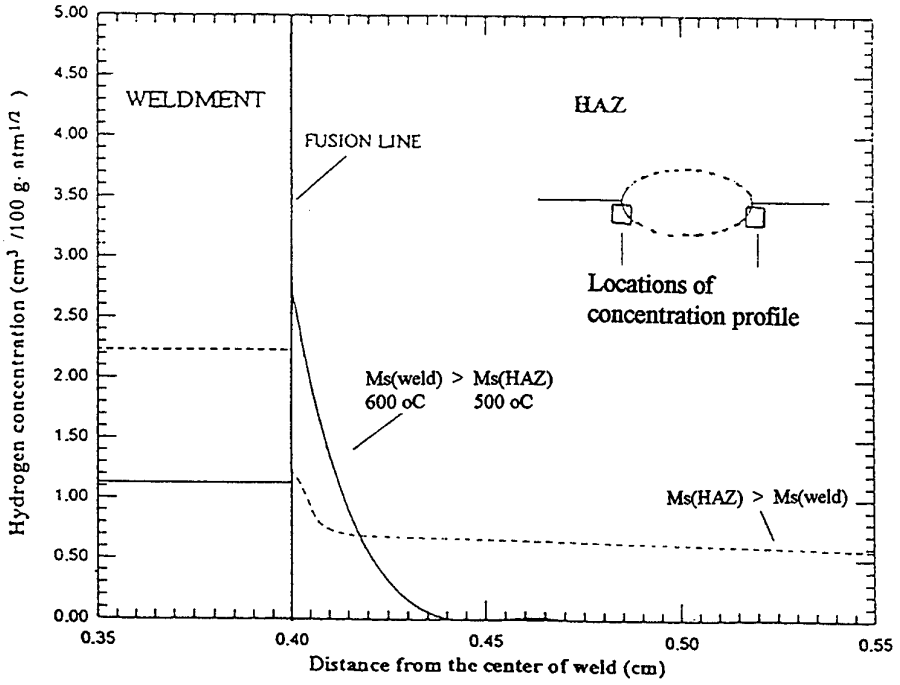

Figure 3. Hydrogen distribution across the fusion line of a steel weldment for $M_{s\ weld} > M_{s\ HAZ}$ and $M_{s\ weld} < M_{s\ HAZ}$.

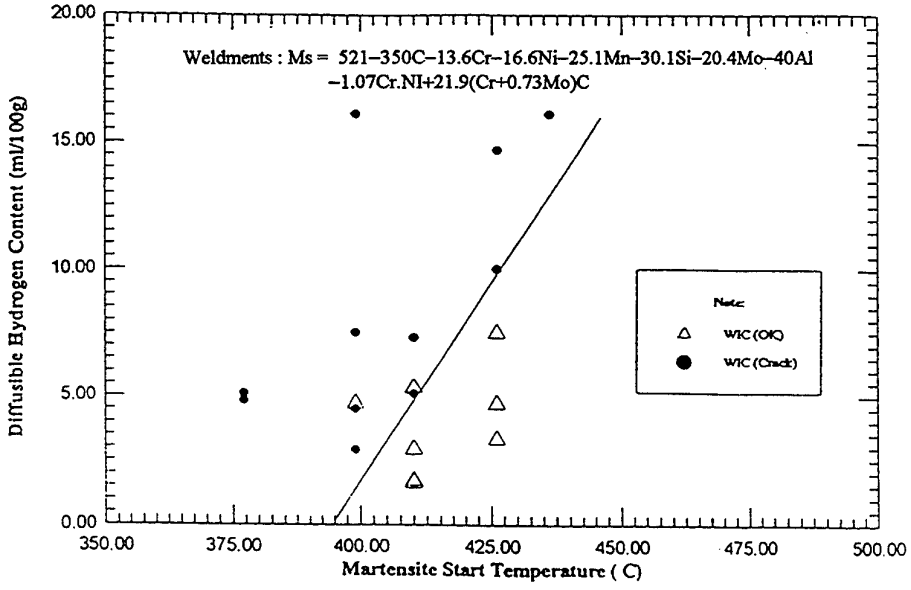

Figure 4. Conceptual illustration of cracking prediction.

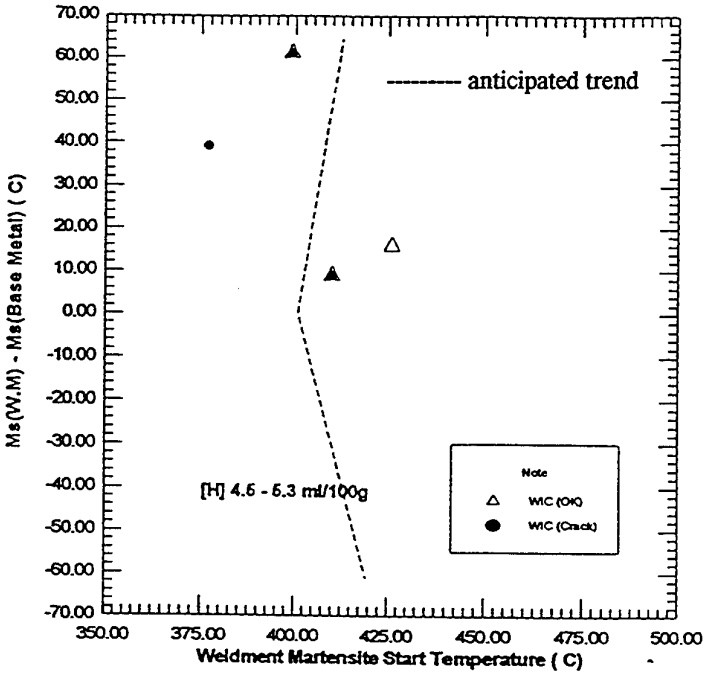

Figure 5. Illustration of hydrogen cracking/uncracking zones by hydrogen content and martensite start temperature.

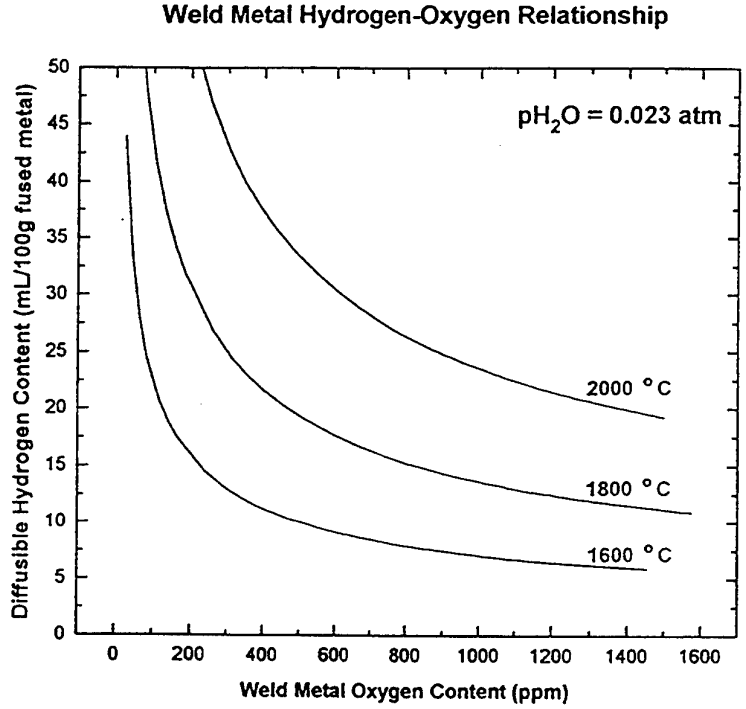

Figure 6. Thermo-chemical reaction between oxygen and hydrogen in the welding plasma.

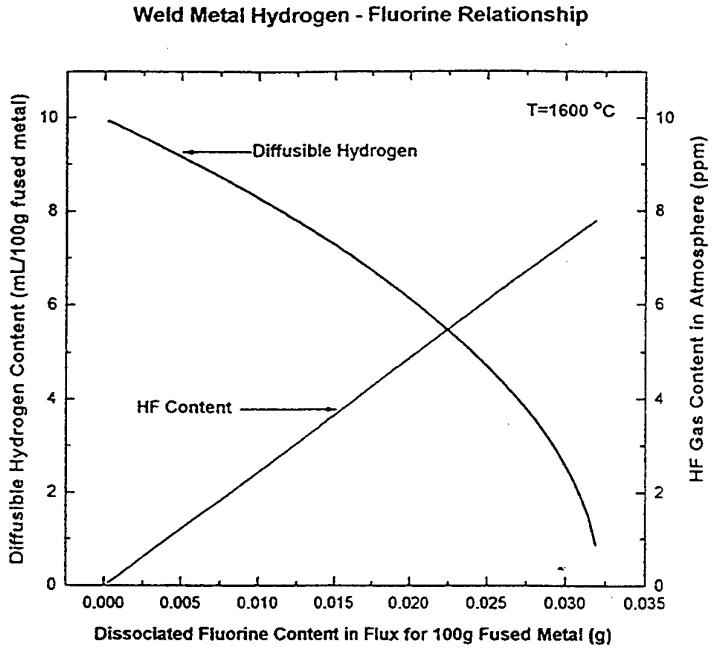

Figure 7. Thermo-chemical reaction between fluorine and hydrogen in the welding plasma.

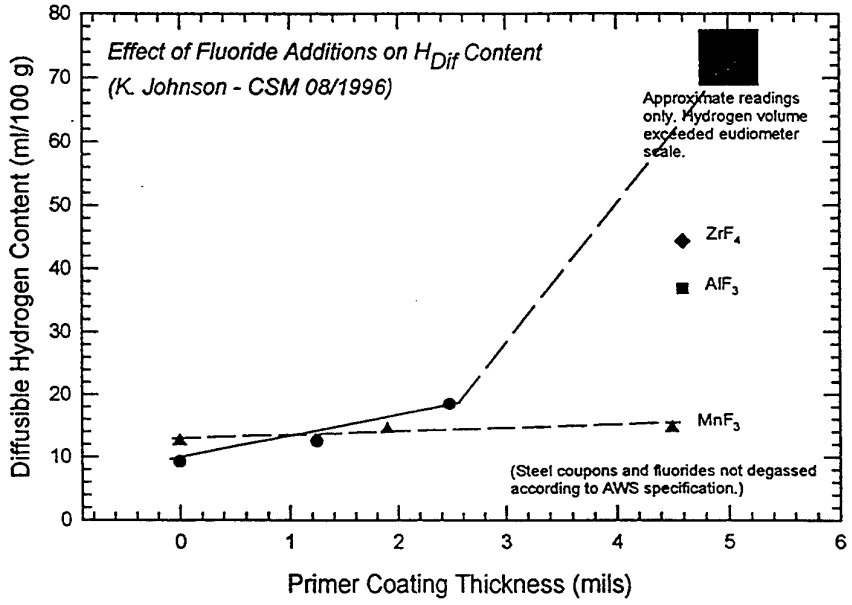

Figure 8. Effect of fluoride additions on H_{diff} content.

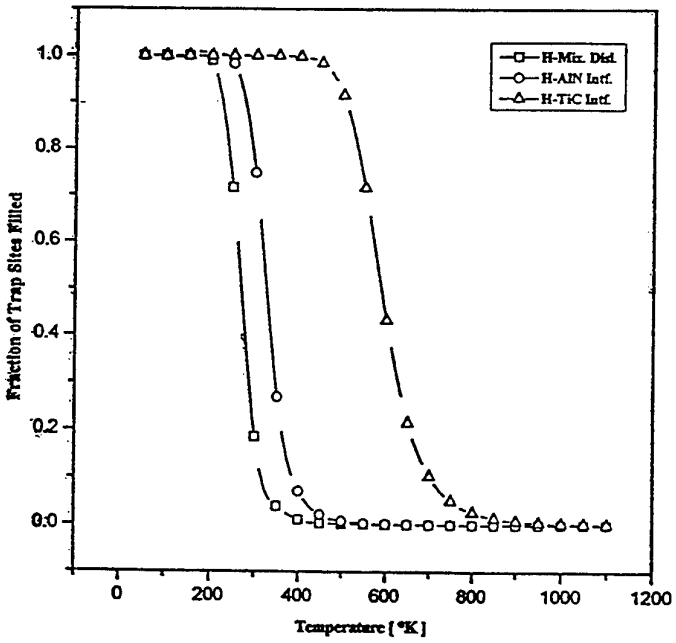

Figure 9. Fraction of trap occupation by hydrogen at trap sites as a function of temperature for various hydrogen-trap binding energies. Partial pressure of hydrogen is 0.0545 Pa.

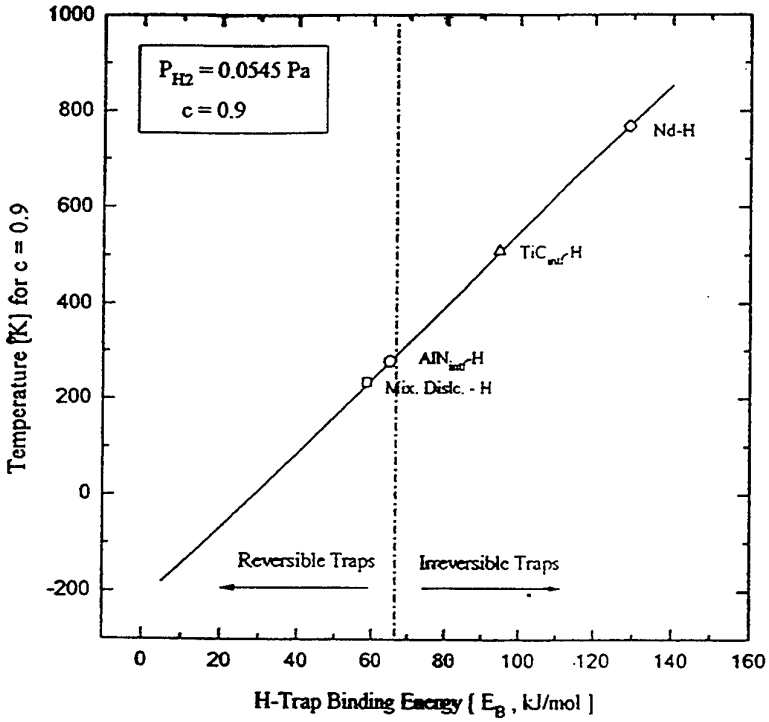

Figure 10. Temperature for ninety percent occupation at various hydrogen trap sites.

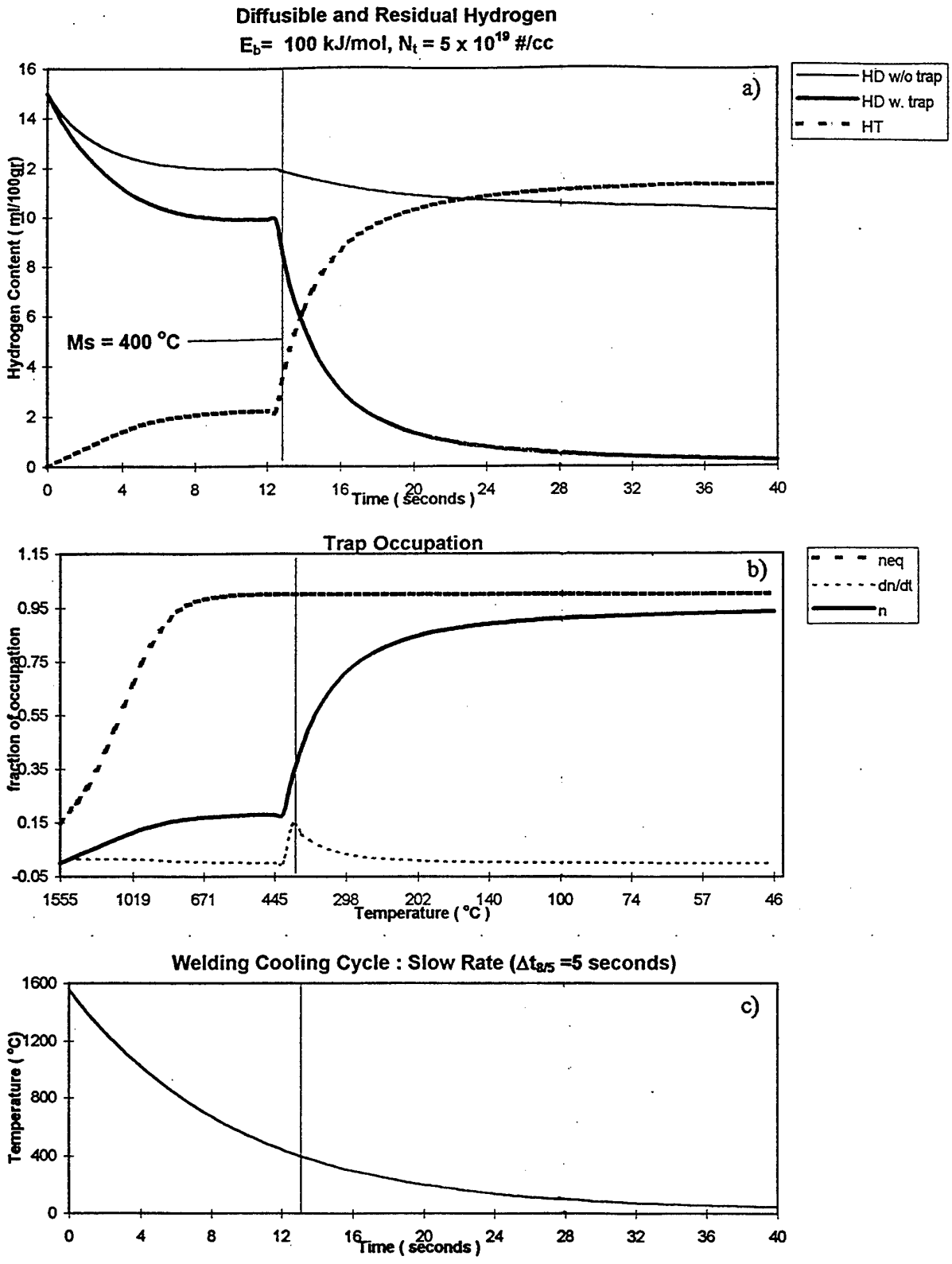

Figure 11. Hydrogen trapping during welding cooling cycle. Initial diffusible hydrogen in weld metal is 15 ml/100g. In (a).,the notation HD stand for diffusible hydrogen, HT is the trapped hydrogen. In (b)., n is the fraction of trap occupation by hydrogen and neq is the equilibrium fraction of occupation determined by the Fermi-Dirac distribution.

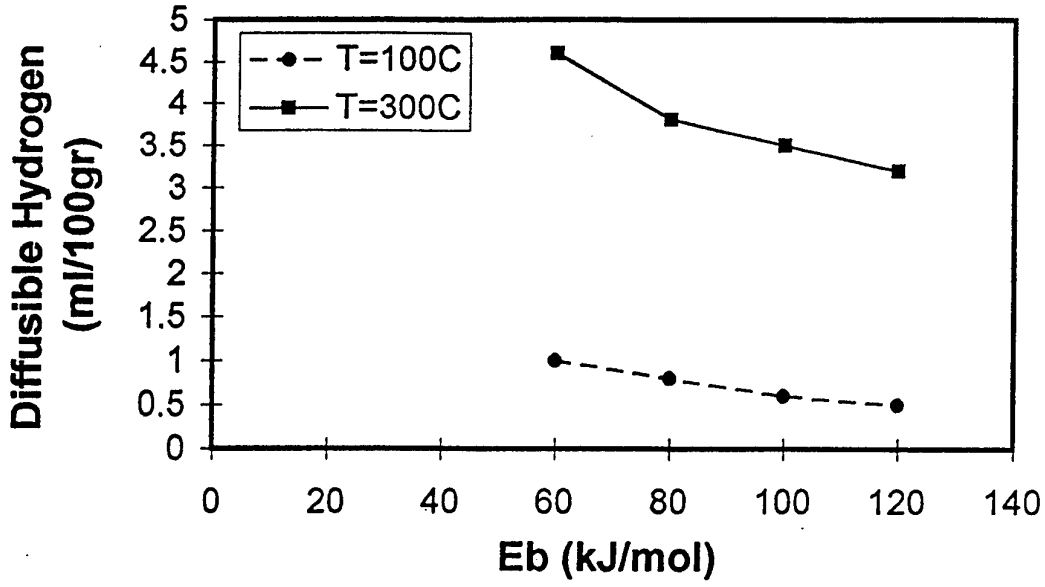

Figure 12. Effect of trap binding energy on the diffusible hydrogen content. Initial diffusible hydrogen content is 15 ml/100g. M_s =400C, $\Delta t_{8/5}$ is 5 seconds, trap density, $N_t = 5x10^{19}$ #/cc.

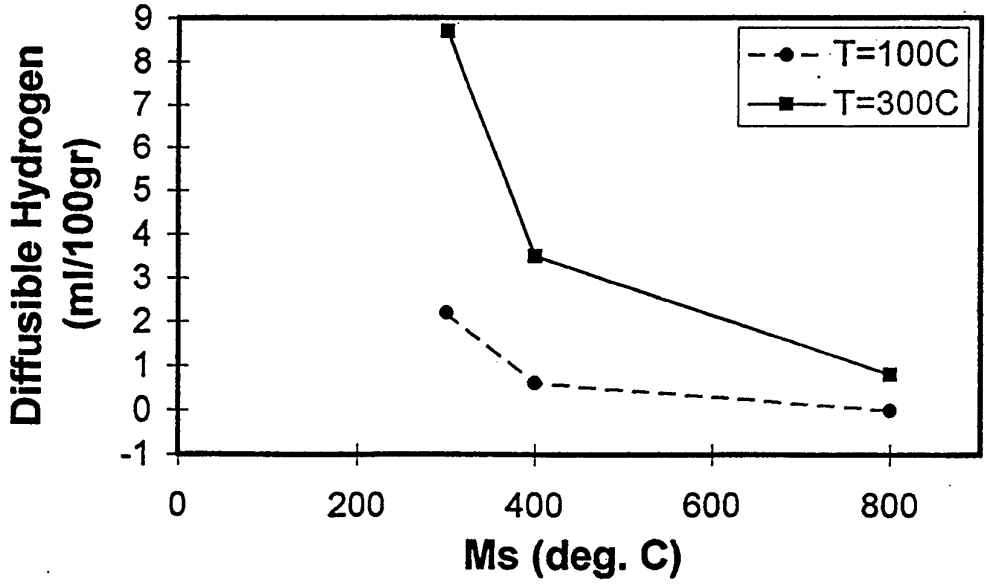

Figure 13. Effect of M_s temperature on the diffusible hydrogen content. Initial diffusible hydrogen content is 15 ml/100g. Eb is 100 kJ/mol, $\Delta t_{8/5}$ is 5 seconds, trap density, $N_t = 5x10^{19}$ #/cc.

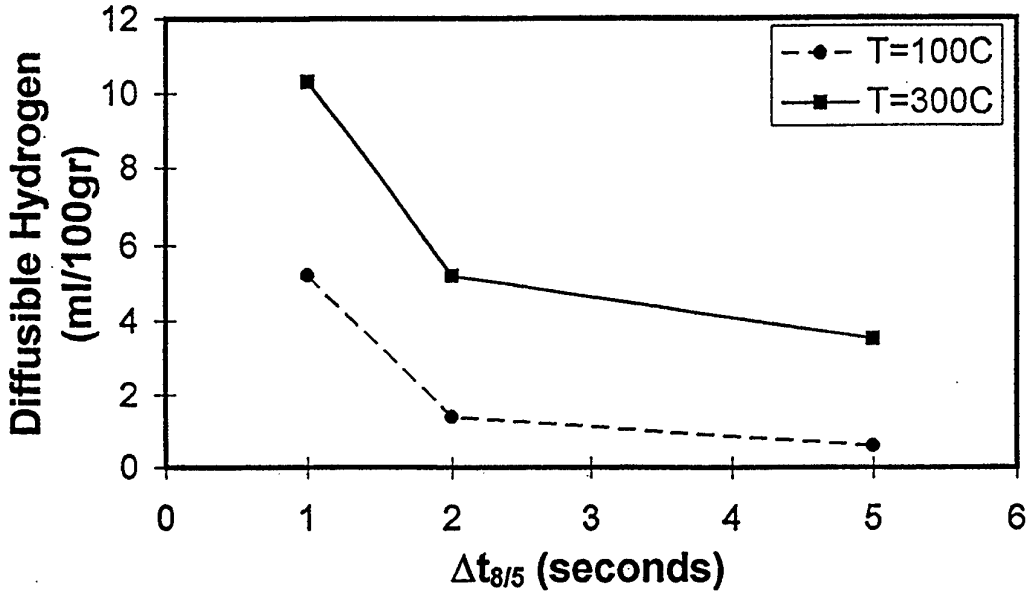

Figure 14. Effect of cooling rate on the diffusible hydrogen content. Initial diffusible hydrogen content is 15 ml/100g. M_s =400C, Eb is 100 kJ/mol, trap density, $N_t = 5x10^{19}$ #/cc.

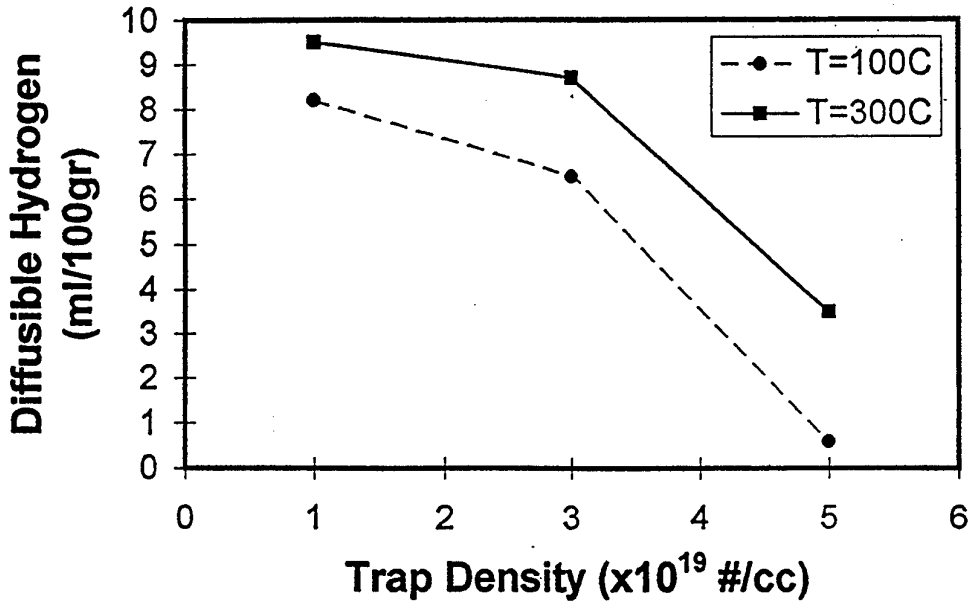

Figure 15. Effect of trap density on the diffusible hydrogen content. Initial diffusible hydrogen content is 15 ml/100g. M_s =400C, $\Delta t_{8/5}$ is 5 seconds, Eb is 100 kJ/mol.

The Relationship Between Hydrogen-Induced Cracking Resistance, Microstructure and Toughness in High Strength Weld Metal

J.L.Davidson, S.P.Lynch and A.Majumdar

Ship Structures and Materials Division
Defence Science and Technology Organisation

1. INTRODUCTION

Increased performance for Naval platforms requires stronger lighter structures which have largely been obtained using high strength steels. As the strength is increased, so is the risk of hydrogen induced cracking after welding. The COLLINS class submarines are fabricated from a 690 MPa yield stress steel. Historically, the risk of hydrogen induced cracking has been greatest in the heat affected zone of the parent metal, where susceptible microstructures can form as a result of the rapid cooling rate experienced during the welding thermal cycle. However, much of this risk has been reduced through the production of low-carbon microalloyed steels which do not develop susceptible heat affected zone microstructures. The risk of weld metal hydrogen induced cracking has been somewhat reduced through the development of low-carbon low-hydrogen welding consumables. However, these developments have not kept pace with advances in the production of the so-called 'preheat free' low-carbon microalloyed steels [1,2,3]. Consequently in modern low carbon microalloyed steels, the focus of attention in the control of hydrogen induced cracking is now on the weld metal [4,5,6].

There is general agreement that the conditions which lead to hydrogen induced cracking during welding are: (1) a critical hydrogen concentration, (2) residual and applied stress above a certain level and (3) a susceptible microstructure [78,5]. All three conditions are interrelated: the critical hydrogen concentration necessary for cracking could be reduced by an increase in the stress or by the presence of microstructures with a greater hydrogen induced cracking susceptibility. Changes in one parameter often affect changes in the other two. For example, a change in welding parameters that changes the weld metal cooling rate is likely to alter the hydrogen concentration, the residual stress, and the microstructure. Twinned martensite has been shown to be more susceptible to hydrogen induced cracking than slipped martensite [9]. This may be due to either the higher residual stresses present in the twinned martensite structure or an inherent susceptibility of the structure itself.

It is unclear which particular aspect of a microstructure makes it susceptible to hydrogen induced cracking. Broadly speaking, the hydrogen induced cracking susceptibility of a microstructure increases with increasing hardness (or strength) [10,11]. A number of workers have indicated that it is the particular microstructure used to achieve the strength which will have a greater influence on hydrogen embrittlement than its strength level *per se* [12,13,14,9,15] and that neither hardness (see Figure 1) [4,16,17,9], nor strength (see Figure 2) [18,19,20,21] are reliable indicators of hydrogen induced cracking susceptibility. The relationship between hardness and hydrogen induced cracking resistance of weld metal is further complicated by the welding parameters used to deposit the weld metal, since they affect the hydrogen concentration as well as hardness. Contours of equal hardness are plotted in Figure 1 as a function of welding parameters for a submerged arc consumable. The solid line is a boundary between the conditions under which hydrogen induced cracking will and will not occur in a Gapped Bead on Plate Test. Since the crack no-crack boundary crosses the hardness contours, a situation arises where cracking will occur at "A", where HV=320, but not at "B" where HV=360. The inherent hydrogen induced cracking resistance of weld metal deposited under conditions at "A" is not necessarily lower than weld metal deposited under conditions

at "B" since the hydrogen concentration will be higher under conditions at "A" than at "B".

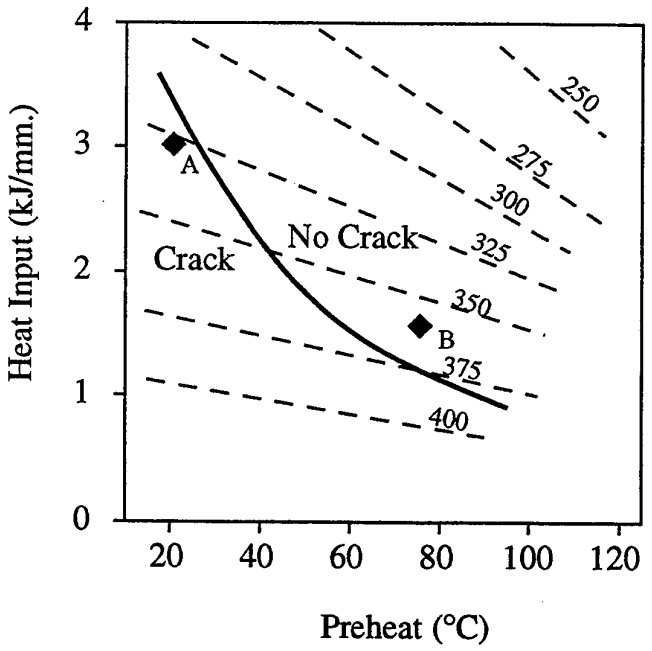

Figure 1. Schematic diagram of hardness contours as a function of welding parameters. Hydrogen induced cracking will occur under the conditions at "A" (HV=320) but not at "B" (HV=360) (hardness data from ref.22)

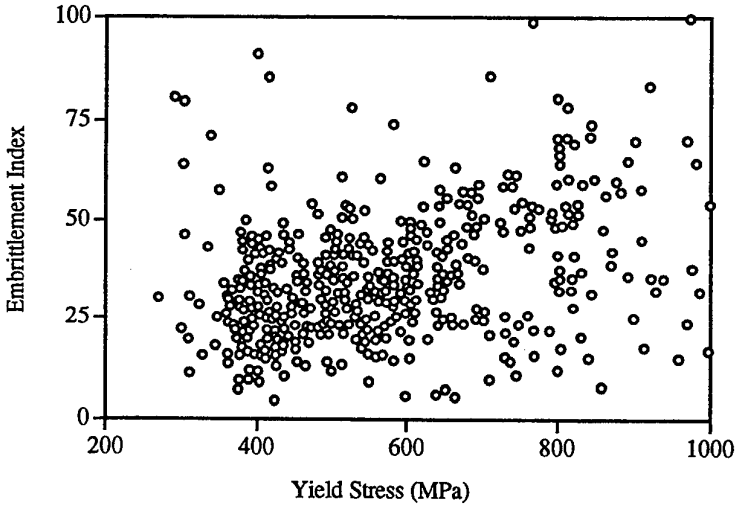

Figure 2. The embrittlement index (percent loss in reduction of area) as a function of yield stress for 34 grades of steel (after ref. 19).

The poor correlation between yield stress and the susceptibility of a steel to hydrogen embrittlement is shown in Figure 2. The scatter in Figure 2 is to a certain extent a result of the many microstructure types which are represented in the data. There is a good correlation between strength and hydrogen induced cracking resistance when the

hydrogen embrittlement is plotted as a function of strength for one microstructure type. Hobson and Sykes [20] examined the hydrogen induced ductility loss of a quenched 3% Cr-Mo steel which was tempered to a range of strength levels (see Figure 3). The hydrogen induced ductility loss decreased with the strength level down to 750 MPa but then increased as the strength was decreased further. The change in behaviour was due to the spherodisation of carbides which occurred at the higher tempering temperatures used to achieve the lower strength levels. This is a good example of the dependence of hydrogen induced cracking resistance on both strength and microstructure.

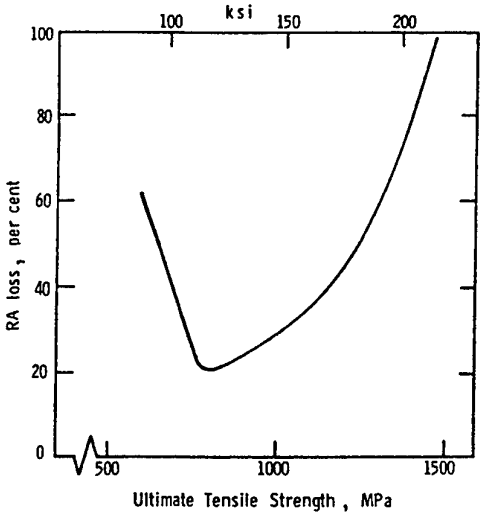

Figure 3. The hydrogen induced ductility loss as a function of UTS for a 3%Cr-Mo steel (after Ref. 20).

It has also been suggested that microstructures with low toughness are more susceptible to hydrogen induced cracking [2,23,24,25,26,27]. Although the correlation between toughness and resistance to hydrogen induced cracking is a useful rule-of-thumb for the welding engineer, the relationship does not always hold [28,29]. For example, a flux cored arc weld metal was shown to have a greater hydrogen induced cracking resistance than a manual metal arc weld metal despite the lower toughness and higher diffusible hydrogen concentration of the flux cored arc weld metal (see Table 1and Figure 4) [28].

Table 1. Properties of a manual metal arc and a flux cored arc weld metal.

	Yield Rel (MPa)	Tensile Rm (MPa)	Charpy Impact Energy (J) -51°C	-18°C	H_D* (ml/100g)
FCAW	735	776	58	86	6.0
MMA	794	844	75	99	3.5

* H_D = diffusible hydrogen content per 100g deposited weld metal

The flux cored arc weld metal may have a greater hydrogen induced cracking resistance due its lower strength relative to the manual metal arc weld metal or because of differences in the inherent hydrogen induced cracking resistance of the weld metal microstructures (see Figure 5).

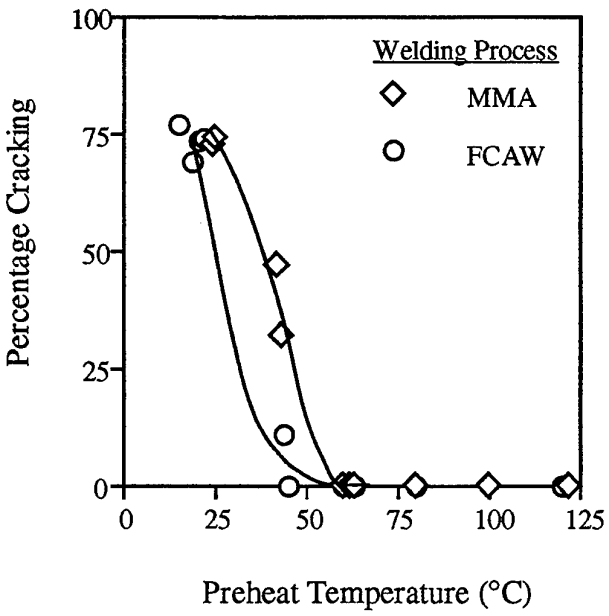

Figure 4. Gapped bead on plate results for a manual metal arc and a flux cored arc consumable. At 40°C the flux cored arc specimens had 0 and 11% cracking whereas the manual metal arc specimens had 32 and 47% cracking.

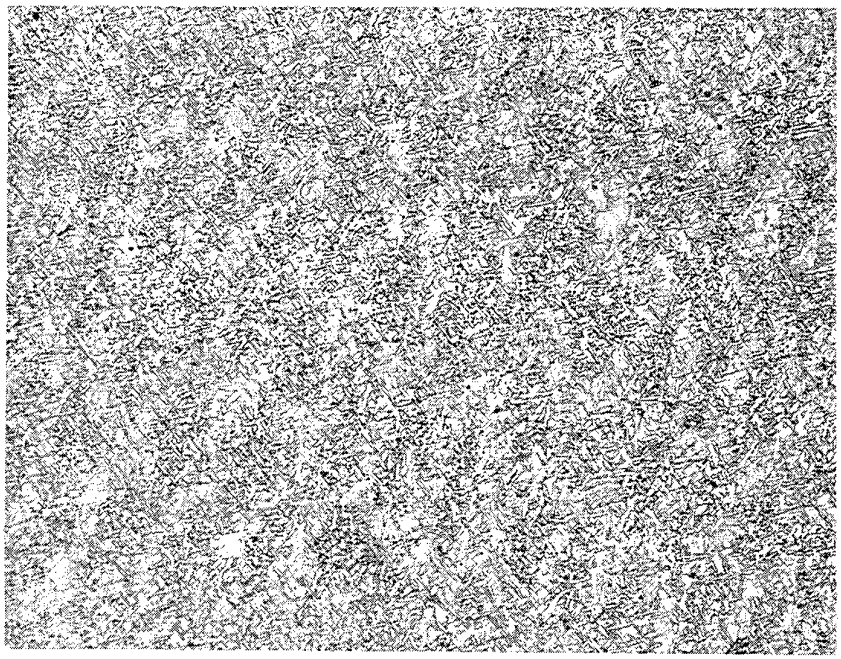

Figure 5. (a) Microstructure of a manual metal arc weld metal. X500

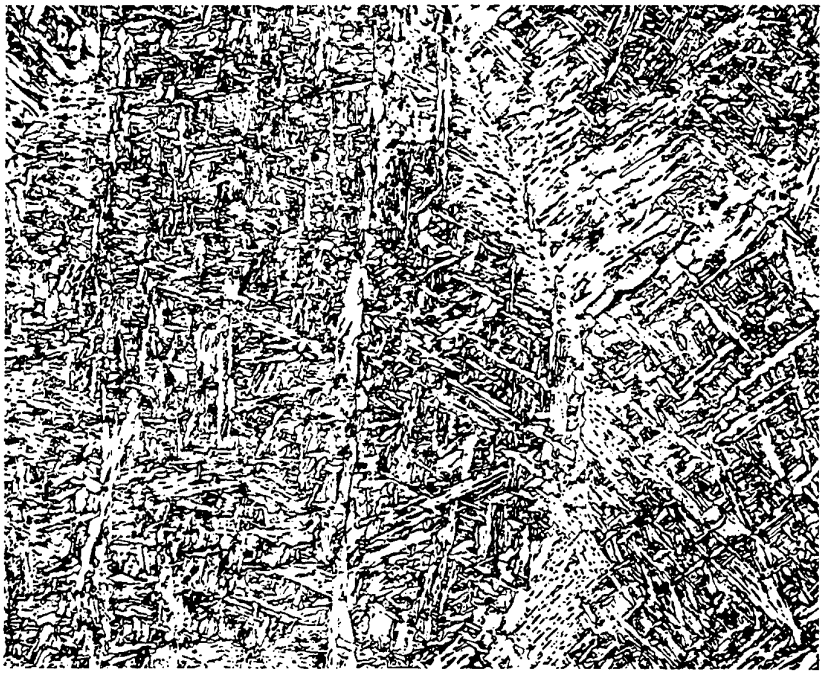

Figure 5. (b) Microstructure of a flux cored arc weld metal. X500

The correlation between toughness and hydrogen induced cracking resistance is not a proof of a causal relationship: ie. the physical process of fracture during hydrogen induced cracking is not normally the same process by which fracture occurs during a toughness test. Furthermore, the fracture mode of hydrogen induced cracking can vary for the same material, depending on the hydrogen concentration at the crack tip and the stress intensity factor [30,31,32,13,33]. Increased stress intensity factor levels can lead to a change in the fracture mode from 'brittle' intergranular fracture to quasi-cleavage and finally transgranular microvoid coalescence [30]. Accordingly, the failure mode in a hydrogen induced cracking test, such as the Gapped Bead on Plate test, is sometimes different to the mode of hydrogen induced cracking observed in a multipass weld (see Figure 6 (a) and (b)).

It is clear that the interrelationship between strength, toughness, hydrogen induced cracking resistance and microstructure is complicated. As an initial attempt to investigate these interrelationships it is the aim of this paper to explore the relationship between toughness and the resistance to hydrogen-induced cracking in weld metal for 690MPa yield stress steel and to demonstrate that the correlation between the two is due to the qualitative mutual dependence of both toughness and hydrogen induced cracking resistance on microstructure. To this end, three microstructural features which influence toughness are discussed in terms of their likely effect on the inherent hydrogen induced cracking resistance of a 690MPa yield stress weld metal. The resistance to cleavage and ductile fracture, as measured by toughness tests, will be treated separately in the discussion, since each occurs by different mechanisms and hence have different dependencies on microstructural features.

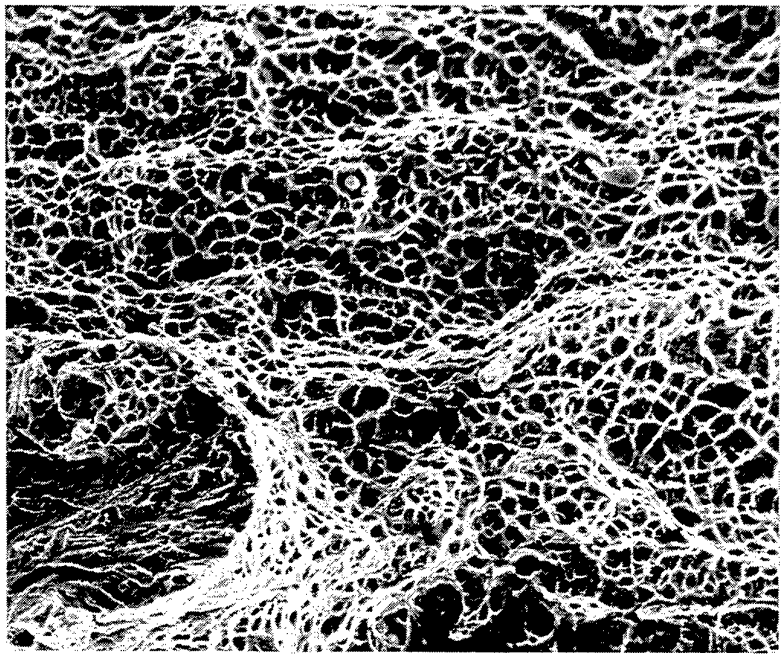

(a)

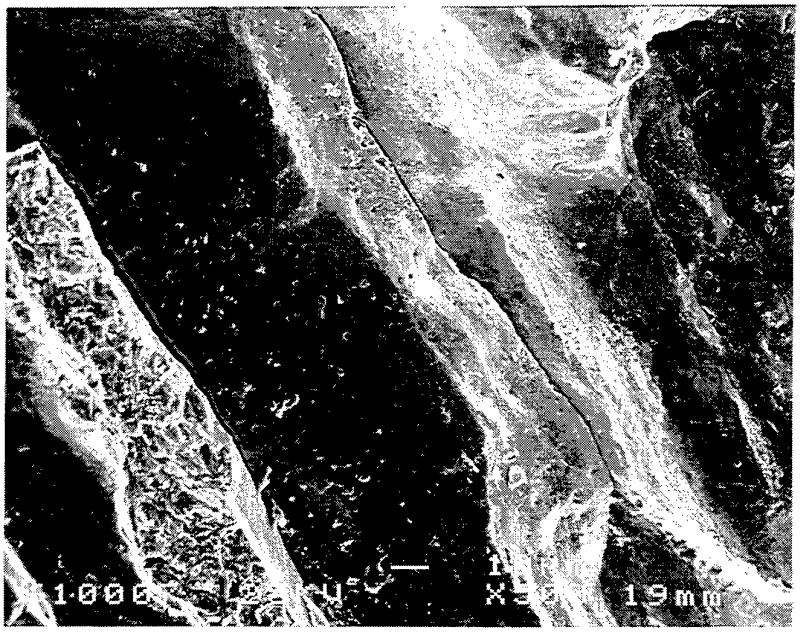

(b)

Figure 6. The variation in the hydrogen induced fracture mode of a flux cored arc weld metal for 690MPa yield stress steel (a) cleavage and microvoid coalescence (taken from a Gapped Bead on Plate Test).(b) intergranular fracture (taken from a multipass weld).

2. EFFECT OF MICROSTRUCTURAL FEATURES ON TOUGHNESS AND HYDROGEN INDUCED CRACKING

2.1 Second phase particles

Inclusions influence the resistance to hydrogen induced cracking, cleavage and ductile fracture in different ways.

Cleavage fracture can initiate through the cracking of brittle second phase particles [34], such as carbides [35] or inclusions [36]. The crack formed by a fractured particle will only propagate into the adjacent ferrite matrix if the stress intensity factor at the newly formed crack tip is large enough to initiate cleavage in the ferrite. Larger particles are more likely to initiate cleavage since the crack formed by their fracture will be longer and hence the stress intensity factor at the crack tip will be higher. It has been observed that cleavage in weld metal is initiated by inclusions at the uppermost end of the inclusion size distribution (>1μm) despite the small number of inclusions of this size [36,37] (see Figure 7). In contrast the propagation of a cleavage fracture is unlikely to be affected by inclusions.

Since ductile fracture occurs by the growth and coalescence of microvoids nucleated at inclusions, ductile crack growth will be promoted by an increased size and decreased separation of inclusions, which to a first approximation will be given by the volume fraction of inclusions [60,38,39].

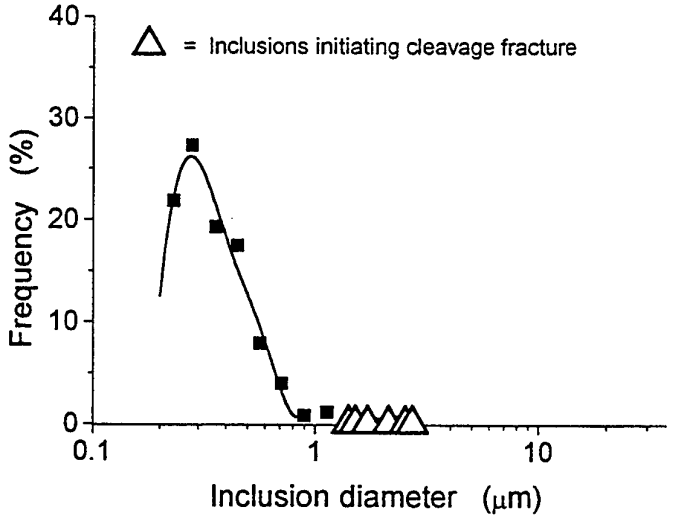

Figure 7. The size of inclusions which have initiated cleavage fracture in blunt notch four point bend test specimens compared to the overall inclusion size distribution.(from ref.40).

Table 2. Identified hydrogen traps with a range of trap energies.

Hydrogen Trap	Activation Energy kJ/mol	Peak Temp. °C	Ref.
Very reversible			
interstitial lattice site	7.7	-	[41]
Reversible			
Ti substitutional atom	26	-	[42]
grain boundaries	17.2	112	[43]
"	26	-	[44]
dislocations	-	270	[45]
"	24	-	[46]
"	24	-	[47]
"	26.8	215	[43]
ferrite/carbide interface		115	[45]
ferrite/cementite interface	18	160	[48]
"	18.4	-	[49]
"	-	123	[43]
ferrite/carbide average	26.8	-	[49]
(tempered martensite)	29.7	-	[49]
(overaged martensite)	36.4	-	[49]
"Irreversible"			
microvoids	48.3	338	[45]
"	35.2	305	[43]
"	36.8	330	[48]
iron oxide	50.6	430	[48]
	69.5	530	[48]
MnS	72.3	496	[45]
Al2O3	79	580	[50]
Al2O3 or SiO2	86.2	630	[48]
	112.1	750	[48]
TiC	88.2	-	[42]

Inclusions can affect hydrogen induced cracking resistance by acting as crack nuclei and/or hydrogen traps. When the weld pool solidifies, hydrogen diffuses due to the concentration gradient. During this process hydrogen becomes trapped by "irreversible" and reversible traps. Traps are classified on the basis of their room temperature behavior: "irreversible" if they act purely as hydrogen sinks or reversible if they accept hydrogen under some circumstances, but act as a hydrogen source under others. The local hydrogen concentration at a potential crack site must reach a critical level for a given stress before cracking will initiate. Hydrogen traps influence the likelihood of cracking by reducing the amount of hydrogen available to diffuse to the critical cracking locations and by reducing the rate at which it can diffuse there [51,52]. Many traps have been identified and some of the traps which could be present in weld metal for 690MPa yield stress steel are listed in Table 2. The trap activation energy is a measure of the traps strength and will dictate the temperature at which hydrogen is released from the trap. Since even 'irreversible' traps release their hydrogen above a certain temperature, knowledge of the trap strength facilitates the optimum usage of hydrogen traps in the science based design of weld metal for maximum hydrogen induced cracking resistance.

Second phase particles can either increase or decrease the resistance to hydrogen induced cracking depending on the nature and distribution of the particle. A microstructure that contains a uniform distribution of particles, such as TiC particles [52], which trap the hydrogen but which are not potential crack nuclei themselves should give the greatest resistance to hydrogen induced cracking [51,53]. Conversely, large acutely shaped particles introduce large areas of incoherent interface into the structure, which trap large amounts of hydrogen at a location which is intrinsically more susceptible to cracking [51,53].

The effect of the oxide inclusion content on the resistance of an HSLA100 and an HY100 weld metal to hydrogen induced cracking has been investigated by varying the weld metal oxygen content [54]. The HY100 weld metal had sufficient inherent hardenability from its alloying content so that with the exception of an increased number of oxides, its microstructure was unchanged by an increased oxygen content and a special quenching technique was employed to ensure a similar consistency of microstructure and strength of the HSLA100 weld metal with increasing oxygen content. For both weld metals an increasing oxygen content reduced the resistance to hydrogen induced cracking and increased the amount of intergranular failure. The decreased hydrogen induced cracking resistance was believed to be due to the increased number of oxide inclusions on prior-austenite grain boundaries. The grain boundary inclusions were believed to promote grain boundary fracture by locally concentrating the hydrogen via a hydrogen trapping mechanism and by acting as a stress raiser. Because the inclusions were relatively small, those inclusions within the prior-austenite grains did not initiate hydrogen induced fracture and may have moderated the effect of the grain boundary oxides by reducing the hydrogen available to diffuse to the grain boundaries.

2.2 Ferrite Grain size

A finer grain size improves the resistance to cleavage initiation [55,56,57] through the influence of dislocation pile-up stresses on the fracture stress [58,59]. A finer grain size also improves the resistance to cleavage propagation. Since cleavage fracture in ferrite occurs along {100} planes, a fracture must change direction when it crosses a high angle boundary between adjacent grains of acicular ferrite. The smaller the grain size the more tortuous the fracture path and the greater the resistance to cleavage fracture propagation. [60].

Although the effect of grain size on the resistance to ductile fracture has not been investigated explicitly, a finer grain size will increase the strength of the weld metal, which in turn is believed to reduce the longitudinal strain needed to cause microvoids to coalesce [61].

Hydrogen induced cracking in weld metals for 690 MPa yield stress steels, occurs in multipass welds predominantly by an intergranular fracture along prior-austenite grain boundaries and is unlikely to be affected by a decrease in the ferrite grain size. However, a decreasing grain size was found to reduce the extent of intergranular hydrogen induced cracking in purified iron and iron-titanium alloys [62,63]. Improvements to hydrogen induced cracking resistance with a decreasing grain size may arise from an increase in the hydrogen-trap density associated with the increased number of grain boundaries per unit volume [32].

2.3 Grain boundary ferrite

The presence of grain boundary ferrite is considered to be deleterious to cleavage fracture initiation and propagation and has been implicated as a contributing factor in hydrogen induced intergranular fracture. Tweed and Knott showed that in a C-Mn weld containing acicular ferrite and grain boundary ferrite, strain will be localised in the grain boundary ferrite until the bulk specimen strain reaches approximately 7%. They suggested that this localisation of strain may promote cleavage initiation in non-metallic inclusions. They also noted a slight tendency for the cleavage fracture to preferentially follow the grain boundary ferrite [36]. However, it seems odd that a phase which "absorbs" 7% of the bulk specimen strain can be considered to be deleterious to toughness.

Grain boundary ferrite has also been associated with the initiation of hydrogen induced cracking [64,5,65,66]. Allen *et al.* suggest that cracks along prior-austenite grain boundaries initiate at grain boundary ferrite whose ductility is reduced by hydrogen, but no detailed evidence or description of a mechanism was offered [65]. It has also been suggested that carbon which is expelled from pro-eutectoid ferrite during the phase transformation from austenite, can segregate to the grain boundary and thereby make the boundary more susceptible to hydrogen embrittlement [66]. Carbon segregates strongly to grain boundaries and is one of the most powerful elements for increasing grain boundary strength [67,68], but, high levels of grain boundary carbon can weaken grain boundaries [69]. This may explain why investigations into the effect of grain boundary carbon on HIC have produced conflicting results. In one study [70] an increased partitioning of carbon to grain boundaries changed the mode of HIC from intergranular to transgranular, while in another [71], exactly the opposite effect was observed.

2.4 Summary

The influence of three microstructural features on ductile fracture, cleavage fracture and hydrogen induced cracking resistance is summarised in Table 2. Although each fracture mode is affected by each of the microstructural features listed, the physical processes by which each fracture mode is affected are different. For example, all three modes are affected by inclusions. However, cleavage initiation is affected most by the largest inclusions, ductile fracture is controlled by the volume fraction of inclusions and hydrogen induced cracking resistance is affected by the number of inclusions on prior-austenite grain boundaries and by the hydrogen trapping effects of inclusions. It is evident from Table 1, that hydrogen induced cracking resistance and toughness are indirectly related through their mutual dependence on microstructural features.

Table 2. The influence of microstructural features on ductile fracture, cleavage fracture and hydrogen induced cracking resistance.

Parameter	Intergranular HIC Resistance	Ductile Fracture Resistance	Cleavage Fracture Resistance
Inclusions	Number on prior-austenite grain boundaries[39] Hydrogen trapping effects	Volume fraction [38,60]	Largest inclusions (>1μm) [36,37]
Ferrite Grain size	Hydrogen trapping effects	Indirect relationship through dependence on strength	Inversely proportional to √d [24]
Grain boundary ferrite	Increase of grain boundary carbon [66]		Localised strain causes cracked inclusions [36]

3. CONCLUSIONS

The interrelationship between strength, toughness and hydrogen induced cracking resistance is complex and microstructure is the primary element from which each is derived. It is suggested that a careful examination of the effects of microstructural features on hydrogen induced cracking resistance will allow for a more scientifically rational development of welding consumables for maximum hydrogen induced cracking resistance rather than a reliance on empirical correlations.

4. REFERENCES

1 P.H.M.Hart: Weld. Inst. Res. Bull., 1978, 320

2 P.H.M.Hart: Weld. J., 1986, **65**, 14s

3 C.D.Lundin: 74th Annual Meeting of the American Welding Society: Hydrogen-Induced Cracking in High Strength Steel Weld Deposits (proc. conf.), Houston, Texas, April 1993

4 B.A. Graville: Weld. J., 1986, **24**, 190s

5 D. Wang and R.L. Apps: Intl. Conf. On Joining of Materials, 1991, Denmark, 438

6 R. J. Pargeter: Effects of arc energy, plate thickness and preheat on C-Mn steel weld metal hydrogen cracking, TWI Report 461/1992

7 S.R.Bala, L.Malik, S.Santyr and A.F.Crawley: Proc. of Weldability of Materials, ASM International, Detroit, Michigan, 8-12 Oct., 1990

8 Y. Ito, M. Nakanishi and Y.Komizo: The Sumitomo Search No. 22, 1979

9 T. Boniszewski and F. Watkinson: Metals and Materials, 1973, Feb., 90

10 P.H.M.Hart and E.Watkinson: Weld.J., 1975, **54**, 288s

11 C. Düren and K.Niederhoff: IIW Doc. IX-1550-88

12 W.M.Cain and A.R. Troiano: Petr. Eng., 1965, 78

13 C.Chen, A.W.Thompson and I.M.Bernstein: Metall. Trans., 1980, **11A**, 1723

14 D.A. Ryder, T. Grundy, and T.J.Davies: Proc. Intl. Conf. On Current Solutions to Hydrogen Problems in Steels, ASM, 1982, p. 272

15 I.M.Bernstein, A.W.Thompson, F.Gutierrez-Solana, L.Christodoulou: Proc. Intl. Conf. On Current Solutions to Hydrogen Problems in Steels, ASM, 1982, p. 259

16 R.B.Lazor and B.A. Graville: Can. Weld. Fabr., 1983, **74**, 21

17 M.McParlan and B.A.Graville: Weld. J., 1976, **55**, 95s

18 A.W. Thompson and I.M.Berstein: Intl. Conf. On the Effect of Hydrogen on the Behaviour of Materials, 1980, Met. Soc. AIME, 291

19 C.Zmudzinski, L.Bretin and M.Toitot: Hydrogen in Metals, 1977, **10**, paper 3A-6

20 J.D.Hobson and C. Sykes: J. Iron and Steel Inst., 1951, **169**, 209

21 I.M.Bernstein, A.W.Thompson, F.Gutierrez-Solana, L.Christodoulou: Proc. Intl. Conf. On Current Solutions to Hydrogen Problems in Steels, ASM, 1982, p. 259

22 B.F.Dixon and K. Häkansson: Weld. J., 1995, **74**, 122s

23 J.A. Davidson, P.J.Konkol and J.F.Sovak: WRC Bull. 345, 1989

24 A.M.Makara et al.: Avt. Svarka, 1971, **11**, 1

25 J.Mikula: Weld. Int., 1994, **8**, 761

26 N.Alam, H.Li.L.Chen, D.Dunne, B.Feng, I.Squires and F. Barbaro: "Fracture-Microstructure Relationship of Hydrogen Assisted Cracking in Steel Weldments", Conf. Proceedings, IMMA, July 1996

27 W.F.Savage, E.F.Nippes and E.I.Husa: Weld. J., 1982, **20**, 233s

28 J.L.Davidson: *The hydrogen-induced cracking resistance of consumables for use in the fabrication of the COLLINS class submarines,* DSTO Technical Report, DSTO-TR-0354

29 S-H. Hwang, B-H.Lee, H-L.Kim and J-Y.Lee: Proc. Intl. Conf. On Current Solutions to Hydrogen Problems in Steels, ASM, 1982, p. 286

30 C.D.Beachem; Metall. Trans., 1972, **3(2)**, 437

31 S.A.Gedeon and T.W.Eager: Weld. J., 1988, **67**, 213s

32 I.M. Bernstein and A.W. Thompson: Intl. Met. Rev., 1976, Review 212, p. 269

33 W.F.Savage, E.F.Nippes and E.I.Husa: Weld. J., 1982, **61**, 233s

34 N.P.Allen, W.P.Rees, B.E.Hopkins and H.R.Tipler: J. Iron St. Inst., 1953, **174**, 108

35 C.J.McMahon,Jr. and M.Cohen: Acta Metall., 1965, **13**, 591

36 J.H.Tweed and J.F.Knott: Acta Metall., 1987, **35**, 1401

37 R.K.Hughes and J.C.Ritter: in 4th Int. Conf. on Trends in Welding, 5-8 June 1995, Gatlinburg, Tenn.

38 L.L-J.Chin: Weld.J., 1969, **48**, 290s

39 R.H.Van Stone, T.B.Cox, J.R.Low,Jr. and J.A.Psioda: Int.Met.Rev.,1985, **30**, 157

40 R.K.Hughes: *Cleavage fracture of high strength weld metal*, PhD. thesis, Monash University, 1996

41 O.D.Gonzalez: Trans. TMS-AIME, 1969, **245**, 607

42 G.M.Pressouyre and I.M.Bernstein: Metall. Trans., 1978, **9A**, 1571

43 W.Y.Choo and J.Y.Lee: Met. Trans., 1982, **13A**, 135

44 I.M.Bernstein: Scr. Metall., 1974, **8**, 343

45 J.L.Lee and J.Y.Lee: Met. Sc., 1983, **17**, 426

46 R.Girbala: Trans. AIME, 1967, **239**, 1574

47 G.M.Pressouyre and I.M.Bernstein: Acta Metall., 1979, **27**, 89

48 K.Y.Lee, J.Y.Lee and D.R.Kim: Mat. Sci. Eng., 1984, **67**, 213

49 W.M.Robertson, and A.W.Thompson: Met. Trans., 1979, **11A**, 553

50 J.L.Lee and J.Y.Lee: Met. Trans., 1986, **17A**, 2183

51 G.M.Pressouyre: Acta Metall., 1980, **28**, 895

52 G.M. Pressouyre and I.M.Bernstein: Met. Trans., 1981, **12A**, 835

53 G.M. Pressouyre and I.M.Bernstein: Met. Trans., 1981, **12A**, 835

54 K.Shinozaki, X.Wang and T.H.North: Metall. Trans., 1990, **21A**, 1287

55 R.E.Dolby: Factors controlling weld toughness-the present position, Part 2- weld metals: Research Report 14/1976/M, TWI, Abington, May 1976

56 R.E.Dolby: in "Fracture '79" , (ed. G.G.Garrett and D.L. Marriott), 117-134, 1979, Oxford, Pergamon

57 E.A. Almond, D.A.Timbres and J.D. Embury: in "Fracture '1969", (ed. P.L.Platt), p. 253

58 A.H.Cotrell: Trans. Metall. Soc. AIME, 1958, p. 192

59 J.H.Tweed and J.F.Knott: Acta. Metall., 1987, **35**, 1401

60 D.J. Abson and R.J.Pargeter: Int. Met. Rev., 1986, **31**, 141

61 J.F.Knott: in The effect of second-phase particles on the mechanical properties of steel, Conf. Proc., Iron and Steel Inst., March 1971, p. 44

62 I.M.Bernstein and B.B.Rath: Metall. Trans., 1973, **4**, 1545

63 G.M.Pressouyre and I.M.Berstein: ASM IMD Abstract Bulletin, 1973, Metals Congress, Detroit

64 F. Watkinson: Weld. J., 1969, **48**, 417s

65 D.J.Allen, B. Chew and P.Harris: Weld. J., 1982, **61**, 212s

66 Symposium on " Welding metallurgy of TMCP steel", (ed. F. Matsuda), 1985, Tokyo, Japan Weld. Eng. Soc., 35-42

67 S.F. Pugh: An introduction to grain boundary fracture in metals, 1991, Institute of Metals, p. 36

68 H. Erhart, H.J. Grabke: Metal Sci., 1981, **15**, 401

69 X. Chen et al: Acta Met., 1990, **38**, (9), 1719

70 I.M. Bernstein and A.W. Thompson: Intl. Met. Rev., 1976, Review 212, p. 269

71 I.M.Bernstein and B.B.Rath: Metall. Trans., 1973, **4**, 1545

Welding Induced Hydrogen In US Navy Structural Steels

By

R. Wong
J. Blackburn
J. DeLoach
R. DeNale

Carderock Division
Naval Surface Warfare Center
Bethesda, MD, USA

1.0 INTRODUCTION

A significant portion of the cost of welding high strength steel structures is in the measures taken to avoid the detrimental effects of hydrogen. The costs include labor and energy used to apply preheat and postweld thermal soaks and the decreased productivity that results from maintaining stringent procedural controls.

Historically, welding controls used to prevent hydrogen cracking (e.g., preheating and post weld soaking) have been dictated by the susceptibility of the heat-affected-zone (HAZ). Advances in steel metallurgy and plate processing have led to significant improvements in the hydrogen-cracking resistance of steel heat-affected-zones. In many applications, these advances, along with the trend toward higher strength steel systems, have shifted hydrogen cracking problems from the HAZ into the weld metal. The nomograms, equations, and algorithms used to estimate safe (crack-free) welding conditions are based on cracking tests and carbon equivalent equations designed to assess the HAZ. Applying these methods to newer steel systems can lead to excessive or inadequate preheat/interpass temperatures and postweld thermal soaks. Excessive controls reduce productivity and increase fabrication costs. Inadequate controls can lead to cracking, increased rework, and service failures. Improved methods are needed to adequately assess the hydrogen cracking resistance of newer high strength steels and associated weld metals.

In response to this need the U.S. Navy is developing improved methods for quantifying the effects of hydrogen on cracking of high strength steel weld metals. The overarching goal of the research is to reduce both the cost of hydrogen management and the risk of hydrogen-related problems. Specific technical objectives are as follows:

- To model the relationship between composition, hydrogen level, and welding conditions on weld metal hydrogen cracking.
- To develop improved tests for assessing weld metal hydrogen cracking.
- To develop a method for estimating weld metal diffusible hydrogen content using in-process monitoring of hydrogen emissions from the welding arc.

This paper discusses three ongoing Naval Surface Warfare Center efforts designed to address these objectives. The first task discussed is developing a sensor to monitor hydrogen emissions in the welding arc. The emphasis of the effort is in using the sensor to predict and estimate weld metal diffusible hydrogen levels. The second task is developing a quantitative understanding of hydrogen transport through a solid state system. The final study is quantifying the influence of hydrogen level and chemical composition on hydrogen cracking susceptibility. These developments will provide the capability to (1) monitor and predict weld metal diffusible hydrogen levels during welding and (2) determine critical levels of diffusible hydrogen as a function of material composition and welding conditions. Such capabilities could provide a powerful, on-line nondestructive means for ensuring that safe (crack-free) welding conditions are maintained. In addition, a quantitative relationship between composition and weld metal hydrogen cracking will be an invaluable design tool in ongoing U.S. Navy efforts to develop preheat-free filler metals.

1.1 ARC HYDROGEN SENSOR

An arc hydrogen sensor is currently under development for in-process monitoring of hydrogen during the welding of high strength steels. The sensor is a spectrometer capable of detecting light within the visible wavelength range. The sensor consists of a spectrometer, containing a 512 element linear photodiode array, and a fiber optic bundle. The fiber optic bundle contains a spherical sapphire lens which collects light from the entire welding arc area rather than line of sight collection. The light travels through the fiber optic bundle to the spectrometer where a 70 nm bandwidth is spread over the photodiode array. The bandwidth contains the peaks for hydrogen (656.2 nm) and argon (675.2 nm). The ratio of the hydrogen peak to the argon peak is used to monitor the level of hydrogen within the welding arc, see equation below. This ratio has been shown to be an effective means for monitoring the hydrogen in an argon-dominated plasma. [1,2,3]

$$I_{rel} = (I_H - I_B)/(I_{Ar} - I_B)$$

where,

I_{rel} = relative intensity,
I_H = intensity of the hydrogen line
I_B = background intensity level, and
I_{Ar} = intensity of the argon line.

The purpose of developing such a sensor is to provide the ability to monitor and predict the weld metal diffusible hydrogen levels. The approach is two-fold. The first approach involves correlating the relative intensity to the AWS A4.3 diffusible hydrogen results. The utilization of this approach would predict diffusible hydrogen test results and allow in-process monitoring during fabrication for fluctuations in hydrogen levels. The second approach is a more versatile one which involves modelling weld metal diffusible hydrogen content and distribution using the amount of hydrogen present in the welding arc as input. The amount of hydrogen present in the welding arc could be extracted from the correlation between the relative intensity and the amount of hydrogen present in the shielding gas. This approach will provide a tool which could not only predict diffusible hydrogen results, but predict hydrogen concentration and distribution in the case of complex welding situations.

Figure 1 shows typical spectra collected from a welding arc with various amounts of hydrogen added to the shielding gas. As the amount of hydrogen in the shielding gas is varied, the hydrogen peaks become larger while the argon peaks remain relatively constant.

Figures 2 and 3 display the relationship between relative intensity and the results of the diffusible hydrogen test for a series of experiments involving hydrogen and moisture additions, and variations in welding parameters. In the development of these relationships, hydrogen gas was added to a standard 98% Ar - 2% O_2 in amounts up to 1% , the dew point of the shielding gas was varied to 1°F, and the welding parameters were varied. The resulting spectra and diffusible hydrogen results were measured.

The data representing a travel speed of 12 ipm shows that the relationship between relative intensity and weld metal diffusible hydrogen is linear regardless of the source of hydrogen. An R^2 analysis indicates a fit of 0.67, indicating some scatter in the data. However, this data set represents a large range in welding electrical parameters. Further isolation of electrical parameters is performed in Figure 3. This isolation of data indicates an improvement in the relationships. This also suggests that changing amperage and voltage affect the relationship between relative intensity and weld metal diffusible hydrogen.

Figure 1. Spectra showing the hydrogen and argon peaks for various levels of shielding gas hydrogen.

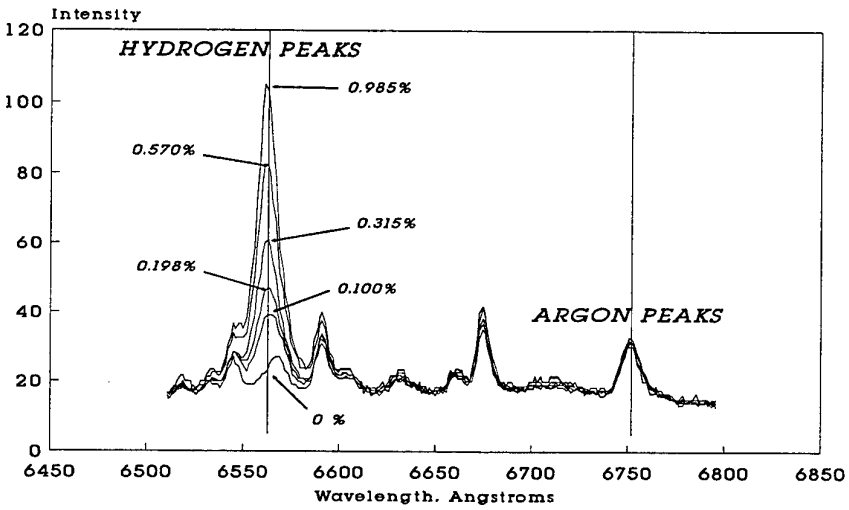

Figure 2 also shows the effect of the welding travel speed. The data for travel speeds of 30 and 55 ipm indicate slightly higher slope values than for 12 ipm. This suggests that other factors relative to the diffusible hydrogen test are acting to influence the slope value.

All of the factors influencing the relationship between relative intensity and weld metal diffusible hydrogen content are not fully understood at this time. However, these factors may interact in a complex manner which may make it difficult to handle variations in welding scenarios. Therefore, the relationships given in Figure 2 do not apply to other sets of welding conditions. However, for a given set of welding parameters, the use of relative intensity to predict weld metal diffusible hydrogen results or fluctuations in results is feasible using this approach.

Due to the complex interactions between welding parameters, plasma characteristics, and diffusible hydrogen results, a second approach is being pursued. The relative intensity data is being coupled with a 3-D finite element modelling effort. In this case, the relative intensity data is used only to identify the concentration of hydrogen in the plasma. This can be accomplished through a relationship such as the one shown in Figure 4.

Figure 2. The relationship between the H/Ar relative intensity ratio and the weld metal diffusible hydrogen content.

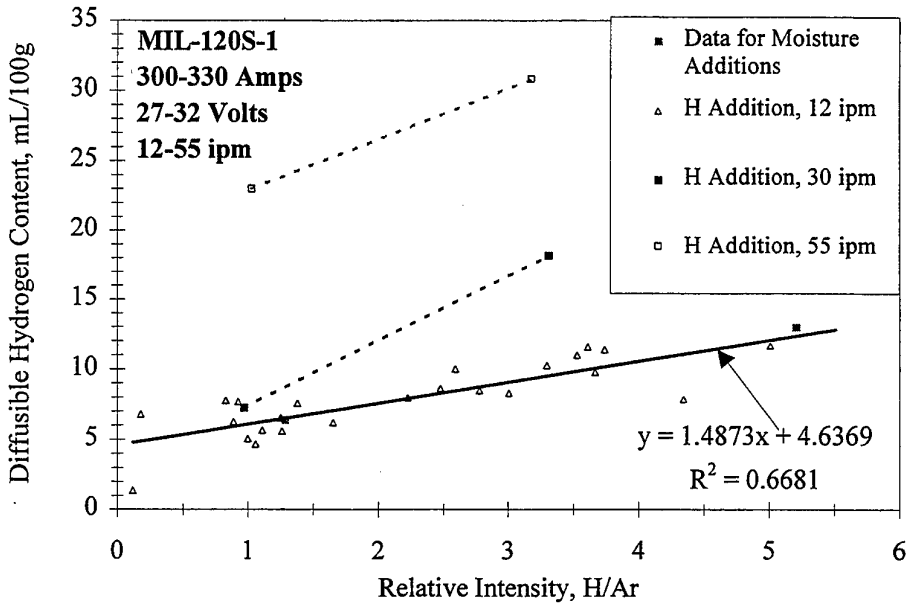

Figure 3. The effect of electrical parameters on the relationship between relative intensity and weld metal diffusible hydrogen.

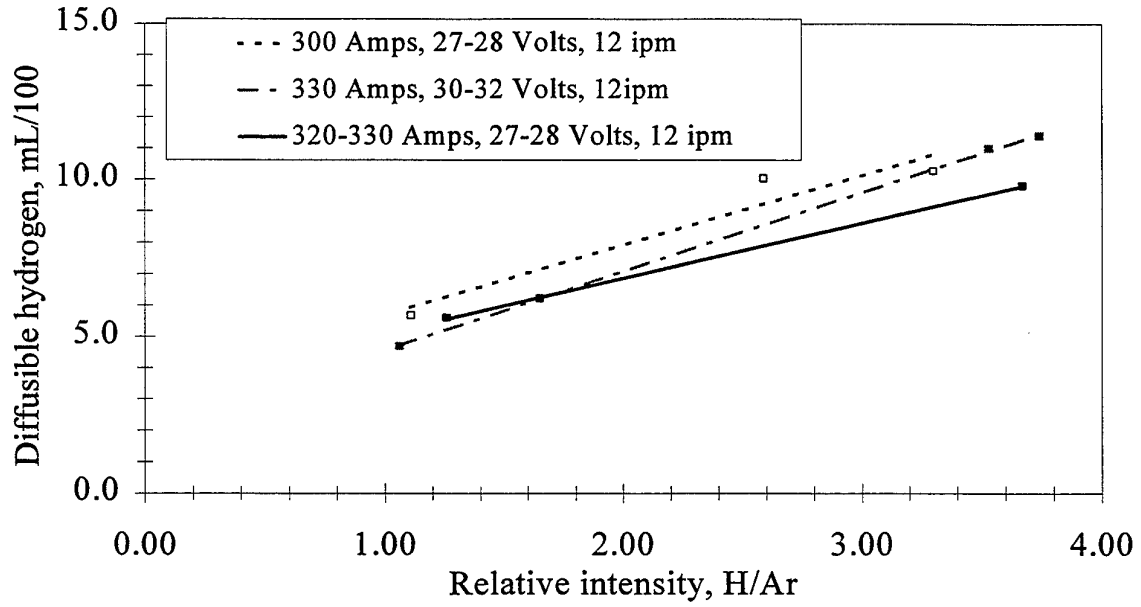

Figure 4. The effect of hydrogen additions on the relative intensity values (H/Ar).

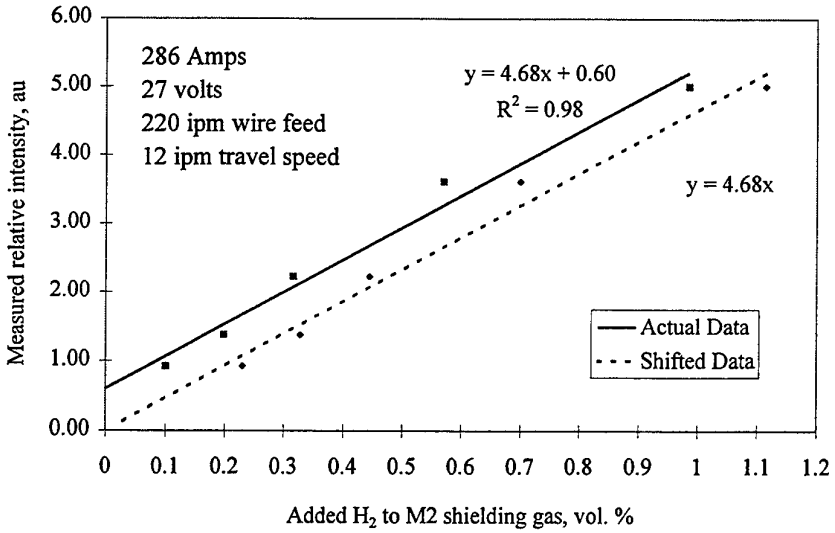

This linear plot shows the relationship between the amount of added hyrogen to the shielding gas and the measured relative intensity value. Theoretically, the relative intensity should be zero when there is no hydrogen present in the welding arc. However, the "actual data" has a non-zero intercept. However, the total amount of hydrogen is actually the sum of the hydrogen in the shielding gas and hydrogen present from other sources (i.e. wire, atmosphere, moisture, etc.). Therefore, the measured relative intensity value at zero added hydrogen indicates the presence of hydrogen from other sources. Using the intercept value of 0.60 and assuming linearity at small values of added hydrogen and relative intensity, the hydrogen present due to other sources is calculated as 0.13 vol. %. Additions of 0.13% to each x-value would then result in a relationship which passes through zero as shown by "shifted data". Just as the relationship in Figure 1 is sensitive to welding parameters, so is the relationship between added hydrogen and relative intensity. However, in this case, diffusible hydrogen testing is not necessary to establish the relationship. Currently, this relationship is being determined for various welding parameters with the intent of establishing a relationship between welding parameters and the slope.

Once the relationship between added hydrogen and relative intensity is established, the relative intensity can be measured during welding,and the amount of hydrogen determined. This hydrogen concentration is assumed to be the plasma hydrogen concentration. This plasma hydrogen concentration is then utilized in a 3-D model being developed at the Pennsylvania State University. This model simulates hydrogen transport from the high temperature plasma, through the molten metal, and into the solidified weld metal. Initial results are shown in Figure 5. There is reasonable agreement between the model and experimental results. However, the model development is in it's initial stages and many details are still under development.

Figure 5. Comparison of experimental and model results.

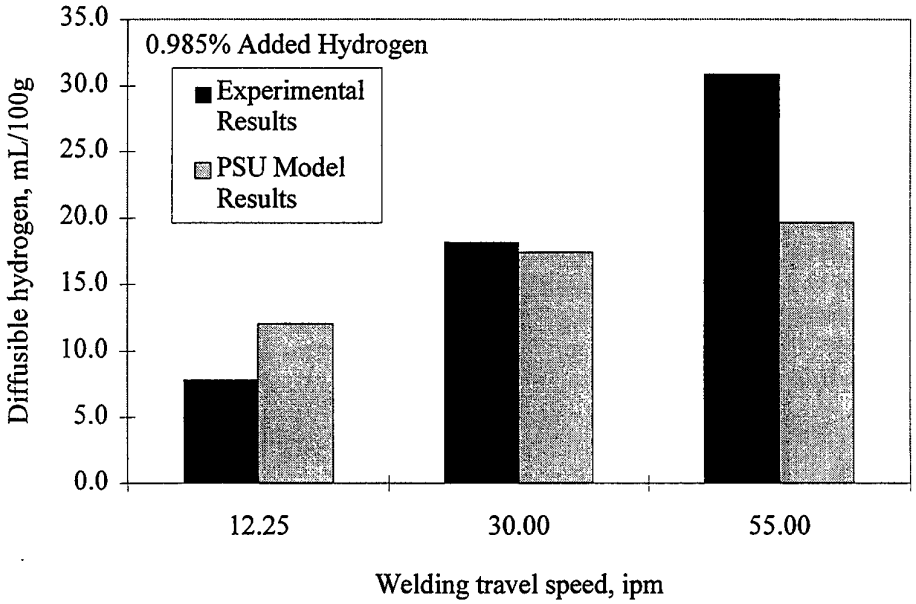

Results of this work have indicated that spectral analysis of hydrogen in the welding arc is a viable means of predicting hydrogen in the weld metal. Results indicate that the use of relative intensity to predict weldmetal diffusible hydrogen results or fluctuations in results is feasible. The combination of a spectragraphic sensor and 3-D finite element modelling show promising results toward being able to predict weld metal diffusible hydrogen test results. The future of this method lies in the development of a similar system which is capable of predicting weld metal hydrogen concentrations at any time during more complex single-pass and multi-pass welding situations.

1.2 HYDROGEN TRANSPORT

The objective of this work is to determine the diffusion characteristics of hydrogen in HSLA-100 steel and to develop the ability to control the hydrogen concentration in steel as a function of distance. Consequently, it will be possible to modify hydrogen concentration ahead of a crack tip. This will be a useful tool for studying the interaction of hydrogen and a propagating hydrogen crack.

Modified Devanathan-Stachurski (D-S)[4] permeation experiments are being performed to characterize the transport of hydrogen. The bi-electrode D-S cell is shown in Figure 6. During a standard permeation experiment the input side of the bi-electrode is cathodically charged producing hydrogen on the input surface of the specimen. Hydrogen is adsorped into the specimen and diffuses to the output side. On the output side of the cell, the hydrogen is oxidized into water. The current of the oxidation reaction is a direct measurement of the hydrogen permeating through the membrane. The reactions occurring in the cell are given by:

Input side: $H_2O \rightarrow OH^- + H^+$ (cathodic polarization), and

Output side $H^+ + OH^- \rightarrow H_2O$ (hydrogen oxidation)

In this work, a modification to a simple permeation experiment was used. It uses a sinusoidally modulated current to cathodically charge hydrogen on the input side of the D-S cell. The current is modulated by superimposing an alternating charging current on a constant mean current. This permits separation of the adsorption and diffusion processes. The effect of using a modulated charging current on hydrogen permeation is schematically illustrated in Figure 7. The phase shift between the input and output current signals is dependent on the diffusivity of hydrogen through the specimen. The relationship between the independent variables and the phase shift (Φ) is given by:

$$\Phi = \tan^{-1}\left\{\frac{(\tan\alpha - \tanh\alpha)}{(\tan\alpha + \tanh\alpha)}\right\}$$

where: $\alpha = (\pi \cdot f / D)^{1/2} \cdot t$

f = frequency

t = thickness of specimen

D = diffusion coefficient

The concentration of hydrogen ($C_{x,t}$) at any point x within the specimen consists of a mean component ($Co_{x,t}$) and an alternating component ($Calt_{x,t}$), as described below.

$$(Calt_{x,t}) = A \cdot \exp(-x / x_o) \cdot \sin\left\{\left(\frac{\omega \cdot t}{\lambda}\right) - \left(\frac{\pi}{4}\right)\right\}$$

where : $x_{o=} = \lambda / 2\pi$

$\lambda = 2\pi(D/\omega)^{1/2}$

$A = \dfrac{c_s}{2\pi mk} \cdot \dfrac{1}{(D\omega)^{1/2}}$

$\omega = 2\pi f$

c_s = concentration at the input surface

The amplitude of the alternating portion of the concentration profile is an exponentially damped wave with a velocity of $(D\omega)^{1/2}$. Consequently, it should be possible to modify the concentration of hydrogen below a surface by modification of input parameters such as amplitude and frequency.

Initial results of the output current from a modulated charging current are shown in Figure 8. Figure 8(a) is an example of the output signal as a result of a single 30 second input pulse. The signal is a result of hydrogen permeating the membrane to the oxidation side of the cell. Figure 8(b) is an example of the output signal as a result of several pulses created with various frequencies. Increasing frequency resulted in increased damping of the output signal as expected from the governing equations. This indicates that the diffusion process can be seperated from the

adsorption process at high frequencies and that it will be possible to vary hydrogen concentration as a function of distance.

Figure 6. Devanathan-Starchurski bi-electrode cell.

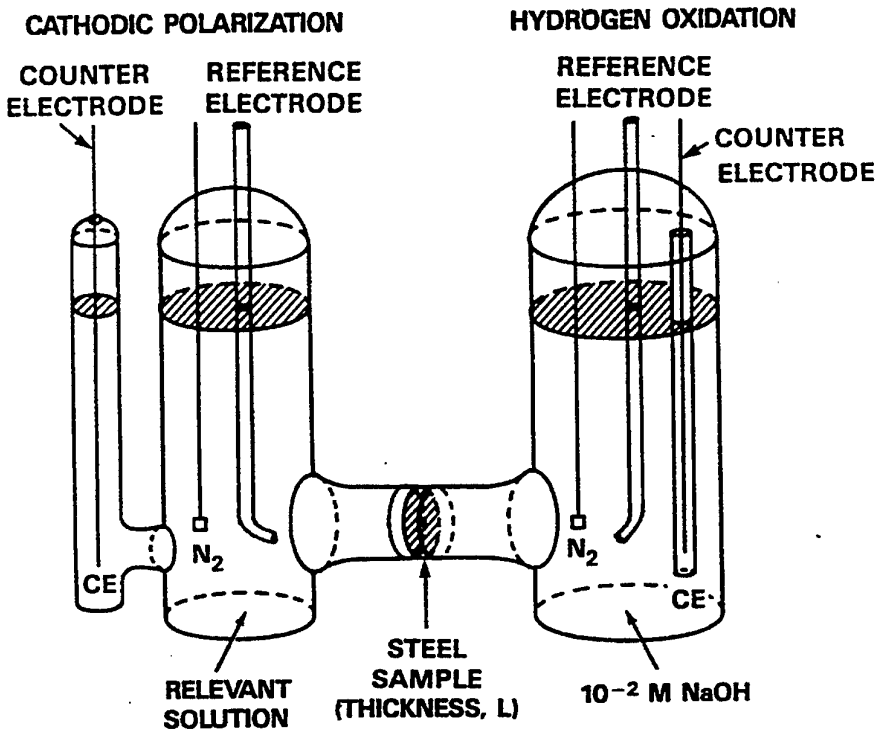

Figure 7. Schematic illustration of the effect of a modulated charging current on permeation of hydrogen through a membrane.

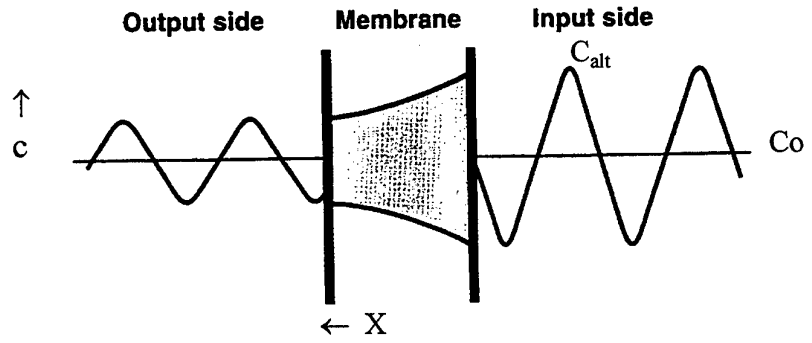

Figure 8. Examples of the output current from a hydrogen permeation experiment using a single pulse and using a modulated charging current.

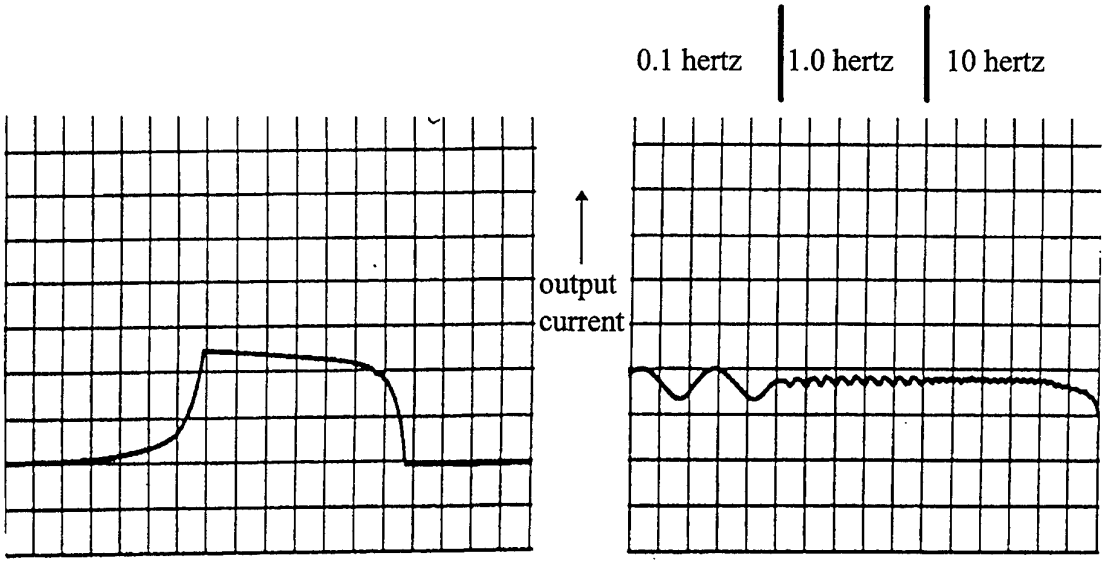

← time (strip chart feed direction)

(a) 30 second pulse (b) modulated charging current

1.3 WELDABILITY METHODOLOGY DEVELOPMENT

The objective of the weldability program is to develop a methodology for determining the hydrogen cracking resistance of high strength steel weldments. The methodology will then be used to identify safe welding procedures and design more weldable materials. A summary of the base plate material used is provided in table 1. Solid wire gas metal arc welding consumables were employed as the filler materials. The welding consumables included MIL-E -120S, MIL-E-100S, and a MIL-E-70S products.

The methodology employs a crack prediction model based on determination of a minimum critical cooling time to cool to 100° C. ($t_{100,\,min}$) [5] . This parameter can be used to evaluate the effect of changes in chemistry and hydrogen content on changes in t_{100} required to avoid cracking. This will allow welding procedure and material development to avoid hydrogen cracking.

The t_{100} is a measure of hydrogen diffusion out of the weld. Hydrogen cracking may occur if the particular welding parameters (such as preheat temperature and heat input) result in a t_{100} that is less than $t_{100,\,min}$. Increasing welding preheat temperature increases t_{100} resulting in more hydrogen removal. The removal of hydrogen reduces the likelihood of hydrogen cracking.

Figure 9. Schematic Illustration of the crack prediction model

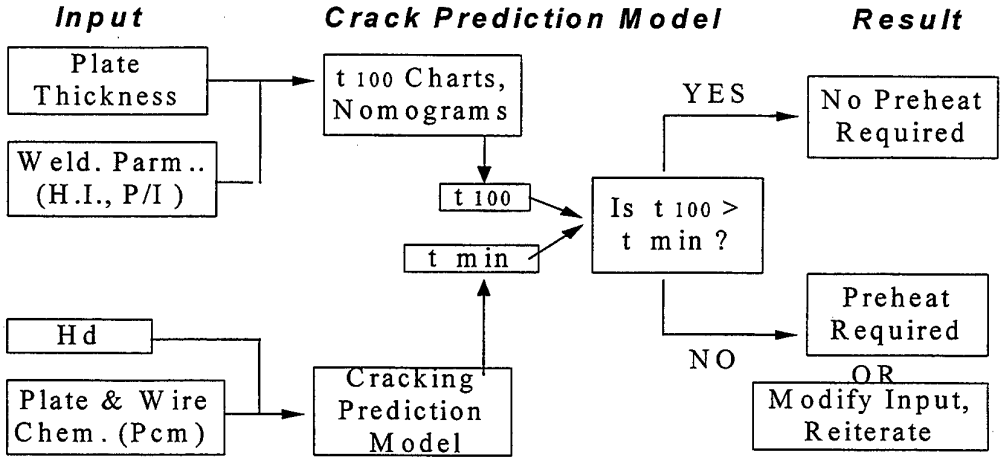

Table 1. Base plate compositions

	C	Mn	Si	P	S	Ni	Mo	Cr	V	Cu	CEN
HY-100	0.053	0.25	0.20	0.005	0.010	2.60	0.26	1.26	0.007	0.12	0.59
HSLA 100[1]	0.037	0.78	0.27	0.013	0.002	3.17	0.62	0.56	0.006	1.36	0.36
HSLA 100[2]	0.056	0.76	0.23	0.005	0.010	3.41	0.59	0.63	0.002	1.51	0.41
HSLA-80	0.06	0.6	0.3	0.005.	0.003	0.87	0.22	0.75	0.002	1.15	0.296
HSLA-65	0.08	1.39	0.22	.005	0.003	0.35	0.06	0.16	0.002	0.25	0.27

1. 19 mm plate used in WIC tests
2. 25 mm plate used in cruciform tests
3. CEN is a Yurioka's carbon equivalent number [5]

The primary weldability tests used in this study included the Welding Institute of Canada's (WIC) single pass high restraint cracking test and multipass cruciform tests. Some gapped bead on plate and implant tests were also performed on some of the materials. The effect of composition was evaluated by using different plate and wire combinations. The various changes in alloying is handled by calculation on a carbon equivalent number. In this study Yurioka's CEN carbon equivalent number [5] was used to assess changes in hardenability (chemistry). Diffusible hydrogen was varied through hydrogen additions to the M-2 shielding gas. The diffusible hydrogen content was measured by gas chromatography in accordance this AWS A4.3 [6].

Cracking versus no cracking regions were identified and empirical equation of the line separating the two regions are derived. The two lines shown in Figures 10 and 11 represent cracking versus no cracking boundary lines.

Figure 10. The effect of CEN and t_{100} on hydrogen cracking.

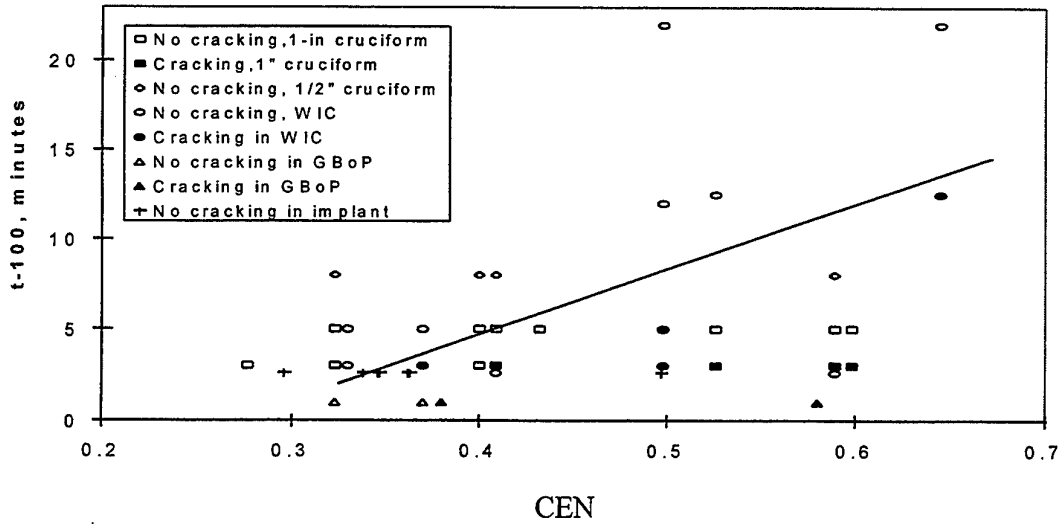

Figure 11. The effect of CEN and diffusible hydrogen on hydrogen cracking

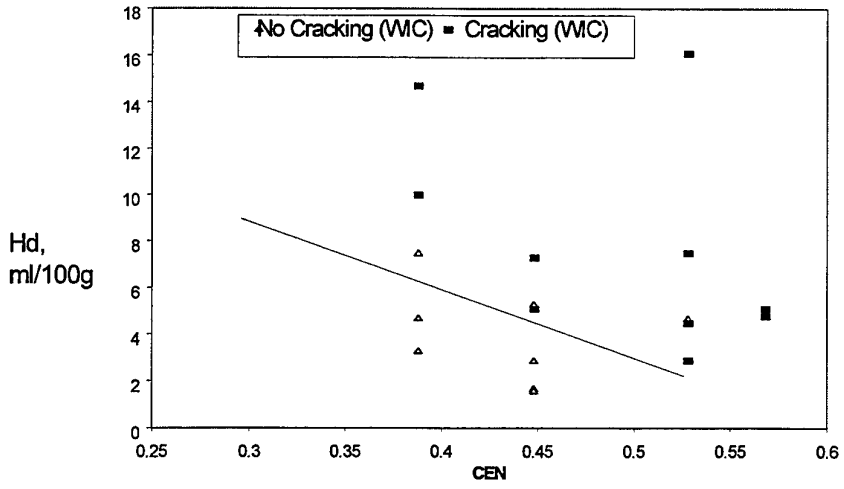

When the equation of these two lines are combined the resulting equation represents a hydrogen cracking response surface of $t_{100,min}$ which is a function of the chemistry of the materials (CEN) and the diffusible hydrogen content (Hd). The resulting relationship (Figures 12 and 13) is given by

$$t_{100,\,min} = 34.1(CEN) + (Hd-5)/3.5 - 9.1$$

Figure 12. Hydrogen cracking response surface of $t_{100,\ min}$ as a function of CEN and diffusible hydrogen (Hd), orthagonal view.

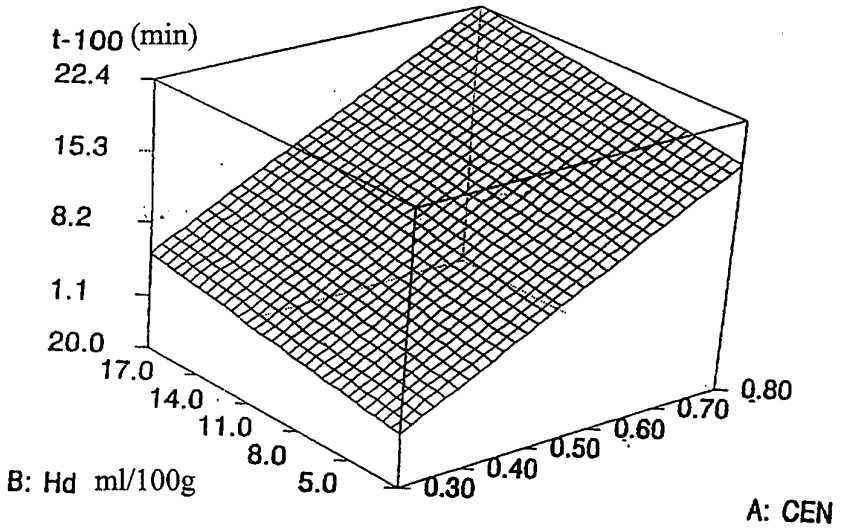

Figure 13. Iso-$t_{100,\ min}$ contours of the hydrogen cracking response surface.

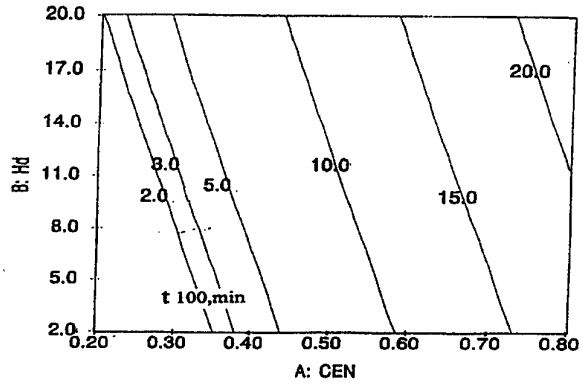

$$t_{\text{100-min}} = 34.1\ (\text{CEN}) + (\text{Hd} - 5)/\ 3.5\ - 9.1$$

The results of this analysis indicate that some high strength steels may need little or no preheat. For example if a line is drawn at CEN = 0.4, representing an HSLA 100 type of material, and a line is drawn at Hd = 8 ml/100g the $t_{100,\ min}$ value is approximately 5 minutes. This is a typical cooling time for a 19 mm thick plate welded without preheat using typical welding conditions. Consequently one should be able to weld 19 mm HSLA-100 as long as the diffusible hydrogen is well below 8 ml/100g. The results in Figure 13 also show that in order to weld thick section materials that will have $t_{100,}$ of two minutes or lower without preheat one will need to require both a low CEN and low Hd.

1.4 SUMMARY

It was demonstrated that spectral analysis of hydrogen in the welding arc is a viable means of predicting hydrogen in the weld metal. Results indicate that the use of relative intensity to predict weldmetal diffusible hydrogen results or fluctuations in results is feasible. The combination of a spectragraphic sensor and 3-D finite element modelling show promising results toward being able to predict weld metal diffusible hydrogen test results. Initial cathodic charging experiments showed that the diffusion process can be seperated from the adsorption process at high input frequencies, and that it will be possible to vary hydrogen concentration as a function of distance. Further development of this technique will allow controlled manipulation of hydrogen concentration in hydrogen cracking experiments. A weldability methodology was described which is under development. The methodology was developed using single-bead and multi-bead cracking tests. The methodology considers chemistry and diffusible hydrogen content as inputs and predicts a cooling time to 100°C to avoid hydrogen cracking. This cooling time can then be translated to appropriate welding conditions. The advancement of these technologies will provide a means for ensuring that safe (crack-free) welding conditions are maintained through in-process monitoring and the development of preheat-free filler metals.

1.5 ACKNOWLEDGMENTS

The authors gratefully acknowledge the Office of Naval Research and the Ship Structure Committee for sponsoring this research.

REFERENCES

1. White, D.R., and W.G. Chionis, "In-Process Prediction of the Diffusible Hydrogen Content of Gas Metal Arc Welds," Hydrogen Embrittlement: Prevention and Control," American Society for Testing and Materials STP 962, ISBN 0-8031-0959-8,(1988)

2. Andalib, A. L. Zhang, and D.G. Howden, "Evaluation of the Capabilities of the Weld Quality Monitor," by The Ohio State University to David W. Taylor Naval Ship Research and Development Center, Contract #N6153387M1892, Id# 50040106, (Sept. 1987)

3. Blackmon, E.R., and F.W. Kearney, "A Real Time Approach to Quality Control in Welding," Welding Journal 62(8), pp. 37-39, August 1983

4. Devanathan, M.A., and Z. Stachurski, Proceeding of the Royal Society, London, Vol. A270, 1962

5. Yurioka, N., H. Suzuki, S. Oshita, and S. Saito,"Determination of Necessary Preheating Temperature in Steel Welding," *Welding Research Supplement*, pps 147s-153s, June 1983

6. AWS A4.3-93, "Standard Methods for Determination of the Diffusible Hydrogen Content of Martensitic, Bainitic, and Ferritic Weld Metal Produced by Arc Welding," The American Welding Society, 1993.

Weldment Cold Cracking -The Effect of Hydrogen and Other Factors

N. Alam*, D. Dunne*, I. Squires**, F. Barbaro** and B.Feng**

*Department of Materials Engineering, University of Wollongong, Australia.
**BHP-Flat Products Division, Wollongong, Australia.

All authors are research members of the CRC for Materials Welding and Joining.

ABSTRACT

Cold cracking in steel weldments is caused by the presence of hydrogen in a susceptible microstructure in association with a high stress concentration at sites such as sharp undercuts or root angles. As the strength of the weld increases the hydrogen sensitivity of cold cracking also increases. In laboratory tests used to assess cold cracking susceptibility the test method itself and the joint design can influence the result which sometimes can be very conservative. Two test methods were used in the present work to study the weldability of two different types of steels: 9-10 mm thick plates of the pipeline grades X70 and X80; and 20-36 mm thick HSLA80 and X80 plate steels. For the pipeline steels high hydrogen cellulosic electrodes were used and for the plate steels welding tests were conducted with medium hydrogen strength matching electrodes.

An attempt was made to elucidate the cause of cold cracking of weldments. The study revealed that for a high heat input the joint design plays a significant role in controlling the crack susceptibility. However, for low heat input welds, microstructure becomes a more dominant influence on cracking. Studies of fracture morphology revealed that for high hydrogen welds crack initiation occurred by microvoid coalescence and for the medium hydrogen electrodes crack initiation occurred by quasi-cleavage or intergranular cracking.

1. INTRODUCTION

Cold cracking in steel weldments is considered to be a limiting factor for high productivity in the structural industry. One of the main conditions for cold cracking to occur is the presence of hydrogen in a susceptible microstructure [1]. In conventional C-Mn structural steels the presence of hydrogen has been proved to be very critical because the relatively high carbon contents promote the formation of martensite in the heat affected zone (HAZ) and diluted weld metal. The presence of hydrogen in the structure reduces the cohesive strength [2] and under restraint conditions the residual stress and restraint stress are relaxed by opening cracks at stress concentrators. The reduction of hydrogen in the weld consumables by drying or baking is essential to avoid cold cracking in such weldments. However, over the last decade the quality and weldability of steels have been markedly improved by lowering the carbon and adding microalloying elements. As a result HAZ microstructures are less susceptible to the effects of hydrogen. This improvement in steel quality has focused attention on the weld metal and other factors which influence weld metal cracking. These include the weld consumable, the joint design, the weld bead shape and location and restraint intensity of the joint. This paper reports the results of weld metal cracking tests conducted using two different tests: the rigid restraint cracking (RRC) and Tekken cracking tests, for various joint conditions with the aim to clarify some of the aspects which contribute to cracking in weldments of low carbon steels.

2. EXPERIMENTAL

The RRC and Tekken cracking tests were used to investigate cracking in weldments of X70, X80 and HSLA80 steels deposited with high hydrogen cellulosic electrodes and medium hydrogen electrodes. The chemical compositions of the steels and the consumables are given Table 1.

The RRC test configuration is shown in Fig. 1 and this test program was conducted by BHP-FPD. The pipeline grade steels X70 and X80, 10 mm and 9 mm thick respectively, were used with three cellulosic electrodes: E6010, E8010G and E9010. For X70 steel the E6010 and E8010G cellulosic electrodes were used and for X80 all three electrodes were used. In testing of the X70 steel both symmetric Y and single bevel joints were used and the heat input was varied from 0.3 to 2.6 kJ/mm. For the X80 steel only a symmetric Y joint with a 2 mm root face was

used and the heat input was varied from 0.5 to 0.8 kJ/mm to deposit a root pass weld. During the test the crack initiation time was monitored using strain gauges attached to the test rig.

In the Tekken cracking test an oblique Y joint was used in which the root was located at the mid-thickness of the plate, see Fig. 2. The HSLA80, plate 25 and 36 mm thick, and 20 mm thick X80 plate were used for investigating weldment cracking. For HSLA80 plate the strength matching electrodes, E8018C3 and E8018B2, containing a medium quantity of hydrogen, were deposited at different heat inputs ranging from 1 to 2.5 kJ/mm; and for X80 only the E8018B2 electrode was deposited for heat inputs from 0.7 to 2 kJ/mm.

3. RESULTS AND DISCUSSION

After weld deposition the test blocks were left for 24 hours for the RRC test and 48 hours for the Tekken test and then the test blocks were sectioned transverse to the welding direction into ten pieces. All sections were polished for metallographic examination. Some sections were fractured to study the fracture morphology of the cold cracks.

3.1 Effect of Joint Design and Restraint Intensity

3.1.1 RRC Tests

The joint design for weld crack testing was found to be a very important factor in assessing the cracking susceptibility of weldments. The joint design was varied for X70 steel, with the influence being most pronounced at high heat input. The incidence of cracking in the X70 steel weld with E6010 and E8010G electrodes is shown in Figs. 3 and 4. It is evident from Fig. 3 that at a heat input of 0.5 kJ/mm both tests exhibited cracking. The microstructures resulting from this low heat input, combined with stress concentration at the weld root appeared to be responsible for cracking. However, when the heat input was increased to 1.9 kJ/mm the cracking was found to be associated with joint geometry. The weld deposited using a single bevel joint was more susceptible to cracking than symmetric Y configuration, even at a heat input of 2.4 kJ/mm.

For X70 welds with the E8010G electrode the heat input was varied from 1.6 to 2.6 kJ/mm. It is evident from Fig. 4 that the symmetric Y joint did not generate any cracking for the heat input used in the program. However, the single bevel joint for this electrode was also found to induce conditions suitable for cracking at all heat inputs.

Although the X70 steel strip was only 10 mm thick, due to the design of test rig the restraint intensity, R_f for the RRC test is estimated to be 64 GPa [3]. This restraint should lead to a general stress level in the weld beyond the yield stress. In the presence of stress concentrators at the root of incompletely penetrated steel weld the general stress level would be expected to exceed the yield stress.

The incidence of cracking in RRC tests using a single bevel joint for X70 steel welds may have been the result of a high stress concentration factor for the single bevel joint [4]. Stress concentration factors for some joints are given in Table 2. The local stress acting at a site where a crack can initiate, rather than the mean stress acting on a weld, is indicative of the incidence of cracking [5]. The local stress is a product of the stress concentration factor and mean stress which is predicted from the restraint intensity. The restraint intensity for the RRC test has been expressed [6] by

$$R_f = \frac{Eh}{l} \quad \text{.....(1)}$$

where E is the modulus of elasticity, h the thickness of the plate and l the length of the weld bead.

For given values of h and l, the local stress in the weld is a function of the stress concentration factor. The high local stress concentration associated with a single bevel joint appeared to be the reason for cracking found in the weld metal at high heat input.

The cracking in the weld metal of X80 steel strip from the RRC test initiated from the root of a *wagon track* at which the local stress was estimated to well beyond yield stress. Although the stress concentration factor for the symmetric Y joint used for the RRC testing of X80 was relatively low, (Table 2), the restraint intensity due to the design of the test rig was already high enough (64 GPa) to cause cracking in the weld. In addition, the alloying effect from Mo and the use of a low heat input resulted in a microstructure which was highly susceptible to cracking (see Section 3.3).

3.1.2 Tekken Tests

In the Tekken cracking tests of 25 mm HSLA80 plate with E8018C3 electrode no cracking was observed in the weld at a heat input of 1.0 kJ/mm. However, when the thickness of the plate was increased to 36 mm, the weld showed cracking at a heat input of 1.5 kJ/mm, which was equivalent to 1 kJ/mm heat input on 25 mm thick plate in terms of to cooling rate. As the local stress is a product of stress concentration factor and restraint stress, the greater thickness of HSLA80 plate resulted in higher restraint intensity which, for a particular joint and weld bead size, increases the local stress. In the Tekken cracking test no equation has been formulated to determine the magnitude of restraint intensity. If Eq. (1) is used the value of R_f for 25 mm plate is estimated to about 50 GPa. The equation for R_f (in MPa) used in the WIC restraint cracking test for a 50 mm long weld bead is [7]

$$R_f = 1600h \quad \text{..... (2)}$$

where h is the thickness of the plate in mm. For 25 mm plate R_f is estimated to be 40 GPa. Whatever equations are used for the Tekken cracking test, the 36 mm plate will induce higher restraint intensity than the 25 mm thick plate. Although the stress concentration factor of the joint used in the Tekken cracking test is slightly lower than that for a single bevel joint (see Table 2) the increased R_f resulting from the greater plate thickness is likely to have generated a higher local stress which initiated cracking in the weld.

3.2 Crack Initiation

The site of the local stress which initiates cracking is dependent on the location of the weld bead on the test strip or plate. In most cases the cracking in the RRC tests for X70 steel welds and the Tekken tests for the X80 and HSLA80 plates started from the root of the weld, see Fig. 5. The Y joint design of the RRC test piece for 10 mm X70 steel was such that the root of the joint was at the mid-thickness of the plate and the weld bead was formed above the centre of the mid-thickness which tended to cause bending. After weld deposition on 10 mm thick X70 plate the bead position above the neutral axis causes the root of the joint to undergo a tensile residual stress and the surface to develop a compressive stress, see Fig. 6a. The tensile residual stress at the weld root causes root cracking during the test [8]. For a high heat input, the weld bead filled the *vee* portion of the joint completely (Fig. 5a) and resulted in a tensile residual stress at the root. A similar condition existed in the Tekken cracking test with the exception that the weld bead was approximately located at the neutral axis as in Fig. 6b. Due to the use of thicker plate in the Tekken cracking test the cross sectional area of the weld bead was relatively low. As the weld bead was located near the neutral axis the

whole bead experienced tensile residual stress. Since a sharp root angle was also present at the root of the weld, the local stress at the root was high enough to cause cracking in the weld. However, the high incidence of cracking for the E8018B2 electrode in the Tekken cracking test was due to the development of a susceptible weld metal microstructure (Section 3.3).

In the RRC tests on 9 mm thick X80 steel plate, cracking started from the root of one of the wagon tracks, see Fig. 7. The root face of the joint for X80 strip was only 2 mm high and the weld resulted in full penetration of the root face. In this situation the root of the weld was in compression and weld surface was in tension, Fig. 6c. The weld bead exhibited quite extensive wagon tracks on the weld surface which provided undercuts. The tensile residual stress at the undercuts of the *wagon* tracks caused cracking in the weld metal. In addition, a low heat input resulted in a small weld metal cross section, increasing the mean stress on the weld bead.

3.3 Susceptible Microstructures and Metallurgical Effects

Cold cracking by hydrogen is facilitated by the presence of a susceptible microstructure which is typically martensitic or bainitic or a combination of these two constituents. The hardness of these microstructures even in low carbon steels is typically higher than 300 HV. Such hard microstructures have a low tolerance for hydrogen and cracking is likely to occur. Below a certain level of heat input the role of microstructure in contributing to cracking appeared to become dominant for the Tekken cracking tests with the E8018B2 electrode. The microstructure of the weld metal was found to contain a high proportion of bainite and some martensite, Fig. 8. The presence of Mo in the E8018B2 electrode increased the hardenability by suppressing the nucleation of ferrite along grain boundaries. This effect was found to be more pronounced when X80 plate, which also contains Mo, was used with the E8018B2 electrode in the Tekken cracking test. Increased Mo can be present in the weld metal of X80 plate due to a dilution effect which can be as high as 40% [9]. The high hardness value of weld metal deposited from E8018B2 electrodes supports this view, see Fig. 9. In addition, low heat input results in a smaller weld bead which significantly reduces the weld cross sectional area for sustaining the reaction stress. The hardness of the weld metal deposited from E8018C3 at 1 kJ/mm heat input was also found to be relatively high, see Fig. 10, but the lack of cracking in the weld metal suggests that high hardness can not be used as a reliable indicative tool for crack prediction. Despite the high hardness value the microstructure consisted of fine acicular type ferrite, see Fig. 11.

A similar heat input effect was observed in RRC tests of X70 steel plate which showed a lower susceptibility to cracking with increasing heat input. However, the weld metal microstructures were not highly susceptible, in conventional terms. In the RRC tests the microstructure for a low heat input generally consisted of fine acicular ferrite, see Fig. 12 and the hardness values in Fig. 13 do not suggest that the weld metal structure should be highly susceptible to cracking. However, cracking was observed to originate from the root of single bevel joints. For X80 steel plate the weld metal from electrodes other than E9010 showed a hardness below 300 HV, see Fig. 14. Despite the lower hardness, cracking occurred in the weld metal which mainly consisted of fine acicular ferrite, Fig. 15. This observation suggests that the susceptibility of the microstructure to cold cracking can not be predicted from hardness and is dependent mainly on the amount of hydrogen at the site of stress concentration and the restraint intensity. The presence of high solute hydrogen in the fine acicular ferrite, in combination with high local stresses resulting from the highly restrained joint, facilitated crack initiation at the sharp root angle.

When heat input was increased in RRC tests of X70 steel plate the microstructure mainly consisted of coarse acicular ferrite and veins of grain boundary ferrite with Widmanstatten side plates, see Fig. 16. The hardness traverse, Fig. 17, revealed that the weld hardness was

well below 300 HV which implies that the susceptibility of the microstructure to cracking is relatively low. Under these circumstances the observed cracking in the weld metal of single bevel joints was due to the high restraint intensity which resulted from the test rig and the high stress concentration factor at the root of the welds.

3.4 Fracture Morphologies

The examination of crack propagation in the weld revealed that the crack was either transgranular or intergranular depending on the columnar grain direction. However, the crack morphology was found to be dependent on the hydrogen content. For the medium hydrogen welds of the Tekken cracking test, crack initiation was in the form of cleavage and intergranular fracture with little sign of plastic deformation, see Fig. 18. It has already been mentioned that the stress intensity is relatively small for the Tekken cracking test and, due to this lower stress intensity and the relatively low hydrogen concentration, the plastic zone ahead of a sharp root angle is likely to be small [10] resulting in quasi-cleavage or intergranular fracture. However, the morphology of fracture at the crack initiation site in the high hydrogen welds in the RRC tests was found to be in the form of microvoid coalescence, see Fig. 19. High hydrogen reduces the yield stress [11] and the high stress intensity at the undercuts or *wagon* tracks gives rise to a large plastic zone which causes microvoid coalescence in the crack initiation area. As the crack grows some hydrogen is lost and the stress intensity is reduced to a level which becomes appropriate for cracking by cleavage fracture.

4. CONCLUSIONS

The results of the investigation of cold cracking in weldments of X70, X80 and HSLA80 steels led to the following specific and general conclusions.

The specific conclusions are summarised as follows:

1. A single bevel joint was found to promote cold cracking at relatively high heat inputs in RRC tests of X70.

2. Increasing the thickness of the test plate in the Tekken cracking test was found to increase crack sensitivity because of the higher restraint intensity.

3. The presence of Mo in the weld metal reduced the incidence of grain boundary ferrite and was found to promote cracking of the weld metal in the Tekken cracking test.

The general conclusions of the investigation are summarised as follows:

1. For low heat input welding the role of microstructure appeared to be more important than the restraint intensity.

2. The fracture morphology of crack initiation site was found to be microvoid coalescence for high hydrogen weld metal and quasi-cleavage for relatively low hydrogen weld metal.

3. The hardness of the microstructure can not be used as a reliable predictive tool for determination of susceptibility to hydrogen cracking.

Table 1: Chemical compositions (wt%) of the X70, X80 and HSLA80 steels and their weld consumables.

Steel	C	Mn	Si	Ni	Cr	Mo	Cu	Al	Ti	Nb	V
X80	0.07	1.62	0.33	0.028	0.03	0.22	0.01	0.031	0.013	0.058	0.003
X70	0.08	1.41	0.10	0.023	0.018	0.004	0.008	0.028	0.011	0.042	0.052
E6010[1]	0.11	1.13	0.23	0.022	0.19	0.115	0.01	0.015	0.021	0.026	0.003
HSLA80	0.06	1.40	0.25	0.85	0.02	-	1.10	-	0.013	0.020	-
E8018C3	0.05	1.10	0.40	1.00	-	-	-	-	-	-	-
E8018B2[2]	0.07	0.80	0.30	-	1.20	0.50	-	-	-	-	-

1: Actual diluted weld metal on X80; 2: Supplier's analysis of the consumable (undiluted).

Table 2: Stress concentration factor, Kt at the root of weld of basic joint geometry [4].

Groove Type	Kt	Groove Type	Kt
Oblique y 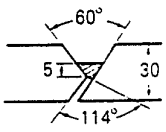	4.0	Single bevel-3 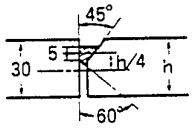	6.9
Double Vee 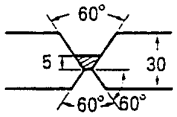	3.7	Single bevel-4 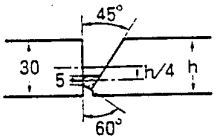	3.5
Single bevel-1 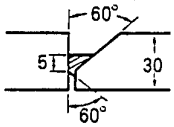	5.8	Symmetric Y 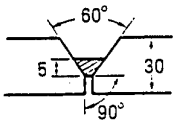	4.2
Single bevel-2 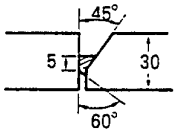	5.4		

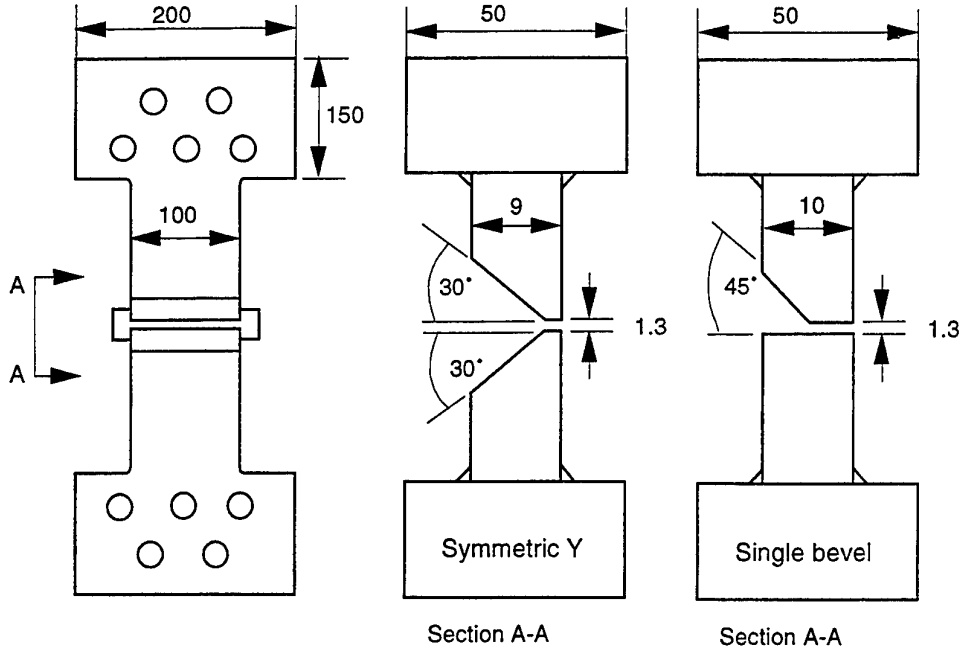

Figure 1: The Rigid Restraint Cracking (RRC) test set up used for 10 mm X70 and 9 mm X80 steel strips [12].

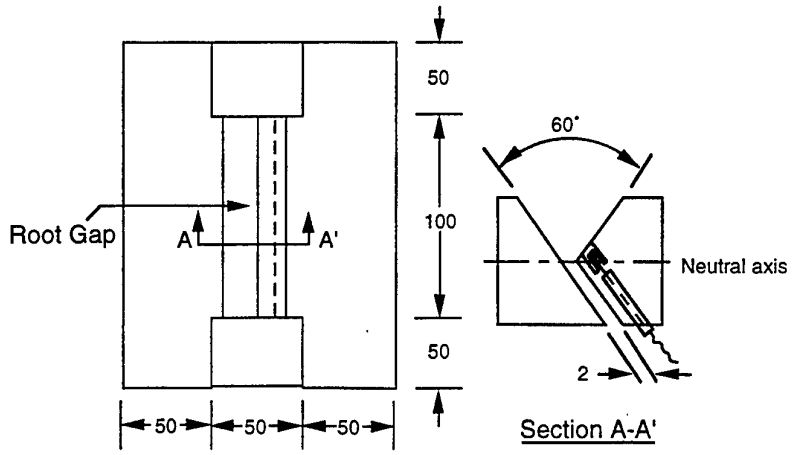

Figure 2: The instrumented Tekken cracking test set up for 25 and 36 mm HSLA80 and 20 mm X80 steel plates.

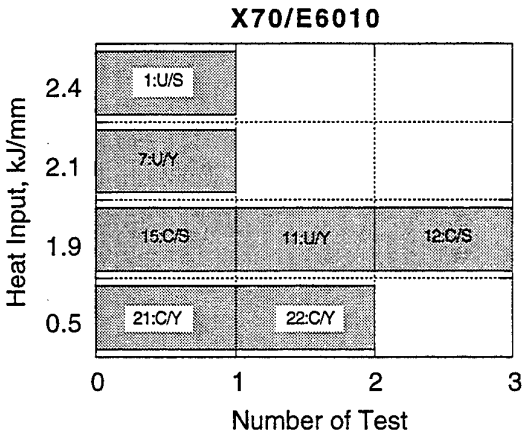

Figure 3: RRC test matrix for X70 and E6010 electrodes. U: uncracked; C: cracked; Y: symmetric Y joint; S: single bevel joint.

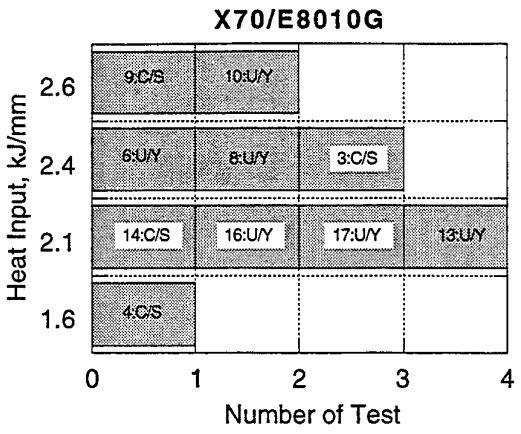

Figure 4: RRC test matrix for X70 and E8010G electrodes. U: uncracked; C: cracked; Y: symmetric Y joint; S: single bevel joint.

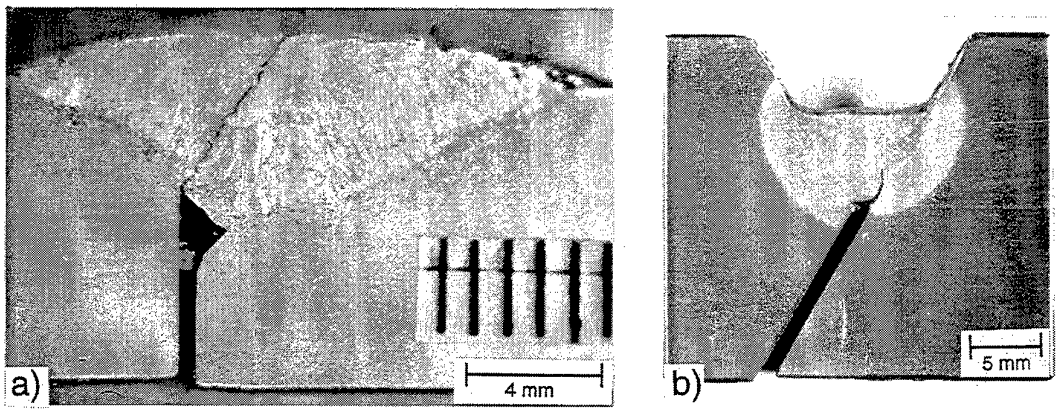

Figure 5: Cross sectional views of weld observed from a) single bevel RRC test and b) oblique Y Tekken test. Note that the crack in both joints initiated from the root of the weld.

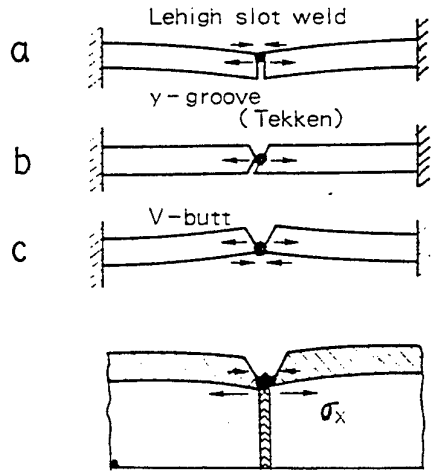

Figure 6: Residual stress across weld throat in flat test specimens with different grooves and in pipe girth [7].

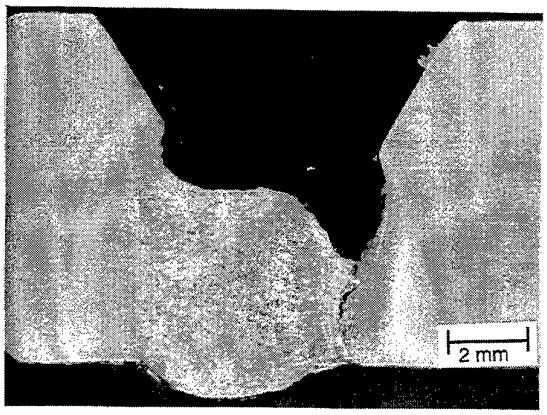

Figure 7: Cross sectional view of RRC weld specimen. Note that the crack in this joint geometry initiated from the root of the wagon track.

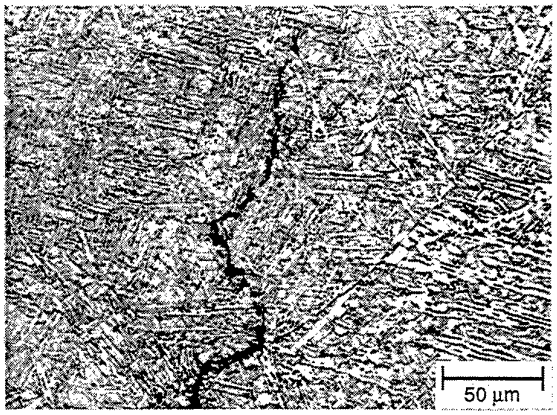

Figure 8: Typical microstructure of HSLA80 weld metal deposited in Tekken cracking test using E8018B2 at 1.0 kJ/mm heat input.

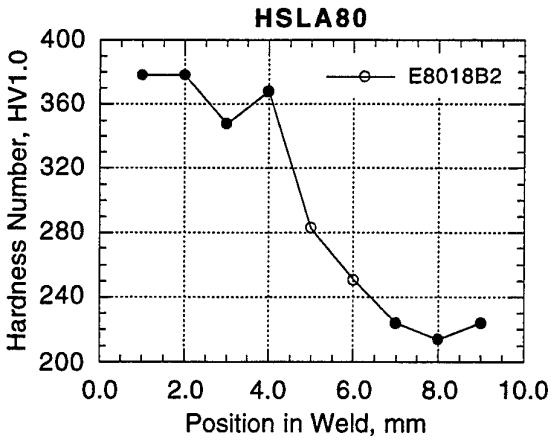

Figure 9: Hardness traverse of weldment deposited in Tekken cracking test at 1 kJ/mm heat input. Filled symbols: weld metal (left) & base metal (right).

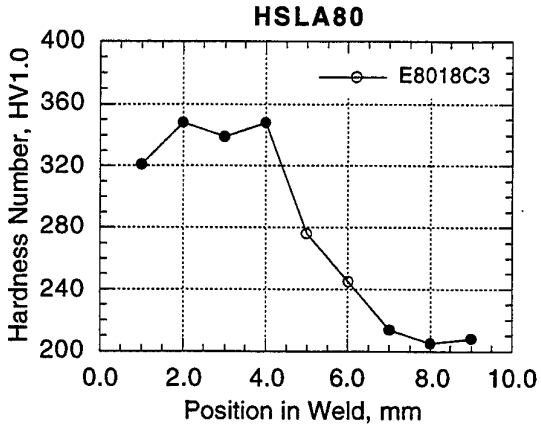

Figure 10: Hardness traverse of weldment deposited in Tekken cracking test at 1 kJ/mm heat input. Filled symbols: weld metal (left) & base metal (right).

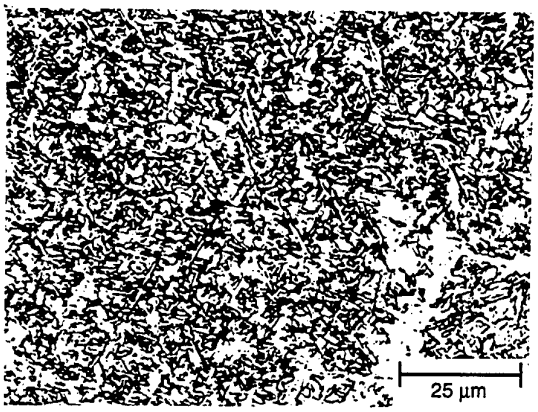

Figure 11: Typical microstructure of HSLA80 weld metal deposited in Tekken cracking test using E8018C3 at 1 kJ/mm heat input.

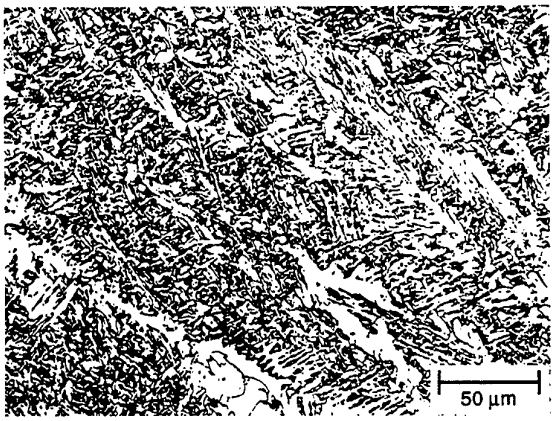

Figure 12: Typical microstructure of X70 weld metal deposited in RRC test using E6010 at 0.4 kJ/mm heat input.

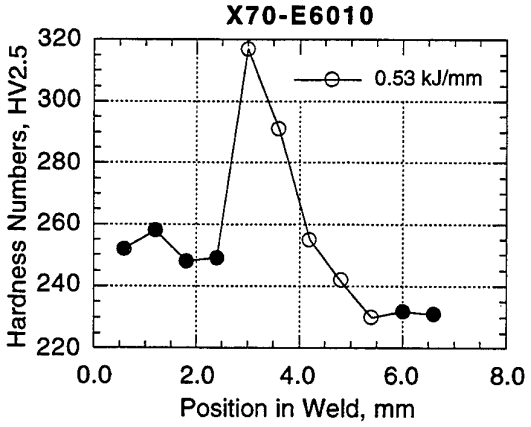

Figure 13: Hardness traverse of weldment deposited at in RRC test 0.53 kJ/mm heat input. Filled symbols: weld metal (left) & base metal (right).

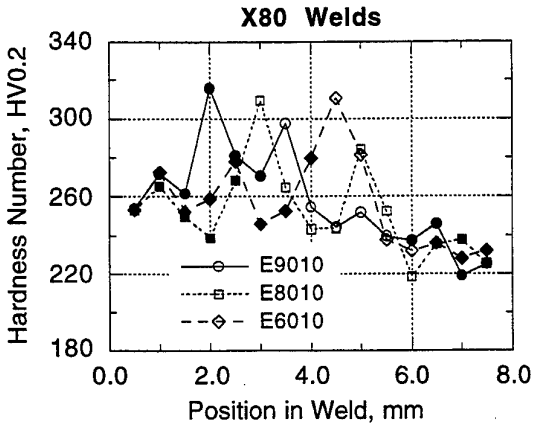

Figure 14: Hardness traverses of low heat input (≤ 0.6 kJ/mm) weldments deposited in RRC test. Filled symbols: weld metal (left) & base metal (right).

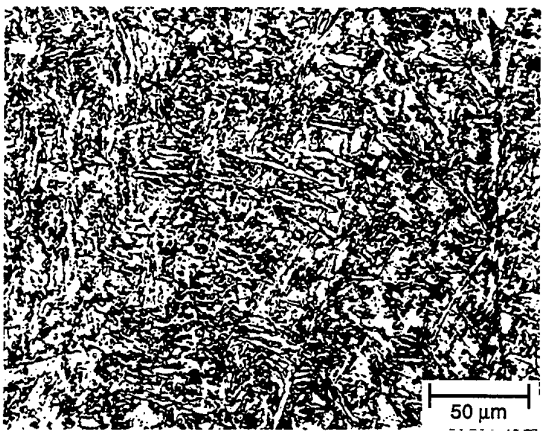

Figure 15: Typical microstructure of X80 weld metal deposited in RRC test using E6010 at 1 kJ/mm heat input.

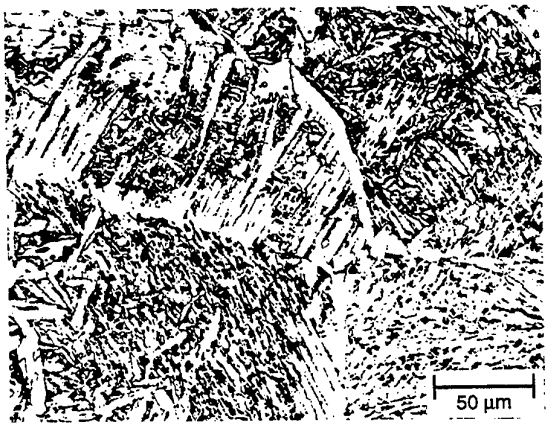

Figure 16: Typical microstructure of X70 weld metal deposited in RRC test using E8010G at 2.4 kJ/mm heat input.

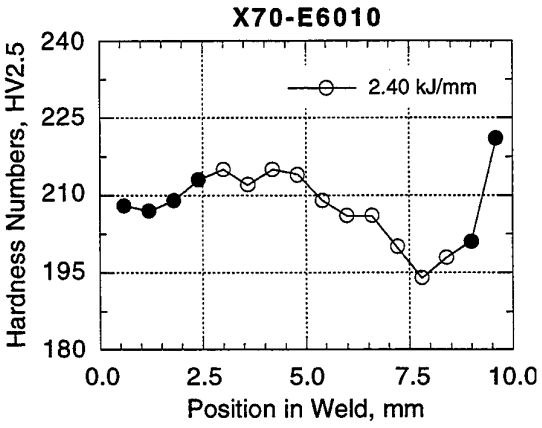

Figure 17: Hardness traverse of weldment deposited in RRC test at 2.4 kJ/mm heat input. Filled symbols: weld metal (left) & base metal (right).

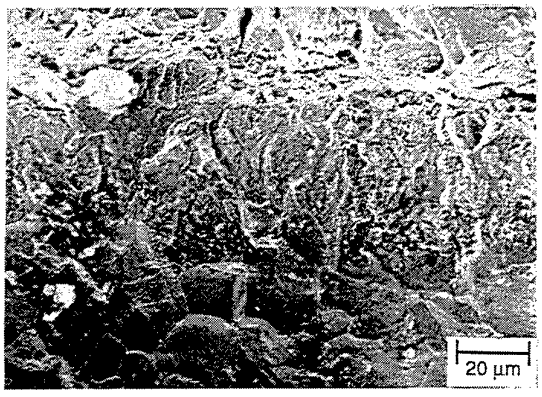

Figure 18: Crack initiation area for medium hydrogen electrode (E8018B2).

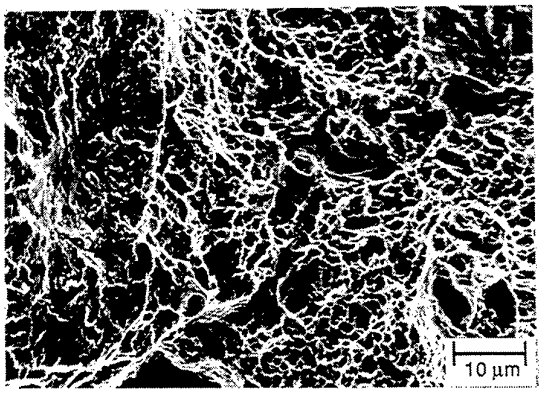

Figure 19: Crack initiation area for high hydrogen electrode (E6010).

ACKNOWLEDGEMENTS

The authors are grateful to Ms L. Chen and Dr. H. Li for providing some of the results. The funding of the CRC for Materials Welding and Joining for this research work is gratefully acknowledged.

REFERENCES

1. Sawhill, J. M., Dix, A. W. and Savage, W. F. *Welding Journal*, 1974, 53, (12), 554s-559s.
2. Troiano, A. R. *Transaction of American Society of Metals*, 1960, 52, (1) 54-80.
3. Squires, I. and Feng, B. The Restraint Effect in HAZ Cold Cracking of Steels, *Asia Pacific Welding Congress*, Auckland, February, 1996, New Zealand.
4. Satoh, K. and Terasaki, T. *Journal of Japanese Welding Society*, 1979, 48, (5), 298-303.
5. Yurioka, N. and Suzuki, H. *International Materials Reviews*, 1990, 35, (4), 217-249.
6. Watanabe, M., Satoh, K. and Matsui, S. *Journal of Japan Welding Society*, 33 (6), 446-457.
7. North, T., Rothwell, A. B. Glover, A. G. and Pick, R. J. *Welding Journal*, 1982, 61, (8) 243s-257s.
8. Suzuki, H. and Yurioka, N. Weldability of Linepipe Steels and Prevention of Cracking in Field Welding, *IIW Doc. IX-1191-81*, 1981.
9. Li, H., Alam, N., Chen, L. and Dunne, D. Cold Cracking in the Weldment of X80 Steel, *WTIA/APIA Panel 7 Research Seminar,* No. 13, Wollongong, October, 1995
10. Beachem, C. D. *Metallurgical Transaction*, 1972, 3 (2), 437-451.
11. Vasudevan, R., Stout, R. D. and Pense, A. W. *Welding Journal,* 1981, 60, (9), 155s-168s.
12. Feng, B., Squires, I. RRC testing of X80 Steel Welds, Report Produced in Central Lab for the CRC Materials Welding and Joining, 1994.

Hydrogen Induced Cracking Tests of High Strength Steels and Nickel-Iron Base Alloys Using the Bolt-Loaded Specimen

G. N. Vigilante
J. H. Underwood
D. Crayon
S. Tauscher
T. Sage
E. Troiano

Army Armament Research Development and Engineering Center, Watervliet, NY, USA

INTRODUCTION

Hydrogen induced cracking failures have been a particular problem in those applications involving high strength materials in aggressive service environments, including armament applications. Recently, a 1.7 m long crack was found at an outside diameter keyway of a gun tube. An investigation concluded that hydrogen stress cracking occurred at a location of tensile residual stress after being exposed to an aggressive electropolish solution [1]. Also, higher energy propellants have been shown to increase the risk of hydrogen damage to bore coatings, liners, and the underlying steel substrate [2]. In addition, Troiano et al. [3] have concluded that premature seal failures in armament were likely caused by the hydrogen rich by-products of the combustion environment.

In this work, a fracture mechanics approach was used to measure the hydrogen induced crack growth rates and thresholds of various steels and nickel-iron base alloys at various yield strength levels. The effects of refinement were also examined for one of the steels tested. The constant displacement bolt-loaded compact sample (Figure 1), henceforth referred to as the bolt-loaded sample, was used in the testing because it provides quantitative information on the crack growth rate, da/dt, and the threshold stress intensity (K_{IHIC}) in a simple test. K_{IHIC} is the threshold stress intensity under which no cracking will occur in a given material in a hydrogen environment. As a crack grows in a bolt-loaded specimen, the load, and therefore the stress intensity, decreases until K_{IHIC} is reached. This test is fundamentally different from constant load tests, where K_{IHIC} is found by testing several specimens at various initial stress intensities until no cracking occurs. One disadvantage of the bolt-loaded specimen is that long test times (up to 10,000 hours) may be necessary when testing insensitive materials, non-aggressive environments, and when testing at low initial stress intensities. This problem may be mitigated by first testing a sample at a high initial stress intensity level approaching K_{Ic}. This will aid in determining the material susceptibility and the initial applied stress intensity levels for subsequent tests. There is currently no recognized standardization of the bolt-loaded specimen; however, an ASTM committee is engaged in incorporating a bolt-loaded compact specimen standard with the recently adopted ASTM standard E 1681-95 on environment-assisted cracking.

MATERIALS AND ENVIRONMENTS

MATERIALS

The materials used in this investigation consisted of martensitic and austenitic forged alloys with yield strengths ranging from 760 MPa-1400 MPa. The martensitic alloys used have a body center cubic (BCC) crystal structure and the austenitic materials have a face centered cubic (FCC) crystal structure. The materials investigated were A723, Maraging 200, and PH 13-8 Mo steels, Alloy 718 and Alloy 706 nickel-iron base alloys, and A286 iron-nickel base alloy. A723, Maraging 200, and PH 13-8 Mo were chosen for their high strength and toughness properties (in air). Alloys 718 and 706 were chosen for their high strength, crystal structure, and hydrogen induced cracking resistance (as compared to the steels tested) [4, 5]. A286 was chosen for its well known resistance to hydrogen induced cracking [6, 7]. Some pertinent mechanical/material properties for the tested materials are listed in Table 1.

A723 is a Ni-Cr-Mo quenched and tempered (Q&T) steel. Both A723 Grade 1 and Grade 2 compositions were evaluated to determine the effects of strength, composition, and refinement on da/dt and K_{IHIC}. A723 Grade 1 material was electric furnace melted and vacuum degassed (EFM-VD). Two different refinement methods of A723 Grade 2 material were examined, electric furnace melted and electro-slag remelted (EFM-ESR) material and vacuum induction melted and vacuum arc remelted (VIM-VAR) material. Both the ESR and VIM-VAR refinement methods increase the homogeneity of the microstructure and reduce the amount of sulfur (S) and phosphorus (P) present as compared to

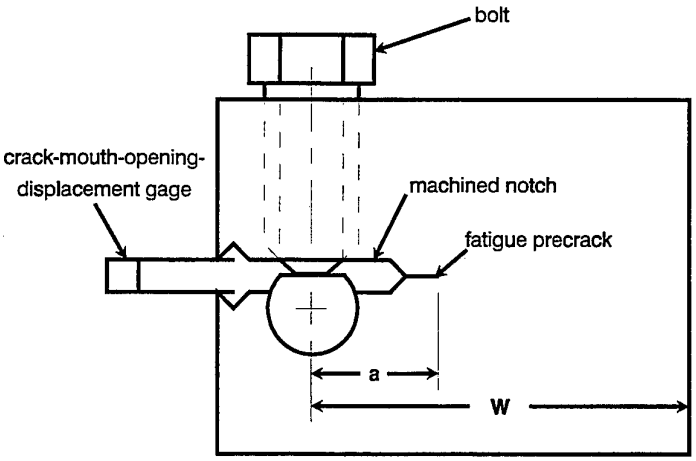

FIG. 1 - Schematic of the bolt-loaded test specimen.

the EFM-VD condition. The levels of S and P in the Grade 1, Grade 2 (ESR), and Grade 2 (VIM-VAR) steels were 0.005/0.006, 0.002/0.005, and 0.0007/0.005, respectively. Additionally, the Grade 2 material contains slightly more Ni to improve fracture toughness. Maraging 200 is a 18Co-8Ni steel which was conventionally austenitized and aged. PH 13-8 Mo is a 13Cr-8Ni-2Mo precipitation hardening stainless steel which was heat treated to two standard overaged conditions. Alloy 718 is a 52Ni-19Cr-19 Fe superalloy which was tested in the direct aged condition for maximum strength and a standard heat treatment condition for maximum ductility and impact strength [8]. Alloy 706 is a

TABLE 1 - Mechanical/material property information on the materials tested.

Material	**Yield Strength (MPa)**	**Fracture Toughness (MPa√m)**	**Crystal Structure**
A723 Grade 1	1160	125	BCC
A723 Grade 2 (ESR)	1130	175	BCC
A723 Grade 2 (ESR)	1275	125	BCC
A723 Grade 2 (VIM-VAR)	1275	170	BCC
Maraging 200	1400	175	BCC
PH 13-8 Mo	1275	145	BCC
PH 13-8 Mo	1035	125	BCC
Alloy 718 (Direct Aged)	1150	135	FCC
Alloy 718	1115	145	FCC
Alloy 706	1110	180	FCC
A286	760	125	FCC

41Ni-38Fe-16Cr superalloy tested in a standard heat treated condition to maximize ductility and impact strength [9]. A286 is an Fe-25Ni-15Cr superalloy which was tested in a standard heat treatment condition. Table 2 lists the various heat treatments of the materials tested.

ENVIRONMENTS

All tests were conducted in either electrochemical cells or in concentrated acid solutions with the exception of A723 Grade 1 (1160 MPa YS) and Grade 2 (1130 MPa YS) and Alloy 706 which were tested in both environments. All tests were conducted at ambient temperature.

The electrochemical cell tests were conducted using a platinum anode and specimen cathode in a 3.5% aqueous NaCl solution. As_2O_3 was used as a "poison" to limit the combination of nascent hydrogen to the diatomic gas [10]. All electrochemical cell test specimens were pre-charged at a current density of 40 mA/cm^2 for eight hours prior to load application. A current density of 40 mA/cm^2 was also applied during testing. This current density was maintained at a constant value using a current controlling power source and by keeping the exposed surface area of the specimen constant throughout the test. The NaCl solution volume was monitored on a daily basis in order to ensure a constant current density and replaced weekly to ensure a constant reservoir chemistry.

All acid cracking tests were conducted in a concentrated 50% sulfuric acid and 50% phosphoric acid solution (by volume). This solution is identical to that used in previous tests [1].

TEST PROCEDURE

All bolt-loaded test specimens were taken in the C-R orientation as described in ASTM E 399, and all tests were conducted following interlaboratory guidelines on the bolt-loaded specimen from Wei and Novak [11]. All tests were conducted in acid or in an electrochemical cell as described in the preceding section. The A723 steels tested in acid were tested in triplicate for each test condition. All

TABLE 2 - Heat Treatments of Materials Tested.

Materials	Heat Treatment
A723 Grade 1 @ 1160 MPa YS	843°C 1 hour Water Quench, Temper 582°C 4 hours Air Cool
A723 Grade 2 @ 1130 MPa YS	843°C 1 hour Water Quench, Temper 627°C 4 hours Air Cool
A723 Grade 2 @ 1275 MPa YS	843°C 1 hour Water Quench, Temper 524°C 4 hours Air Cool
PH 13-8 Mo @ 1275 MPa YS	927°C 1/2 hour air cool, Refrigerate -73°C, 2 hours Air Warm, Age 556°C 4 hours Air Cool
PH 13-8 Mo @ 1035 MPa YS	927°C 1/2 hour air cool, Refrigerate -73°C, 2 hours Air Warm, Age 579°C 4 hours Air Cool
Maraging 200	816°C 1 hour Water Quench, Age 482°C 3 hours Air Cool
Alloy 718 Direct Aged	718°C 8 hours Furnace Cool to 621°C 18 hours Air Cool
Alloy 718	1038°C 1/3 hour Air Cool, Age 760°C 11 hours Furnace Cool to 649°C 9 hours Air Cool
Alloy 706	982°C 1 hour Air Cool, Age 718°C 8 hours Furnace Cool 38°C/hour to 621°C 8 hours Air Cool
A286	816°C 1 hour Water Quench, Age 718°C 16 hours Air Cool

bolt-loaded specimens were tested at an initial stress intensity of 55 MPa√m with the exception of one Alloy 706 specimen which was tested at 110 MPa√m. The low stress intensities of 55 MPa√m were chosen from previous experience in order to avoid the problem of a deep crack growing too near to the back edge of the specimen. The stress intensity in the bolt-loaded sample is related to the mouth opening through the following relationship [1]:

$$K_{applied} = f(a/W)\, Ev(1-a/W)^{1/2} \;/\; W^{1/2}$$

$$f(a/W) = 0.654 - 1.88(a/W) + 2.66(a/W)^2 - 1.233(a/W)^3$$

where v is mouth opening and E is Young's Modulus. This K expression is valid for $0.3 \leq a/W \leq 1$. For the acid cracking tests the acid was introduced to the crack tip prior to load application in order to expose fresh surfaces produced by the subsequent loading. The crack extension of the specimens was monitored optically on both sides of the specimen on a regular basis in order to determine $K_{applied}$ as a function of time and to obtain da/dt information. The mouth opening of the test specimen and the solution pH were checked frequently to ensure no relaxation or solution contamination, respectively. The duration of the tests depended on the material tested and its yield strength. Typically, tests were conducted for durations ranging from 1500-6000 hours. After test termination the final crack length was measured to determine if the test conformed to plain strain test conditions and the fracture surface was examined visually and by scanning electron microscopy to determine the fracture morphology. From previous experience it was believed that all materials would easily conform to plane strain conditions because of low hydrogen induced cracking threshold values.

RESULTS AND DISCUSSION

In general, all of the body center cubic materials tested exhibited similar cracking characteristics. Both da/dt and K_{IHIC} information were similar, though both the PH 13-8 Mo materials tested had lower crack growth rates and slightly higher K_{IHIC} than the average BCC materials tested. With the face centered cubic materials tested, the crack growth rate was lower than with the BCC materials. This was expected in part because diffusivity of hydrogen through an open cell BCC structure is higher than through a closed cell FCC structure. In the technical literature, crack growth rates have been shown to be orders of magnitude less in FCC structures than in BCC structures, e.g. Ritchie et al. [12].

In the following sections, discussion of the results from the various materials is given. Table 3 shows a summary of the results of the hydrogen induced cracking tests conducted on all materials.

A723 Steel

The hydrogen induced cracking tests conducted on A723 steels in acid environments showed dramatic results when plotted as applied stress intensity versus time (Figure 2). Figure 2 shows the trend of the data, illustrating the incubation time, subsequent crack growth, and threshold. Though the Grade 1 and Grade 2 materials were tested at about the same yield strength level (1160 and 1130 MPa, respectively), the incubation time required to promote a growing crack increased from approximately from 200 hours to over 2000 hours. Additionally, when the yield strength of the Grade 2 material was increased 13% from 1130 MPa to 1275 MPa, the incubation time decreased over two orders of magnitude from over 2000 hours to less than 12 hours. After the incubation time was exceeded, the crack grew steadily until K_{IHIC} was reached. Incubation time has been observed to decrease with an increase in strength or applied stress, for example as cited by Steigerwald et al. [13] and Jones [14].

TABLE 3 - Summary of K_{IHIC} test results

Material	Yield Strength (MPa)	K_{IHIC} (MPa√m)	Test Environment
A723 Grade 1	1160	16/10	acid/cell
A723 Grade 2 (ESR)	1130	16/16	acid/cell
A723 Grade 2 (ESR)	1275	10	acid
A723 Grade 2 (VIM-VAR)	1275	11	acid
Maraging 200	1400	12	cell
PH 13-8 Mo	1275	17	cell
PH 13-8 Mo	1035	19	cell
Alloy 718	1150	11	cell
Alloy 718	1115	-	cell
Alloy 706	1110	-	acid/cell
A286	760	-	cell

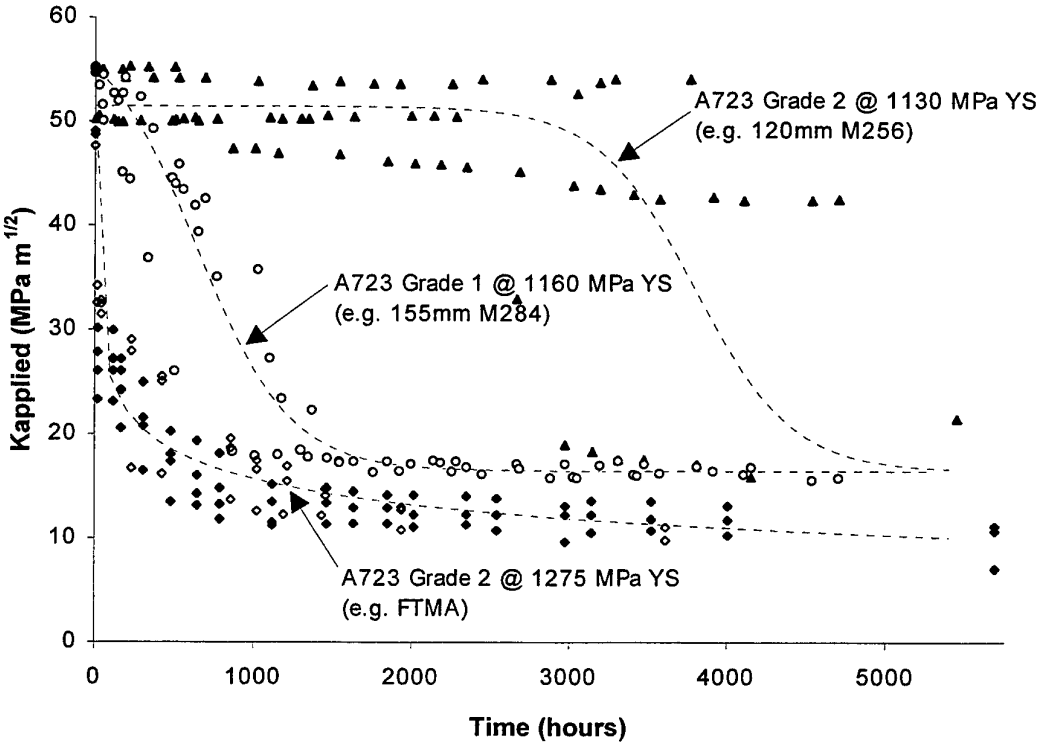

FIG. 2 - Applied K versus time for A723 steels exposed to a 50% sulfuric - 50% phosphoric acid solution.

However, both the strength and applied stress intensity levels were nearly identical in the lower yield strength Grade 1 and Grade 2 materials tested. This suggests that the local crack tip chemistry may have been the controlling factor. Therefore, the longer incubation time of the lower strength Grade 2 material may be attributed to the refinement and increased Ni content as compared to the Grade 1 material.

The crack growth rates of the A723 steels conducted in acid are shown in Figure 3. A five point moving average was used to analyze the data. This curve shows the stage I and a portion of the stage II crack growth regimes. For the lower strength Grade 1 and Grade 2 steels, da/dt in the stage II regime appeared to be constant at approximately 10^{-5} mm/s, the same as that found by Underwood et al. [1]. The constant da/dt data in the stage II regime for the lower strength steels were independent of K and were solely a result of diffusion controlled crack growth. For the higher strength Grade 2 steel, da/dt in the stage II regime was approximately an order of magnitude higher (10^{-4} mm/s). Note the wide scatter in both of the lower strength steels at the initial applied stress intensity of 55 MPa$\sqrt{m}$. This scatter occurred during the incubation period when little or no crack growth was observed. After incubation the crack grew significantly and the scatter was eliminated. The average K_{IHIC} for the lower strength Grade 1 and Grade 2 steels was approximately 16 MPa$\sqrt{m}$. The average K_{IHIC} for the higher strength ESR and VIM-VAR processed Grade 2 materials was approximately 10 and 11 MPa$\sqrt{m}$, respectively.

The electrochemical cell tests on the lower strength Grade 1 and Grade 2 steels exhibited incubation times of approximately 325 and 450 hours, respectively, then cracked rapidly and reached K_{IHIC} levels of approximately 10 and 16 MPa$\sqrt{m}$, respectively. Figure 4 shows the applied stress intensity as a function of exposure time for all materials tested in the electrochemical cell tests.

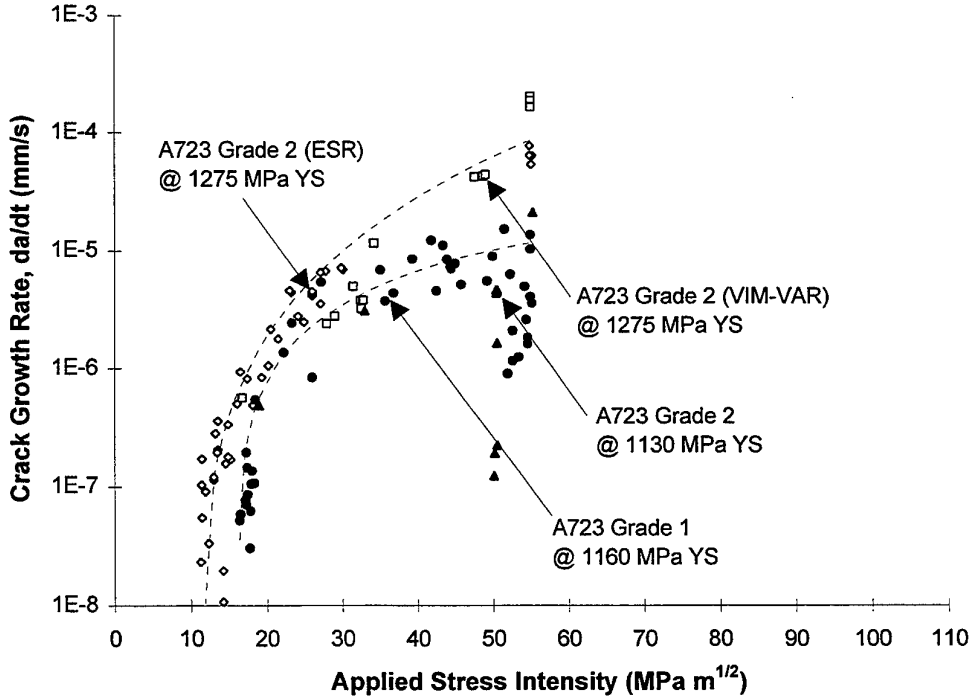

FIG. 3 - Crack growth rate versus applied K for A723 steel exposed to a 50% sulfuric - 50% phosphoric acid solution.

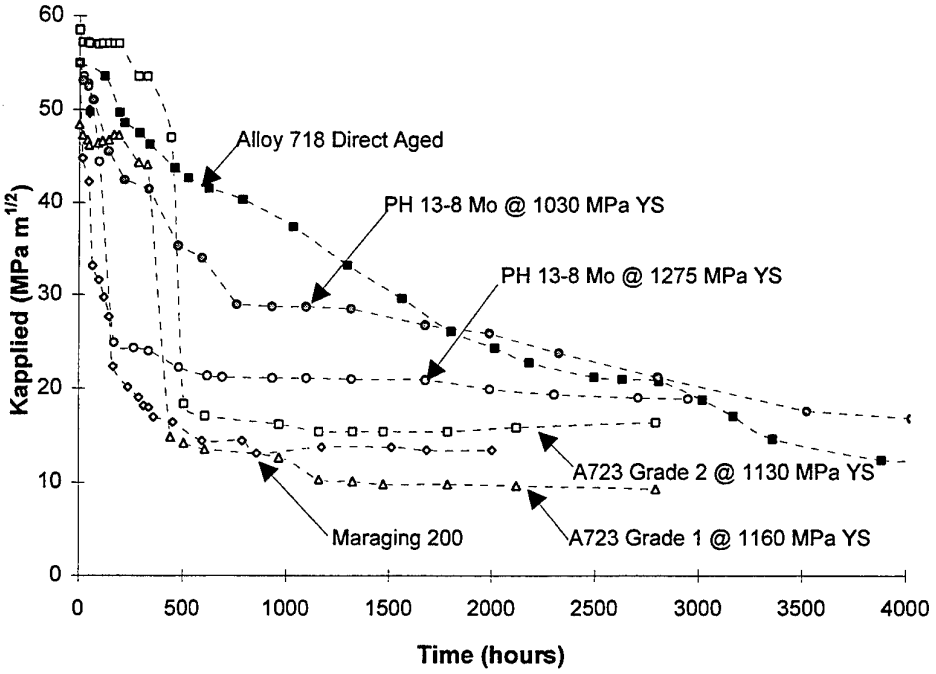

FIG. 4 - Applied K versus time for high strength steels and nickel-iron base alloys tested in an electrochemical cell.

In the electrochemical cell tests, there was little distinction in the incubation time between the Grade 1 steel and the Grade 2 steel tested. It is believed that the high current density and precharging procedure liberated much more hydrogen than the acid tests thereby increasing the severity of cracking in both steels and reducing the incubation time in the Grade 2 steel. If the current density was decreased significantly, a more notable distinction may have been apparent. It is also interesting to note that only the A723 steels tested in the electrochemical cell exhibited a classical incubation period. This appears to more than just a strength effect since the 1035 MPa yield strength PH 13-8 Mo material tested did not exhibit an incubation time.

The crack growth rates of the A723 steels tested in the electrochemical cell were approximately 10^{-5} mm/s as can be seen in Figure 5. A five point moving average was used to plot the data. In Figure 5 the initial scatter was omitted from the A723 steels for clarity.

The fracture surface near the crack tip of the higher strength ESR processed Grade 2 material is shown in Figure 6a. In this figure the intergranular fracture morphology is evident as is the chemical attack of the fracture surface caused by the acid solution. Much more chemical attack was observed at lower a/W values as would be expected due to longer exposure to the acid. The remaining ligament of this specimen was forced open by tensile overload after testing was completed. Figure 6b shows predominantly a ductile fracture morphology of microvoid coalescence. However, notice the island of intergranular fracture. This intergranular area is believed to have resulted from the remaining ligament being embrittled by hydrogen during immersion in the acid solution. When the tensile load was applied to break the remaining ligament, a portion of it failed in a brittle intergranular manner.

In the A723 steels examined, there were little differences in the S and P content between the EFM-VD and EFM-ESR refinement methods. The VIM-VAR processed steel contained approximately the same amount of P and much less S than either the VD or ESR processed steels. Because the S is

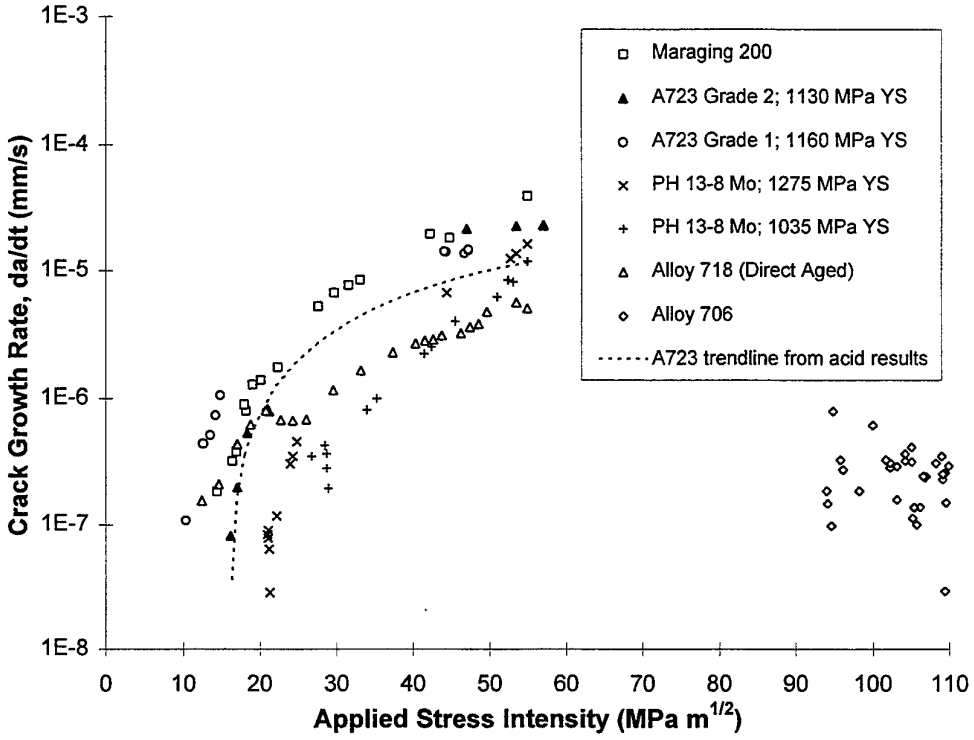

FIG. 5 - Crack growth rate versus applied K for high strength steels and nickel-iron base alloys tested in an electrochemical cell.

"tied up" as manganese sulfide stringers in A723 steels and the P content remained essentially constant, there is no direct correlation which can be made here on the effects of these impurities on incubation time, da/dt, or K_{IHIC}. Previous studies have shown no strong effect of impurities on hydrogen induced cracking of high strength steels with yield strengths greater than 1250 MPa [15].

PH 13-8 Mo

The PH 13-8 Mo material tested in the 1275 MPa yield strength condition resulted in a K_{IHIC} of approximately 17 MPa$\sqrt{m}$. The material tested at a lower yield strength level of 1035 MPa resulted in a K_{IHIC} of approximately 19 MPa$\sqrt{m}$. It was surprising that the lower yield strength condition did not provide an improved K_{IHIC}. More dramatic results may have been evident if the PH 13-8 Mo material was tested in a peak aged and an overaged condition rather than two overaged conditions, since the mechanical properties from a highly overaged condition result in lower strength but also lower toughness due to precipitate incoherency. Fracture toughness tests by Young et al. [16] on H charged PH 13-8 Mo specimens at a yield strength level of 1275 MPa showed results similar to those obtained in these tests.

Maraging 200

The Maraging 200 material tested in the electrochemical cell exhibited a K_{IHIC} value of approximately 13 MPa$\sqrt{m}$.

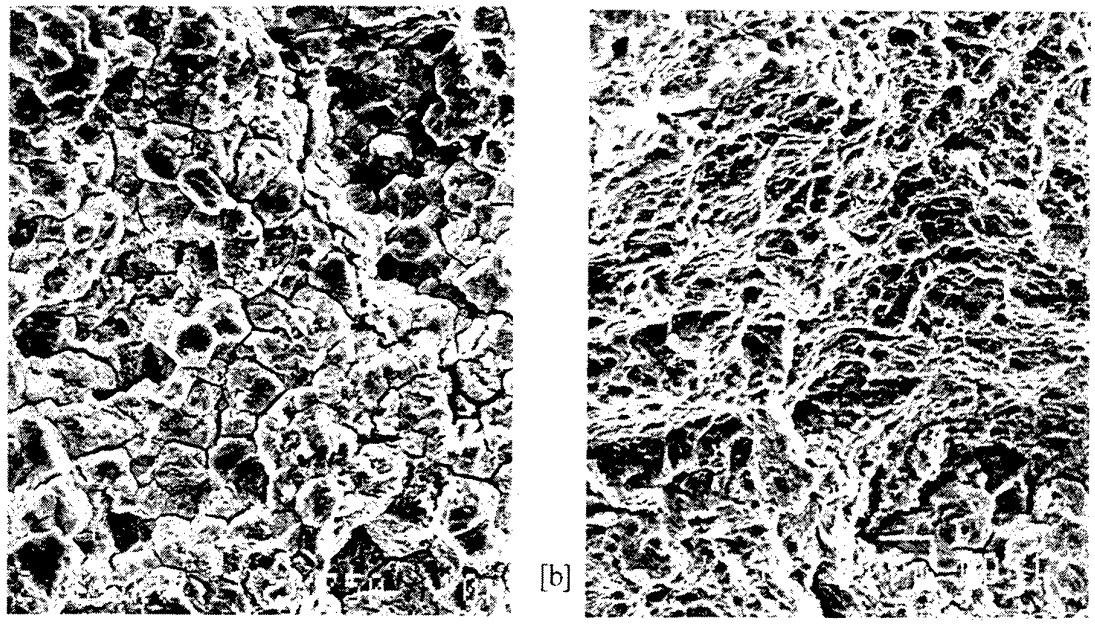

FIG. 6 - SEM fractographs of a 1275 MPa YS A723 steel exposed to an acid solution for 1100 hours; 750x magnification: [a] intergranular cracking near the crack tip and [b] microvoid coalescence in the ruptured remaining ligament.

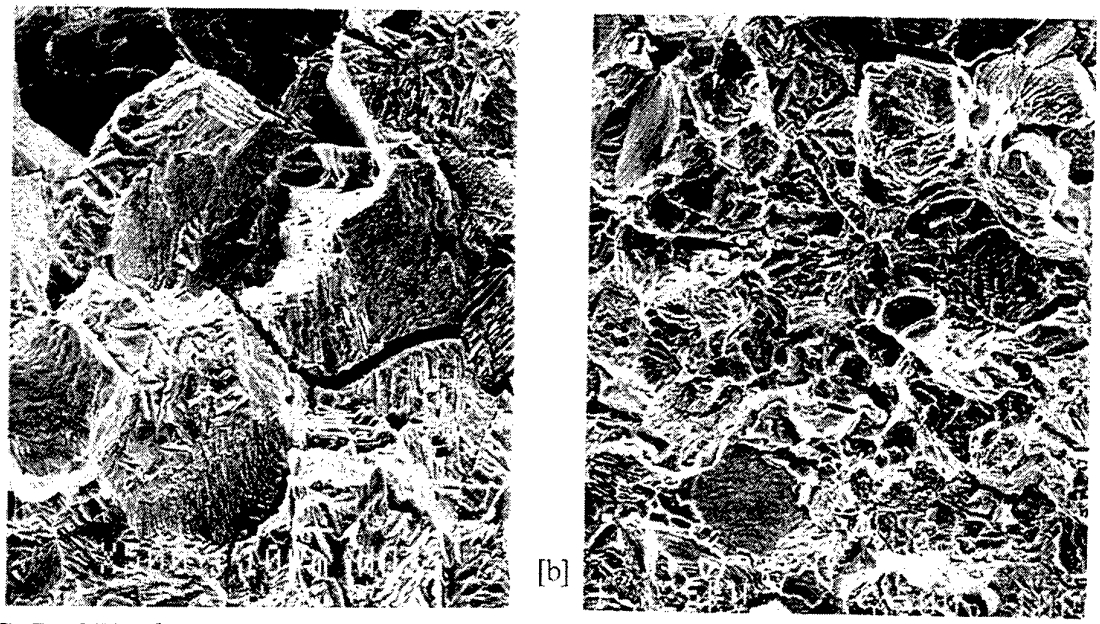

FIG. 7 - SEM fractographs of direct aged Alloy 718 tested in an electrochemical cell; 500x magnification: [a] intergranular cracking in the cracked portion of the specimen and [b] mixed mode failure in the ruptured remaining ligament.

Alloy 718

The Alloy 718 material tested in the direct aged condition exhibited no distinctive incubation time. As seen in Figure 4, the crack grew much slower and did not exhibit any gross crack advances as with the BCC materials, an advantage attributed to the lower diffusivity of H through the FCC crystal structure. However, K_{IHIC} for the direct aged Alloy 718 specimen was similar or less than that of the BCC materials tested. The lower than expected yield strength and low K_{IHIC} values are believed to be attributed to an undesirable δ phase present at the grain boundaries [17]. Figure 7a shows the fracture surface in the cracked portion of the Alloy 718 material tested in the direct aged condition. The fracture surface is entirely intergranular in nature with evidence of the second phase present at the grain boundaries. Figure 7b shows the fracture surface of the ruptured remaining ligament. The fracture morphology is brittle, containing both quasi-cleavage and intergranular fracture.

The Alloy 718 material heat treated to provide maximum ductility and impact strength exhibited no appreciable cracking after 5000 hours of exposure. If given enough time, it is believed that the K_{IHIC} of Alloy 718 in this condition could be as high as 42 MPa√m based on environmental fracture tests conducted by Walter and Chandler [4].

Alloy 706

After over 3000 hours in acid and 5000 hours in the electrochemical cell, no appreciable cracking was observed in the Alloy 706 specimens at both the 55 MPa√m and 110 MPa√m initial applied stress intensity levels. For example, after 5000 hours of exposure in the electrochemical cell at an initial applied stress intensity of 110 MPa√m the current applied stress intensity is 90 MPa√m which corresponds to crack growth of only approximately 3.7 mm. It is believed that the K_{IHIC} of Alloy 706 will be higher than that of Alloy 718 because slow strain rate notched tensile tests conducted on both alloys [18] showed a higher notched tensile strength ratio for Alloy 706 than for Alloy 718. The slow strain rate notched tensile tests were conducted on specimens which were hydrogen charged and compared to control specimens tested in laboratory air. The notched tensile strength ratio of the Alloy 706 specimens were 0.91 as compared to 0.84 for the Alloy 718 specimens. High pressure hydrogen notched tensile tests also showed a higher ratio for Alloy 706 than for Alloy 718 [4].

A286

After over 2300 hours in the electrochemical cell, no visible cracking occurred with the A286 material. The K_{IHIC} is expected to be higher than that of Alloys 718 and 706 because slow strain rate notched tensile tests conducted [18] show a ratio of 0.98 for A286 as compared 0.84 and 0.91, respectively. In addition, high pressure hydrogen notched tensile tests conducted on A286 also show an improved resistance to hydrogen as compared to Alloys 718 and 706 [4].

SUMMARY AND CONCLUSIONS

1. Hydrogen induced cracking studies were conducted on A723, Maraging 200, PH 13-8 Mo, Alloy 718 Direct Aged, Alloy 718, and A286 alloys using the constant displacement bolt-loaded compact specimen. All tested were conducted in either 50% sulfuric-50% phosphoric acid solutions or in electrochemical cells at room temperature. All tests, with the exception of Alloy 706, were conducted at an initial stress intensity of 55 MPa√m. Information on crack growth rates and hydrogen induced cracking threshold stress intensities were obtained from these tests.

2. The bolt-loaded specimen has provided closely repeatable hydrogen induced cracking tests and allows

for accurate crack growth rate and threshold measurement.

3. With the lower strength A723 steels tested in an acid environment, an incubation period was observed followed by crack growth and asymptotic approach of a threshold. At the lower strength levels (e.g. 1130 MPa YS) refinement and alloying have an effect on the hydrogen induced cracking susceptibility of A723; however, at high strength levels (1275 MPa YS) there was no apparent benefit. In A723, yield strength had the most pronounced effect on hydrogen induced cracking susceptibility. As the strength of A723 increases, the incubation time, crack growth rate, and K_{IHIC} all decreased. Crack growth rates in the Stage II cracking regime for the lower strength A723 Grade 1 steel were approximately 10^{-5} mm/s. Crack growth rates in the Stage II regime for the higher strength Grade 2 steels were about an order of magnitude larger.

4. The electrochemical tests were more severe than the acid cracking tests for A723 steel. A shorter incubation time was observed for the A723 Grade 2 steel and a lower threshold was evident for both Grade 1 and Grade 2 steels tested in the electrochemical cell.

5. Alloy 718 tested in the direct aged condition has a low K_{IHIC} value of 11 MPa$\sqrt{m}$, due to a deleterious δ phase present at the grain boundaries. Alloy 718 tested under a standard high ductility heat treatment condition appears to be much more resistant to hydrogen induced cracking since no cracking was observed after 5000 hours of exposure.

6. A286 and Alloy 706 did not exhibit any measurable crack growth in bolt-loaded tests conducted at 55 MPa$\sqrt{m}$ after 2400 and 3000 hours of exposure, respectively. Though Alloy 706 tested at 110 MPa$\sqrt{m}$ exhibited a small amount of crack extension after 5000 hours of exposure, it proved to be very resilient to hydrogen induced cracking.

7. The martensitic materials tested in this investigation exhibited similar crack growth rates and hydrogen induced cracking threshold stress intensity values with the exception of the two PH 13-8 Mo specimen tested at 1130 MPa YS and 1275 MPa YS which had slightly lower crack growth rates.

8. The austenitic, face centered cubic materials tested exhibited up to three orders of magnitude lower crack growth rates than the body centered cubic materials tested.

ACKNOWLEDGEMENTS

Thanks to Mr. A. Kapusta for fractography of the bolt-loaded specimens.

REFERENCES

[1]Underwood, J. H., Olmstead, V. J., Askew, J. C., Kapusta, A. K., and Young, G. A., "Environmentally Controlled Fracture of an Overstrained A723 Steel Thick-Wall Cylinder", *ASTM STP 1189*, 1993, pp. 443-460.

[2] Dalley, A.M., Buckman, R.W. Jr., and Bagnall, C., "Physical and Chemical Interactions at the Bore Surface of a Ta-10W Gun Barrel Liner", *MPIF-APMI International Conference on Tungsten and Refractory Metals, Their Alloys, Composites and Carbides*, Washington D.C., November 1995.

[3] Troiano, E., Underwood, J. H., Scalise, A., O'Hara, G. P., and Crayon, D., "Fatigue Analysis of a Vessel Experiencing Pressure Oscillations", *Fatigue and Fracture Mechanics: 28th Volume, ASTM STP*

1321, J. H. Underwood, B. D. MacDonald, M. R. Mitchell, Eds., American Society for Testing and Materials, 1997.

[4] Walter, R. J. and Chandler, W. T., "Influence of Gaseous Hydrogen on Inconel 718", *Hydrogen in Metals*, 1974, pp. 515-524.

[5] *Handbook of Corrosion Data*, ASM International Materials Data Series, 1989, p. 333.

[6] Thompson, A. W. and Brooks, J. A., "Hydrogen Performance of Precipitation-Strengthened Stainless Steels Based on A-286", *Metallurgical Transactions A*, Volume 6A, July 1975, pp. 1431-1442.

[7] Papp, J., Hehemann, R. F., and Troiano, A. R., "Hydrogen Embrittlement of High Strength FCC Alloys", *Hydrogen in Metals*, 1974, pp. 657-669.

[8] Product Literature on Inconel Alloy 718, Inco Alloys International, 1968.

[9] Product Literature on Inconel Alloy 706, Huntington Alloys, Inc., 1974.

[10] Spencer, G.L., "Hydrogen Embrittlement of Gun Steel", Master's Thesis, Rensselaer Polytechnic Institute, Troy, NY, August 1987.

[11] Wei, R.P. and Novak, S.R. "Interlaboratory Evaluation to KISCC and da/dt Determination Procedures for High-Strength Steels", *Journal of Testing and Evaluation*, Vol. 15, No. 1, Jan. 1987.

[12] Ritchie, R. O., Castro Cedeño, M. H., Zackay, V. F., and Parker, E. R., "Effects of Silicon Additions and Retained Austenite on Stress Corrosion Cracking in Ultrahigh Strength Steels", *Metallurgical Transactions A*, Vol. 9A, 1978, pp. 35-40.

[13] Steigerwald, E. A., Schaller, F. W., and Troiano, A. R., "The Role of Stress in Hydrogen Induced Delayed Failure", *AIME Transactions*, Vol. 218, October 1960, pp. 832-841.

[14] Jones, D. A., *Principles and Prevention of Corrosion*, Prentice Hall, Inc., Saddle River, NJ, 1996, p. 249.

[15] Craig, B., "Limitations of Alloying to Improve the Threshold for Hydrogen Stress Cracking of Steels", *Hydrogen Effects on Material Behavior*, 1989, pp. 955-963.

[16] Young, L. M., Eggleston, M. R., Solomon, H. D., and Kaisand, L. R., "Hydrogen-assisted cracking in a precipitation hardening stainless steel: effects of heat treatment and displacement rate", *Materials Science and Engineering*, 1995, pp. 377-387.

[17] Vigilante, G. N. and Fusco, D. R., "Evaluation of High Strength Materials for the Regenerative Liquid Propellant Gun Program", Army Armament Research Development and Engineering Center Technical Report #95035, Watervliet, NY, 1995.

[18] Tauscher, S. and Sage, T., Unpublished Research, 1995.

Hydrogen Activity Coefficients in The Weld Zone

M Tchaikovsky
BHP Flat Products Division
Port Kembla Steelworks

I Squires
Cooperative Research Centre
for Material Welding and Joining

1.0 INTRODUCTION

Hydrogen assisted cold cracking is perhaps the most serious of all weld cracking problems and is dependent on three interacting requirements: sufficient hydrogen concentration, an applied stress and a susceptible microstructure. Cracking is associated with the accumulation of hydrogen at weak internal interfaces and under the action of a stress initiates cracking which can be delayed for some considerable hours after welding. Unfortunately however the interaction of hydrogen distribution and the role of stress have not been experimentally determined. In an attempt to determine the critical conditions for crack initiation a project utilising the rigid restraint cracking (RRC) test has been undertaken by the CRC for Materials Welding & Joining.

In order to develop a finite element analysis (FEA) model to predict cracking it is essential to determine the activity coefficients for hydrogen in the weld zone, ie, weld metal, HAZ and adjacent parent metal. A review of the literature showed that a considerable amount of information exists on hydrogen diffusion coefficients for steels but extremely little data exists for either diffusion coefficients or activity coefficients for weld metals[2]. It would be expected that, particularly because of the differences in oxygen content, and hence inclusion content, between different weld consumable types, substantial differences in activity coefficient could exist and at present limit data is available in the open literature[3]. The work reported here was thus initiated to establish and verify a methodology for the determination of weld metal hydrogen activity and establish values for weld metals used in the experimental RRC test program.

2.0 MATHEMATICAL METHOD OF EVALUATION OF HYDROGEN ACTIVITY COEFFICIENT

The method of evaluation of the hydrogen activity coefficient proposed in previous work[4] , based on steady-state diffusion, does not predict the actual distribution of hydrogen in real welds.

The use of samples approaching approximately 2 mm in thickness in this work simulates non-steady-state diffusion which better describes the distribution of hydrogen in real welds. The proposed method of determining the activity coefficient was based on electrochemical generation of hydrogen. Consider the instantaneous production of a maximum level of hydrogen at the sample surface which can be assumed to be a constant (C_o = constant) with a large concentration gradient.

Thus for Fick's second law of diffusion:

$$\frac{\partial C}{\partial t} = D \frac{\partial^2 C}{\partial x^2} \tag{1}$$

where D = constant.

Initial and boundary conditions are respectively:

$$C\,(x > 0, t = 0) = C_i = 0 \tag{2}$$

$$C\,(x = 0, t > 0) = C_o = \text{const.} \tag{3}$$

Using the Laplace transformation[5], equation (1) for the conditions (2) and (3) has the following solution:

$$C(x, t) = C_o \operatorname{erfc} \frac{x}{2\sqrt{Dt}} \tag{4}$$

where,

D - diffusion coefficient
C - hydrogen concentration
C_o - hydrogen concentration on specimen surface
t - diffusion time
x - distance

then,
$$\operatorname{erfc}(z) = 1 - \operatorname{erf}(z) \tag{5}$$

$$\operatorname{erf}(z) = \frac{2}{\sqrt{\pi}} \int_o^z \exp(-u^2)\, du \tag{6}$$

Hence, the mass of the hydrogen diffused into a specimen can be expressed as follows:

$$M(t) = \int_o^L C(x, t)\, dx \tag{7}$$

where, L - specimen thickness

In non-steady-state diffusion the total amount of hydrogen migrated into a specimen during time (t) is as follows[6]:

$$M(t) = 2 C_o \sqrt{\frac{Dt}{\pi}} \quad \text{per unit of diffusion surface area} \tag{8}$$

For a given diffusion surface area (A) equation (8) becomes:

$$M(t) = 2 A C_o \sqrt{\frac{Dt}{\pi}} \tag{9}$$

From equation (9) the diffusion coefficient is:

$$D = \frac{\pi}{4} \frac{M^2}{A^2 C_o^2 t} \tag{10}$$

The diffusion coefficient calculated in equation (10) is the result of a complex real process of transportation of hydrogen mass thus it can be consequently applied to the calculation of the actual hydrogen activity coefficient (γ) as well as to the simulation of the distribution of diffusible hydrogen in steel weldments. According to Yurioka et al[3], "from the condition of mathematical continuity in chemical potential or activity, equation (11) must be held regardless of hydrogen trapping portion and untrapped portion".[7]

$$D/\gamma = \text{constant} \tag{11}$$

Where γ is the activity coefficient representing occlusibility and diffusibility of hydrogen in steel.

Analysing equations in the work of Yurioka et al[3] the D/γ = const. becomes:

$$D/\gamma = \text{const.} = 0.14 \exp(-3200/RT) \quad (12)$$

where, $R = 1.9872$ cal/mol °K, and T°K .

The constant represents the diffusion coefficient for unstrained and pure iron without hydrogen trapping sites experimentally obtained by Johnson and Hill[8].

Analysis of equation (12) indicates that the activity coefficient (γ) is a dimensionless numerical value.

Substituting equation (10) into equation (12) one obtains:

$$\gamma = \frac{1}{0.14 \exp(-3200/RT)} \frac{\pi}{4} \frac{M^2}{A^2 C_o^2 t} \quad (13)$$

3.0 EXPERIMENTAL PROCEDURE

3.1 SAMPLE PREPARATION

AS1594-HA300 steel has been used to prepare samples for determining the activity coefficient (equ.13) of hydrogen in steel weldments. The chemical composition of this steel is shown in Table 1.

Table 1 - Chemical Composition of Steel (%)

C	P	Mn	Si	S	Ni	Cr	Mo	Cu	Al	Sn
0.185	0.014	0.78	0.015	0.014	0.028	0.022	0.007	0.029	0.044	0.004

The samples of parent metal, simulated HAZ and weld metal had dimensions 30 mm x 60 mm x 2 mm.

The single weld bead sample has been manually produced with AS1553.1 E4113, 5 mm electrodes and deposited on 8 mm thick HRS sample with a prepared groove of 14 mm width and 3 mm depth. The welding parameters were as follows: 300A, 27V, t = 3 mins 20 secs, and weld length of 450 mm.

The chemical composition of the weld metal is shown in Table 2.

Table 2 - Chemical Composition of Weld Metal (%)

C	P	Mn	Si	S	Ni	Cr	Mo	Cu	Al	Sn	Oxygen
0.080	0.010	0.50	0.10	0.007	0.018	0.031	0.009	0.007	0.005	0.004	0.0006

The HAZ samples have been heat treated using a HAZ simulator to a maximum temperature of 1250°C with a cooling time between 800 and 500°C of 90 sec and a total cooling time of 445 sec between 1250 and 100°C. All prepared samples were degassed at 400°C in an argon stream for not less than 6 hours to remove any hydrogen present in the samples prior to determining hydrogen permeability[9].

The samples were ground and finally polished using 8μm diamond paste. Some HAZ samples were strained by 2%, 3%, 5% and 6.5%.

3.2 HYDROGEN PERMEATION TEST

The samples were used to determine hydrogen permeability by an electrochemical method at a temperature of 20°C. The instrument PHERM MOD. HM403[10] for determination of hydrogen permeability consists of two circuits; one, to impose a cathodic current constant over the whole surface; and the other to reveal the current produced by the oxidation of hydrogen and the passivation of the exposed area at the exit surface.

The instrument contained two compartments: a detector compartment and a cell compartment (Figure 1)[10].

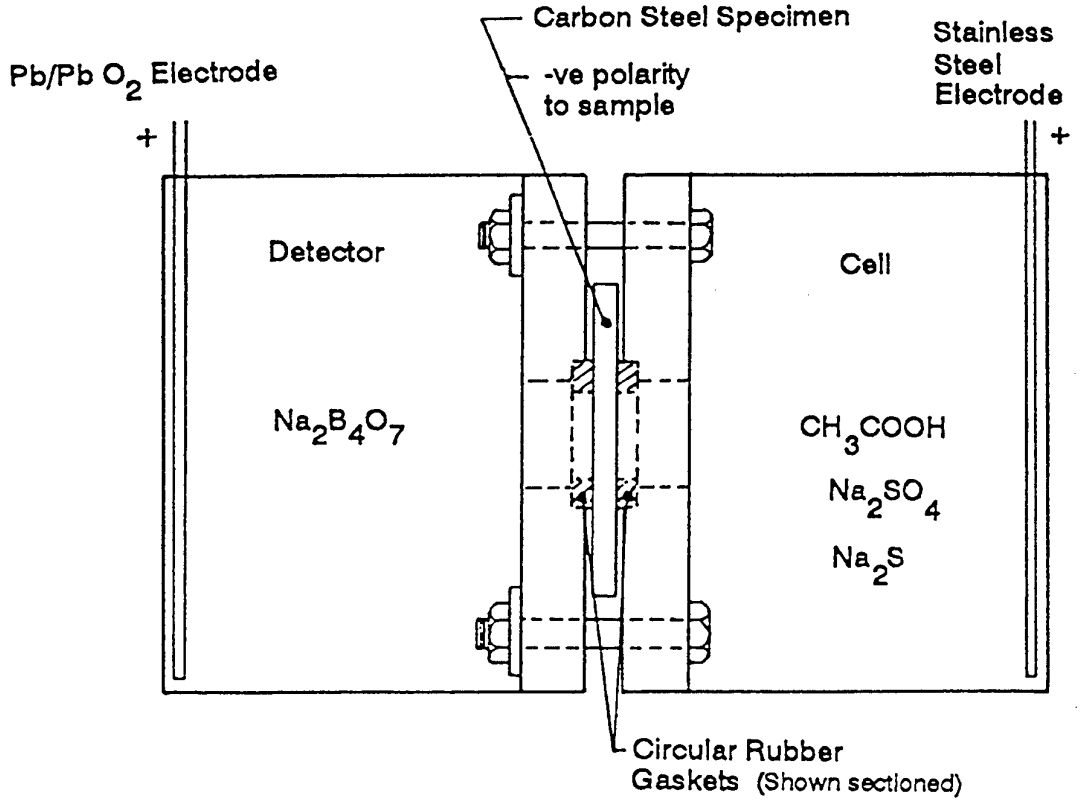

Figure 1: Electrolytic compartments of Atel Hyperm Model HM403.

The solution in the detector compartment constituted saturated borate of sodium $Na_2B_4O_7$ and the cell compartment contained CH_3COOH, Na_2SO_4, Na_2S with pH from 4 to 4.2. Analysis of hydrogen content in the samples after hydrogen permeation testing was carried out using Strohlein H-MAT 251 instrument. The H-MAT 251 is a hydrogen analyser for steel and other metals by fusion extraction or hot extraction in a carrier gas stream. Experimental results are shown in Table 3.

Table 3 - Experimental Results of Hydrogen Permeability in Steel

	Samples	Sample Area (mm^2)	Sample Thickness (mm)	Time (s)	Average Hydrogen (ppm)
		A	L	t	$\bar{C}$
	Parent Metal	226.98	1.79	150	0.33
AS1594-HA300	HAZ 0% Strained	226.98	0.86	31	2.37
	2%	226.98	1.80	235	0.96
	3%	226.98	1.80	288	1.32
	5%	226.98	1.75	377	1.87
	6.5%	226.98	1.79	472	2.45
	Weld Metal AS1553.1 E4113	164.0	1.90	204	1.23

4.0 EVALUATION OF HYDROGEN DIFFUSIVITY AND ACTIVITY COEFFICIENT

The kinetics of hydrogen entry into the steel samples and the experimental permeability results were used to determine the diffusion coefficient (D) and the activity coefficient (γ). The diffusion coefficient has been evaluated using equation (10) where the coefficient is given with respect to the hydrogen mass contained in steel samples, sample area exposed to hydrogen and hydrogen concentration on the sample entry surface.

$$D = \frac{\pi}{4} \frac{M^2}{A^2 C_o^2 t}$$

Where C_o was obtained from approximation of hydrogen distribution by the following equation:

$$C(x, t) = C_o \exp(-kx^n) \qquad (14)$$

where, t = const.
k = const.
$n = \frac{1}{2}$
$0 \leq x \leq L$

Hence: $C(x) = C_o \exp(-k\sqrt{x})$ (15).

when: $C(x = 0) = C_o = \text{const.}$
$C(x = L) = 0$

$$\int_0^L \bar{C}dx = \int_0^L C_o \exp(-k\sqrt{x})\,dx \;;\; \bar{C} \text{ - average hydrogen concentration} \quad (16)$$

$$\bar{C}\int_0^L dx = C_o \int_0^L \exp(-k\sqrt{x})\,dx = M \quad (17)$$

where: M - hydrogen mass migrated into the steel sample.

However, the hydrogen activity coefficient has been evaluated from equation (13) based on the parameters designated previously (C_o and M). The results of the evaluation are shown in Table 4.

Table 4 - Hydrogen Diffusivity and Activity Coefficient of Steel at 20°C

	Samples	C_o (g/mm^2)	M (g)	D (mm^2/s)	γ
AS1594-HA300	Parent Metal	0.267×10^{-12}	12.051×10^{-12}	2.07×10^{-4}	35.90×10^{-2}
	HAZ 0% Strained	1.917×10^{-12}	41.581×10^{-12}	2.31×10^{-4}	40.10×10^{-2}
	2%	0.777×10^{-12}	35.253×10^{-12}	1.34×10^{-4}	23.26×10^{-2}
	3%	1.068×10^{-12}	48.473×10^{-12}	1.09×10^{-4}	18.92×10^{-2}
	5%	1.513×10^{-12}	66.762×10^{-12}	7.87×10^{-5}	13.66×10^{-2}
	6.5%	1.982×10^{-12}	89.468×10^{-12}	6.58×10^{-5}	11.42×10^{-2}
	Weld Metal AS1553.1 E4113	0.995×10^{-12}	34.448×10^{-12}	1.72×10^{-4}	29.86×10^{-2}

The results of diffusion and activity coefficients for HAZ strained samples are shown on the graphs in Appendix A.

5.0 DISCUSSION

Evaluated diffusivity and activity coefficients in relation to the degree of steel deformation clearly show that the hydrogen diffusivity and activity coefficients fall with increasing deformation (refer Table 4 and Appendix A). These results indicate the same tendency and are in agreement with results of N Yurioka et al[3] [7] [8]. The results obtained in this work, as well as those obtained by N Yurioka et al, have been compared in Appendices B and C.

Certain small deviations arose from the differences of heat treatment temperatures of the HAZ samples (of this work 1250°C, and 1400°C for Yurioka's) and different cooling time between 800 and 500°C which was 90 sec for this work and 6.7 sec for Yurioka et al[3]. There are also differences in alloy element contents between the steels. The differences outlined above have apparently caused differences in the HAZ structures and consequently in the results for D and γ. The substantial differences in Mn content (1.4% - Yurioka samples and 0.78% in this work) have no significant influence on the hydrogen diffusion coefficient, because Böllinghaus et al[11] suggest the differences in Mn content up to the level of 3% do not change the hydrogen diffusivity in steel but could be expected to influence HAZ properties through the formation of different transformation products.

Publication[11] quotes the results for the hydrogen diffusion coefficients in micro alloyed and low carbon structural steels for austenitic decomposition structures: ferrite-pearlite, martensite (HAZ structures) ranging from 7×10^{-6} to 1.5×10^{-3} mm^2/s at 20°C. The comparative result in this work 2.31×10^{-4} mm^2/s at 20°C fits well into the above range.

Also Böllinghaus et al[11] discussed experimental results of many researchers which show that hydrogen diffusion coefficients in steel depend on cold working and applied stress from 2 to 5% and were within the range of 6×10^{-5} to 7×10^{-3} mm^2/s at 20°C. The experimental results of this work in the range of 7.87×10^{-5} to 1.34×10^{-4} mm^2/s at 20°C are in good agreement with those above.

6.0 CONCLUDING COMMENT

The results of this investigation have demonstrated that the diffusion coefficient (D) and activity coefficient (γ) for hydrogen in a weldment can be experimentally determined. The results for D and γ obtained in this work are in good agreement with those available in open literature and validate the methodology as a means of determining the weld metal coefficients. The values of $D = 1.72 \times 10^{-4}$ mm^2/sec and $\gamma = 29.86 \times 10^{-2}$ are thus considered representative of rutile weld metal at 20°C deposited under the conditions used in this work.

7.0 ACKNOWLEDGEMENTS

The authors thank their many colleagues who contributed to this work, especially the efforts of F Bararo and J Williams for discussion on the manuscript and L Brown in connection with setting up and carrying out the hydrogen measurements. The work was carried out as part of a project for the CRC for Materials Welding & Joining, established under the Cooperative Research Centres initiative of the Australian Commonwealth Government.

7.0 REFERENCES

[1] I F Squires, B Feng, D Mercer, W Payten, D Dunne, N Alam: WTIA 42nd National Welding Conference 1994 Melbourne, Volume 3, Paper 51.

[2] Th. Böllinghaus, H Hoffmeister, C Middel: "Scatterbands for Hydrogen Diffusion Coefficients in Low and High Alloyed Steels with and Austenite Decomposition Microstructure and High Alloyed Steels with an Austenite Microstructure at Room Temperature", IIW Document IX-1812-95.

[3] N Yurioka, S Ohshita, H Nakamura: "An Analysis of Hydrogen Accumulation at Weld Heat Affected Zone", Hydrogen in Metals Proceedings of Second JIM International Symposium, 1979.

[4] M Tchaikovsky: Report of BHP Steel - Slab & Plate Products Division, PK/TIC/95/063.

[5] J Crank: "The Mathematics of Diffusion", Oxford at the Clarendon Press, 1967.

[6] L Kalinowski, M Czajkowski: Mechanik, Nr 4-1976, (179-180).

[7] K Kohira, N Yurioka: IIW Document IX-951-76 (1976) (After [3]).

[8] K Kohira, T Yatake, N Yurioka: "Numerical Analysis of the Diffusion and Trapping of Hydrogen in Steel Weldments", IIW Document IX-951-76.

[9] Australian Standard AS3752-1990: Welding Methods for Determination of the Diffusible Hydrogen Content of Ferritic Weld Metal Produced by Arc Welding.

[10] ATEL, HYPERM Mod. HM403, Operation and Maintenance Manual.

[11] Th. Böllinghaus, H Hoffmeister, A Dongeleit: "A Scatterband for Hydrogen Diffusion Coefficients in Micro Alloyed and Low Carbon Structural Steels", IIW Document IX-1767-94.

APPENDIX A

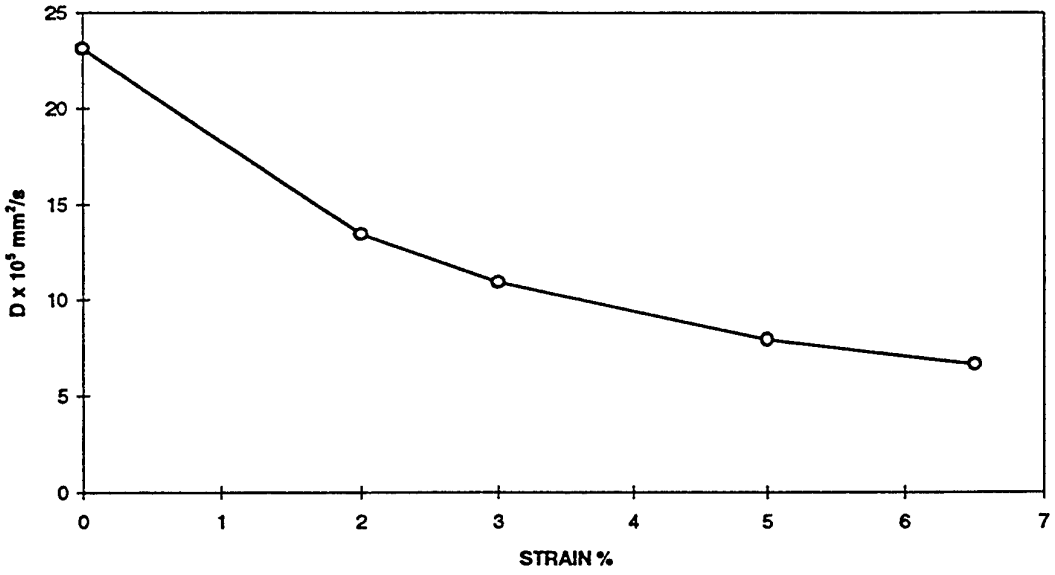

Figure A1: Hydrogen diffusivity in HAZ of AS1594-HA300 Steel at 20°C as a function of strain.

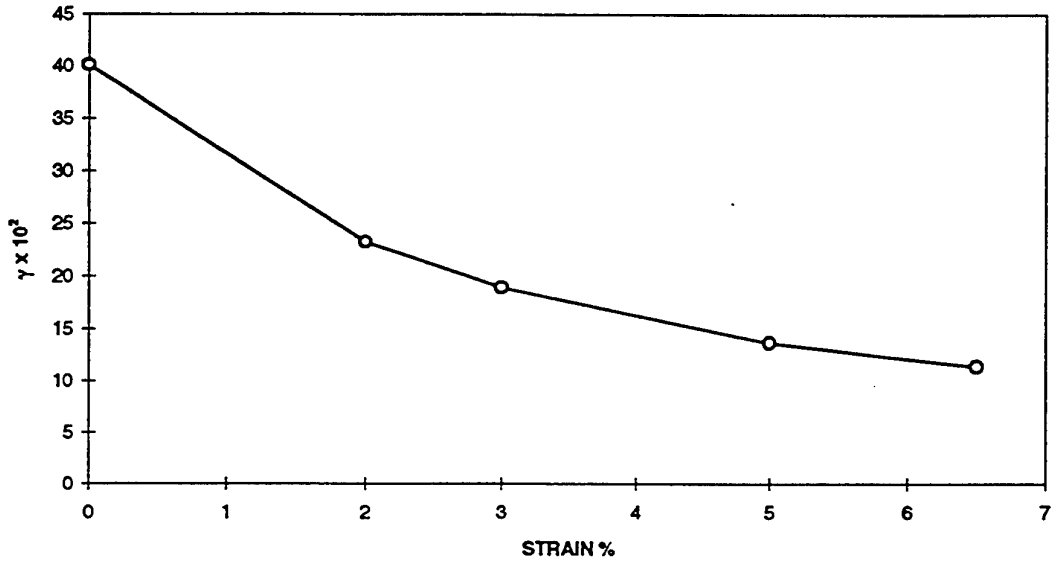

Figure A2: Hydrogen activity coefficient for HAZ of AS1594-HA300 Steel at 20°C as a function of strain.

APPENDIX B

Table B1 - Comparison of Hydrogen Diffusivity and Activity Coefficients for Weld Metal and HAZ at 20°C as a function of strain in this work with values calculated from the work of Yurioka et al[3].

Strain %	D mm^2/s		γ	
	AS1594-HA300	JIS SM50B*	AS1594-HA300	JIS SM50B**
HAZ 0% Strained	2.31×10^{-4}	1.8×10^{-4}	40.10×10^{-2}	31.50×10^{-2}
2%	1.34×10^{-4}	0.76×10^{-4}	23.26×10^{-2}	13.31×10^{-2}
3%	1.09×10^{-4}	-	18.92×10^{-2}	-
4%	-	5.6×10^{-5}	-	9.80×10^{-2}
5%	7.87×10^{-5}	-	13.66×10^{-2}	-
6%	-	4.4×10^{-5}	-	7.69×10^{-2}
6.5%	6.58×10^{-5}	-	11.42×10^{-2}	-
7%	-	4.0×10^{-5}	-	7.00×10^{-2}
Weld Metal AS1553.1 E4113	1.72×10^{-4}	1.6×10^{-4}	29.86×10^{-4}	26.72×10^{-2}

* The hydrogen diffusivity from [3]

** The hydrogen activity coefficients (γ) were evaluated from the date of reference[3] where:

R = 1.9872 cal/mol °K
T = 293.16 °K

APPENDIX C

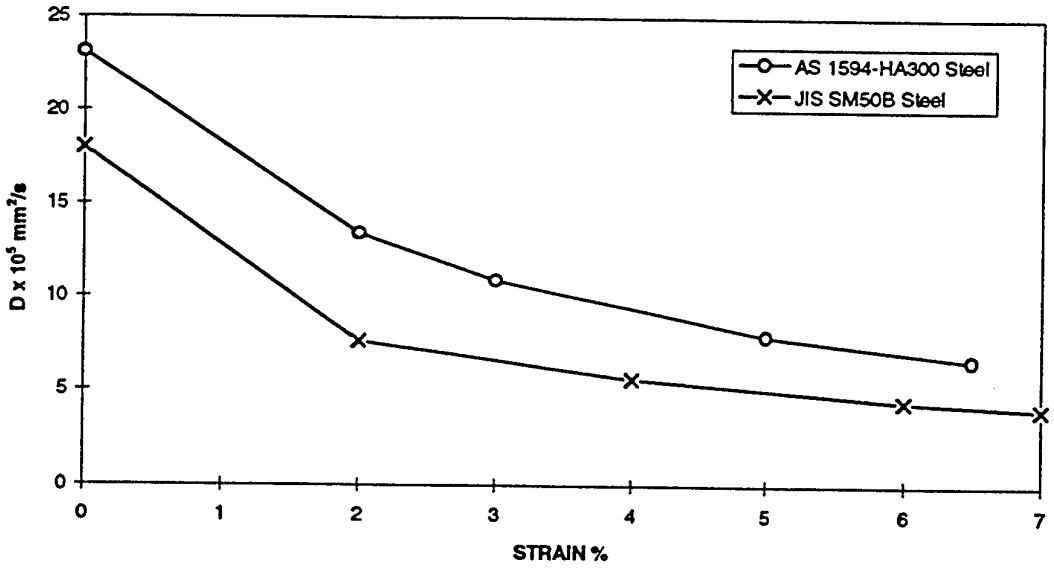

Figure C1: Comparison of Hydrogen Diffusivity in HAZ at 20°C as a function of strain in this work with the results of Yurioka et al[3]

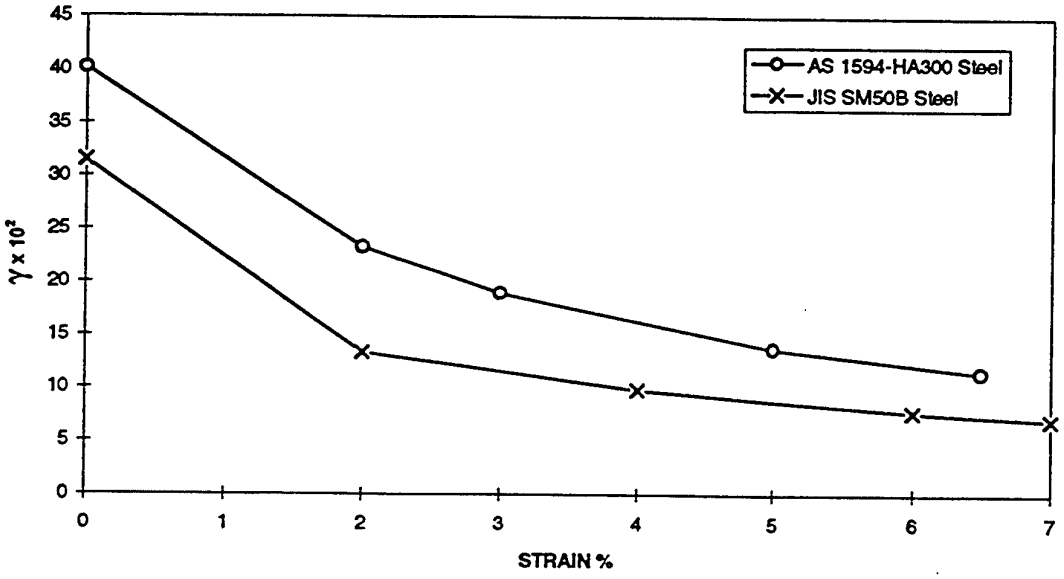

Figure C2: Comparison of Hydrogen Activity Coefficient for HAZ at 20°C as a function of strain in this work with values calculated from the work of Yurioka et al[3]

Hydrogen Measurement and Standardization

D.J. Kotecki

The Lincoln Electric Company

INTRODUCTION

For more than fifty years, the role of diffusible hydrogen in delayed cracking of weldments in carbon steels and low alloy steels has been recognized. It is well known that cracking is promoted by higher strength microstructures such as martensite, by higher stresses such as those imposed by welding in restrained heavy sections, and by higher levels of diffusible hydrogen. Shortly after recognition occurred, attempts at measurement of diffusible hydrogen and standardization of test methods began.

Diffusible hydrogen, however, is unlike other elements in steels, in that it is a transient element. Other interstitial elements, such as boron or nitrogen, remain in the steel awaiting analysis. Once a suitably sensitive and accurate method of analysis is developed, standard samples can be prepared and distributed to various laboratories, allowing for calibration of a particular laboratory's analytical procedure. But, because diffusible hydrogen is a transient, continually escaping from the steel even at temperatures below 0°C, it has not proven possible to prepare standard samples of accurately known diffusible hydrogen content. Therefore, calibration of diffusible hydrogen analytical procedures has proven to be a daunting task.

A second complicating factor in diffusible hydrogen measurement is the levels of interest. It is common today to express diffusible hydrogen measurements in units of milliliters per 100 grams of deposited weld metal. But in units more common in other chemical analysis of steel, 1 mL/100 g amounts to 0.892 ppm, or 0.0000892 weight percent. In order for a measurement to be meaningful in standardization, it must be reproducible from one laboratory to another. To put such measurement levels in perspective, it is instructive to consider interlaboratory reproducibility of measurement of other trace elements in steel welds. The Welding Institute has examined this (Ref. 1), and reports, for example, the interlaboratory reproducibility of boron measurement, at the level of approximately 10 ppm interlaboratory average, as about ± 2 ppm. This means that one laboratory could conceivably measure, for example, 8 ppm B, while another laboratory could measure 12 ppm B, on identical samples, and these two results could not be considered as different. Similar considerations need to be kept in mind when setting limits for diffusible hydrogen.

STANDARD METHODS FOR DEFINING LOW HYDROGEN ELECTRODES

There have been two basic approaches to setting limits for hydrogen-controlled electrodes. One has been to rapidly quench a single weld bead, then collect and measure the diffusible hydrogen as it escapes from the steel, which is applicable to a number of welding processes. The other has been to measure the potential for introducing diffusible hydrogen into the weld by determining the coating moisture content of covered electrodes.

In 1948, AWS Specification A5.5-48T (ASTM A316-48T) for low alloy steel electrodes defined a "low-hydrogen electrode" as one meeting a maximum limit of 0.1 cm^3 of gas collected per gram of deposited metal (10 mL/100 g, in units commonly used today for expressing diffusible hydrogen) when hydrogen from the quenched bead was collected over glycerin in an eudiometer. Shortly after this specification was published, however, doubt was cast (Ref. 2) on the suitability of glycerin as a hydrogen collecting medium because hydrogen and other gases are appreciably soluble in glycerin. By the 1954 revision of AWS A5.5, the glycerin test had disappeared from that specification. In the 1964 revision of that specification, a new definition of a low-hydrogen electrode was introduced, as one having no more than 0.6% coating moisture by weight, with lower limits for higher strength

electrode classifications. Coating moisture is determined by heating the coating sample in an oxygen stream at 980°C (1800°F), collecting the water that is evolved with anhydrous magnesium perchlorate, and determining the moisture by the weight gain of the magnesium perchlorate. This definition of low-hydrogen electrodes entered the nonmandatory appendix of the carbon steel electrode specification, AWS A5.1, in its 1969 revision, and entered the mandatory portion of the specification in the 1981 revision. It remains in both standards to this day.

Although the AWS abandoned assessing the low-hydrogen quality of electrodes by collection of hydrogen over glycerin, others took up this test. For example, the American Association of State Highway and Transportation Officials (AASHTO) adopted the glycerin test for their *Guide Specifications for Fracture Critical Non-Redundant Steel Bridge Members*. The U.S. Navy adopted it for defining low-hydrogen flux cored wires in MIL-E-24403. The glycerin test for assessing low-hydrogen electrode quality became a Japanese standard (JIS Z3113) also.

Beginning about 1956, Commission II of the International Institute of Welding (IIW) undertook (Ref. 3) to develop a standardized test for determining diffusible hydrogen from steel covered electrodes using collection of hydrogen over mercury. Mercury has virtually no solubility for hydrogen or any of the atmospheric gases. After much evolution and testing, the "IIW method" was adopted as an international standard (ISO 3690) in 1977. Due to fear of the toxicity of mercury vapor, the IIW test method evolves hydrogen from the test specimen in a sealed Y-tube at about 25°C. In order to obtain nearly complete diffusible hydrogen release in a reasonable time period (three days), small test specimens are employed (30 mm long by 15 mm wide by 10 mm thick). The standard also provides for sub-dividing the 30 mm specimen length into two 15 mm pieces, or into four 7.5 mm pieces to speed hydrogen release. A run-on piece and a run-off piece are included in the test assembly, but are broken off when the assembly is chilled to -78°C, or colder, after iced water quenching, and are discarded before analysis takes place. The assembly is tightly clamped in a copper fixture, which serves as a heat sink to prevent specimen overheating during welding. Figure 1 shows the test assembly and fixture of ISO 3690.

Recently, Commission II of the IIW have prepared a draft revision (Ref. 4) of ISO 3690 which provides for re-orienting the test piece so that the method can be extended to GMAW, SAW, and FCAW. In this modification, the central test piece is oriented with its 30 mm dimension as the width, and its 15 mm dimension as the length. Then the run-on and run-off pieces are appropriately widened and lengthened to accommodate the higher heat input of these additional welding processes. The revision calls for adjusting the welding travel speed to obtain a deposit weight on the central test piece of 4.0 g (± 0.5 g) to improve interlaboratory reproducibility. For this reorientation, a new, larger copper fixture is necessary, as shown in Figure 2. Since three days at 25°C as the reference method has not proven to release all diffusible hydrogen from the central test piece, hydrogen evolution is now required to be carried out until there is no change in the quantity collected from one day to the next. In practice, this often means a total evolution time at 25°C of 14 to 21 days. Use of higher evolution temperature, and of alternate equipment such as a gas chromatograph, are allowed so long as the variant is shown to correlate to the reference method. While this draft revision of ISO 3690 has not yet been approved by ISO, an agreement has been reached with the relevant Committee for European Standardization (CEN TC121) over the details of the revision, and approval seems likely.

The Filler Metal Committee of the American Welding Society followed development of the draft revision of ISO 3690 in IIW Commission II, while re-examining its own position regarding definition of low hydrogen electrodes (Ref. 5). After round robin examination of glycerin testing following the

method of JIS Z3113, the Filler Metal Committee decided against that avenue due to the observation that the glycerin test measures zero diffusible hydrogen when the IIW method is still finding low levels of diffusible hydrogen. Instead, it concluded that collection of hydrogen over mercury, or in a gas chromatograph, was more suitable since these methods do not lose part of the diffusible hydrogen as the glycerin method does. However, the Filler Metal Committee was not satisfied with the small specimen size of the IIW draft method because it resulted in very small hydrogen volume with very low hydrogen consumables, and because it required an arbitrary decision about when to re-orient the central test piece for higher heat input welding (Ref. 5). Instead, a test specimen 80 mm long by 25 mm wide by 12 mm thick, more like that of JIS Z3113, with run-on and run-off pieces that could be broken off and discarded, was chosen for the AWS method (Ref. 6). Figure 3 shows the weld test assembly and welding fixture of ANSI/AWS A4.3.

To speed diffusible hydrogen evolution using its method, the AWS standard provided for evolution of hydrogen at 45°C for 72 hours, or at 150°C for 6 hours. Due to the hazards associated with heated mercury, the 150°C hydrogen evolution is probably only applicable to gas chromatography. These two time-temperature combinations were shown to produce equal results. And comparison of gas chromatograph results with collection over mercury results showed no difference between the two analytical techniques with the AWS method (Ref. 5).

Meanwhile, the Japanese standard, JIS Z3113, has been replaced by JIS Z3118, which includes SMAW, GMAW, FCAW, and SAW consumables, and allows for analysis by gas chromatography or collection over glycerin. Glycerin collection is only allowed for consumables providing at least 2 mL/100 g by this method, and Equation 4, above, is used to convert the glycerin results to IIW (gas chromatography) values, which are considered as the reference values. JIS Z3118 provides for copper fixtures, run-on and run-off pieces which are broken off and discarded, and rapid quenching after welding. It provides for use of four center test piece sizes, including the 30 by 15 by 10 mm IIW/ISO 3690 size, the 80 by 25 by 12 mm AWS size, a 40 by 25 by 12 mm size, and a 100 by 25 by 12 mm size (the latter for glycerin only, while the first three are for gas chromatography only).

REPRODUCIBILITY OF LOW HYDROGEN ELECTRODE DETERMINATION

An axiom of measurement is that the results of measurement must be reproducible from one laboratory to another. For the present discussion, it is essential that there can be assurance of agreement concerning the low hydrogen quality of a given lot of welding consumables among the electrode producer, the electrode user (fabricator), the contractor responsible for the overall engineering project, and any oversight authority such as an insurance company, safety agency, or government office. A common means of assessing reproducibility of measurement is by round robin testing. There have been many round robin tests in which welding consumables from a particular lot were distributed to several laboratories, each of which were then asked to conduct a given test for low hydrogen quality following a standardized procedure, and report the results to a central point for evaluation. Then reproducibility of the test can be assessed by examining the interlaboratory standard deviation of the results, especially as compared to the interlaboratory mean value. A most useful comparison is the percent variability (% Var.), usually defined as twice the standard deviation, multiplied by 100, and divided by the interlaboratory mean value. Then better reproducibility means a smaller percent variability.

Reproducibility of coating moisture determination was examined in an AWS round robin (Ref. 7). There were two parts to this round robin - coating moisture as-manufactured, and coating moisture after exposure in a commercial moving air humidity cabinet for 9 hours to 80% relative humidity and 27°C (80°F). The first part of the round robin evaluated the reproducibility of the coating moisture test alone, while the second part examined the combination of the exposure test and the coating moisture test. Table 1 summarizes the results. It can be seen that the reproducibility of the coating moisture test alone is much better than the reproducibility of the combination of exposure and coating moisture test.

Table 1. AWS Round Robin of Coating Moisture Tests

	Part 1 - Coating Moisture, %, of Electrodes As-Manufactured						
Lab	MRA	MRB	MRC	MRD	X	Y	Z
1	0.019	0.033	0.047	0.048	0.086	0.425	0.220
2	0.074	0.054	0.083	0.108	0.104	0.432	0.238
3	0.070	0.060	0.073	0.113	0.110	0.380	0.257
4	0.065	0.062	0.087	0.104	0.084	0.411	0.215
5	0.040	0.040	0.100	0.100	0.073	0.357	0.197
Avg.	0.054	0.050	0.078	0.095	0.091	0.401	0.225
SD	0.021	0.011	0.018	0.024	0.014	0.028	0.020
% Var.	78.2	45.7	45.5	50.1	29.8	14.1	18.2
	Part 2 - Coating Moisture, %, of Electrodes after Exposure						
Lab	MRA	MRB	MRC	MRD	X	Y	Z
1	0.075	0.059	0.034	0.032	0.154	1.540	1.015
2	0.197	0.153	0.133	0.217	0.300	3.163	2.493
3	0.393	0.303	0.167	0.420	0.577	3.940	4.030
4	0.345	0.356	0.215	0.353	0.615	3.776	3.757
5	0.230	0.175	0.165	0.265	0.245	2.955	2.155
Avg.	0.248	0.209	0.143	0.257	0.378	3.075	2.690
SD	0.113	0.107	0.060	0.133	0.184	0.851	1.101
% Var.	90.7	102.3	84.6	103.1	97.4	55.3	81.9

Reproducibility of glycerin testing along the lines of JIS Z3113 (or Z3118) was examined by the AWS Task Group on Hydrogen in 1983 (Ref. 8). With electrodes producing an interlaboratory average value of 3.3 mL/100 g, the interlaboratory standard deviation was 0.88 mL/100 g and the percent variability was 53%.

In 1982, The Welding Institute completed a study (Ref. 1) of interlaboratory reproducibility of diffusible hydrogen measurements from covered electrodes. Five laboratories participated, using the method of ISO 3690 (full 30 mm specimen length), with hydrogen evolution carried out to fourteen days to assure complete evolution of hydrogen and improve reproducibility of measurement. The results, with electrodes averaging diffusible hydrogen of about 10 mL/100 g of deposited metal, showed an interlaboratory reproducibility (average of three tests per laboratory) of about ± 1 mL/100 g.

In 1984, the AWS Task Group on Hydrogen conducted a series of round robins of diffusible hydrogen measurements with SMAW electrodes, GMAW wires, FCAW wires, and SAW consumables, all producing diffusible hydrogen in the vicinity of 5 mL/100 g of deposited metal. Each round robin produced an inter-laboratory standard deviation of diffusible hydrogen measurement of about 1 mL/100 g (Ref. 5). All of the above examinations of reproducibility of diffusible hydrogen testing compare favorably with the reproducibility of measurement for other trace elements in steel (Ref. 1).

CORRELATIONS AMONG VARIOUS TESTS FOR LOW HYDROGEN FILLER METALS

Since there are at least four means of assessing low hydrogen electrode quality, it is useful to understand correlations among them. In three separate studies, the method of ANSI/AWS A4.3 was shown to produce results virtually identical to those of the method of the IIW draft standard or the present ISO 3690 (Ref. 5). So it can safely be said that:

$$H_{AWS} = H_{IIW} \quad (1)$$

where H_{AWS} is the diffusible hydrogen measured using the method of ANSI/AWS A4.3, and H_{IIW} is the diffusible hydrogen measured using either the method of ISO 3690 or of the IIW draft revision of ISO 3690, both measurements expressed in mL/100 g of deposited metal.

The Japanese have conducted at least three studies of correlation between the glycerin test used in JIS Z3113 (or Z3118) and the mercury or gas chromatography method of the IIW draft or of ISO 3690. Each produced a correlation equation:

(Ref. 9) $$H_{GL} = 0.64\ H_{IIW} - 0.93 \quad (2)$$

(Ref. 10) $$H_{GL} = 0.67\ H_{IIW} - 0.8 \quad (3)$$

(Ref. 11) $$H_{GL} = 0.79\ H_{IIW} - 1.73 \quad (4)$$

where H_{GL} is the diffusible hydrogen, mL/100 g of deposited metal, measured with the method of JIS Z3113 (or Z3118). Note that all of these correlations indicate that the method of JIS Z3113 (Z3118) does not collect all of the diffusible hydrogen that the method of ISO 3690 collects. While these three correlations look different, plotting them, as is done in Figure 4, reveals that, over the range of interest in low hydrogen electrodes, there is little or no significant difference among the three correlations. At most, the differences are within the scatter of experimental error.

The Japanese have also examined the correlation between coating moisture and diffusible hydrogen for E7018-type electrodes. Included in the Japanese study (Ref. 14) were as-manufactured coating moisture, moisture picked up during exposure, and atmospheric moisture at the time of welding which finds its way into the arc. The correlation obtained is as follows:

$$H_{IIW} = [260\ a_1 + 30\ a_2 + 0.9\ b - 10]^{1/2} \quad (5)$$

where a_1 is the as-manufactured coating moisture weight percent, a_2 is the weight percent coating moisture picked up by exposure, and b is the partial pressure of water vapor (mm Hg) in the air at the time of welding. If the electrode has not been exposed, then a_2 is zero and the second term on the

right side of Equation 5 drops out. The AWS Task Group on Hydrogen collected data during some of its round robin work, where the atmospheric moisture at time of welding was about 10 mm Hg partial pressure, and the E7018 electrode coating moisture was adjusted by varying the final bake temperature of the electrodes (Ref. 5). Then these as-manufactured coating moisture data versus diffusible hydrogen could be examined, as shown in Figure 5, along with Equation 5 above. Figure 5 shows that the Japanese equation rather well reflects the experimental data up to a coating moisture of about 0.3%, but appears to understate the effect of coating moisture above 0.3%.

The Japanese study and Equation 5 indicate that moisture picked up by electrode exposure is less effective at introducing diffusible hydrogen into the weld metal than is the as-manufactured moisture. This seems reasonable in view of the fact that as-manufactured coating moisture is likely to be distributed uniformly throughout the coating, while moisture picked up on exposure is likely to be concentrated on the coating surface. Evans (Ref. 13) provided data, shown in Figure 6, to the AWS Task Group on Hydrogen, which demonstrated that this is the case. Electrodes were progressively dried at higher and higher temperatures, sampling diffusible hydrogen after each baking temperature to generate the "On Drying" part of the curve, until a very dry condition was achieved. Then these very dry electrodes were progressively exposed to pick up more and more moisture, sampling diffusible hydrogen after various exposures to generate the "On Exposure" part of the curve.

Equation 5 points out the fact that there is an effect of atmospheric moisture at the time of welding upon the measured diffusible hydrogen with a covered electrode. As a result of this observation, the AWS specifies a reference atmospheric condition for welding the diffusible hydrogen test specimens. This is 1.43 grams of water per kilogram of dry air, or a moisture partial pressure of 1.735 mm Hg. A diffusible hydrogen test piece must be welded at or above this condition and satisfy the requirement. In practice, it is often found that welding for the diffusible hydrogen test in summer months must be done in an air conditioned room to bring the atmospheric moisture down to near this level to satisfy requirements for very low hydrogen electrodes.

BENCHMARKS FOR LOW HYDROGEN FILLER METALS

Benchmarks are useful in classifying filler metals, and in selecting appropriate preheat and welding heat input for a given base metal and restraint condition. It is logical to expect benchmarks to be realistic in terms of the state of the art of producing filler metals commercially, and to expect different benchmarks to indicate significant differences in low hydrogen quality. It is useful to consider these various benchmarks as regards reproducibility of measurement among laboratories and as regards significance of differences in consumable quality.

Table 2 lists the basic coating moisture limits for covered electrodes of various strength levels in ANSI/AWS A5.1-91 (carbon steel electrodes) and A5.5-96 (low alloy steel electrodes). Some more stringent limits are also used in these standards.

Table 2. Coating Moisture Limits (As-Manufactured) for Low Hydrogen Electrodes, versus Weld Metal Strength Levels in ANSI/AWS A5.1 and A5.5

ANSI/AWS Standard	A5.1	A5.5	A5.5	A5.5
Minimum Tensile Strength, ksi (MPa)	70 (480)	70 (480)	80 (550)	90 (620)
Maximum Coating Moisture, weight %	0.6	0.4	0.2	0.15

With the test of ISO 3690, IIW Commission II defined a "hydrogen controlled electrode" as one providing no more than 15 mL of diffusible hydrogen per 100 g of deposited metal. Further, Commission II recommended (Ref. 3) a linear system of benchmarks of no more than 15 mL/100 g of deposited metal ("medium hydrogen"), no more than 10 mL/100 g ("low hydrogen"), and no more than 5 mL/100 g ("very low hydrogen"). In contrast to the AWS coating moisture benchmarks in Table 2, the IIW benchmarks are not directly connected to weld metal strength level. Besides weld metal strength, base metal hardenability, restraint, and preheat need to be taken into account before deciding upon a safe diffusible hydrogen level.

The AWS (Ref. 5) examined considerable data correlating diffusible hydrogen levels with critical cracking stress, critical preheat temperature, and the like, for avoiding hydrogen cracking. These data showed linear correlations with the logarithm of the diffusible hydrogen content of the weld metal, not with the diffusible hydrogen level itself. Figure 7 (Ref. 15), from implant test results, shows one such correlation. This suggested that a system of benchmarks based upon equal increments in the logarithm of the diffusible hydrogen content was more logical and useful than the IIW system based upon equal increments in the numerical diffusible hydrogen content. This logarithmic approach is also supported by Yurioka and Kasuya (Ref. 14). At the present time, the AWS benchmarks for diffusible hydrogen, as given in ANSI/AWS A5.1-91 (mild steel covered electrodes), ANSI/AWS A5.5-96 (low alloy steel covered electrodes), ANSI/AWS A5.18-93 (mild steel GMAW wires), ANSI/AWS A5.20-95 (mild steel flux cored wires), and ANSI/AWS A5.23-90 (low alloy steel SAW wires and fluxes), are no more than 16.0 mL/100 g ("H16"), no more than 8.0 mL/100 g ("H8"), and no more than 4.0 mL/100 g ("H4"). As with the IIW system, any of these benchmarks can be attached to any low hydrogen consumable, depending upon successful test results, without regard to strength level of the weld metal. Revisions of ANSI/AWS A5.17 (mild steel SAW wires and fluxes), ANSI/AWS A5.28 (low alloy steel GMAW wires), and ANSI/AWS A5.29 (low alloy steel flux cored wires) are in process, which will include these same diffusible hydrogen benchmarks. Consideration is being given by AWS to including the next lower benchmark (no more than 2.0 mL/100 g, or "H2") in appropriate filler metal standards.

The Japanese electrode classification standards, JIS Z3211 for mild steel electrodes, and JIS Z3212 for high tensile strength electrodes, establish a single maximum diffusible hydrogen limit for each tensile strength level, more like the AWS coating moisture benchmarks, and unlike the IIW and AWS diffusible hydrogen benchmarks. These limits are given in Table 3. Limits for diffusible hydrogen are not established for classifying consumables other than covered electrodes by the Japanese standards.

Table 3. Diffusible Hydrogen Limits versus Deposited Weld Metal Minimum Strength Level in JIS Z3211 (Mild Steel Electrodes) and JIS Z3212 (Low Alloy High Strength Steel Electrodes)

JIS Standard	Z3211	Z3212	Z3212	Z3212	Z3212	Z3212	Z3212
Minimum Tensile Strength, MPa	420	490	520	570	610 & 690	750	780
Maximum Allowable Diffusible Hydrogen, mL/100 g Deposited Metal	15	15	12	10	9	7	6

The U.S. Military standard MIL-E-22200/10C (SH) sets classification benchmarks for covered electrodes for high tensile steels as 0.10% coating moisture as-manufactured, 0.20% coating moisture after exposure for 9 hours to 27°C air at 80% relative humidity, and diffusible hydrogen limits

(measured by ANSI/AWS A4.3) of 3.5 mL/100 g deposited metal for electrodes of 4.0 mm diameter and larger, 3.2 mL/100 g for electrodes of 3.2 mm diameter and smaller. On the other hand, both ANSI/AWS A5.1-91 and ANSI/AWS A5.5-96 set exposed coating moisture limits for moisture resistant electrodes at 0.4% maximum, in view of the larger scatter in round robin testing of exposed electrode coating moisture (Part 2 of Table 1) as compared to as-manufactured coating moisture.

DISCUSSION

There are two aspects to determination of low hydrogen welding consumable quality that are of interest from the viewpoints of measurement and standardization. These are the measurement method itself, and the benchmarks used for assessment of quality.

The measurement of weld metal diffusible hydrogen, for electrode quality purposes, seems to have reached a desirable situation where the reference method can be considered to be the IIW method, and the AWS methods and the JIS gas chromatography method, despite using different test piece sizes, arrive at essentially the same result. So a diffusible hydrogen test, performed using any of these methods, can be directly related to the other methods, on a one-to-one basis. However, the effect of atmospheric moisture at the time of welding needs to be taken into account. The AWS system has introduced a reference atmospheric condition (1.43 g of water vapor per kg of dry air), at or above which the welding must be conducted for the diffusible hydrogen test. The IIW draft standard (Ref. 4), proposed to revise ISO 3690, now includes a reference atmospheric condition also, but it is 3 g of water vapor per kg of dry air. This could require humidification of the air in cold climates during winter, as well as requiring air conditioning in warm humid climates. While the difference in reference atmospheric conditions between IIW and AWS is not major, it is a difference. The ANSI/AWS A4.3 standard allows welding at above 3 g of water vapor, provided that the electrode meets the requirements for diffusible hydrogen.

The proliferation of numerous benchmarks for assessing low hydrogen electrode quality leaves a confused situation. In view of the interlaboratory reproducibility of measurement of as-manufactured coating moisture, exposed coating moisture, or diffusible hydrogen, the proliferation of so many benchmarks seems unrealistic. It is clearly not possible to state with any certainty that a given electrode meets a limit of 3.5 mL/100 g deposited metal, but does not meet 3.2 mL/100 g, as is proposed by the U.S. MIL-E-22200/10C (SH) standard, since the reproducibility of the diffusible hydrogen test is no better than ± 1 mL/100 g. It is also not realistic to state that a given electrode meets 10 mL/100 g but does not meet 9 mL/100 g, as is proposed by the JIS Z3212 standard. The seven benchmarks of the JIS system shown in Table 3, which span a smaller range of diffusible hydrogen values than either the three benchmarks of the IIW system or the three benchmarks of the AWS system, seem to be an unnecessary and unrealistic complication of the situation, especially in view of the fact that many electrodes are used to weld base metals of non-matching strength. As a practical matter, in the manufacture of low hydrogen electrodes, the manufacturer uses the same coating binder and minerals, and the same bake schedule, for electrodes of 480 MPa minimum tensile strength as for electrodes of much higher minimum tensile strength. Then the weld metal diffusible hydrogen which results will be indistinguishable, and the electrodes will meet the same benchmark. Therefore, reducing the number of benchmarks will not be a hardship for the electrode manufacturer.

Furthermore, it is not possible to state with much certainty that an electrode meeting the IIW benchmark of 15 mL/100 g is really different from an electrode meeting the AWS H16 benchmark,

nor that an electrode meeting the IIW benchmark of 5 mL/100 g is really different from an electrode meeting the AWS H4 benchmark. On the other hand, an electrode meeting the IIW benchmark of 10 mL/100 g could be very likely be different from one meeting the AWS H8 benchmark. In view of the numerous linear relationships between various crack susceptibility measures and the logarithm of the diffusible hydrogen content, the AWS logarithmic system of hydrogen benchmarks seems more logical than the IIW linear system of hydrogen benchmarks. It is also more amenable to logical extension to lower diffusible hydrogen limits (e.g. H2) than is the IIW linear system, if the quality of consumables and the reproducibility of measurement can be shown to warrant this extension. It is the opinion of this writer that the logarithmic system of benchmarks, with three, or, at most, four benchmarks, is the most appropriate in view of the technology of diffusible hydrogen damage and in view of the reproducibility of diffusible hydrogen tests.

By using Figures 4, 5, and 6, it is possible to make approximate correlations among several benchmarks, which can put some of these benchmarks in perspective. For this examination, the IIW method is considered the reference method, and is taken to be equal to the AWS methods or the gas chromatography method of JIS Z3118. Table 4 makes these correlation attempts. It is possible to argue with any given specific correlation, but the approximate correlations seem reasonable in view of the figures and in view of the interlaboratory reproducibility of the various methods.

Table 4. Correlations among Various Benchmarks for Classifying Low Hydrogen Welding Consumables

Benchmark	Correlation by:	H_{IIW}, mL/100 g Deposited Metal
0.6% Coating Moisture	Figure 5	15 or 16
0.4% Coating Moisture	Figure 5	8, 9, or 10
0.2% Coating Moisture	Figure 5	6, 7, or 8
0.15% Coating Moisture	Figure 5	5 or 6
0.10% Coating Moisture	Figure 5	3, 4, or 5
10 mL/100 g by Glycerin	Figure 4	15 or 16
5 mL/100 g by Glycerin	Figure 4	8, 9, or 10
0.4% Coating Moisture after Exposure	Figure 6	6, 7, or 8
0.20% Coating Moisture after Exposure	Figure 6	5 or 6

The round robin test results of Table 1, Part 2, indicate that the U.S. MIL-E-22200/10C (SH) coating moisture limit of 0.20% after exposure seems very unrealistic. With each of the four electrodes generally considered to be moisture resistant (MRA, MRB, MRC, and MRD), at least one of the five participating laboratories would conclude that the electrode failed the test, and at least one laboratory would conclude that the electrode passed the test. One laboratory would pass all four electrodes, and one laboratory would fail all four electrodes. From this data, it would seem to be nearly impossible for one laboratory (e.g. a shipyard) to consistently verify the certification of another laboratory (e.g. an electrode producer) that a given lot of electrodes met the requirement. The AWS limit of 0.4% coating moisture for a moisture resistant electrode seems much more realistic, considering the reproducibility of the combination of the exposure test variability and the coating moisture test variability. It is also unrealistic to expect an electrode to meet the same benchmark both before and

after exposure, unless the electrode is initially much lower in diffusible hydrogen than the as-manufactured benchmark suggests.

CONCLUSION

Internationally, standardization of measurement for assessing the low hydrogen quality of welding consumables has made great strides in the past ten years. However, corresponding standardization of diffusible hydrogen benchmarks internationally has not taken place. The proliferation of numerous benchmarks seems to reflect a lack of appreciation for the reproducibility of measurement. Standardization on three, or, at most four, benchmarks, preferably based upon a logarithmic scale, seems most appropriate.

REFERENCES

1. The Welding Institute, September, 1982. The measurement of diffusible hydrogen in manual metal arc weld deposits. A study group report. Project 9327.
2. Stern, I.L., Kalinsky, J., and Fenton, E.A. 1949. Gas evolution from weld metal deposits. *Welding Journal* 28(9):405s-413s.
3. Coe, F.R. 1986. Hydrogen measurements - current trends versus forgotten facts. *Metal Construction* 18(1):20-25.
4. Commission II of the International Institute of Welding, *IIW Document II-1055-91 (revised November, 1995)*, The determination of the hydrogen content of ferritic arc weld metal (draft revision of ISO 3690). International Institute of Welding, Paris.
5. Kotecki, D.J. 1992. Hydrogen reconsidered. *Welding Journal* 71(8):35-43.
6. ANSI/AWS A4.3-93. 1993. Standard methods for determination of the diffusible hydrogen content of martensitic, bainitic, and ferritic weld metal produced by arc welding. American Welding Society, Miami, Florida.
7. Minutes of the AWS A5 Committee meeting of 10-11 March, 1987. American Welding Society, Miami, Florida.
8. Kotecki, D.J., and LaFave, R.A. 1985. AWS A5 Committee studies on weld metal diffusible hydrogen. *Welding Journal* 64(3):31-37.
9. Coe, F.R. 1972. The comparison of hydrogen levels. *IIW Document II-A-305-72.* The International Institute of Welding, Paris.
10. Japan Welding Engineering Society. 1974. Relation between hydrogen contents by IIW and JIS methods. *IIW Document II-698-74.* International Institute of Welding, Paris.
11. Japan Welding Engineering Society. 1986. Method of measurement for hydrogen evolved from steel welds. *IIW Document II-1073-86.* International Institute of Welding, Paris.
12. Hirai, Y., Minakawa, S., and Tsuboi, J. 1980. Prediction of diffusible hydrogen content in deposited metals with basic type covered electrodes. *IIW Document II-929-80.* International Institute of Welding, Paris.
13. Evans, G.M. 1982. Report of 30 August, 1982 to AWS A5A Task Group on Hydrogen.
14. Evans, G.M., and Christensen, N. 1971. Correlation of weld metal hydrogen content with HAZ embrittlement. *British Welding Journal* 3:188-189.
15. Yurioka, N., and Kasuya, T. 1994. A chart method to determine necessary preheat in steel welding. *IIW Document II-1230-94.* The International Institute of Welding, Paris.

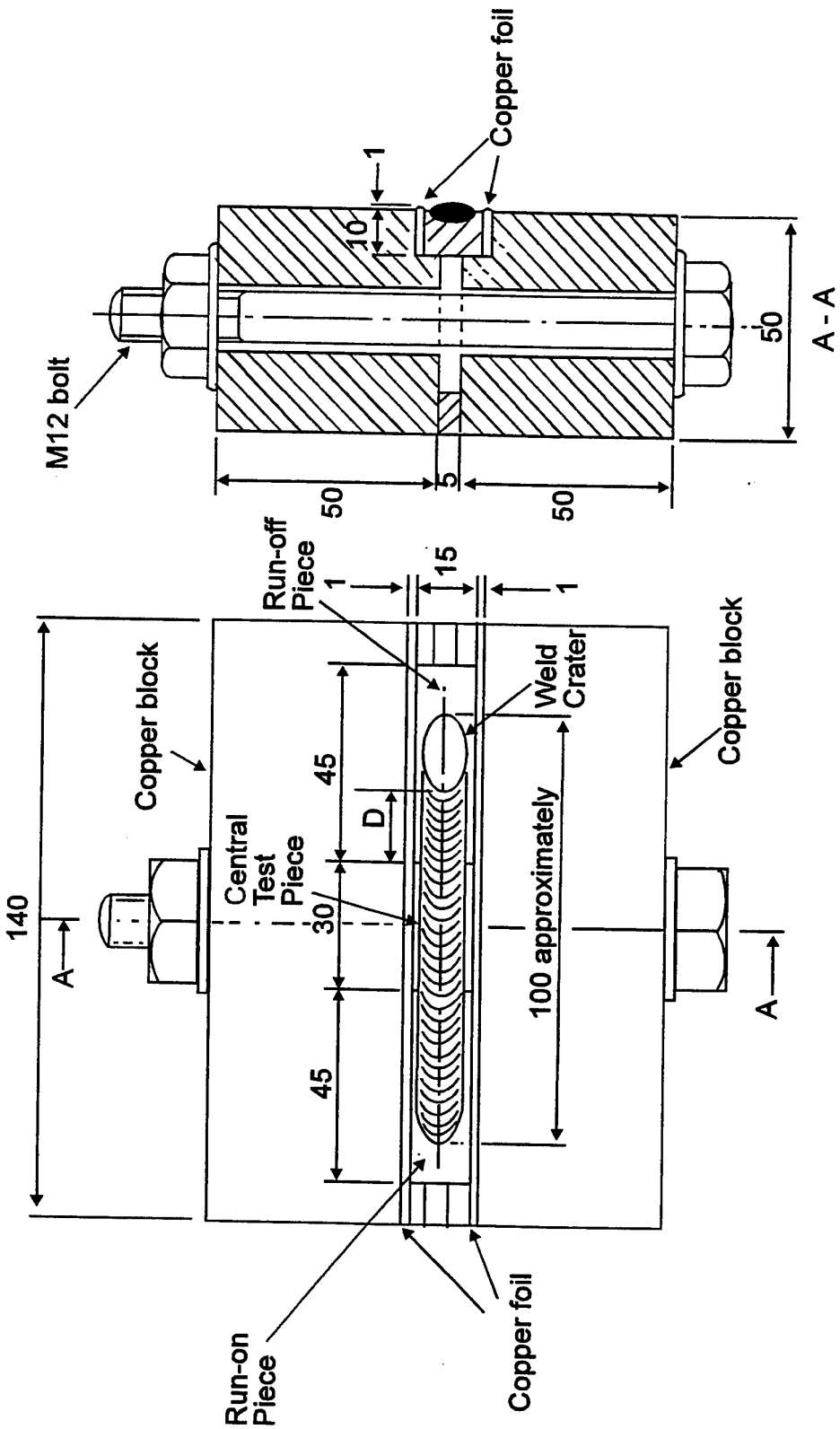

All dimensions are in millimeters. Distance D not more than 25mm
NOTE 1. Water cooling channels may be used.
NOTE 2. Overall weld traverse length is 100mm.
NOTE 3. The weld test assembly consists of the run-on piece, the central test piece, and the run-off piece.

Fig. 1 Welding fixture and testpiece assembly for weld deposits made with energy inputs up to 2.0 kJ/mm.

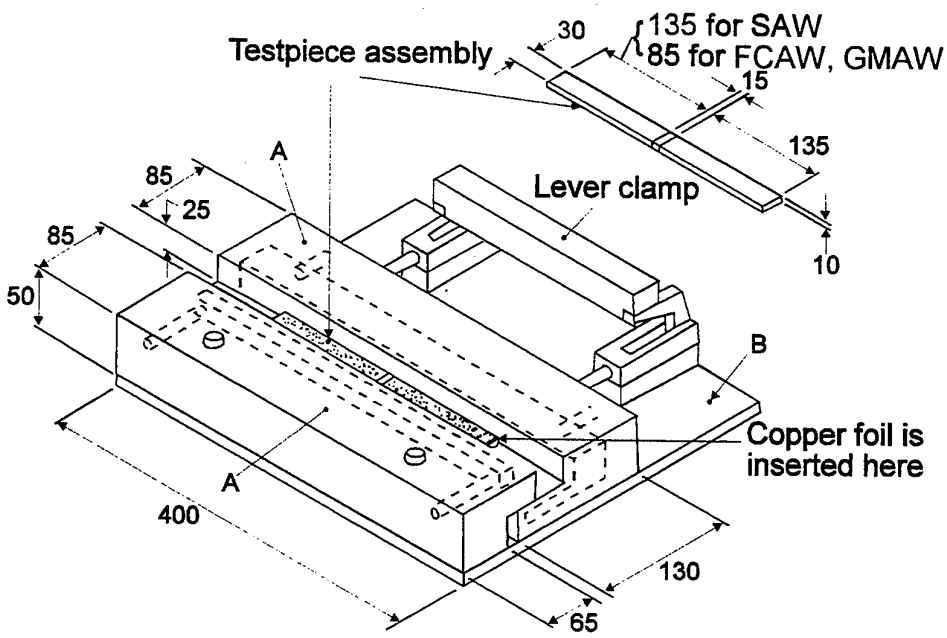

Key

---------- Water cooling

Materials

A. Copper
B. Mild steel

All dimensions are in millimeters.

Fig. 2 Welding fixture and testpiece assembly for weld deposits made with energy inputs greater than 2.0 kJ/mm up to 3.0 kJ/mm.

Notes to Figure 2:

Note 1. Overall weld traverse is 200 mm for SAW, and 140 mm for GMAW.

Note 2. 1 mm copper foil inserts (not shown) for SAW are 300 mm x 40 mm for the 10 mm thick test piece, or 300 mm x 45 mm for 15 mm thick test piece.

Note 3. The run-off bead length shall be such that the trailing end of the crater is on the run-off piece but within 25 mm of the test piece. See Distance D in Figure 1 for clarity.

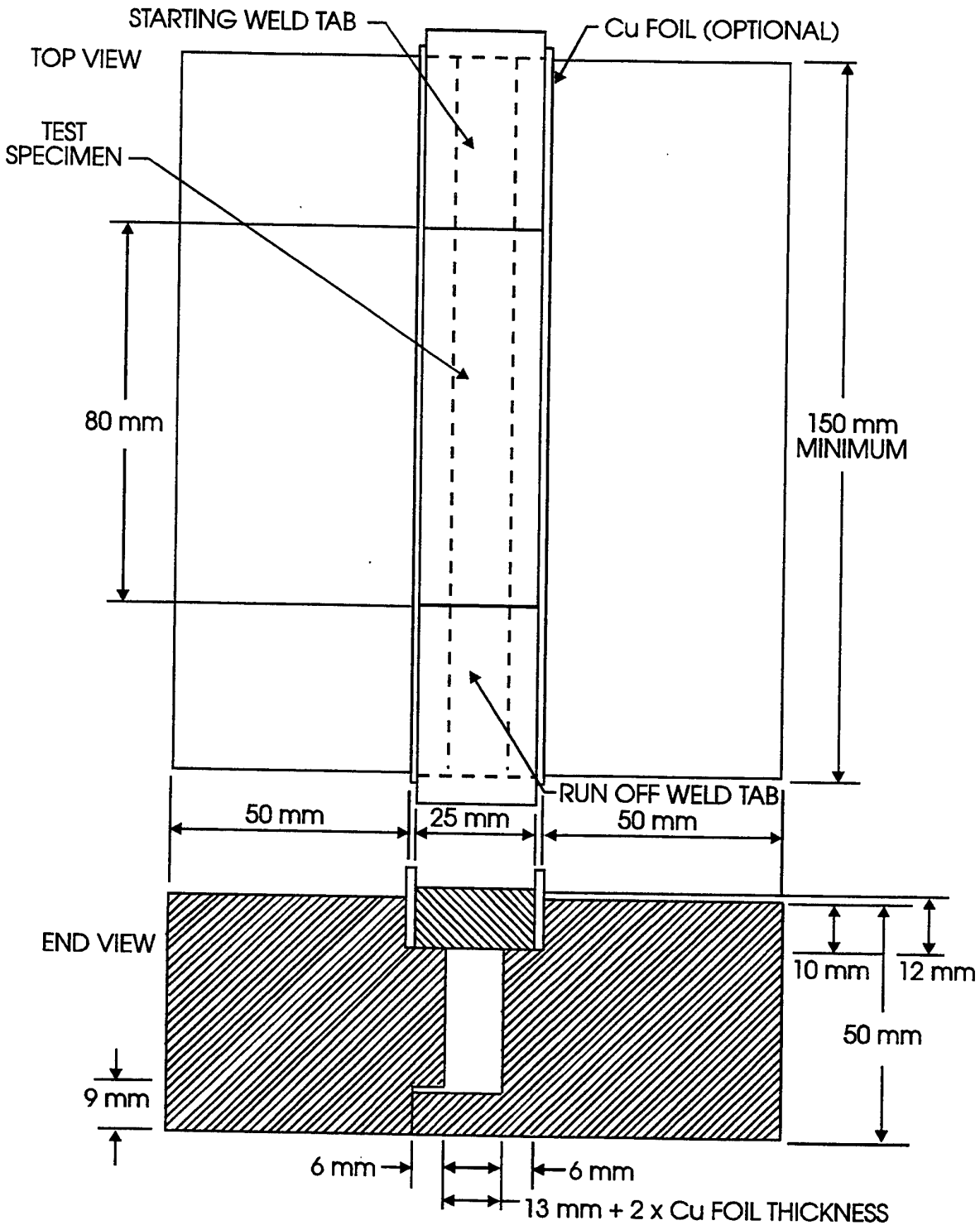

Figure 3. Weld Test Assembly for Diffusible Hydrogen Testing According to ANSI/AWS A4.3

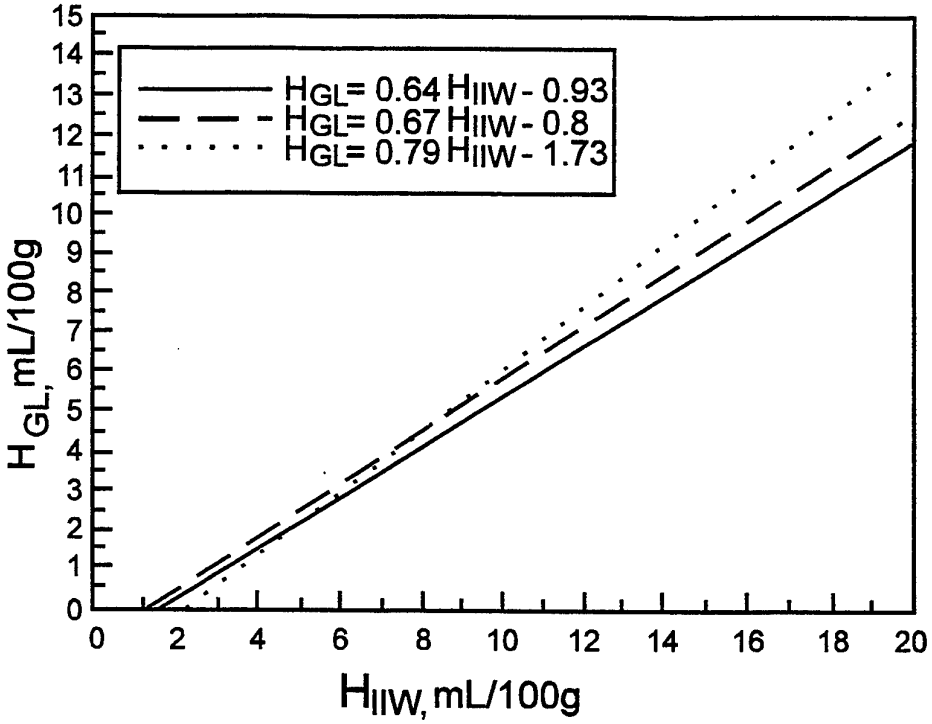

Figure 4. Equations 2, 3, and 4, Correlating Diffusible Hydrogen by Glycerin with Diffusible Hydrogen by the IIW Method

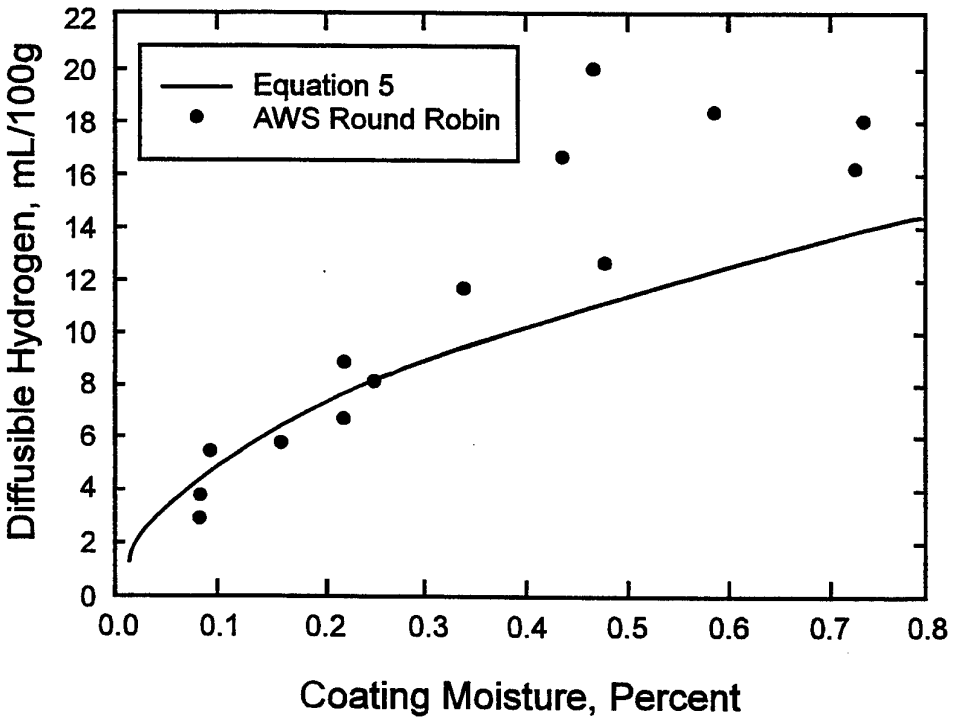

Figure 5. AWS Round Robin of As-Manufactured Coating Moisture versus Diffusible Hydrogen, with Equation 5

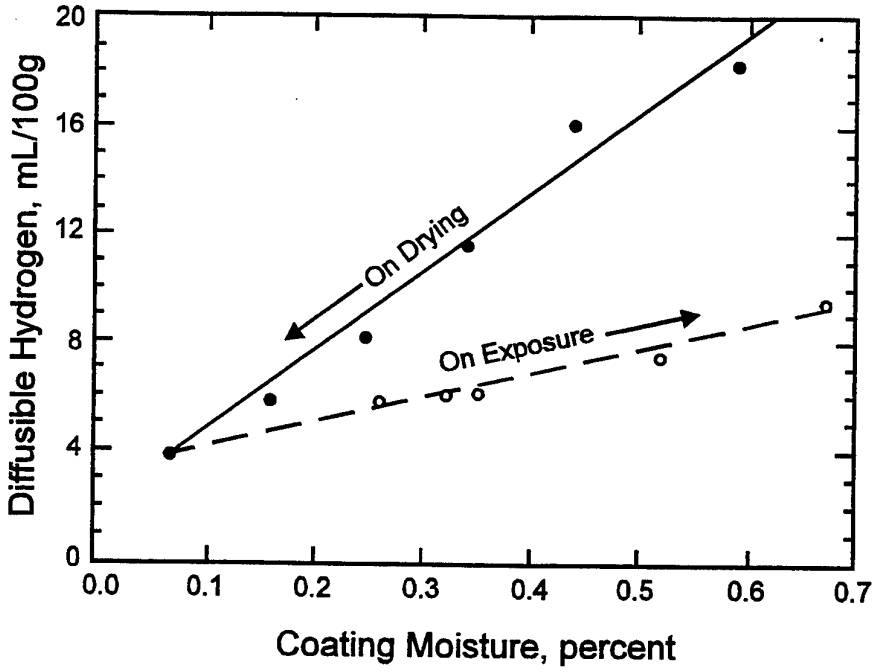

Figure 6. As-Manufactured Coating Moisture and Exposed Coating Moisture versus Diffusible Hydrogen by IIW Method (Ref. 13)

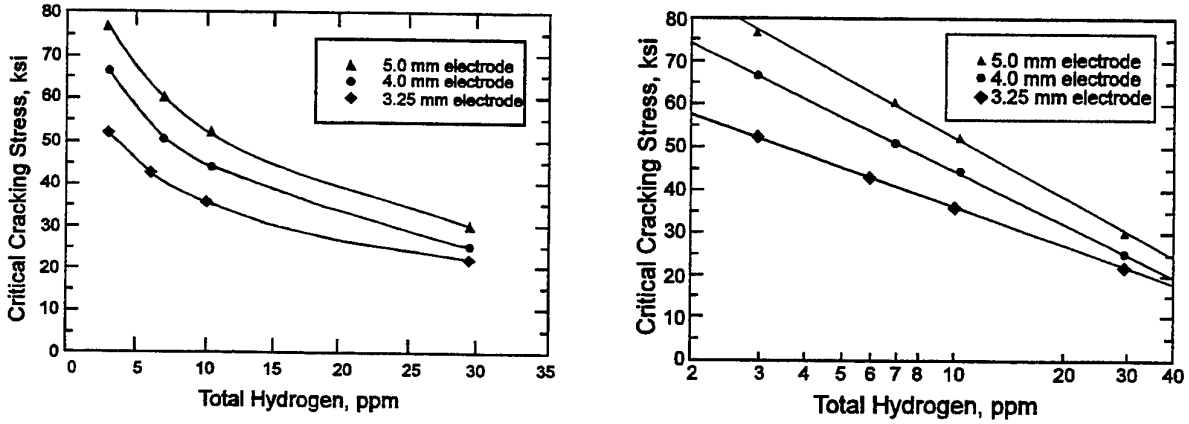

Figure 7. Critical Cracking Stress versus Diffusible Hydrogen (Ref. 13)
Left: Diffusible hydrogen plotted using a linear axis
Right: Diffusible hydrogen plotted using a logarithmic axis

MeV Ion Beam Analysis for Hydrogen

William A. Lanford
Department of Physics
SUNY Albany
Albany, New York 12222 U.S.A.

INTRODUCTION

Because of its low mass and low atomic number, hydrogen is difficult to detect by most modern physical methods of analysis. Hydrogen has too low a Z to emit either X-rays or Auger electrons. It is too light for Rutherford backscattering. It cannot be detected by neutron activation. To further complicate its analysis, hydrogen is a nearly ubiquitous contaminant in analysis chambers. Hence, effective analysis requires not only that hydrogen be detected and quantified, but also that the location of the hydrogen within the sample be determined. This situation has led to development of a number of MeV ion beam analysis techniques which are particularly well suited for measurement of hydrogen concentration profiles in solid samples. The purpose of this paper is to give a brief overview of these methods with the hope that through subsequent discussions, it will become clear if these methods can be usefully applied to the hydrogen in weldments problem.

There are two distinct approaches that use MeV ion beams to probe solids for hydrogen. One is nuclear reaction analysis (NRA) [1] and the second is elastic recoil detection (ERD) [2,3]. Both rely only on the properties of the nucleus of the hydrogen atom and, consequently, are insensitive to how the hydrogen is bound in the solid being analyzed. This insensitivity to matrix effects allows both these methods to be easily quantified without reference to standard calibration samples.

NUCLEAR REACTION ANALYSIS

Nuclear reaction analysis is shown schematically in Figure 1 .

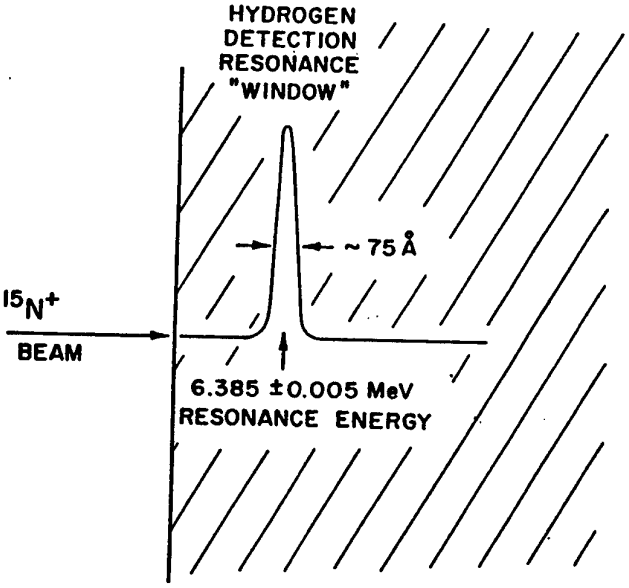

Figure 1: A schematic representation of the ^{15}N nuclear reaction method. Because of an isolated resonance in the cross section, hydrogen concentration profiles can be determined by measuring reaction yield *versus* beam energy. From reference [1].

To probe a sample for hydrogen, the sample is bombarded with ions that can undergo nuclear reactions with hydrogen (protons) in the target. To be specific, the ^{15}N nuclear reaction method will be discussed to illustrate the method. Reactions based on ion beams of ^{19}F and ^{7}Li have also been used. For recent reviews, see references [4,5].

The ^{15}N NRA method relies on the nuclear reaction:

$$^{15}N + {}^{1}H \rightarrow {}^{12}C + {}^{4}He + \gamma\text{-ray}. \qquad (1)$$

To use this reaction as a probe for hydrogen (^{1}H), the sample is bombarded with ^{15}N and the yield of characteristic gamma-rays is measured. The cross-section for this reaction is very small, except at a particular ^{15}N energy (6.385 MeV), i.e. this is a resonance reaction with a resonance energy of $E_r = 6.385$ MeV. Hence, if a sample is bombarded with ^{15}N at the resonance energy, the yield of gamma-rays is proportional to the amount of hydrogen on the surface of the sample. If the beam energy is raised above E_r, there are no reactions with surface H because the beam energy is too high. However, as the ^{15}N ions penetrate the sample, they lose energy reaching the resonance energy at some depth. Now the yield of gamma-rays from this reaction is proportional to the hydrogen content at that depth. Hence, by measuring the yield of gamma-rays *versus* beam energy, the hydrogen concentration *versus* depth is determined [1].

Figure 2 shows typical ^{15}N NRA data. These figures show both raw data (counts vs beam energy) and concentration profiles (H concentration vs depth).

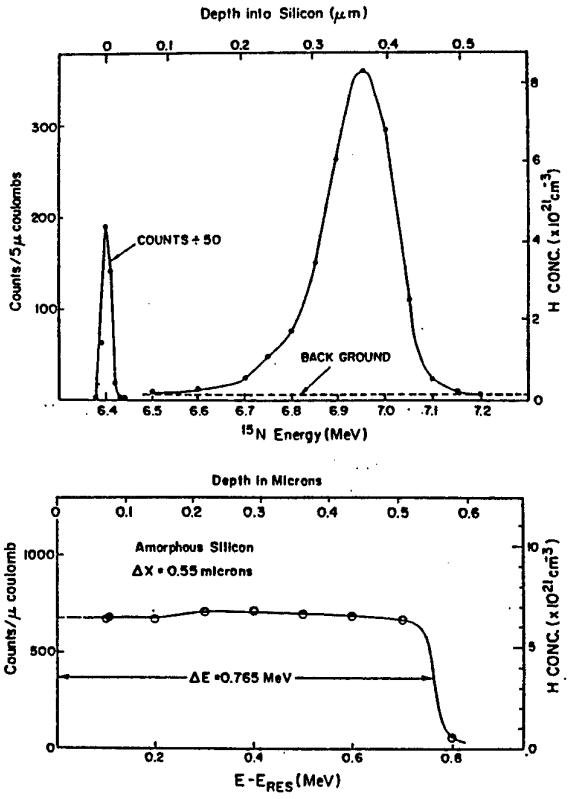

Figure 2: Typical NRA hydrogen profiling data, showing both raw data (counts *versus* beam energy) and final profiles (hydrogen concentration *versus* depth). The upper figure is a profile for a Si sample implanted with 10^{16} H/cm^2 at 40 keV. The lower figure is a profile of a thin film of hydrogenated amorphous Si with the solid datum a repeat measurement made after the profile had been completed. From reference [4].

The analytical characteristics of this method depend to a degree on the particulars of the sample being analyzed, the amount of ^{15}N beam used, and the detector used to measure the gamma-rays, but as commonly practiced, this method has a sensitivity on the order of 100 ppm (atomic), a depth resolution on the order of 100 A, and a maximum probing depth on the order of 3 microns.

ELASTIC RECOIL DETECTION

The elastic recoil detection (ERD) method is shown schematically in Figure 3.

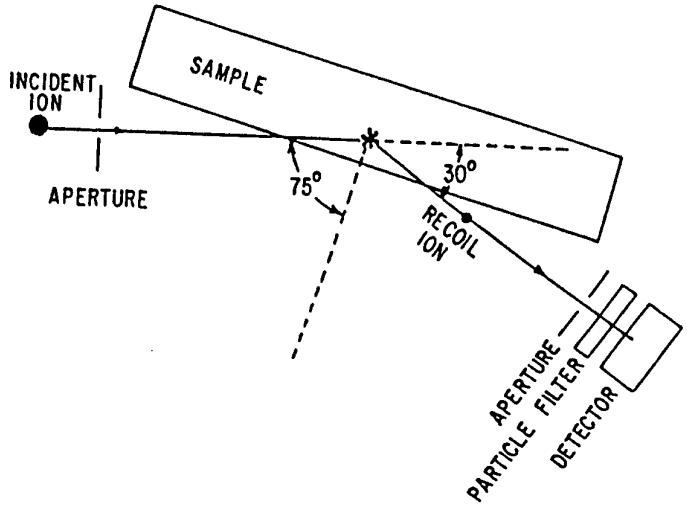

Figure 3: A schematic representation of the usual ERD method for glancing angle geometry. From reference [3].

ERD relies on elastic scattering between the incident ion and protons in the target to scatter (recoil) some of the protons out of the target where they are detected. Simple twobody kinematics determines the energy of the recoiling protons to be:

$$E = \{4Mm \cos^2\theta/(m+M)^2\}E_o \qquad (2)$$

where M is the mass of the incident projectile, m is the mass of the recoiled target atom (hydrogen), θ is the angle between the beam direction and the detector and E_o is the beam energy. For illustration, assume the incident beam is 2 MeV ^4He and the detection angle is 30°. From the formula above it follows that the recoil protons have an energy of 0.96 MeV. It is important that protons of 0.96 MeV have about twice the range (6.5 microns in iron) compared to the 2 MeV ^4He incident beam. This large range difference allows for simple and complete identification of recoil protons from the much more intense flux of elastically scattered incident ions. This identification is accomplished by placing a thin foil (particle filter) in front of the detector. The thickness of this foil is chosen such that recoil protons pass through this foil but ^4He cannot.

Depth profiling is possible since the energy of protons that have recoiled out of the target is reduced from that of formula (2) because both the incident ^4He and recoiling ^1H lose energy as they penetrate the target. Hence the energy spectrum of recoil protons can be read as a depth profile with the highest energy protons coming from the surface and lower energy protons coming from deeper within the target.

Figure 4 shows a typical ERD spectrum [6] showing both data (counts vs energy) with a superimposed depth scale (across top of figure) and approximate H concentration indicated within the figure.

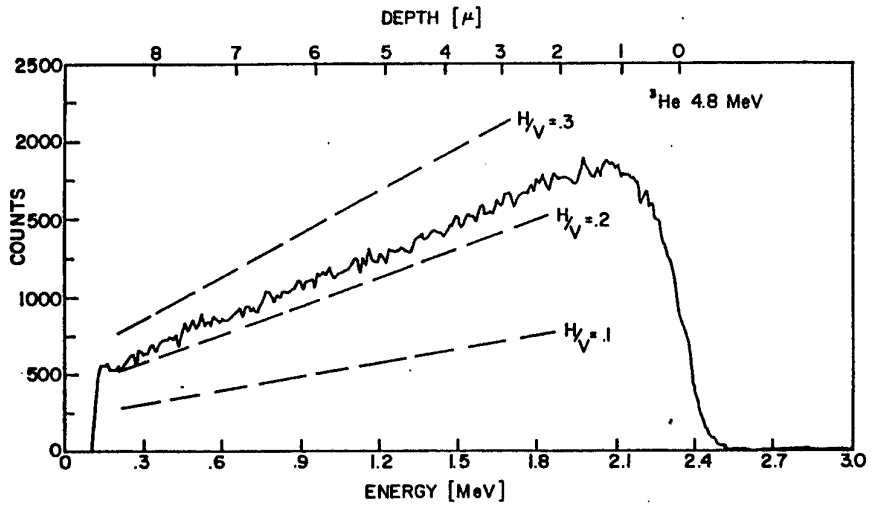

Figure 4: An ERD spectrum recorded from a sample of V electrolytically charged with hydrogen to $VH_{0.23}$. From reference [6].

ERD for hydrogen can have extremely high sensitivity. This follows because recoil cross sections are large and background in particle detectors is low. However, as commonly practiced (using a geometry similar to that shown in Figure 3), ERD has a relatively poor sensitivity. This poor sensitivity comes not from the lack of signal but rather from the incomplete separation of signals from bulk hydrogen from signals from the universally present layer of surface hydrogen. What happens is that the tail from the surface hydrogen peak extends into the bulk of the sample making it difficult to measure low levels of hydrogen present there.

There are at least two approaches that can be used to improve the sensitivity of ERD. One is to replace the low energy resolution detection system (consisting of a "particle filter" followed by a surface barrier detector) with a higher energy resolution detector. This has been done at low energy by Ross [7] who replaced the foil used as a particle filter with a purely electromagnetic (E x B) filter which rejects the elastically scattered particles

but passes the recoil protons. This E x B filter has the great advantage of passing the recoil protons without changing their energy. Use of a material foil filter has the unfortunate consequence of introducing considerable energy straggle (i.e. fluctuations in the energy loss) of protons that pass through the foil. This straggle is a primary contributor to the depth resolution of the method. At MeV incident energy, Gosset [8] at NRL has used a magnetic spectrometer to measure recoil protons. This provides both higher energy resolution than the usual surface barrier detector and automatically filters out the elastically scattered particles. Both the E x B filter and magnetic spectrometer approaches have demonstrated dramatic improvement in depth resolution (to a few nm) but apparently have not yet been applied to get high sensitivity.

Transmission Geometry

The glancing angle geometry is convenient in that it can be used for any flat sample, regardless of the sample thickness. However, for thin samples (on the order of a few tens of microns thick or less), ERD in a transmission geometry can be used [6,9]. This geometry is illustrated in Figure 5. This geometry has several advantages over the glancing angle geometry shown in Figure 3. One advantage is that kinematic broadening of the proton energy is much less. Namely, equation (2) gives the recoil energy as a function of recoil angle. Because cos(θ) changes slowly with angle at 0° but changes rapidly with angle at 30°, a much larger detector solid angle can be used at 0° without having a large energy spread due just to different recoil angles. In addition, surface roughness and multiple scattering effects are much less important in a transmission vs glancing angle geometry.

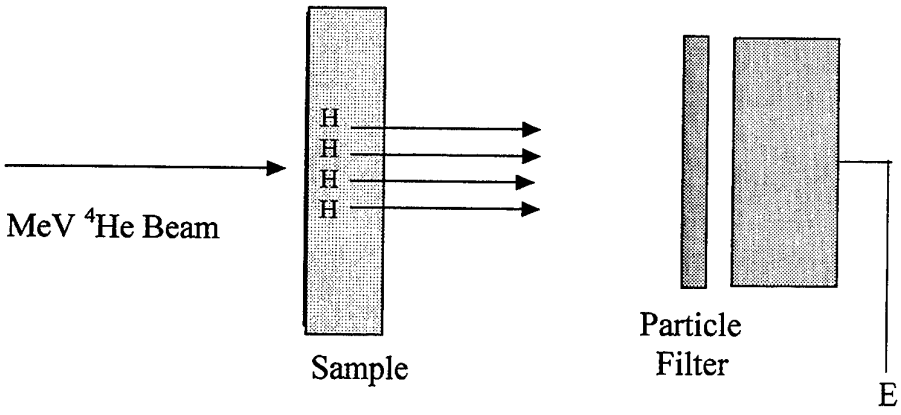

Figure 5: A schematic representation of a ERD setup in a 0 degree transmission geometry. An advantage of this system is the possibility of a large detection solid angle.

Figure 6 shows hydrogen recoil data taken in a transmission geometry [9]. This figure shows the energy spectrum of recoil protons observed to come from a 13 micron nickel foil bombarded with 5.8 MeV ^{4}He. This spectrum was recorded at $\theta = 0^\circ$ (i.e the protons recoiled through the 13 micron Ni foil) with a 12.5 micron Ni filter covering the detector. The large peak at the right side of the figure comes from hydrogen on the surface of the Ni target. To the left of the surface peak, there is a continuous low count spectrum. Converting these data to hydrogen concentrations, the surface peak corresponds to about 2 10^{15} H/cm^2 at the surface of the sample and the low energy spectrum corresponds to 10 ppm (atomic) of hydrogen in the bulk of the Ni. When this sample was *in situ* sputter cleaned, the surface peak was reduced by an order of magnitude while the bulk hydrogen amount was only reduced by about 30%.

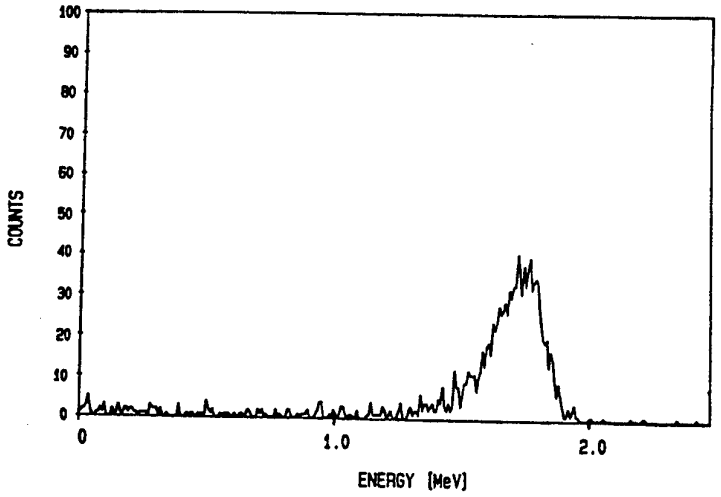

Figure 6: ERD data recorded from a 13 micron thick Ni foil bombarded with 5.8 MeV He. The peak to the right comes from 2 10^{15} H/cm^2 on the surface of the foil. The low counts to the left correspond to 10 ppm (atomic) H in the bulk of the film. From reference [9].

LATERAL SPATIAL RESOLUTION

From the above, it is clear that both NRA and ERD can be used to measure concentration profiles of hydrogen in materials. MeV ion beams typically have a beam spot on the order of 1 mm diameter. Hence, these methods automatically have lateral resolutions on the order of mm, which may be good enough for some applications.

MeV ion beams can be focused down to diameters on the order of 1 micron. Hence, in principal, lateral resolutions on this scale would seem possible. It seems unlikely that microbeam NRA for hydrogen will prove useful. The problems are both the difficulty in getting usable currents of micron diameters heavy ion beams (such as ^{15}N) and the more fundamental problem of the high intensity radiation associated with such beams. Such a

high density radiation is likely to cause the hydrogen within the sample to be mobile, making quantitative measurements difficult or impossible.

However, because of the very large recoil cross sections and the lower energy loss rates of ^{4}He beams (compared with ^{15}N beams), analysis of hydrogen by recoil using micron diameter microbeams should be possible. This approach would seem to offer unique analytic opportunities for quantitative measurement of 3 dimensional concentration distributions of hydrogen within solid samples.

MeV Neutron Recoil

MeV recoil analysis can also be conducted using high energy neutrons. The approach has been developed by Skorodumov in Tashkent [10,11] and is shown schematically in Figure 7.

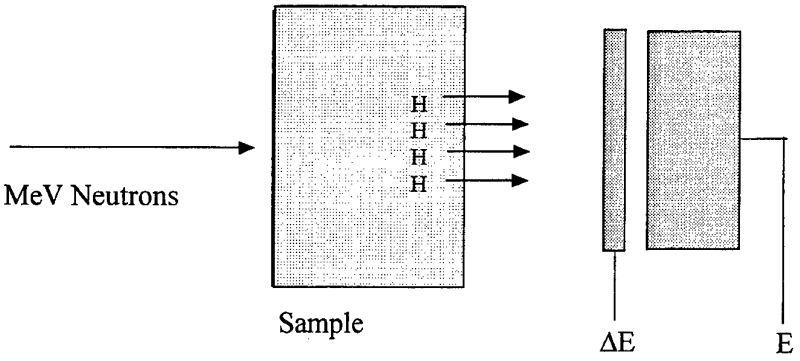

Figure 7: A schematic representation of a neutron induced ERD system. The ΔE detector is used to identify the recoiling protons from other possible ions (deuterium, alphas, etc.)

Conceptually, this is perhaps the simplest of all methods. The sample to be analyzed is bombarded with 14 MeV neutrons and elastically scattered recoil protons are detected. Since the neutrons do not lose energy continuously (as charged particles do), essentially all protons recoils come from full energy neutrons. The limitations of this method are its relatively poor sensitivity (due to (n,p) nuclear reactions in the target or the detector) and relatively poor depth resolution. However, this method has the potential of measuring hydrogen profiles into depths of hundreds of microns on thick samples [11].

Figure 8 shows profiles of hydrogen in electrolytically charged Pd measured using this neutron induced recoil method.

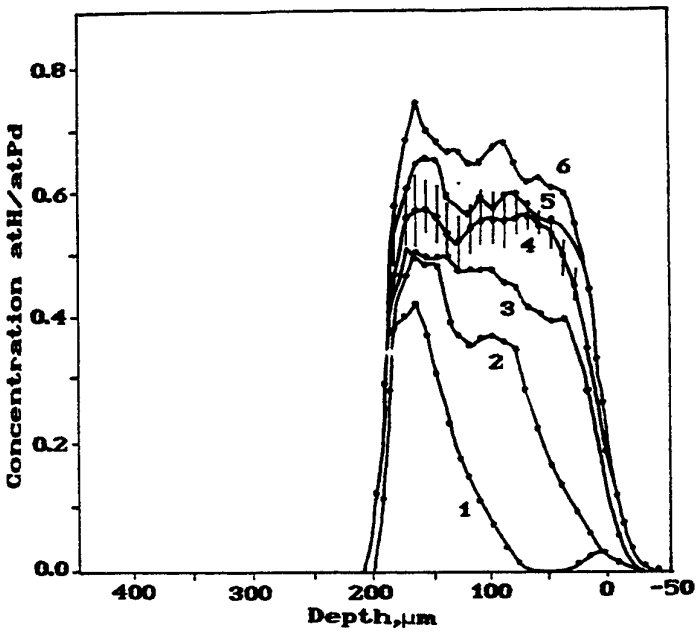

Figure 8: Hydrogen concentration profiles recorded by neutron ERD from 175 micron thick Pd samples electrolytically charged with hydrogen to various degrees. From reference [11].

SUMMARY

The above is intended to be a brief overview of some of the ways MeV ions have been used to probe solids for hydrogen. Much more technical detail is available in the literature, including some recent reviews. It is clear that these methods have some unique analytical characteristics that have allowed their application to supply needed information in a number of diverse fields. It will be interesting to see if any of these methods can fill analytic needs in the control of hydrogen in the welding of high strength steels.

References

1. W. A. Lanford, H. P. Trautvetter, J. F. Ziegler and J. Keller, Applied Physics Letters, 28 (1976)566.

2. J. L'Ecuyer, C. Brassard, C. Cardinal, J. Chabbal, L. Deschenes, J. P. Labrie, B. Terreault, J. G. Martel and R. St. Jacques, Journal of Applied Physics 47(1976) 381.

3. B. Doyle and P. S. Peercy, Applied Physics Letters 34 (1979) 811.

4. W. A. Lanford, Nuclear Instruments and Methods B66 (1992) 65.

5. J. R. Tesmer and M. Nastasi, Handbook of Modern Ion Beam Materials Analysis, Materials Research Society (Pittsburgh), 1995.

6. L. S. Wielunski, R. E. Benenson, and W. A. Lanford, Nuclear Instruments and Methods 218(1983) 120.

7. G. G. Ross, B. Terreault, G. Gobeil, G. Bael, C. Coucher and G. Veilleus, Journal of Nuclear Materials 128/129 (1978) 730.

8. C. R. Gossett, Nuclear Instruments and Methods B15 (1986) 481.

9. L. Wielunski, R. Benenson, K. Horn and W. A. Lanford, Nuclear Instruments and Methods B15 (1986) 469.

10. P. Khabibullaev and B. Skorodumov, Determination of Hydrogen in Materials, Springer (Berlin) 1989.

11. B. Skorodumov, I. O. Yatsevich and O. Zhukovsky, Nuclear Instruments and Methods B85 (1994) 301.

Detection of Hydrogen in the Welding Arc

Robert A. Weber

US Army Construction Engineering Research Laboratories

1. Introduction

In the late 1970's through the early 1980's, the DoD supported a wider variety of research. The Corps of Engineers (COE) had a full construction program underway and there was concern about the presence of hydrogen in high strength welds and the possible problems it could cause. Welding in general was of concern because the COE had implemented a division of responsibilities for quality control between the contractor and the COE. The contractor had sole responsibility for quality control and the COE took on the role of quality assurance. The large force of experienced weld inspectors was dwindling fast and the need for some type of system to control quality was becoming evident. The COE instituted a research program to develop a Weld Quality Monitor. The original concept was to monitor the electrical characteristics of the weld arc and use this information to flag areas where problems might exist. This information source was very limited and the light emitted from the weld arc was investigated as another data source for the workings inside the arc. A simple spectroscopic system was first developed that looked at five bands of the arc spectrum in the range from 400 to 1000 nanometers (nm). With this device it was possible to separate and quantify segments of the weld spectrum and to correlate the energy distribution among these segments to specific weld parameters. This suggested that it may be possible to classify weld flaws based on the energy distribution in the arc spectrum. To supplement and extend this work, a high-resolution, microprocessor-controlled spectrograph was developed by USACERL. This device made possible detailed studies of the near-infrared, visible, and ultraviolet spectra of the weld arc. These spectra could then be related to welding conditions. One of the concerns and the main driving force in the development of the spectrograph was the need to determine the extent of hydrogen in welding arcs and how this related to the amount of hydrogen remaining as a residual in the weld metal.

2. Instrumentation

A high resolution spectrograph was constructed and interfaced with a Digital Equipment Co. LSI 11/23 microprocessor. This system made it possible to monitor the weld arc spectrum in real time. Hardware and software were developed to permit the computer to also monitor the arc current and voltage, and to calculate weld quality parameters.

Figure 1 shows a schematic of the spectrographic system. The light from the weld arc is gathered by a lens and focused on the end of a non-coherent fiber optic bundle. The bundle is designed to withstand the high temperatures near the weld arc. The bundle terminates at a monochromator entrance slit. The light is shown on a concave holographic grating that breaks the light into its component wavelengths. The grating used for the early work was a 400 line diffraction grating. The later work required more resolution so a 1200 lines/in. 0.32-m Czerny-Turner type diffraction grating was instaled. Higher resolution can be attained with a diffraction grating that has 2400 lines/in. but the higher resolution requires more light be conducted into the monochromator for useful information to be gather by the photodiode array. The exit slit of the monochromator was replaced by a linear photodiode array. A section of the spectrum 600 nm wide with the low resolution grating and 500 Angstroms (Å) wide with the high resolution grating is imaged onto the photodiode array. The grating can be rotated to allow the entire spectrum to be observed from near infrared to ultraviolet. The photodiode array contains 1024 separate diodes that can be scanned at a frequency of up to

1000 Hertz (Hz). The voltage levels from each diode are interfaced with an A/D converter into a 16-bit LSI 11/23 microcomputer. The voltage, curent and travel seed are interfaced to the microcomputer through a parallel input/output port. The spectral data and the arc current, voltage and travel speed data can be processed in real time or stored on disk for later processing.

The spectral response of the silicon photodiodes, Figure 2, and the transmission characteristics of the glass fibers, Figure 3, limit the useful spectral range to about 350 to 1050 nm. The highest theoretical resolution of the spectrograph is about 0.4 Å. This resolution is comparable to the Doppler line widths of argon and hydrogen. Although the photodiodes can be scanned up to 1000 Hz, the sensitivity of the photodiodes decreases as the scanning rate increases. Typically, the scanning rate was kept to 10 Hz, which means that the weld arc spectrum could be sampled once every 100ms. During data collection, 5 to 10 successive scans were usually averaged and then stored on disk for later analysis.

Data are graphed as diode voltage versus wavelength. Resolution of the system is such that the individual atomic emission lines can be easily resolved. The area under the curve is calculated and this value is used in the calculation for the quantity of hydrogen in the arc. An argon line nearby the hydrogen line is used in the calculation of quantity. The background is measured and subtracted from the two lines.

3. Experimental Work

Several experiments were performed with the equipment as described above. This paper will outline only three of the experiments. The first two experiments used the Low resolution diffraction grating. The last experiment used the high resolution diffraction grating. All experiments were conducted with a fully automatic gas metal-arc welding system depositing bead-on-plate welds. The welding shield gas was Ar-2% O_2. The electrode was 0.062 inch diameter E70S-3.

Experiment 1

In the first experiment, the shield gas was interrupted during the welding process and the resultant changes in the arc spectrum, voltage, and current were observed. The arc was stabilized at 300 A welding current. Data was collected for 50 s. Data was averaged for ½ s and then stored to disk. Because of disk access times of ½ s data was collected at 1 s intervals. After 10 s the shield gas was shut off. At 20 s the shield gas was turned on. At about 30 s the gas shut off and then on again at 40 s.

Figure 4 is a plot of the arc voltage and current vs time. The times when the shield gas was off are clearly evident by the dramatic shift in current and voltage. Figure 5 is a sample of the arc spectrum taken during this experiment. Figure 5a is a sample from 28.71 s into the experiment showing normal welding conditions with the shield gas flowing. Figure 5b shows the spectrum at 29.7 s when the shield gas has been shut off. The loss of longer wavelength spectra is evident when the shield gas is removed. Total spectral energy is plotted vs time in Figure 6 for the wavelength range of 700 to 1000 nm. Again, the change in total energy is evident when the shield gas is turned off. Figure 7 shows the total energy for the range of 814 to 816 nm. The energy at this wavelength went down to background levels when the shield gas was turned off. This showed us that it would be possible to construct a

narrowband filter and photodetector to measure the spectral energy in this region and determine the presence or lack of shield gas.

Experiment 2

The second experiment was designed to determine the correlation between heat input and the total spectral energy emitted from the arc. For this experiment, the current was varied from 360 A to 200 A. The travel speed remained constant at 10 in./min. The heat input varied from 36 to 55 kJ/in. Figure 8 is a plot of the voltage and current vs time for this experiment. Figure 9 shows the total energy vs time for the entire spectrum. The energy goes down as the heat input rises because by changing the current and nothing else, the arc length in shortened as the wire moves into the overdriven mode and the arc may even bury itself in the base material. Both of these would reduce the amount of light energy that would reach the fiber optic bundle.

Experiment 3

The third experiment described here took advantage of the finer grating to get better resolution. This grating put a 50 nm bandwidth onto the photodiode array instead of 600 nm. This experiment was designed to determine if the system could detect the presence of hydrogen and then determine amount in the weld arc. The weld shield gas was modified with hydrogen additions by volume. The hydrogen was increased in the shield gas in ½ % increments from 0 to 3 % additions. The test run lasted approximately 25 s during which time 50 spectra were acquired and stored to disk. Nominal welding values for weld voltage and current were 30 V and 300A. Travel speed was varied from 4 ipm to 24 ipm.

Hydrogen has two prominent lines in the visible region of the spectrum and either one can be used for monitoring concentration. One is the Balmer series alpha line at 6563 Å and the other is the Balmer series beta line at 4861 Å. The beta line could not be used for determining the hydrogen concentration because several of the base metal emission lines interfered. Additionally, there are several argon emission lines in the region of the alpha line that can be used for normalization. Figure 10 is a spectral sample taken with the monochromator centered on 6725 Å and a hydrogen shield gas concentration of 2.0%. The spectral lines in this region are due primarily to hydrogen, argon, and iron. The hydrogen line is by far the broadest line in the spectrum. It is due to the Stark broadening mechanism.

The series of experimental runs were performed and the data analyzed. Figure 11 is the graph of the relative intensity of the hydrogen line vs hydrogen concentration in the weld arc. This graph shows the need for normalization of the data. Normalization is done by dividing the hydrogen intensity by the intensity of a nearby spectral line. To be effective, intensity variations in the ratioing line should be highly correlated with variations in the hydrogen line. Table 1 shows the correlation coefficients between the intensity fluctuations of hydrogen and the major iron and argon lines in the vicinity of the hydrogen line. The correlation coefficients for the argon line at 6965 Å is the most highly correlated with the hydrogen line. This probably arises from two factors. The first is the excitation energies of the two lines. The argon line energy is 13.3 eV and the hydrogen line excitation energy is 12 eV. Since these two values are close the temperature dependence of the two lines should be similar. Second, the argon lines are from the argon in the shield gas while the iron lines are from the iron vapor in the arc atmosphere from the weld wire and the base metal. The shield

gas flow should remain relatively constant during welding which implies that the volume of argon gas should remain relatively constant in the weld arc plasma. Metal transfer processes and arc instabilities can vary the volume of iron vapor in the weld plasma considerably. The ratio of the hydrogen line intensity with the argon line intensity can be expressed simply as:

$$R = \frac{I_H - I_B}{I_A - I_B}$$

Where I is the intensity profile for each line and the background.

Table 1
Correlations Coefficients between Hydrogen, Argon, and Iron

Element	λ	1 % Hydrogen ρ	2 % Hydrogen ρ
Argon	6965 Å	0.8380	0.900
Argon	6752Å	0.8264	0.831
Iron	6495Å	0.0500	0.0183
Iron	6546Å	0.3451	0.4319
Iron	6593Å	0.0702	-0.6754
Iron	6678Å	0.0308	-0.2468

The intensity ratio given by the above equation is plotted in Figure 12 versus the hydrogen concentration for three separate data sets. This plot shows that the intensity ratios are very nearly a linear function of the hydrogen concentration. A linear regression analysis of the three data sets was used and the resulting best fit lines and coefficients are presented in Table 2.

Table 2
Results of Linear Regression Analysis of Intensity Ratio and Concentration

Data Set	Slope	Intercept	Coefficient of Determination
1	0.7974	0.0283	0.98
2	0.7548	0.0363	0.97
3	0.6819	0.1156	0.97
Combined	0.7501	0.0010	0.97

4. Conclusions

The spectroscopic technique described in this paper is capable of measuring the absolute hydrogen concentration in the weld arc plasma in the range that has been shown to cause weld failure (0.1% to 0.2% of the shield gas). The techniques described in this paper can be applied to other constituents in the weld plasma and used to determine the concentrations in the arc. Additional work not presented here included correlating the amount of hydrogen in the arc plasma to residual amounts in the weldment, determination of consistency of flux distribution in flux-cored electrodes, and determination of oxygen concentrations in zirconium welds.

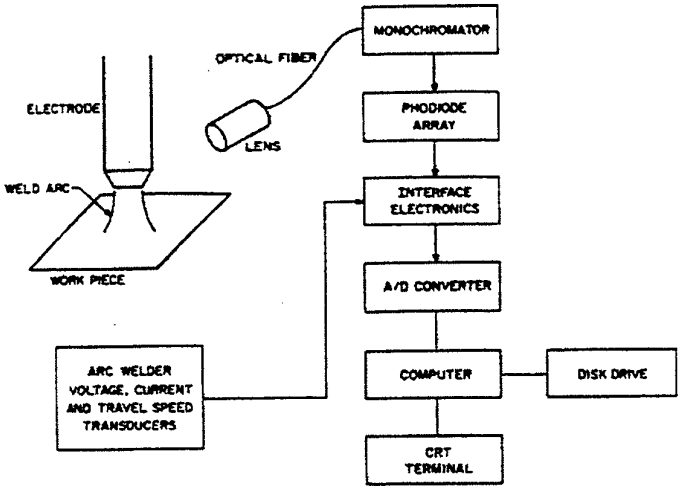

Figure 1 Block diagram of the monochrometer.

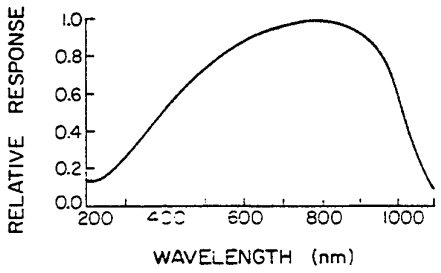

Figure 2. Photodiode array optical responsevs wavelength.

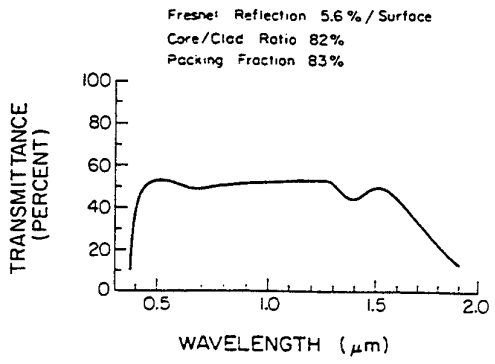

Figure 3. Optical fiber transmittance vs wavelength.

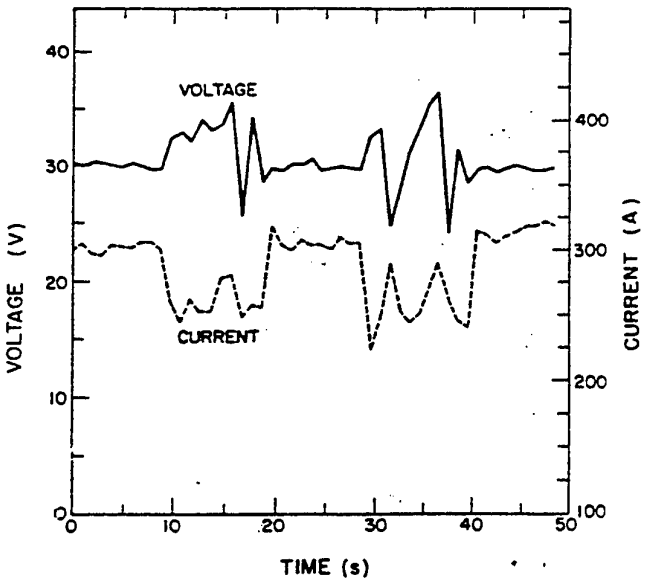

Figure 4. Variation of voltage and current vs time showing interuption of shield gas flow.

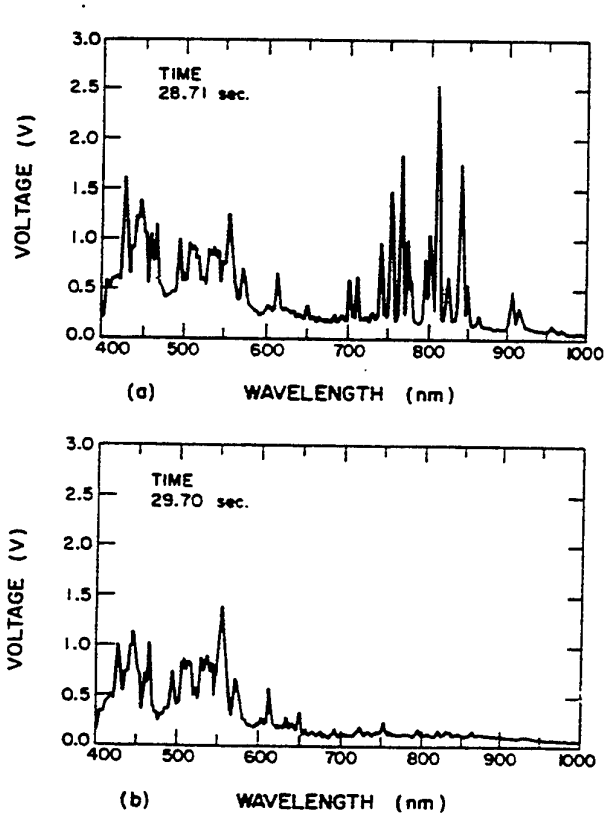

Figure 5. Typical example of the arc emission spectra. a) Spectrum obtained when shield gas is on. b) Spectrum obtained when shield gas is turned off.

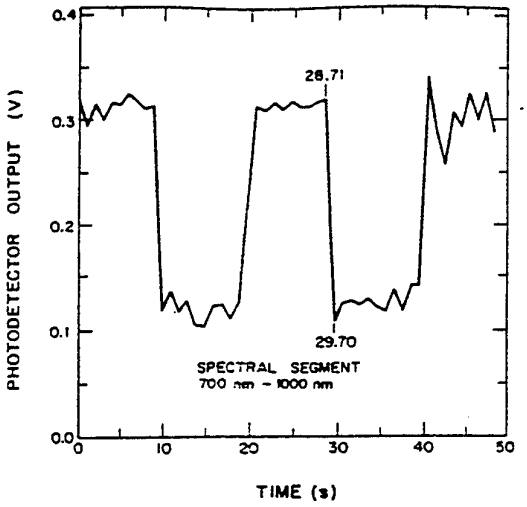

Figure 6. Total energy vs time for the spectral segment from 700 to 1000 nm showing the change with loss of shield gas.

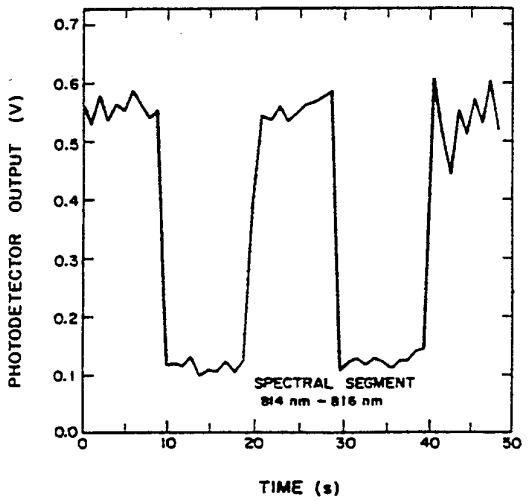

Figure 7. Total energy vs time for the spectral segment from 814 to 816 nmshowing the change with the loss of shield gas.

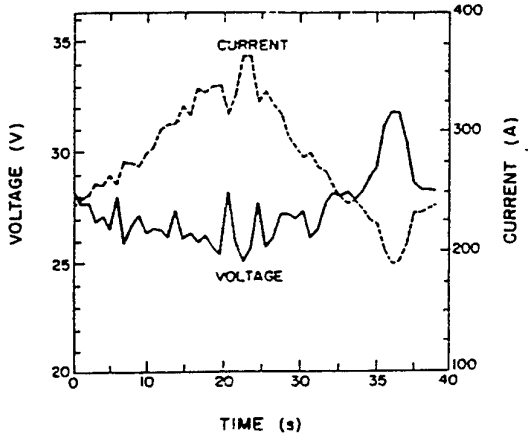

Figure 8. Variation of the arc voltage and current with time for the second experiment.

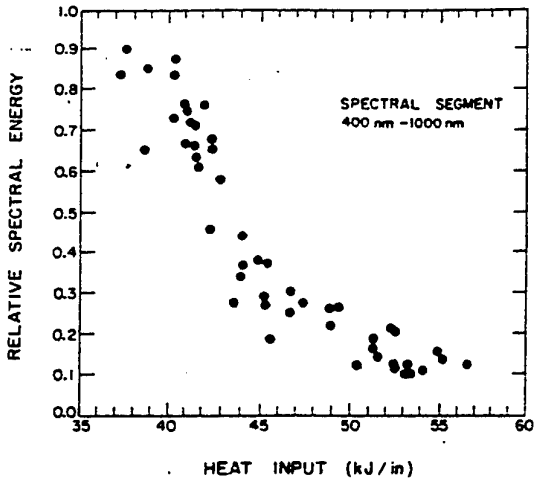

Figure 9. Variation of the total energy in the spectral segment 400 to 1000 nm vs heat input.

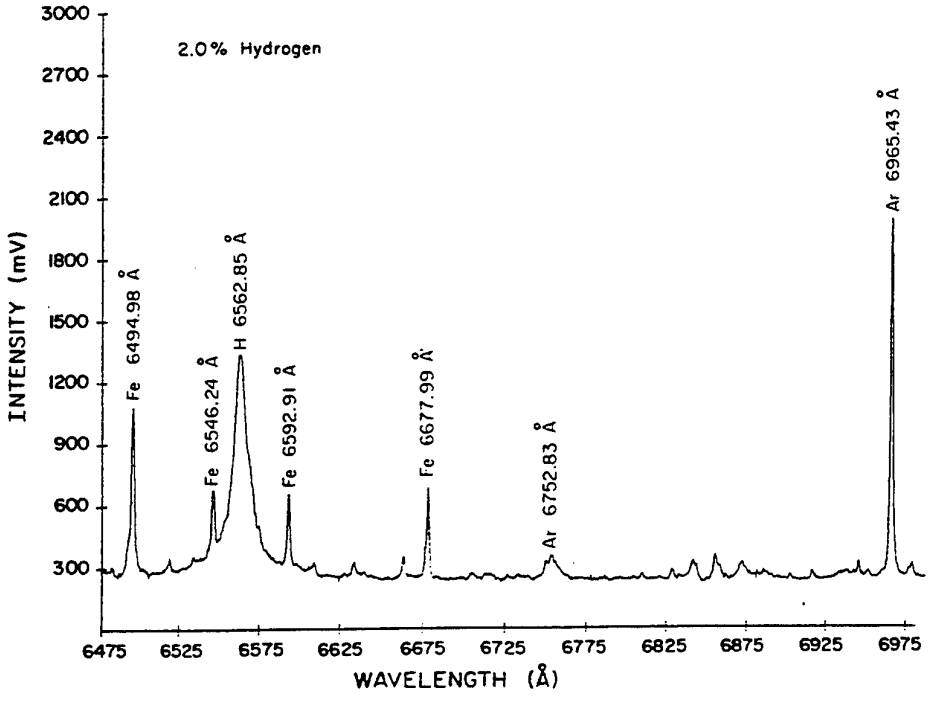

Figure 10. Sample from spectral segment 6475 Å to 6975 Å with 2% hydrogen added to the shield gas.

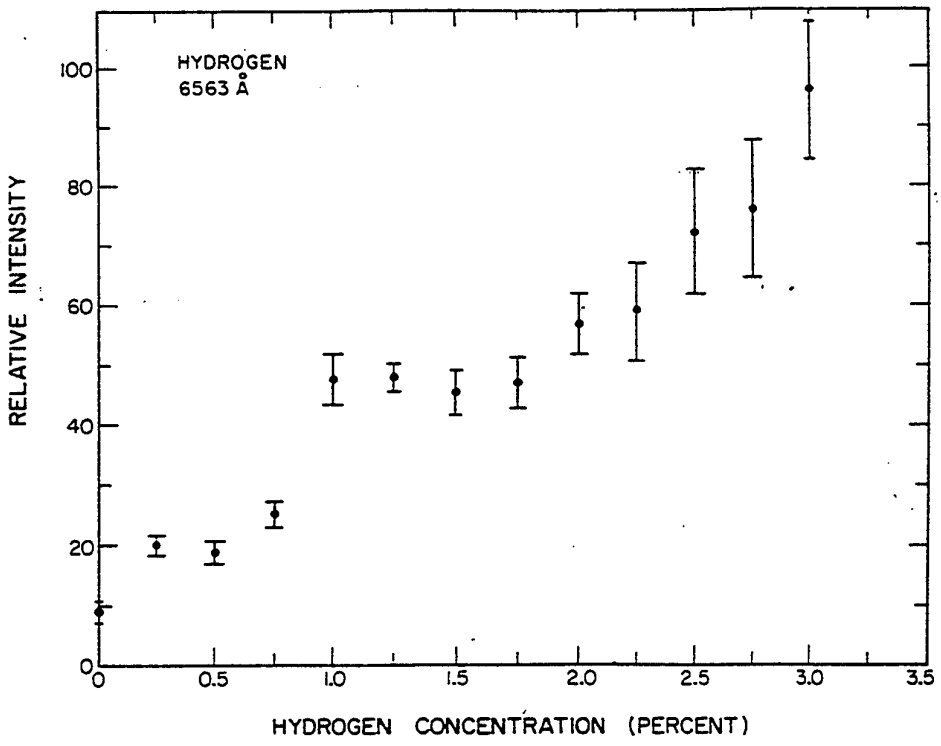

Figure 11. Hydrogen line intensity vs hydrogen concentration in the weld arc.

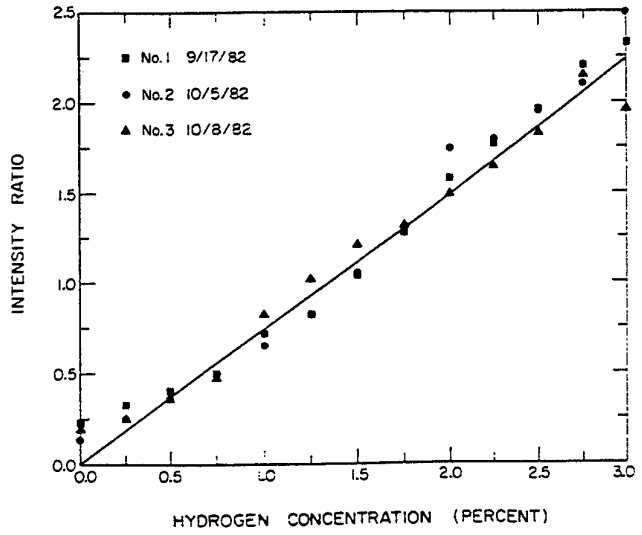

Figure 12. Intensity ratio vs hydrogen concentration in the weld arc.

Control Of Hydrogen Cracking In COLLINS Class Submarine Welds

by B.F. Dixon
Ship Structures and Materials Division
Defence Science and Technology Organisation

and J.S.Taylor
Welding Manager, Australian Submarine Corporation

1. INTRODUCTION

The new COLLINS class (Type 471) submarine being constructed for the Royal Australian Navy by Australian Submarine Corporation (ASC) incorporates a number of material advances in the main pressure hull. In particular, the steel designated BIS 812 EMA represents one of the first uses of 690 MPa. yield stress high strength low alloy (HSLA) steel in a blue water submarine [1]. To meet the necessary high levels of shock resistance and fracture toughness, particular attention was given to all aspects of welding, from first article qualification [2,3] to development of welding procedures [4]. As a consequence, the quality of welding has been high and the rework rate has been relatively low (<1%).

Sensitivity to hydrogen cracking is often considered to be the most important factor in the weldability of high strength steels. In a recent investigation it was found that even slight relaxation in the welding procedure (most notably preheat and interpass temperature) can lead to extensive transverse hydrogen cracking in submerged arc welds, such as those used on COLLINS. For example, Figure 1 shows the extent of cracking which occurred in an experiment to determine the efficacy of using alloy powder additions for the submerged-arc welding of 690 MPa yield stress steel [5].

Furthermore, detection of sub-surface transverse cracking is extremely difficult, particularly in T-butt or cruciform joints and it is generally found that radiography is incapable of detecting such cracks. Ultrasonic testing is capable of detecting cracks but it is highly sensitive to the orientation of the crack, the presence of other reflectors close to the crack and the skill of the operator. It is therefore essential to develop welding procedures that minimize the risk of hydrogen cracking.

The purpose of this investigation was to review the causes of hydrogen cracking in high strength steels and assesses the risk of cracking in hull steels that have been welded using the higher carbon filler metal.

2. STEELS AND WELDING CONSUMABLES

The submarine hull is largely constructed from two steels and two welding consumables. The first is designated BIS 812 EMA, a High Strength Low Alloy (HSLA) steel with small additions of potent micro-alloying elements such as copper, titanium, niobium, boron and vanadium to achieve an extra boost in strength. BIS 812 EMA steel is supplied in rolled form and heat treated using firstly a spray quench from a temperature of about 920°C and then a temper at 590°C

The second steel is a conventional quenched and tempered steel similar to HY 80 and designated HY 590 (composition in Table 1) It has larger quantities of the traditional alloying elements chromium, nickel and molybdenum and negligible quantities of the micro alloying elements which are used in the BIS 812 EMA steel.

Most of the welding on Collins is undertaken using the submerged arc, FCA and MMA processes and a relatively small amount of welding fabrication is undertaken using the GTA process. In this work welding is undertaken using the submerged-arc (SA) and manual-metal arc (MMA or 'shielded metal arc', SMA) processes. The MMA consumable used to join BIS 812 EMA plate is a low hydrogen welding electrode class E12018-M2. Submerged-arc welding is undertaken with a MIL-120S-1 wire combined with a commercial OP 121 TT flux.

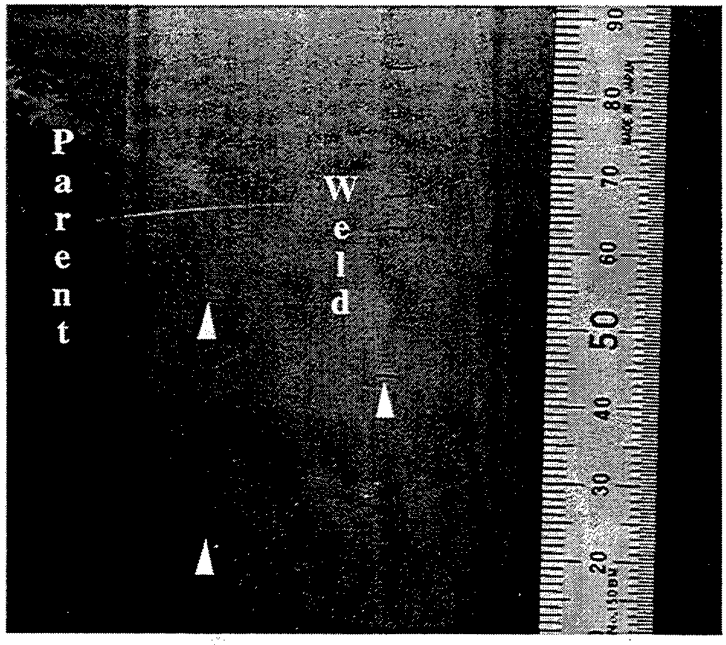

Figure 1 Segment of submerged-arc weld which has been polished down from the weld surface to reveal subsurface transverse cracking. These particular cracks have been deliberately created by adding iron powder to the weld deposit (For details see Ref. 5).

2. HYDROGEN CRACKING

Hydrogen cracking [also known as Hydrogen Induced Cold Cracking (HICC)] occurs by entrapment of hydrogen atoms in the weld zone. It may take very small quantities of hydrogen (from contaminants such as moisture, rust, paint, dirt, etc.) to cause cracking, which may occur in weld metal or base material heat affected zone (HAZ) next to the weld. The most effective way to prevent cold cracking in high strength steel is, therefore, to keep the hydrogen contamination low, which means careful control of electrodes and fluxes, and a high level of cleanliness. Hydrogen soaks out of the weld over a period of days or months (Fig. 2) at room temperature, so the risk gradually disappears. In practice it is found that cracking may occur up to seven days after completion of the weld. Therefore NDT is delayed at least 48 hours after welding in order to increase the probability of detecting nearly all of the statistical population of cracks that are likely to form.

Carbon is traditionally considered to be the most potent of the crack-promoting alloying elements. Furthermore, other elements are considered to be crack-promoting in proportion to their effect on steel hardenability. Two formulae are commonly used for estimating the effect of carbon and the other alloying elements on crack sensitivity. Both are based on values of 'carbon equivalent' (CE). A formula traditionally used is that adopted by the International Institute of Welding (IIW):

$$CE_{IIW} = C + \frac{Mn}{6} + \frac{Cr + Mo + V}{5} + \frac{Cu + Ni}{15} \qquad \text{.... (1)}$$

A more recent formula, attributed to Ito and Bessyo [6] is said to be more appropriate for quenched and tempered (QT) steels. As shown in Equation 2, this formula has less weighting for the solid solution and carbide forming elements (e.g. manganese and nickel) than the IIW formula and includes elements, notably silicon and boron, not covered by in the IIW formula:

$$P_{cm} = C + \frac{Mn + Cu + Cr}{20} + \frac{Si}{30} + \frac{Ni}{60} + \frac{Mo}{15} + \frac{V}{10} + 5B \qquad \text{..... (2)}$$

When these two formulae are applied to either base material or weld metal compositions to estimate the risk of HICC in weld and heat affected zone material, they show that more highly alloyed base metals, such as HY-100, would be expected to have greater crack sensitivity than comparatively lean formulations, such as BIS 812 EMA. This is found in practice, and the risk of *parent metal* cracking in these steels is found to be relatively low.

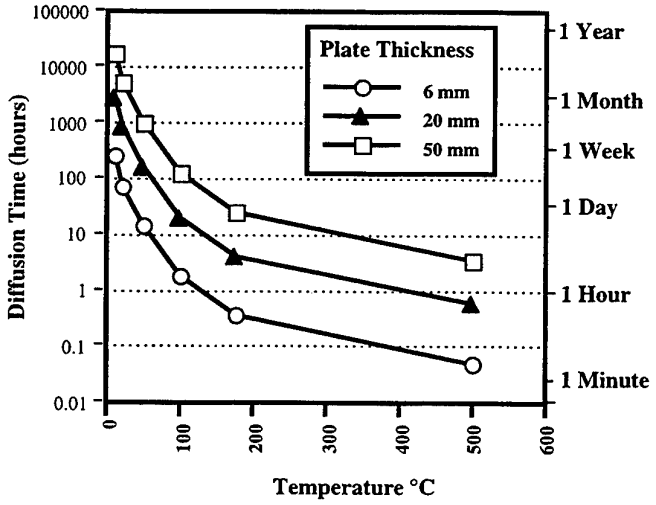

Figure 2 Graph showing, for three different plate thickness, the time required at various temperatures for half of the hydrogen present at the plate centre to diffuse to the surface (data obtained from reference 6).

TABLE 1: TYPICAL COMPOSITION AND MECHANICAL PROPERTIES OF STEELS AND ALL-WELD-METAL WELD DEPOSITS.

a) TYPICAL COMPOSITION (weight percent)

Element	BIS 812 EMA	HY 590	MMA filler E 12018-M2	MIL-120S-1 filler & OP 121 TT ™ flux
C	0.13	0.17	0.04	0.08
Si	0.24	0.24	0.20	0.34
Mn	0.93	0.29	1.55	1.74
P	0.01	0.007	0.010	0.009
S	0.002	0.002	0.008	0.004
Cr	0.48	1.39	0.03	0.31
Ni	1.28	3.06	3.67	2.72
Mo	0.39	0.50	0.26	0.62
V	0.02	0.008	0.01	<0.01
Ti	0.01	0.002	-	0.01
Cu	0.21	0.06	Nil	0.02
Al	0.07	-	-	-
Nb	0.01	0.001	-	<0.01
B	0.0066	Nil	-	-
N	-	-	-	0.0081
Ca	23 ppm.	-	-	<3 ppm
O	0.009	-	-	-
Fe	Bal	Bal	Bal	Bal

b) TYPICAL MECHANICAL PROPERTIES[1]

0.2 % proof stress (MPa)	750	700	800	760
UTS (MPa)	840	800	850	850
Elongation (A5,%)	18	18	19	21

Charpy impact energy (J)

at -18°C	90		100	120
-51°C			73	87
-60°C	75			
-84°C		130		

[1] Note that weld metal mechanical properties may vary slightly, depending upon the procedures actually employed for welding of test coupons and the precise location of test specimens in the weld joint.

However, the filler metal formulations used for steels of similar strength level are identical, and *weld deposits* in BIS 812 EMA are found to have a cracking risk similar to welds in traditional quenched and tempered steels, such as HY-100, when the same welding procedure is used for both parent metals.

Fabricators have little control over the composition of steel and filler metal used in construction, and they have limited control over the hydrogen content of the flux and filler metal. The responsibility for steel and electrode quality resides with the suppliers.

Fabricators do, however, have control over welding procedures employed during fabrication. They can also ensure that the correct electrode handling procedures are followed and that weld cleanliness is maintained at all times.

Factors affecting the risk of hydrogen cracking in parent metal are well understood and various empirical methods for determining preheat levels for given combinations of arc energy, material composition, hydrogen level and quench severity are successfully used to avoid HAZ cracking[7,8]. The risk of hydrogen cracking in weld metal is less well understood and further work is required to establish rules for the control of cracking.

Hydrogen cracking in conventional structural steels is often controlled by regulating the weld cooling rate. Cooling rate is a function of both the temperature of the weldment (preheat and interpass temperatures) and the arc energy per unit length of weld; as determined by Equation 3.

$$\text{Arc Energy} = \frac{A \times V \times 60}{1000 \times \text{Travel speed}} \quad \text{kJ.mm}^{-1} \qquad \ldots.(3)$$

Where 'A' is the mean welding current (in Ampere), 'V' is the mean arc voltage (Volts), and the arc travel speed is expressed in millimeters per minute.

Low heat input and interpass temperatures allow the weld bead to cool quickly after solidification giving hard, martensitic microstructures and trapping more hydrogen in the weld, thereby increasing the risk of HICC. High preheat temperatures combined with high heat input causes larger weld pools that cool more slowly with a reduced risk of cracking. Unfortunately, this approach to control of cracking is unsuitable for QT steels because high preheats and heat input values can also result in reduced toughness[9].

The relationship between heat input and preheat on the properties of welds in high strength steels is illustrated in Figure 3. This shows that insufficient heat input can lead to cracking, however excessive preheat and heat input can lead to undesirable properties such as reduced strength or toughness.

In addition to using the appropriate preheat and input values, maintaining the correct workpiece temperature during and after welding helps hydrogen to diffuse from the weld joint before it cools to a temperature where embrittlement is a problem. It has been found from practical experience that the highest risk of cracking occurs in high restraint joints,

such as in small repair welds, where preheat is maintained only for short periods. The major joints, such as longitudinal and circumferential seam welds in pressure vessels, may take several days to complete and heat is maintained throughout the welding process. Over these long holding times, hydrogen content in the weld zone is reduced considerably and the risk of cracking is relatively low.

It has been argued [11] that high yield and tensile stresses can give a first indication of sensitivity to cracking. For example, it is well known that higher strength electrode formulations, such as E12018-M2 manual metal arc filler metals are more prone to cracking than lower strength designations, such as the E7018-G filler metal. It is also noted that high weld deposit yield stresses are associated with increased sensitivity to stress corrosion cracking (SCC). Tensile tests on weld procedure qualification coupons might therefore be screened for evidence of excessive strength (high yield and tensile stress) or reduced ductility (as measured by low values of elongation or reduction in area).

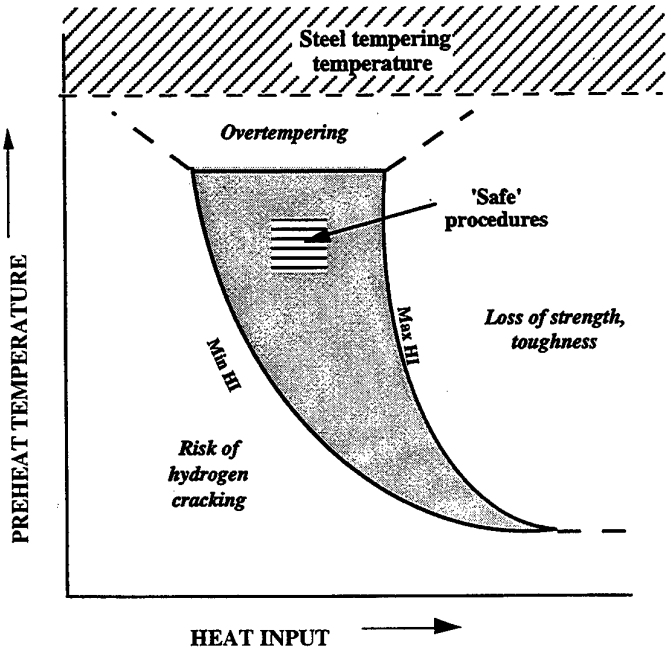

Figure 3 Unscaled graph (after Reference 10) showing the effect of preheat and heat input on weld zone properties. Acceptable properties are only obtained in the shaded region.

This investigation specifically set out to study the effect of a small variation in carbon content on the risk of hydrogen cracking in the resulting weld deposits. It was presumed that weld deposit tensile stress could be used as a measure of sensitivity to embrittlement and cracking.

4. INVESTIGATIONS UNDERTAKEN

4.1 Weld Metal Yield Stress

There is a minimum yield stress requirement of 690 MPa for weld metal in the QT steel plate used for the COLLINS submarines, and a maximum yield stress value of 900 MPa has been prescribed in order to minimize the risk of stress corrosion cracking.

Welding procedure qualification records provide information on filler type, brand and batch number; weld joint design; detailed records of actual welding parameters; and mechanical test results for each joint type. The yield stress values obtained in 188 procedure qualification tests were reviewed and only four yield stress tests exceeded 900 MPa. Histograms showing the distributions of yield stress values for all the qualified procedures are given in Fig. 4; Fig. 4(a) shows the distribution for MMA welds and Fig. 4(b) for submerged-arc weld deposits. Cross-hatched results in Fig. 4 are those outside the acceptable range.

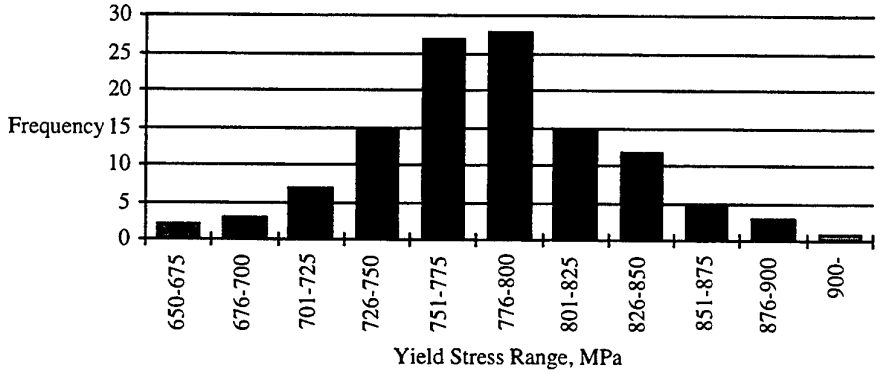

a) E12018-M2 Manual Metal Arc, All Welding Procedures

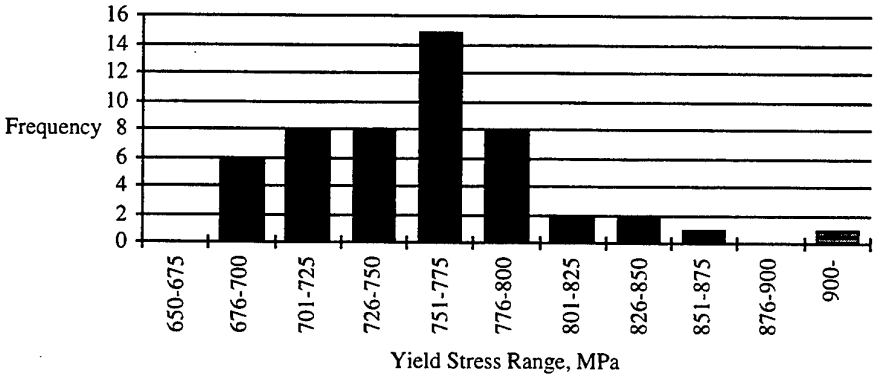

b) E120S-1 Submerged Arc, All Welding Procedures

Figure 4. Distribution of Yield stresses for all weld metals. Results with cross hatching are outside the specified range.

The distribution for MMA welding shows a classic normal distribution with a mean value of about 780 MPa. For the submerged-arc welds, where fewer test results were available, the mean value (about 760 MPa), was slightly lower than for the MMA welds.

Two of the procedure tests that exceeded 900 MPa were made with the GMAW process. In addition, it was noted that GMA welds generally gave lower elongation figures and a high incidence of lack of fusion defects. Consequently GMAW is not used in fabrication of the COLLINS submarines.

TABLE 2(a) **Tensile Test Results for Welding Procedure 1** (an SA weld)

Qualification Test Results	**1(a)** **[Original result]**	**1(b)** **[1(a) Retest]**
Yield Stress	928 MPa	725 MPa
Tensile strength	1024 MPa	841 MPa
Elongation	20%	24%
Reduction of Area	55%	72%

TABLE 2(b) **Tensile Test Results for Welding Procedure 2** (an MMA weld)

Qualification Test Results	**2(a)** **[Original result]**	**2(b)** **[2(a) Retest]**
Yield Stress	908 MPa	772 MPa
Tensile strength	1006 MPa	821 MPa
Elongation	18%	21%
Reduction of Area	61%	65%

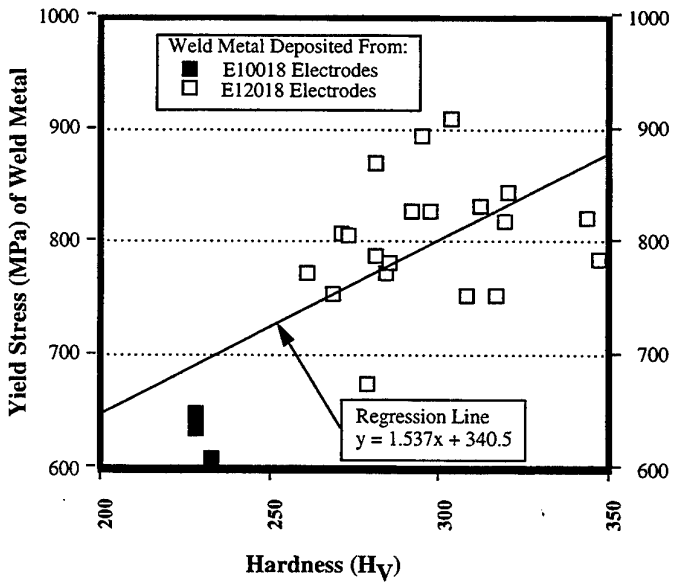

Figure 5. Relationship between yield stress and hardness for procedure qualification tests. Although there is considerable scatter, hardness generally increases with yield stress. The E12018 electrode deposits are clearly harder than the three E10018 deposits.

One of the remaining procedures [Designated 1(a) in this report] which exceeded 900 MPa was welded with the MMA process and the other [2(a)] was with the SA process. In view of the concern about high yield stress in weld deposits, it was decided to re-test these procedures using an identical set of qualification trials. Repeat tensile results of Procedure 1 and Procedure 2 , as shown in Table 2, were much lower than the original results and easily meet the existing requirements.

The welding conditions for Procedure 1 and Procedure 2 were also compared with other successful procedure tests, to see if the high yield stress could be attributed to the way in which they were welded. Heat input, actual interpass temperatures and actual batches used were examined in detail, however no technique differences could be found. Other than normal experimental scatter of results, no explanation can be offered at this stage for the high values of yield stress in these particular weld deposits.

The relationship between hardness and yield stress for all of the procedure qualification tests is presented in Figure 5. It is clear that, for the E12018 electrode formulations used in this work, considerable scatter may occur in both hardness and yield stress. The linear regression for E12018 electrode data is shown in Figure 5, and the significance is low. However, the results in Figure 5 clearly show that the E12018 formulations are significantly harder and stronger than the E10018 formulations. Problems of hydrogen cracking and stress corrosion cracking are therefore more likely to occur in the E12018 electrodes when random variations cause local hard or high stress regions to occur. Greater emphasis is therefore placed on inspection of welds deposited with the E12018 electrodes.

4.2 Composition of Filler Metals

Chemical analysis of Heat B filler wire has been compared with analyses of other heats of the same wire and the relevant specification (MIL-E-23765/20) in Figure 6. Fig. 6(a) shows that the carbon content of Heat B is slightly higher than the other wires examined, however it is well within specification. Comparison of carbon equivalent values according to the IIW formula (Fig. 6(b)) shows that there is little variation from one heat of wire to the next and that Heat B is close to the carbon equivalent value described by the electrode manufacturer as being 'typical'(denoted by 'Typ' in Fig 6). Comparison of compositions according to the Ito-Bessyo P_{cm} formula (Fig. 6(c)) shows a similar result, however Heat B has a somewhat higher value of carbon equivalent than the others.

It should be noted that the carbon equivalent formulae are intended to be applied to base materials and that application of the formulae to filler metals in this case is to simplify the comparison of different compositions only. As a consequence of the slag/metal interactions and parent plate dilution, the weld metal composition may be significantly different to filler metal composition. As an example, Table 3 shows the composition of Heat B electrode and the composition of a weld deposit made using the electrode. Welding variables such as current, voltage and dilution cause variations in weld metal composition even though the flux may be described as 'neutral' in terms of alloying

activity. In other words, variation in weld metal composition depends on both the welding variables and batch-to-batch variation in filler wire composition.

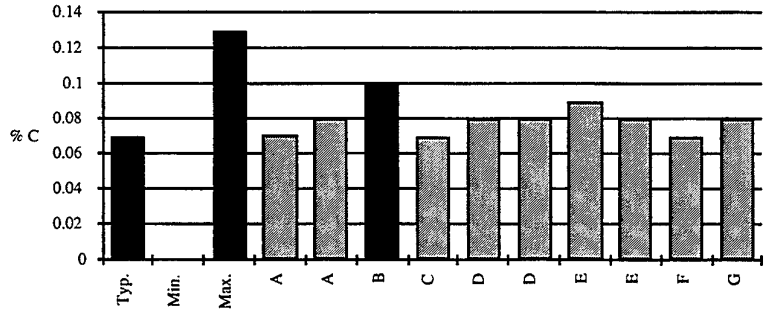

a) Carbon content (Wt. %)

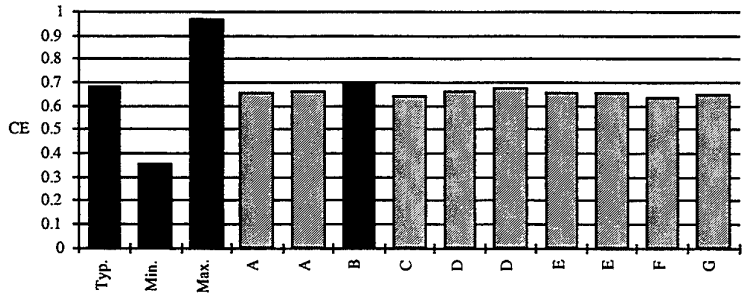

b) Carbon Equivalent according to the IIW Formula (CE_{IIW}, defined in Eq. 1).

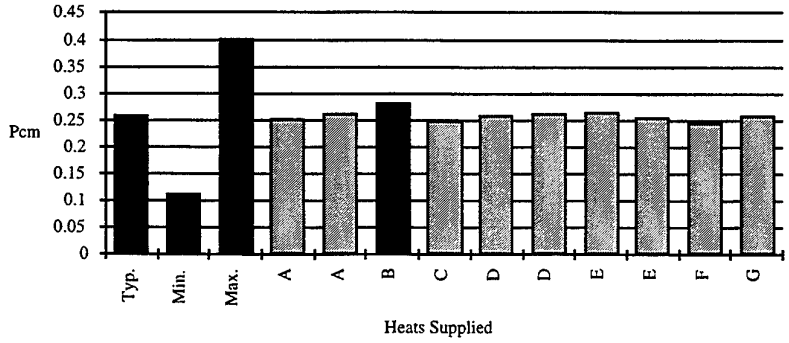

c) Carbon Equivalent according to the P_{cm} Formula (Eq. 2)

Figure 6. Carbon and Carbon Equivalent values of electrodes. Letters A to G denote different heats of the same (MIL-120S-1) filler wire.

TABLE 3 Comparison of Composition of Weld Metal and Electrode Wire. Welding was undertaken using the submerged arc process with OP 121 TT flux

Element	Wire Composition Heat B	Corresponding Weld Metal Composition
Carbon	0.10	0.07
Manganese	1.66	1.42
Silicon	0.35	0.39
Phosphorus	0.009	0.015
Sulphur	0.003	0.002
Nickel	2.36	2.25
Chromium	0.28	0.30
Molybdenum	0.50	0.50
CE_{IIW}	0.693	0.620
P_{cm}	0.283	0.239

4.3 Relationships between Composition and Yield Stress

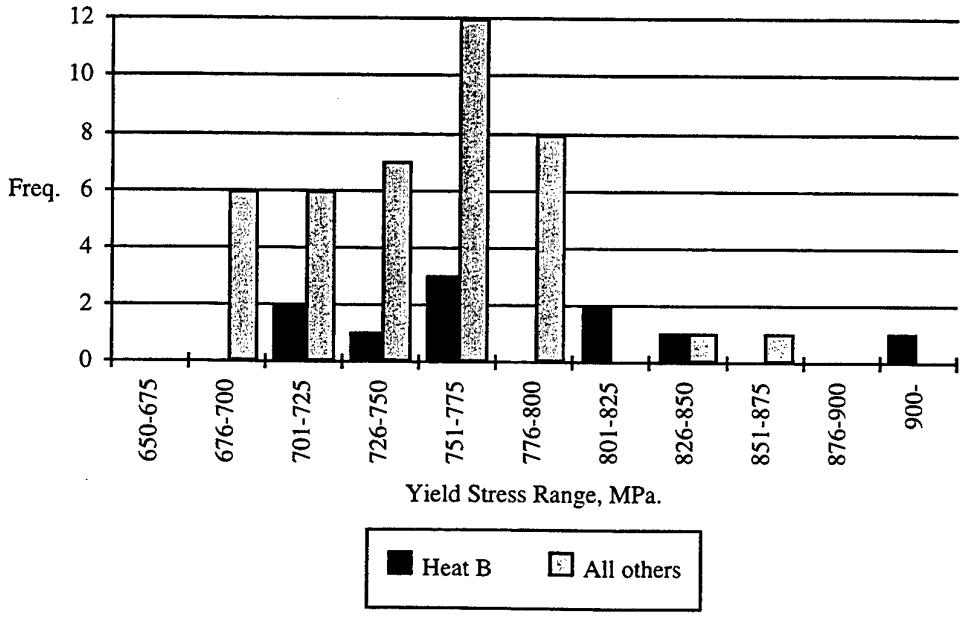

Figure 7 Distribution of yield stress results for welds made with Heat B filler metal and all other submerged arc welds. Although the sample size is small, the distributions

The distribution of yield stress values for Heat B is compared with the distribution for other procedure qualification tests undertaken in Fig. 7. This shows that (allowing for the relatively small sample size) the distribution of yield stress values overlap. The graph shows one value of yield stress greater that 900 MPa [Procedure 1(a) in Table 2], however it also shows that some of the Heat B weld deposits gave comparatively low yield stress values, despite the marginally higher values of CE. As discussed previously, the scatter in yield stress may be attributed to variations in welding procedure. Figure 7 does not take into account that welding parameters vary considerably. Over the range of procedures used at ASC, heat input varies between 1.3 and 2.2 $kJ.mm^{-1}$, with most welding being at heat inputs of 1.8 $kJ.mm^{-1}$ or greater. Preheat and interpass temperatures are controlled within the range 120°C to 200°C.

It is also noted that procedure tests are done on small plates with relatively low restraint, but over a relatively short time scale. Production welds vary widely in the degree of restraint and the time that preheat is maintained. The fact that cracking did not occur in procedure tests is therefore no guarantee it will not occur in production.

4.4 Metallographic Examination of High Strength Welds

The two tensile specimens that gave yield stress values greater than 900 MPa have been examined. The MMA (SMA) weld fractured by a fully ductile mechanism and showed a classic 'cup and cone' appearance.

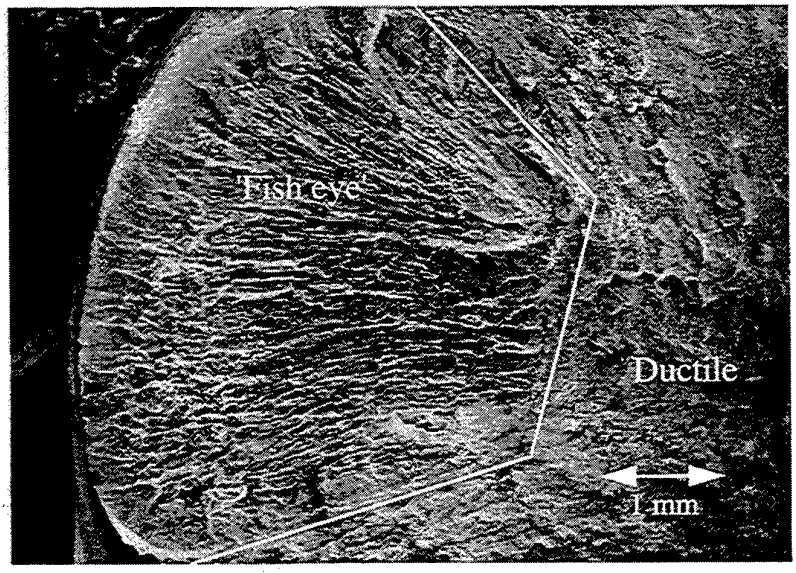

Figure 8 Part of the fracture surface of a tensile test specimen in 928 MPa yield stress submerged-arc weld deposit. This shows a brittle region often referred to as a 'Fish eye' or 'Hydrogen flake'.

Visual inspection of the fracture surface of the tensile specimen removed from the submerged arc weld deposit showed some evidence of low ductility fracture. There was a small area of flat, low ductility fracture commonly described as a 'fish eye'. Detailed examination of this region in the scanning electron microscope (Figs. 8 and 9) showed that failure occurred by a mixture of grain boundary and cleavage fracture, typical of hydrogen embrittlement. The tensile test specimen was radiographed for evidence of hydrogen cracking, however none could be found. roughly coincide.

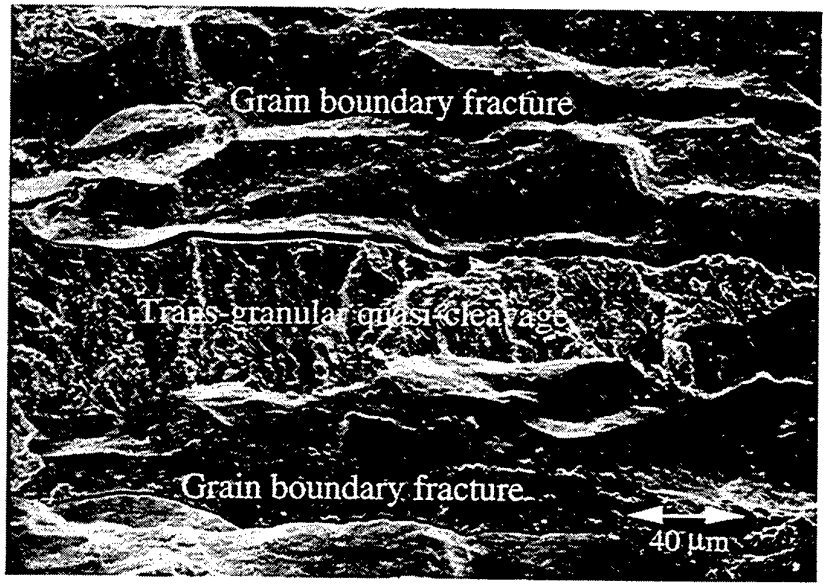

Figure 9 Detail of the 'Fish eye' in Fig. 8 Showing that fracture has occurred by a mixture of grain boundary fracture and trans-granular cleavage fracture. These are low ductility fracture modes commonly associated with hydrogen embrittlement.

Metallographic examination of this submerged arc weld (Fig. 10) showed a fine acicular ferrite microstructure with small regions of ferrite, martensite or Bainite. This microstructure is often considered to provide good toughness at these high values of yield stress. Hardness in the weld zone varied from 283 to 325 Hv_{10}, which is not exceptionally high.

The microstructure of this weld deposit has not been assessed using the higher magnification techniques (such as TEM). It is possible that the fine microstructure which appears as acicular ferrite in the optical microscope may in fact be martensite under TEM.

4.5 Non-Destructive Examination of Welds

The extent of non-destructive examination of welds carried out on the COLLINS submarines depends upon the location and type of each particular weld. No inspection technique is infallible. While specifications call for no cracking, in practice there is a chance it will remain undetected. To overcome this, each weld is inspected with several complementary inspection techniques. Visual and magnetic particle inspection is applied to all welds for the detection of surface cracking and internal cracking may be detected by ultrasonic testing radiographic examination or both.

The type of cracking which occurs may be either longitudinal or transverse to the weld. Surface inspection techniques such as dye penetrant and magnetic particle inspection are able to detect both longitudinal and transverse cracks which reach the surface. Radiography is able to detect both transverse and longitudinal cracks, but they may be missed if they are fine or not aligned parallel to the radiation beam. Radiography is more suited to the detection of volumetric defects rather than planar ones. It is unsuitable for examining Tee joints and fillet welds. Standard ultrasonic inspection techniques are able to detect fine longitudinal cracks in butt and tee joints, but special techniques are required to examine for transverse cracking.

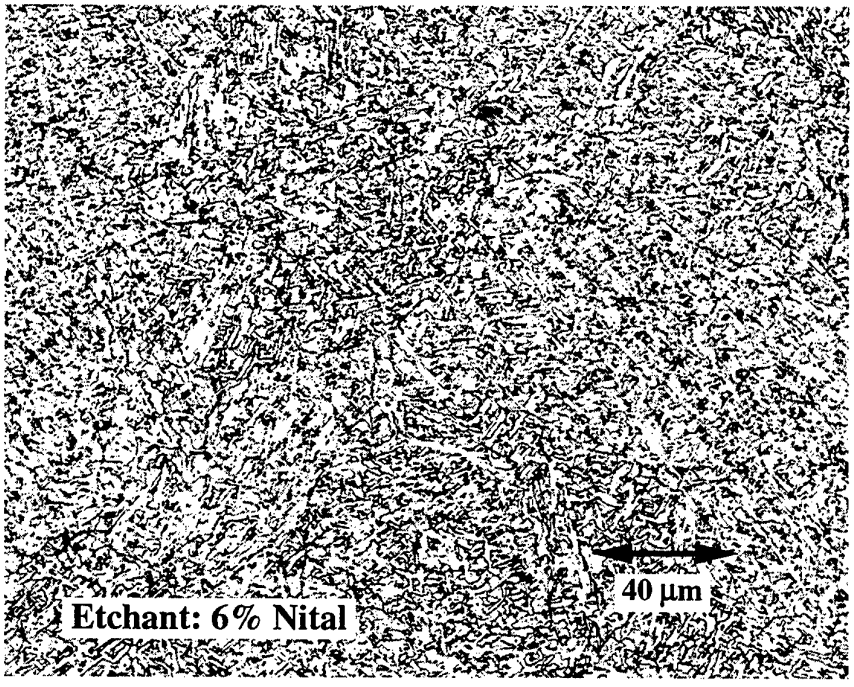

Figure 10 Photomicrograph of weld deposit that obtained 928 MPa yield stress during tensile testing. The microstructure is mainly acicular ferrite but contains secondary structures which may be martensite, pro-eutectoid ferrite or Bainite. The weld provides satisfactory ductility and toughness despite the exceptionally high yield stress.

Inspection of welds on the COLLINS class submarines is extensive. Welds are required to be examined visually during and after completion. MPI is undertaken if preheat is accidentally lost and on the backgouged weld before welding the second side. MPI is required after removal of defects and before rewelding. Completed butt welds in pressure hull are given 100% visual examination, 100% standard ultrasonic examination, 5% ultrasonic examination for transverse cracks, 100% magnetic particle examination and 10% radiography. The magnetic particle examination is undertaken after the external weld cap has been ground off. With this extent of inspection, it is believed there is little risk of an undiscovered cracking problem.

Cracking has occasionally been found during construction of COLLINS class submarines. In each case, the cause of cracking is assessed and steps are taken to prevent recurrence of the problem. The cracks discovered are always rectified. In the light of experience, the method for ultrasonic examination for transverse cracks has been reviewed and upgraded. The revised inspection method has been used to re-evaluate early work on a random basis, without revealing undiscovered cracking. In this way the risk of cracking is effectively managed.

4.5.1 Validation of Technique for Detection of Transverse Defects

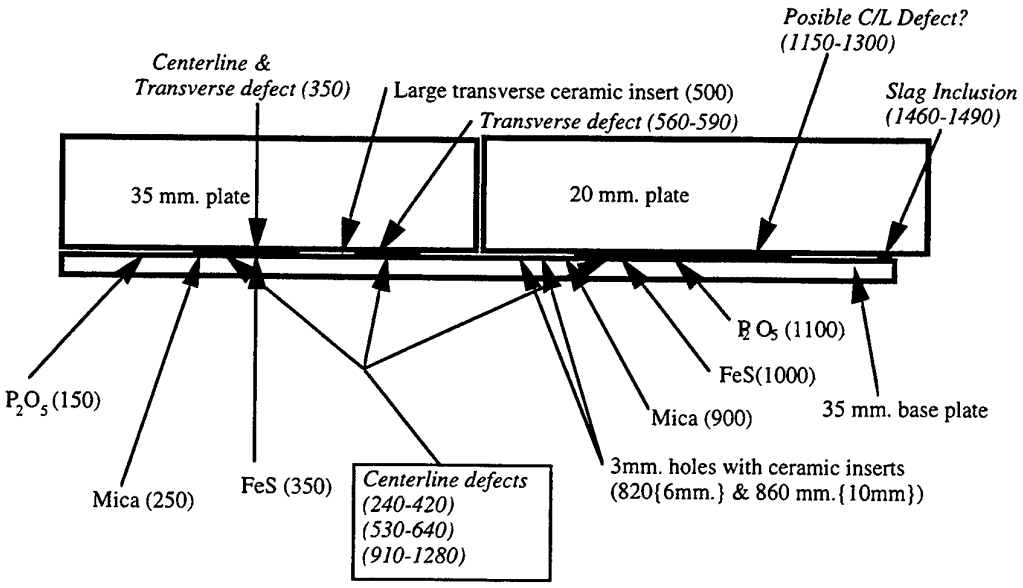

Figure 11 Design of test plate for ultrasonic assessment, showing the location of known cracks and introduced artificial defects. Defects in italics are located on the far side of the joint. Numbers refer to distances from the plate edge at the left hand side. Distances in braces ({}) refer to the depth of drilled holes.

It is evident from this work that reliable procedures are urgently required for ultrasonic inspection of T-butt joints for transverse cracking. This is necessary for routine inspection of the joints and could be required for any auditing of work already completed.

In one investigation at AMRL, two welds of T-butt configuration were produced using welding procedures found to give extensive transverse cracking. The design of the test coupon is illustrated in Figure 11. It consists of one 35 mm and one 20 mm plate welded to a 35 mm base plate. In addition to using crack sensitive welding procedures, a number of artifacts were deliberately added to the weld pool with the intention of producing artificial defects. The artifacts were P_2O_5 (gives excessive porosity), sheets of mica (to simulate cracks), FeS (to give extensive transverse and longitudinal solidification cracking) and ceramic inserts in drilled holes. The procedure for ultrasonic inspection for transverse defects in this case was that used in practice and the results showed that transverse defects can be readily detected, but difficult to size. With the exception of the small ceramic insert, all of the artificial defects were detected and most of the pre-existing cracks were found. This gives confidence that the procedure is adequate for the detection of transverse cracks.

4.6 Inspection of Test Section

It happens that a range of candidate welding procedures were used in a Test Section that was fabricated before starting construction. This section was made as part of the work developing welding procedures, and coincidentally most of the submerged arc welding of this section was made with the high carbon, Heat B wire. Welds on this section have been re-inspected with the specified ultrasonic test procedure and only one transverse defect was found. This was associated with a longitudinal slag defect which would normally have been detected and repaired. It was deduced from this that cracking was relatively uncommon and required unusual events, such as slag entrapment, to occur.

5.0 RISK EVALUATION

Results of the investigations may be summarized as follows:

a) Four of the 188 welding procedure qualification tests undertaken gave values of yield stress of over 900 MPa. Of these four, two were used as the basis for production welding procedures. Re-testing of these two procedure qualifications gave yield stress results that were significantly lower than the original and well within the current requirements.

b) The weld deposit giving the highest yield stress (>900 MPa.) nonetheless gave high values of elongation (20%) and had a desirable, acicular ferrite microstructure.

c) One welding wire that has higher carbon equivalent value has been used during fabrication of the COLLINS. This wire was also used on a test can which was used to develop welding procedures. Extensive non-destructive

and destructive investigation of the can has produced little evidence of cracking.

d) For a given 690 MPa welding wire designation, the yield stress and hardness of the weld deposit may vary considerably depending upon the welding parameters used. Minor variations in the carbon composition of the filler wire can have an influence on yield stress however, in the case of Heat B wire investigated here, the influence composition is insignificant compared to the influence of welding parameters.

e) Current NDE techniques are revealed to be efficient at detecting cracks in a weld deposit, however the sizing of cracks is imprecise. Extensive NDE inspection has been carried out on COLLINS without discovering large numbers of cracks. Cracking has been discovered on occasions, but it has been minor and was not endemic. On each occasion steps have been taken to prevent a recurrence of the problem.

On the basis of experience in fabricating COLLINS submarine hulls, the overall risk of undetected hydrogen cracking is considered to be relatively low.

6.0 DISCUSSION

Results of the investigations show that considerable scatter may occur in the yield stresses of welds deposited with similar welding consumables. As illustrated in Figure 4, the spread of yield stress results can vary from below 675 MPa to values greater than 900 MPa. The results presented in Figure 7 show that there is little difference between the distribution of yield stress results for welds deposited with the high carbon (Heat B) electrode and the distribution of results for all other electrodes. Furthermore, the weld deposit giving the highest yield stress (>900 MPa.) was a Heat B electrode. Nonetheless, this gave high values of elongation (20%) and had a desirable, acicular ferrite microstructure.

The scatter in yield stress may be partly attributable to variations in welding procedure. Figure 7 does not take into account that welding parameters vary considerably. Over the range of procedures used here, heat input varied between 1.3 and 2.2 $kJ.mm^{-1}$, with most welding being undertaken at heat inputs of 1.8 $kJ.mm^{-1}$ or greater. Preheat and interpass temperatures are controlled within the range 120°C to 200°C.

As illustrated by the results for re-testing two of the welding procedures which gave high weld deposit yield stress (Table 2), however, significant scatter of results may also occur when the same welding consumable is used with identical welding parameters. This shows that reproducibility of tensile properties for these high strength weld deposits is not good, and that the fabricator actually has limited control over the weld mechanical properties obtainable in a weld deposit.

When compared to the effect on yield stress of either welding parameters or minor variations in the filler wire carbon composition for these weld metals, it is clear that random scatter has a significant influence.

It is noted that procedure tests reported here are done on small plates with relatively low restraint, but over a relatively short time scale. Production welds vary widely in the degree of restraint and the time that preheat is maintained.

It happens that a series of welds was undertaken on a test section designed to simulate part of the structure. These welds were undertaken on plate having realistic levels of restraint and a wide range of procedures were used. The fact that only one transverse defect was found and that this was associated with a longitudinal slag defect suggests that cracking was relatively uncommon and required unusual events, such as slag entrapment, to form.

Although limited evidence of cracking was found in the welded test section, the wide range of tensile stress results suggest that problems of hydrogen cracking and stress corrosion cracking are a significant consideration when welding with E12018 electrodes. Consequently, care should be taken in the preparation of welding procedures for these steels and greater emphasis should be placed on inspection of welds deposited with the 690 MPa yield stress electrodes.

The work described here also casts doubt on the value of using the carbon equivalent formulae *alone* as a measure of sensitivity to cracking. Strictly, these formulae were developed as a means of estimating *parent metal* hardness and their use as a measure of crack sensitivity has developed from empirical evidence that higher carbon equivalent weld metals have a higher risk of cracking. The authors know of no equivalent formulae for estimation of *weld metal* hardness, and the results of Figure 7 shows that a weld metal containing higher carbon equivalent may none-the-less give a distribution of yield stress that is indistinguishable from the norm.

6. SUMMARY

The risk of hydrogen cracking and embrittlement in high strength steels has been reviewed and an assessment has been made about the risk of increased crack sensitivity associated with a slight increase in filler metal carbon content.

The experimental technique involved reviewing procedure qualification test records for any relationship between composition and weld mechanical properties. It was found that a wide variation in weld metal yield stress that may occur during fabrication with 690 MPa electrodes and that this scatter was sufficient to hide any effect of small variations in composition.

Regions of weld on an experimental fabrication which were welded with the higher carbon electrodes and a wide range of welding procedures have been examined by

ultrasonic testing and negligible evidence of cracking was found. This gives confidence that the procedures used in fabrication have a low risk of cracking.

REFERENCES

1. Ritter, J.C., Dixon, B.F and Phillips R.H. '*Assessment of Welded Steel of 690 Yield Stress for the Type 471 Submarine*' MRL Technical Report MRL- TR-90-1

2 Phillips, R.H., Dixon, B.F. and Ritter, J.C. (1989) ' *Qualification of New Steel for Australian Submarine Construction*' Proceedings of the 37 th. Annual Conference, Welding Technology Institute of Australia, Sydney.

3 Dixon, B '*Evaluation of Welding Consumables and Procedures for Submarine Construction*' MRL Technical Report MRL - TR - 94-3.

4 TS-009 '*Welding Specification for Hull and Hull Attachments*' Confidential Technical Specification, Kockums AB.

5 Håkansson, K. and Dixon, B. (1996) *'Submerged Arc Welding with Alloy Powder Additions for High Strength Steels'* Int. J. for the Joining of Materials, 8, (1), 14-21.

6 Ito,Y. and Bessyo, D. (1968) *'Weldability Formula of High Strength Steels Related to Heat Affected Zone Cracking'* IIW Doc. IX-467-68

7 Australian Welding Research Association (AWRA) Technical Note 1.

8 Bailey, N. Coe. F. R., Gooch T. G., Hart, P. H. M., Jenkins, N. and Pargeter, R. J. 'Welding Steels Without Hydrogen Cracking', 2nd edn, 1973, Abington Publishing and ASM International.

9 Dixon, B. F. and Håkansson, K (1995) *'Effect of Welding Parameters on Weld Zone Hardness and Toughness in a 690 MPa Steel.'* Welding Journal Research Supplement, April, 1995, 122-s - 132-s.

10 Australian Welding Research Association (AWRA) Technical Note 16.

11 Davidson, L., and Lynch, S.'Seminar paper to be presented at the joint Defence Science and Technology Organization / Welding Technology Institute of Australia Seminar, Melbourne, Australia, October 23, 1996.

Hydrogen Behaviour in Welded Joints

Igor K. Pokhodnya*

E.O.Paton Electric Welding Institute, National Academy of Sciences of Ukraine, Kyiv, Ukraine

* I.K.Pokhodnya - Head of the Department for Welding Metallurgy and Consumables at the E.O.Paton Electric Welding Institute, Professor, Doctor of Technical Sciences, Member of the National Academy of Sciences of Ukraine.

In this presentation a review of investigations conducted at the E.O.Paton Electric Welding Institute on behaviour of hydrogen in welded joints is given.

The problems considered are as follows:

1. Hydrogen mass transfer in steels and welded joints:
   - analytical equipment;
   - effect of element composition of weld metal and electrode coatings;
   - effect of traps;
   - effect of deformation of weld metal.
2. Mechanism of hydrogen embrittlement.
3. Effect of hydrogen on mechanical properties of steels and welds:
   - evaluation procedure and equipment;
   - experimental results;
   - lines of future research.
4. Hydrogen and delayed fracture of welded joints.
5. Technology and metallurgy methods for decreasing the content of diffusible hydrogen:
   - sources of hydrogen;
   - sampling and analysis;
   - effect of current and welding speed;
   - distribution of hydrogen in welded joints;
   - thermodynamic studies of interaction of oxy-fluoride melts with water vapours;
   - effect of fluorides and oxides;
   - effect of composition of coating, flux and flux-cored wire;
   - hydrides.
6. Consumables for welding low-alloy high-strength steels:
   - electrodes;
   - agglomerated fluxes.
7. References.

Cold cracks are one of the basic defects formed in low-alloys steels during welding. Many-year research conducted by scientists and engineers in the USA, Great Britain, Japan, France, Australia and the former Soviet Union resulted in identifying the factors which primarily contribute to the formation of cold cracks. They are: element composition of steels and weld metal, thermal-deformation cycle, phase transformations, content and distribution of hydrogen in welded joints.

Determination of a mechanism of the effect of hydrogen proved to be the most difficult problem. Physical nature of this effect is as yet little understood. Behaviour of hydrogen is a subject of investigation of a team of scientists at the E.O.Paton Electric Welding Institute. In this presentation an attempt to review some of these investigations associated with the behaviour of hydrogen in welded joints will be made.

1. HYDROGEN MASS TRANSFER IN STEELS AND WELDED JOINTS

There are the following types of Hydrogen transfer in steels an d welded joints:

a) diffusion in the field of concentration gradient;
b) diffusion in the stress field;
c) thermal diffusion;
d) surface diffusion;
e) diffusion along the microstructure defects;
f) transfer by dislocations.

Fig. 1 shows a laboratory unit used to study effusion of hydrogen from steel samples within the temperature range from 20 to 250^{o}C. A sample has a cylindrical shape, it is 6 mm in diameter and 15 mm long. We use a chromatographic analyzer and computer processing of a signal. Fig. 2 shows the investigation results on the effect of chemical composition of metal on characteristics of the hydrogen mass transfer. Alloying of metal with molybdenum, chromium and especially manganese decreases diffusability of hydrogen. The effect of a composition of welds made using electrodes with basic and rutile coatings is illustrated in Fig. 2. The rate of the hydrogen mass transfer in welds made using basic electrodes is higher than that in welds made using rutile electrodes. This is associated with a large amount of traps, i.e., non-metallic inclusions, present in welds made with the rutile electrodes.

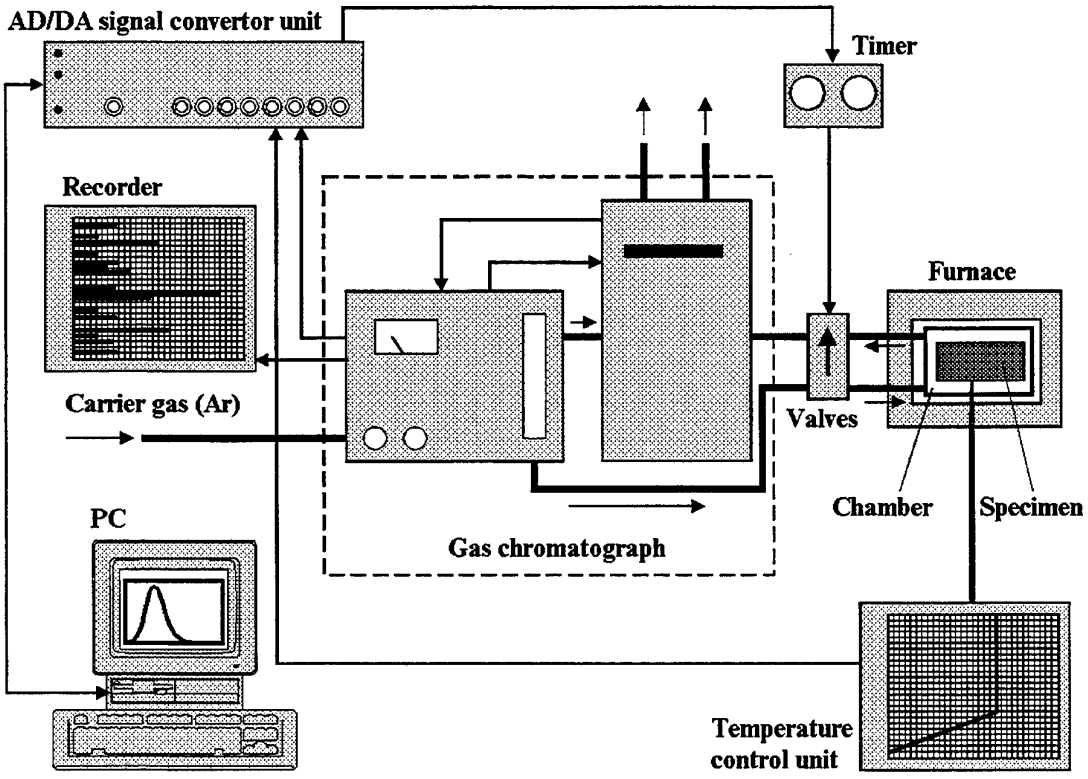

Fig. 1. Computerized analytical system for measuring the hydrogen effusion.

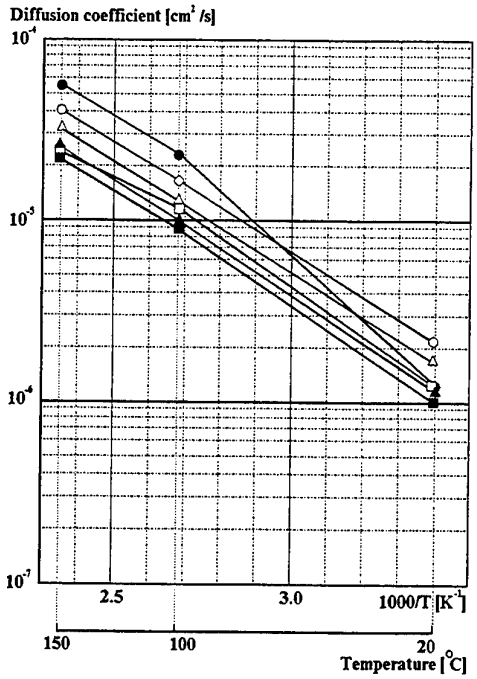

Fig. 2. Influence of alloying on hydrogen diffusion coefficient in steels.

Table 1

Chemical composition of the steels on the Fig. 2

Test number		[H], cm³/100 g	Element content, wt.%						
			C	Si	Mn	Ni	Mo	S	P
1	○	4.3 ... 5.1	0.082	0.21	0.59	2.69	0.51	0.020	0.015
2	●	2.7 ... 3.3	0.078	-	0.58	0.79	0.17	0.018	0.014
3	△	5.7 ... 6.0	0.110	-	1.77	0.93	0.19	0.018	0.013
4	▲	7.3 ... 9.1	0.094	-	1.79	2.80	0.47	0.019	0.014
5	□	7.4 ... 8.6	0.099	-	2.31	1.27	0.23	0.021	0.022
6	■	8.2 ... 8.5	0.083	-	2.21	3.00	0.54	0.022	0.018

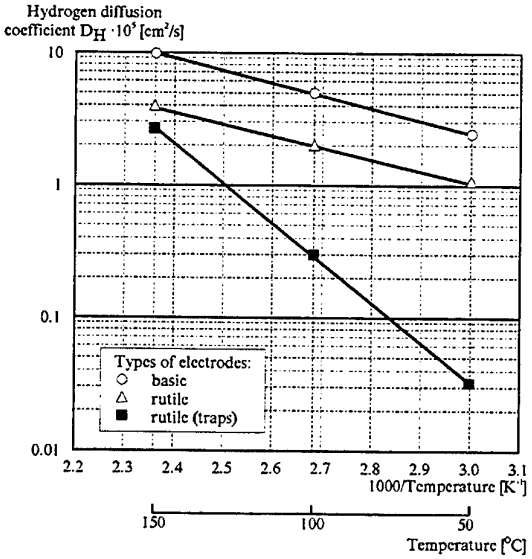

Fig. 3. Temperature dependence of diffusion coefficients of hydrogen in deposited metal from basic and rutile coated electrodes and temperature dependence of the rate constant of hydrogen evolution from traps (rutile-(traps)).

The effect of the hydrogen traps on the effusion process can be well seen from Fig. 4. Experimental kinetic curves (dependence of the rate of evolution upon the hydrogen content of a sample) substantially deviate from the calculated ones in the region of the low hydrogen concentrations. A decrease in temperature adds to a delay of evolution of hydrogen from the reversible traps. Solution of the Fick's equation gives:

$$\frac{\partial C}{\partial t} = \frac{1}{r} \cdot \frac{\partial}{\partial r} \cdot \left(r \cdot D \cdot \frac{\partial C}{\partial r} + \frac{\partial}{\partial y} (D \cdot \frac{\partial C}{\partial y}) \right), \tag{1}$$

$$C(0, r, y) = C_0 \text{ and } C(t, r, 0) = C(t, r, L) = C(t, R, y) = 0, \tag{2}$$

where: C is a hydrogen concentration; D is its diffusion coefficient; t is a time; r and y are cylindrical coordinates; C_0 is an initial concentration of hydrogen in the specimen of radius R and length L.

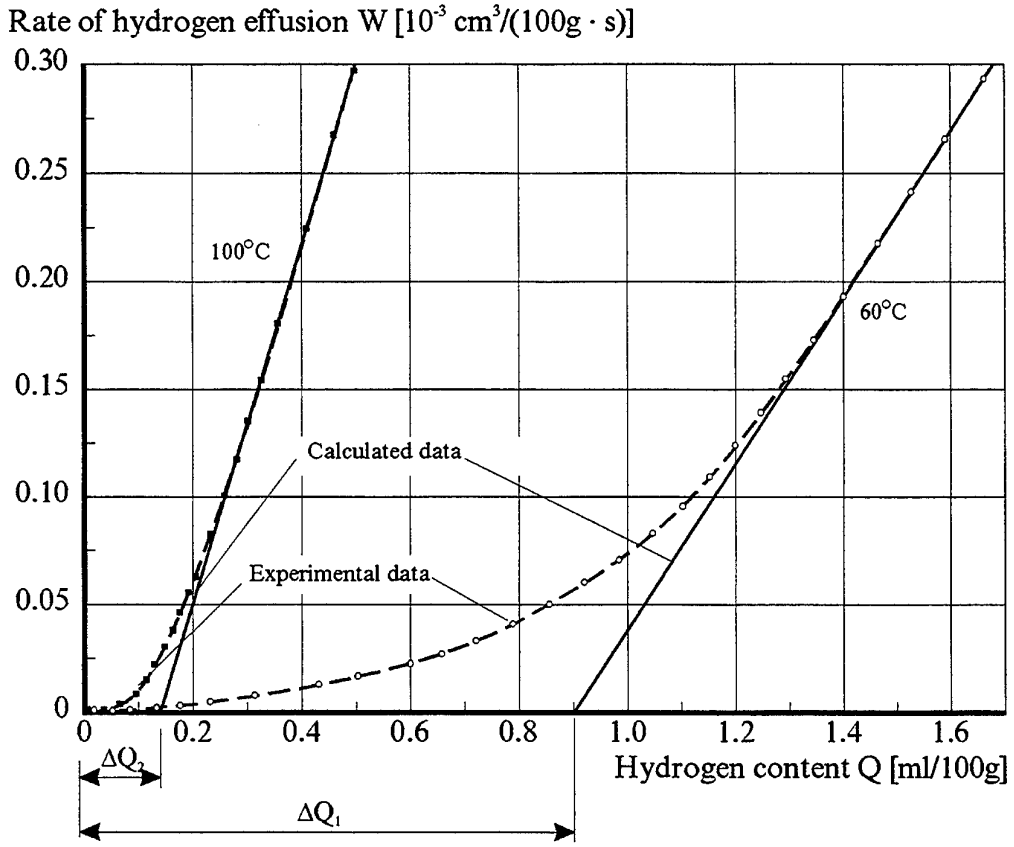

Fig. 4. Influence of traps on the behaviour of effusion curves at low hydrogen content in specimen for analysis temperature 60 and 100°C (rutile type coated electrodes).

Fig. 5 shows a diagram of an experimental cell used to determine the effect of deformation on the hydrogen mass transfer. A hollow sample is fixed in the testing machine holders. A stationary flow of hydrogen through the sample wall was formed by continuous electrolytic hydrogenation. This flow was registered by a chromatograph. Dependencies shown in Fig. 6 illustrate the effect of plastic deformation on the mass transfer. The diffusion slowed down with an increase in the number of defects in metal, while at the moments of loading the spikes of the flow were observed during the intensive plastic deformation, this being caused by the dislocation transfer of hydrogen.

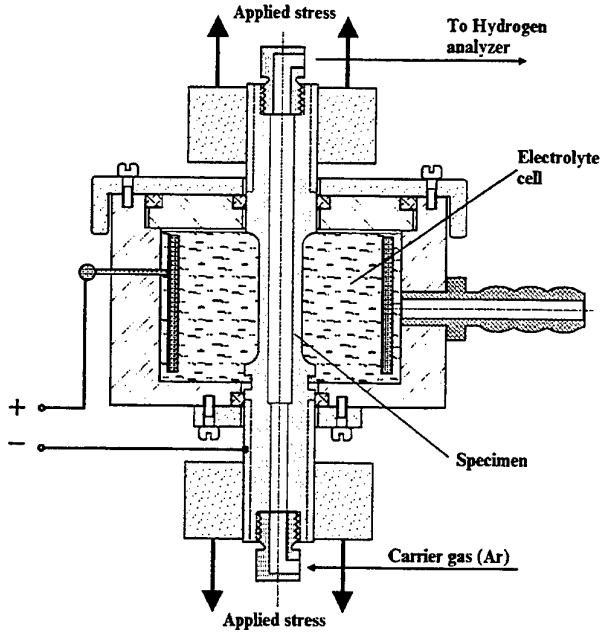

Fig. 5. Experimental cell for investigation of hydrogen behaviour during deformation of steels.

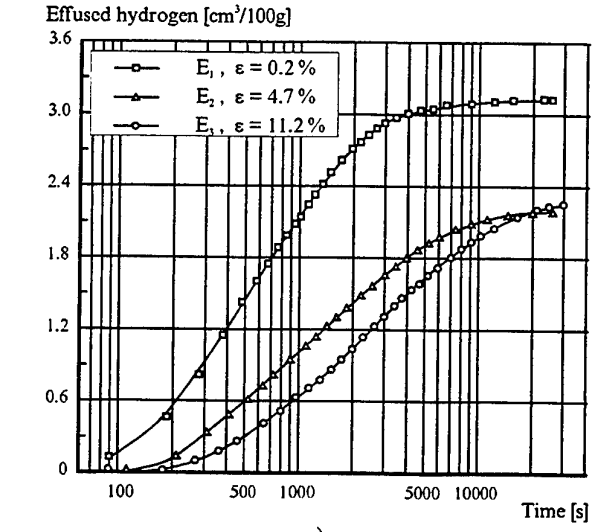

a)

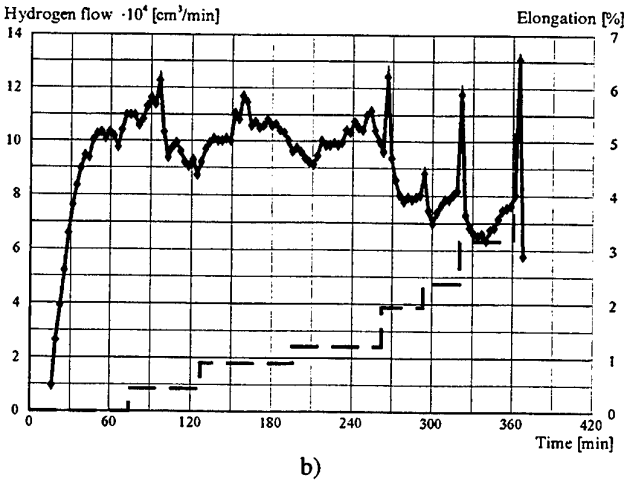

b)

Fig. 6. Hydrogen mass-transfer in steel during its deformation (a) and hydrogen permeation through the mild steel under stress and deformation (b).

2. MECHANISM OF HYDROGEN EMBRITTLEMENT OF METAL

The state of hydrogen in iron was studied by secondary-ion mass spectrometry (SIMS method). This methods provides resolution to the depth of an atomic monolayer. Flow diagram of the method and schematic of the experimental unit to employ it are shown in Fig. 7.

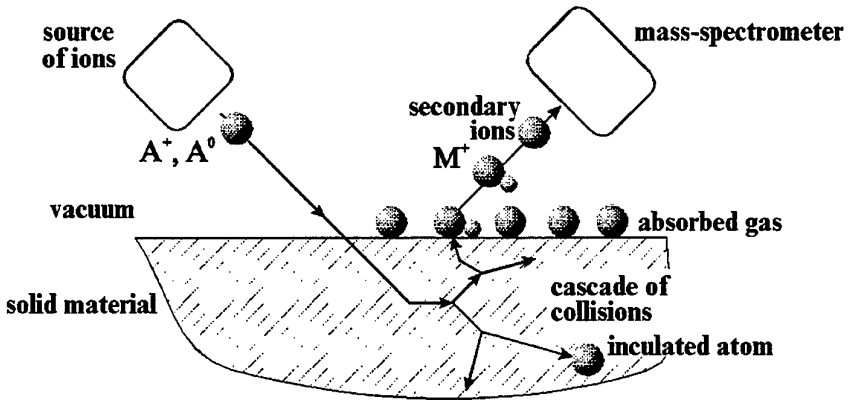

a)

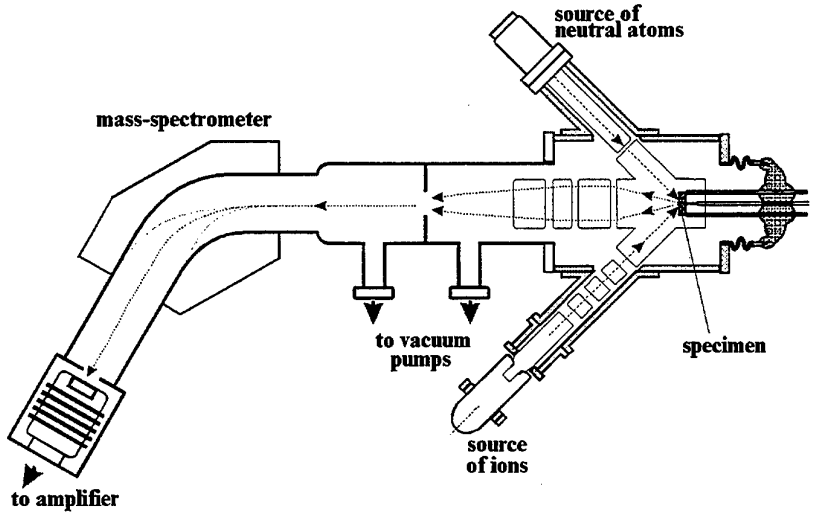

b)

Fig. 7. Investigation of the state of hydrogen using Secondary-Ion Mass-Spectrometry method (SIMS) (a) and Mass-spectral instrument applying SIMS-method (b).

An intensive emission of secondary negative hydrogen ions H^- which decreased with time was found in the hydrogen-saturated samples. In this case the emission of the positive ions H^+ did not depend upon time (Fig. 8). This observation showed that it was a diffusible hydrogen that caused the emission of anions H^-. Besides, the iron surface work function (4.5 eV) considerably raised the electron affinity of a hydrogen atom (0.75 eV). Therefore, the intensive emission of secondary ions H^- is possible only in the case when the atoms of hydrogen at the iron surface already had a negative charge: at a high initial velocity (as compared to the thermal velocity) of the secondary particles there is a high probability that they will "survive" in the initial charge state (in this case it is a negative charge state).

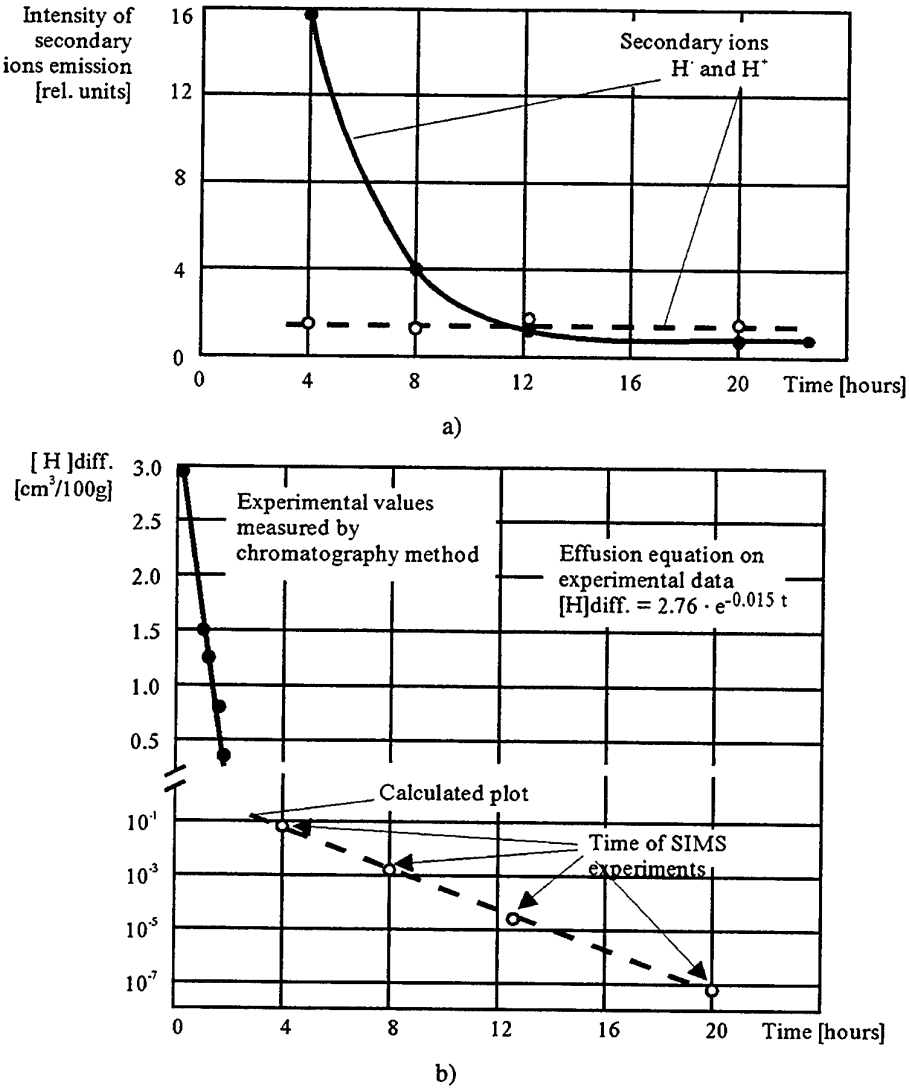

Fig. 8. Time dependence of secondary emission ions H^+ and H^- from hydrogenated steel specimen (a) and hydrogen effusion from the specimen using SIMS experiment (b).

These experimental facts were used for formulation of a new hypothesis of hydrogen embrittlement: Formation of a layer of the negative hydrogen ions at the juvenile surface of a crack initiated in the bulk of metal should lead to a decrease in the surface tension and this, in turn, should lead to a change in its behaviour in the field of stresses.

According to the new notions of metals physics about micromechanisms of fracture, a critical stage of fracture is a change to the Griffits growth of the intragranular embryo submicrocracks, rather than a loss of stability of a micro- or macrocrack, as it is suggested in the traditional approaches.

These submicrocracks are initiated in a local field of dislocation ensembles formed during the process of plastic deformation (Fig. 9). A macrofracture is caused by the submicrocrack which, in the total field of dislocation clusters and external stresses, loses its stability at the moment of its initiation. Additionally to the intragranular cracks, the cracks can initiate also inside the secondary phase particles or the brittle inclusions which fail usually before the sufficiently large dislocation clusters are formed in the matrix.

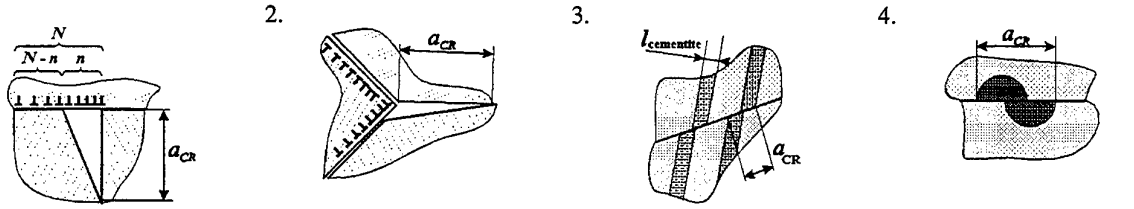

cluster of dislocations sopped by obstacle | crossing of the shifted planes | cutting of the cementite planes | cutting of the globular inclusion

Fig. 9. Some schemes of the cracks formation.

$$
\begin{aligned}
W &= W_1 + W_2 + W_3 + W_4 \\
W_1 &= \frac{(n\cdot b)^2\cdot\mu}{4\cdot\pi\cdot(1-\upsilon)}\cdot\ln\frac{4\cdot R}{a} \\
W_2 &= (N-n)^2\cdot\frac{b^2\cdot\mu^2}{4\cdot\pi\cdot(1-\upsilon)}\cdot\ln\frac{4\cdot\pi\cdot\sqrt{e}\cdot(1-\upsilon)\cdot R\cdot(\tau_\upsilon-\tau_i)}{b\cdot\mu\cdot(N-n)}, \\
W_3 &= 2\cdot\gamma\cdot a \\
W_4 &= -\frac{\pi\cdot\sigma_1^2\cdot a^2\cdot(1-\upsilon^2)}{2\cdot E}
\end{aligned}
\qquad (3)
$$

where W_1 is an energy of super-dislocation; W_2 is an energy of dislocation retained in the cluster; W_3 is an energy of a new surface and *W4* is an energy of sub-microcrack in the field of external stress σ_1.

So, the hydrogen embrittlement model could be described as follows. Critical stage of hydrogen induced fracture is the loss of equilibrium state of intragrain embrio sub-microcrack at the moment of its occurrence in the local stress field of the dislocation cluster during plastic deformation. Also, the formation of such cracks is probable inside the second phase or in brittle inclusions. And, thus:

1.Hydrogen reduces the energy of new surface.

2.The embrio microcrack overcomes the potential barrier at lesser external stress σ_1.

3.After that the motion of the crack is accelerated by external stress.

4.Reduction of the σ_1 value means the increase of brittleness.

Plot of energy *W* against the crack lenght *a*

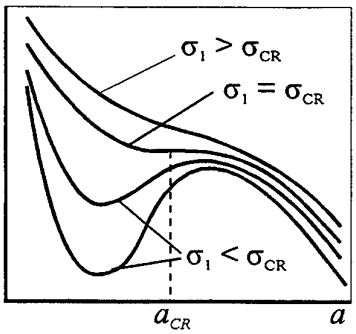

Fig. 10. Plot of energy *W* against the crack length *a*.

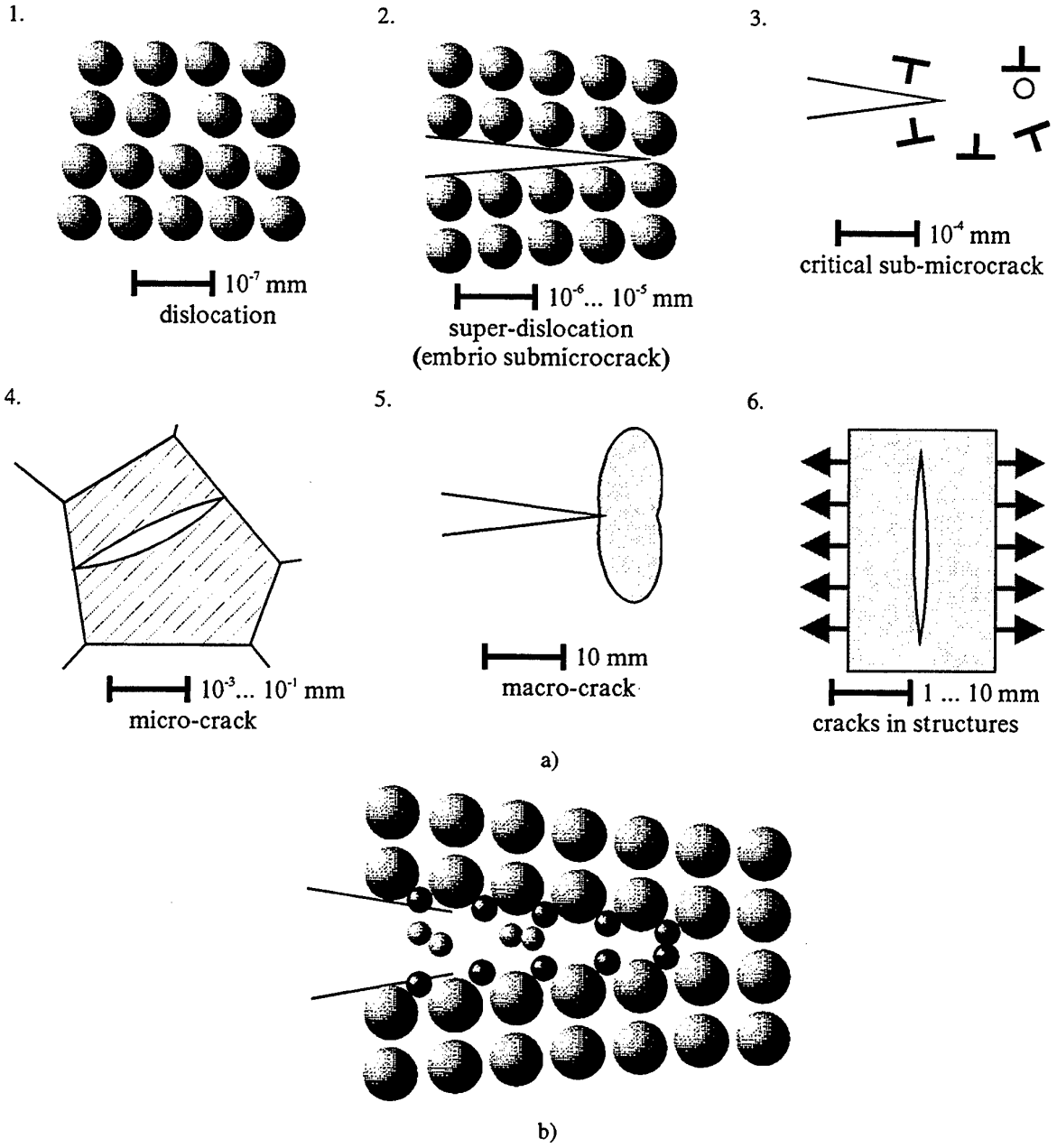

Fig. 11. A hypothesis of hydrogen embrittlement: scheme of defects scale classification (a) main attention should be given to embrio sub-microcrack (position 2, a) (b).

The presence of negative ions of hydrogen on the surface of the crack makes its growing to macrosize according to Griffith's mechanism during initial stage.

According to these notions, the mechanism of the effect of hydrogen on the fracture process can be described as follows.

Mechanism of the effect of hydrogen on the steel fracture process (model conditions).

(1) Concentration of hydrogen is 5 ... 10 cm^3/100 g.

(2) Irreversible traps (pores, cracks, interfaces) are absent.

(3) Hydrogen fills in the irreversible traps - dislocations.

Hydrogen, during the plastic deformation of metal, is transported by the moving dislocations to a point of initiation of a fracture crack. Initiation of a submicrocrack is described by the Ziner-Stro model (submicrocracks are formed at the apex of a dislocation cluster and the dislocation cluster is stopped by a grain boundary). Behaviour of the submicrocrack in the field of external stresses is determined by the energy of the 'dislocation cluster - submicrocrack' system. The submicrocrack can be collapsed, remain in the state of elastic equilibrium or indefinitely grow. Hydrogen which is evolved from the dislocations is chemisorbed at the surface of the initiated cracks to decrease its surface energy. The level of normal stresses required for transformation of the submicrocrack into a state of autocatalytic propagation is decreased. A decrease in the fracture stress under the effect of hydrogen shows up on a microlevel as its embrittlement effect. Some elements of the model studied experimentally proved validity of the suggested mechanism.

Experimental and theoretical proof of the model of the effect of hydrogen on the fracture process.

(1) While dissolving in metal, hydrogen is condensed at the dislocations [1].

(2) The effect of hydrogen is local [2].

(3) Hydrogen is transported to a point of initiation of a submicrocrack by the dislocations [3].

(4) Hydrogen which is evolved from the dislocations is chemisorbed at the surface of an embryo crack causing a change in its energy state [4].

(5) The submicrocrack which has overcome a potential barrier is autocatalytically propagated under the effect of hydrogen into the field of stresses to form a macrocrack [5-8].

The data in Fig. 12 illustrate the effect of diffusible hydrogen on the ratio of values of reduction in area of the high-strength chrome-nickel steel samples, ψ_H/ψ, after hydrogenation ψ_H and before hydrogenation ψ. It can be seen that the effect of hydrogen shows itself in the case of an unfavourable microstructure of steel after heat treatment at the average atomic concentration of 0.3 $cm^3/100$ g, which is much lower than that estimated in the studies by G.V.Karpenko, i. e., one atom of hydrogen per 10^6 atoms of iron. These data confirm the concept of a local character of the hydrogen effect.

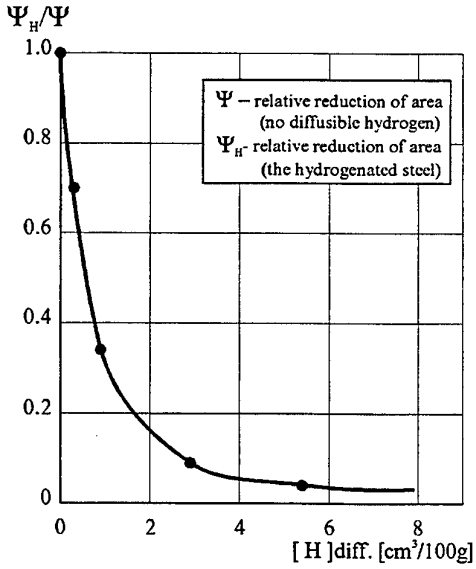

Fig. 12. The dependence of hydrogen embrittlement degree of the steel on concentration of diffusible hydrogen.

Table 2

Chemical composition of the steel [%] in Fig. 12.
Heat treatment: heating to 860°C, aging for 40 min and then cooling in air.

C	Mn	Si	P	S	Cr	Ni	Mo
0.14	0.75	0.25	0.025	0.012	1.0	3.5	0.14

The effect of the deformation rate is illustrated in Fig. 13. At the minimal deformation rate the effect of hydrogen is high. With an increase in the deformation rate the effect of hydrogen is little seen.

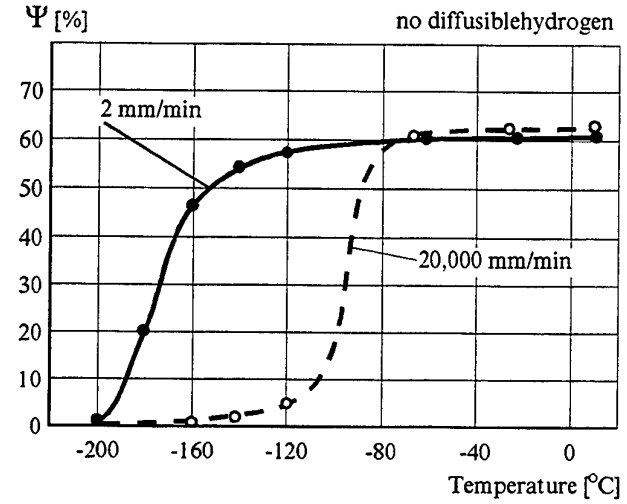

a)

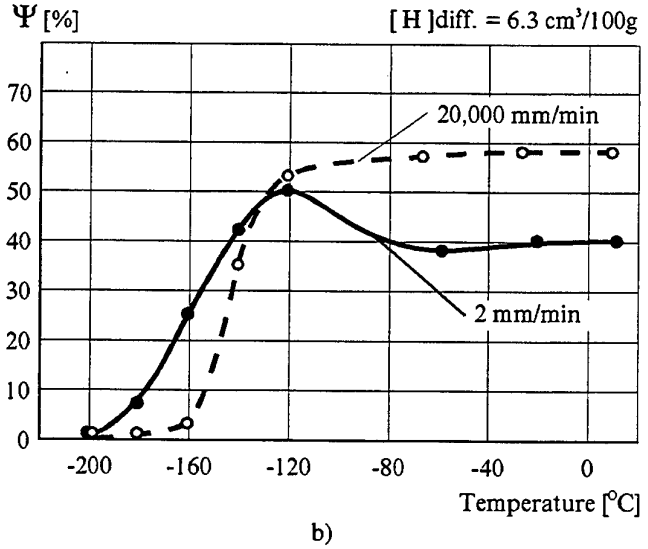

b)

Fig. 13. The effect of deformation rate on the relative reduction of area.

These data prove that the decisive role in the hydrogen embrittlement is played by the transfer of hydrogen to the point of its local effect. Efficiency of the hydrogen transfer is determined by parameters of the deformation process which is known to occur in the plastic region by the dislocation mechanism.

Mechanism of the effect of hydrogen on properties of steels and weld requires further investigations.

3. EFFECT OF HYDROGEN ON MECHANICAL PROPERTIES OF STEELS AND WELDS

Evaluation Procedure and Equipment

Scientists at the Paton Electric Welding Institute made an attempt to develop a procedure for investigation of susceptibility of steels to brittle fracture at the presence of hydrogen using modern theories and methods of metals physics.

The Institute of Metals Physics of the National Academy of Sciences of Ukraine suggested a method for evaluation of brittle fracture resistance of steels using criteria which are unambiguously related to parameters of the metal grain structure.

The flow diagram of the method is shown in Fig. 14. Specimens of metal are subjected to uniaxial tension. Basic mechanical characteristics of metal, such as tensile strength, yield strength, reduction in area and the true fracture stress, are determined within the temperature range from normal to cryogenic one. Parameter *Rmc* - the minimal stress of brittle fracture at a limiting yield strength is estimated from the temperature dependencies of these values.

$$Rmc = 4 \cdot \sqrt{\frac{\gamma \cdot E}{\pi \cdot d}} \cdot \left(\frac{G \cdot \sqrt{b}}{\alpha \cdot \pi \cdot (1-\upsilon) \cdot K_T} \right), \tag{4}$$

In case of the metal deformation : $Rmce = Rmc \cdot (1 + a_1 \cdot e + a_2 \cdot e^2)$. (5)

where $a_1 = 2.01$; $a_2 = -1.14$.

The experimental procedure of hydrogen embrittlement (HE) degree measuring (Fig. 14, b) is the following:

1. A standard cylindrical specimens for mechanical testing is prepared and used.
2. After hydrogenation the specimens are subjected to uniaxial tension (the specimen without hydrogen as well) in the temperature range from ambient to cryogenic temperature.
3. The main mechanical characteristics are measured: ultimate tensile strength (σ_B) yield point ($\sigma_{0.2}$), reduction of area (Ψ), actual fracture stress (S_K).
4. Their temperature dependencies are plotted (see Fig. 14, b, upper part).
5. Using this experimental data, the *Rmce* criterion is determined. The *Rmce* is the microcleavage resistance of metal been deformed to the '*e*' degree.
6. The Bridgeman's formula is used to calculate *Rmce*:

$$Rmce = S_K \cdot \frac{1 + \ln(1 + \eta/2)}{(1 + 2/\eta) \cdot \ln(1 + \eta/2)}, \tag{6}$$

where $\eta = 0.92 \cdot (e - 0.1)$; $e = \ln \frac{1}{1 - \Psi}$.

7. The ratio $Rmce^{[H]}/Rmce$ is a measure of hydrogen embrittlement degree. It is determined at the identical deformation degree of origin and hydrogenated specimens. To do this, the experimental plot $S_K = f(e)$ is used (see Fig. 14, b, lower part).

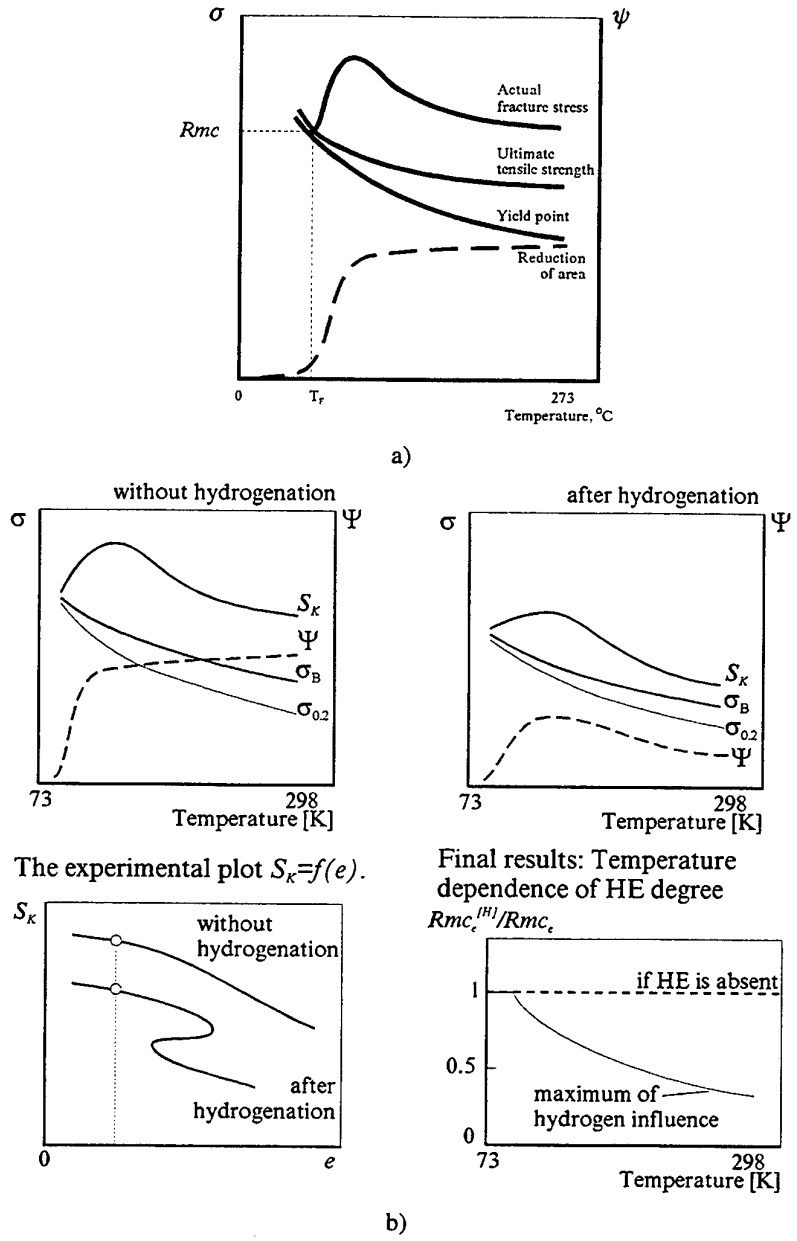

Fig. 14. Schematic diagram to determine the *Rmc* value experimentally (a) and an experimental procedure of hydrogen embrittlement (HE) degree measuring (b).

As shown by experiments, this criterion is determined by the grain structure of metal and does not depend upon experimental conditions, such as temperature, deformation rate and a type of a stress state.

This method was proposed for investigation of the effect of hydrogen on brittle fracture. Parameter *Rmc* reveals the ability of metal to resist brittle fracture at the tough-brittle transition temperature, where the effect of hydrogen is manifested to a lower degree. For investigation of the effect of hydrogen on mechanical properties of steels it is more appropriate to use parameter *Rmce* which is defined as a microcleavage resistance of a deformed metal. Parameter *Rmce* indicates the level of strength within the wide temperature range with allowance for the values of plastic deformation preceding the fracture at the above temperatures.

Bridgeman's formula shown in Fig. 15 is used to calculate the value of *Rmce*.

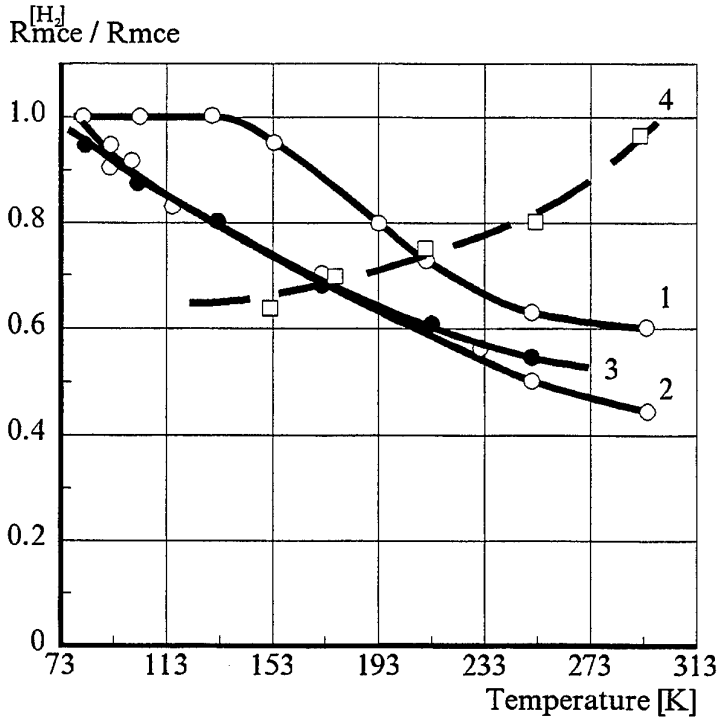

Fig. 15. Hydrogen embrittlement of the mild steels.

Table 3

Chemical composition of the steels [wt.%] in the Fig. 15.

	Steel grade	C	Mn	Si	P	S	Cr	Ni	Cu
1	St. 3	0.18	0.45	0.07	0.04	0.050	0.30	0.30	0.30
2	St. 45	0.45	0.65	0.27	0.035	0.040	0.25	0.25	0.25
3	St. 09G2S	0.12	1.5	0.65	0.035	0.040	0.30	0.30	0.30
4	St. U8	0.8	0.25	0.25	0.030	0.028	0.20	0.20	0.25

Two batches of standard cylindrical uniaxial tension samples were used in the experiment. Samples of batch 1 were hydrogenated, for instance, electrolytically. The preferred hydrogenation conditions were those which provided a uniform distribution of hydrogen over the sample section.

A degree of the effect of hydrogen was estimated from the value of ratio $Rmc_e^{[H]}/Rmc_e$ which was determined at the similar degree of deformation of hydrogenated and non-hydrogenated samples. The values of the true fracture stress S_K required to estimate Rmc_e were set from the plot of the deformation degree against the fracture stress (see Fig. 15). A diagram of the final experimental result is presented in the poster: if there is no effect of hydrogen, the temperature dependence of the criterion will have the form of a horizontal straight line.

Deviation from this dependence will characterize a degree of the hydrogen effect.

Experimental Results

Figs. 16 to 18 show typical dependencies of the effect of hydrogen deduced for steels the compositions of which are presented in the poster.

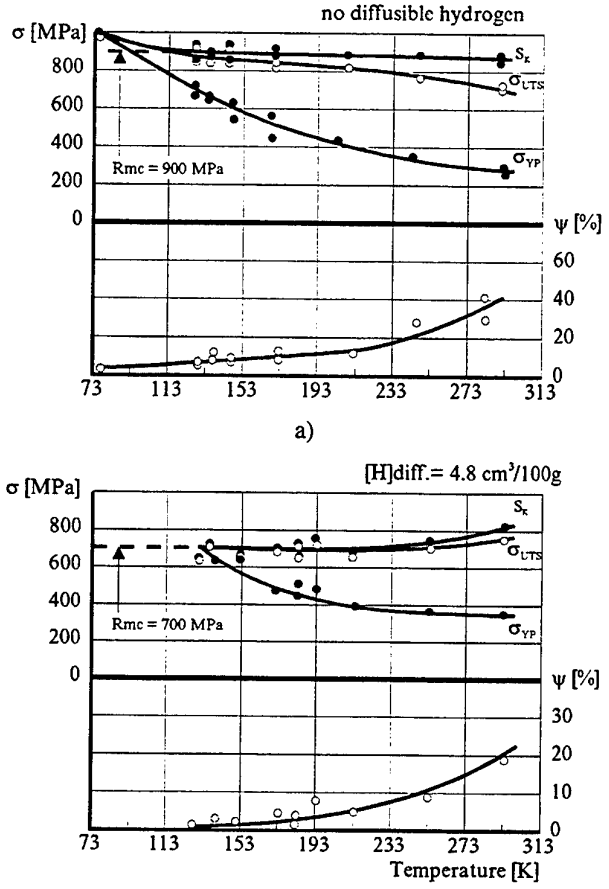

Fig. 16. Typical plots of hydrogen influence on brittleness of the mild steels: [C] = 0.8 wt.% (U8 grade steel). S_K is actual fracture stress; σ_{YP} is yield point and σ_{UTS} is ultimate tensile strength.

As can be seen from the tables of compositions of steels, their carbon content varies significantly. The temperature dependence of the embrittlement criterion for steel with the maximal value of [C] = 0.8 wt.% has a totally different course, as compared to similar dependencies for other steels under investigation. The effect of hydrogen is maximum at the decreased temperature, rather than at the normal one. It means that in this case the effect of hydrogen is not associated with its transportation in the bulk to the point of initiation of a crack. It can be formed as a result of cleavage of carbide particles the interface with which serves as a hydrogen collector. Also, it can be noted that hydrogen has a high effect on a heat-treated high-strength low-alloy steel (Fig. 18).

After heat treatment that simulates probable structural transformations within the heat-affected zone, the presence of hydrogen causes a catastrophic embrittlement.

Some conclusions:

(1) The proposed unique procedure allows the effect of hydrogen on properties of steels and welded joints to be evaluated within the wide ranges of temperatures.

(2) The criterion suggested for evaluation of the hydrogen effect is physically grounded and allows for an analytical description.

(3) The new procedure makes it possible to determine the effect of every factor, such as element composition and metal structure, values of stresses, temperature, deformation rate, content and distribution of hydrogen.

(4) The use of the new procedure is promising for development of new steels, welding consumables and technologies.

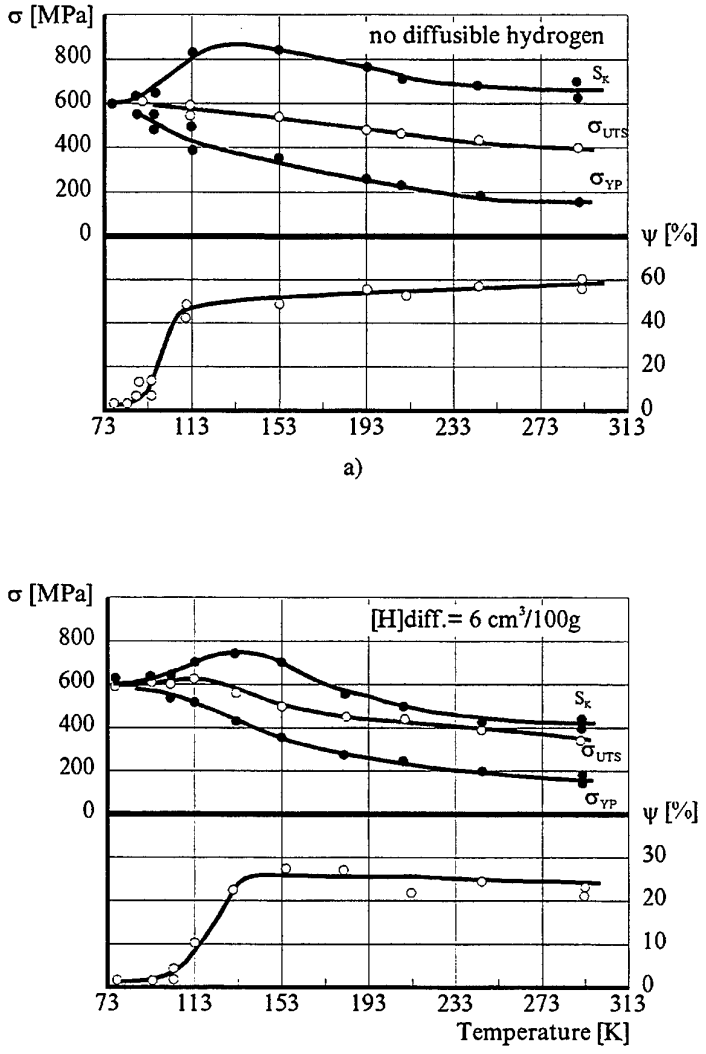

Fig. 17. Hydrogen influence on mild steels S_K is actual fracture stress; σ_{YP} is yield point and σ_{UTS} is ultimate tensile strength.

Table 4

Chemical composition of the steel [wt.%] in Fig. 17.

C	Mn	Si	P	S	Cr	Ni	Cu	As
0.18	0.40	<0.07	<0.04	<0.05	<0.30	<0.30	<0.30	<0.08

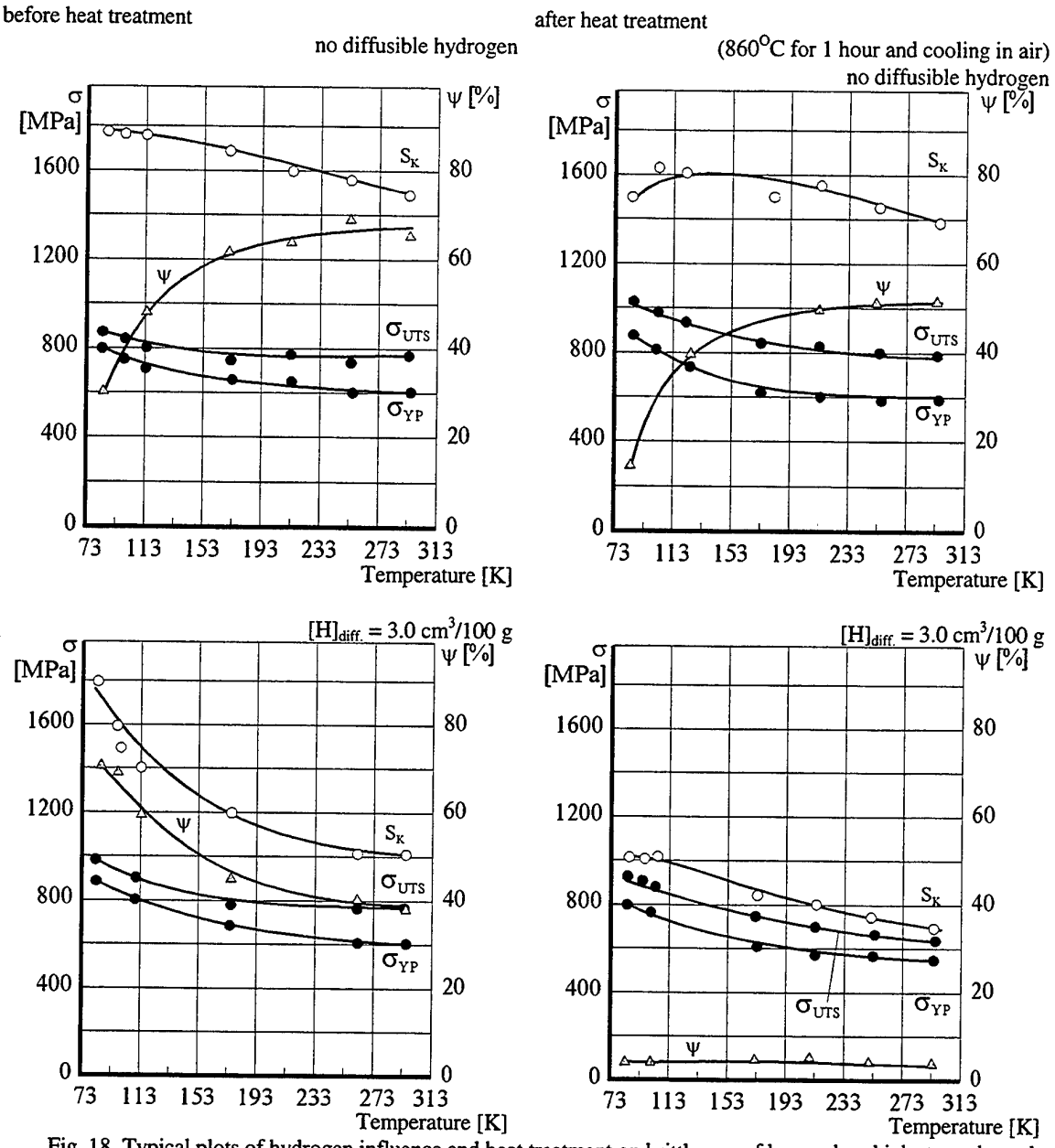

Fig. 18. Typical plots of hydrogen influence and heat treatment on brittleness of low carbon high strength steels. σ_{YP} is yield point; σ_{UTS} is ultimate tensile stress; S_K is actual stress.

4. HYDROGEN AND DELAYED FRACTURE OF WELDED JOINTS

The process of cold cracking during welding of high-strength steels is a subject of the many-year studies conducted at some department of the Paton Electric Welding Institute. The quantitative relationships between a level of alloying, characteristics of the thermal-deformation cycle, a content of diffusible hydrogen and formation of cold cracks were determined as a result of the studies. The list of papers and reviews written at the Paton Electric Welding Institute mostly during the recent years is given in the references.

Let me give you the results of just some of the studies conducted on the delayed fracture resistance of one-pass low-alloy high-strength steel welds of the chrome-manganese-nickel-molybdenum system.

Welded were the composite specimens with the X-groove preparation, parent metal was steel 14KhGN2MCuNFB (alloyed with Cr, Mn, Ni, Mo, Cu, N, V and Nb). After cooling to 120 ... 100°C the welded specimens were subjected to tension at a constant loading. The value of stress σ_{CR} at which the specimens did not fail during 24 hours was assumed to be a criterion. Composition and mechanical properties of weld metal, content of diffusible hydrogen and parameters of a microstructure are given in Table 5.

Table 5

Chemical composition, microstructure and properties of the welds

Weld number	Welding consumables	Element content in weld metal [wt.%]							
		C	Si	Mn	Cr	Ni	Mo	V	Cu
1	SMAW UONI-13/55 (type E50)	0.078	0.45	1.2	0.35	0.35	0.11	0.01	0.30
2, 2'	SMAW ANP-6P (type E70)	0.071	0.31	1.4	0.34	1.60	0.34	0.01	0.31
3	SMAW ANP-2 (type E70)	0.070	0.18	1.3	0.82	1.75	0.32	0.015	0.30
4	SMAW ANP-7 (type E85)	0.078	0.25	1.3	0.50	1.85	0.46	0.045	0.33
5	SMAW 48N-13 (type E85)	0.082	0.22	0.85	0.75	2.65	0.45	0.02	0.56
6	GMAW Sv-08GSMT + {CO_2}	0.082	0.30	0.87	0.37	0.28	0.28	0.01	0.22
7	GMAW Sv-07KhN3GMFTYu + {Ar+CO_2}	0.065	0.22	0.82	0.60	2.4	0.45	0.04	0.20
8	GMAW Sv-10KhN2GSMFTYu + {CO_2}	0.078	0.29	0.95	0.65	2.1	0.49	0.03	0.21
9	GMAW Sv-08KhN2GMYu + {CO_2}	0.076	0.17	0.82	0.75	2.2	0.55	0.01	0.20
10	GMAW Sv-08KhN2GMYu + {Ar+CO_2}	0.066	0.28	1.05	0.7	2.2	0.50	0.01	0.20
11	GMAW Sv-07KhG2SN2MDYu + {CO_2}	0.070	0.34	1.30	0.8	2.2	0.55	0.06	0.45

Weld number	Welding consumables	Carbon equivalent P_C %	$D_{avreage}$ μm	Phase composition of microstructure	$\sigma_{0.2}$ MPa	δ_5, %	[H]diff., $cm^3/100g$
1	SMAW UONI-13/55 (type E50)	0.192	110	50% F + 50% B	500	25	9.0
2, 2'	SMAW ANP-6P (type E70)	0.232	35	30% F + 70% B	620	20	9.0
3	SMAW ANP-2 (type E70)	0.248	55	20% F + 80% B	650	16	4.0
4	SMAW ANP-7 (type E85)	0.278	30	90% B + 10% M	820	19	3.0
5	SMAW 48N-13 (type E85)	0.274	40	80% B + 20% M	850	20	3.0
6	GMAW Sv-08GSMT + {CO_2}	0.181	80	40% F + 60% B	520	24	6.0
7	GMAW Sv-07KhN3GMFTYu + {Ar+CO_2}	0.225	30	85% B + 15% M	730	22	5.0
8	GMAW Sv-10KhN2GSMFTYu + {CO_2}	0.242	35	80% B + 20% M	800	17	5.0
9	GMAW Sv-08KhN2GMYu + {CO_2}	0.241	65	70% B + 30% M	800	15	5.0
10	GMAW Sv-08KhN2GMYu + {Ar+CO_2}	0.243	60	70% B + 30% M	830	18	5.0
11	GMAW Sv-07KhG2SN2MDYu + {CO_2}	0.285	35	50% B + 50% M	900	13	5.0

The rate of cooling the weld metal was regulated by varying temperature of preheating the specimens.

An index of crack resistance $\sigma_{CR}/\sigma_{0.2}$ suggested by Dickenson and Ries ($\sigma_{0.2}$ is a proof stress determined on the cylindrical specimens) was used in the studies.

Allowing for conditions of the tests and values of the stress concentration factor at the apex of a notch equal to 1.7, the value of ratio $\sigma_{CR}/\sigma_{0.2}$ was estimated as equal to 0.5.

Fig. 19 shows the ratio $\sigma_{CR}/\sigma_{0.2}$ against the diffusible hydrogen content of weld metal. It can be seen from this Fig. that the relative crack resistance of welds decreases with an increase in the share of the martensite component in welds and an increase in their strength and diffusible hydrogen content.

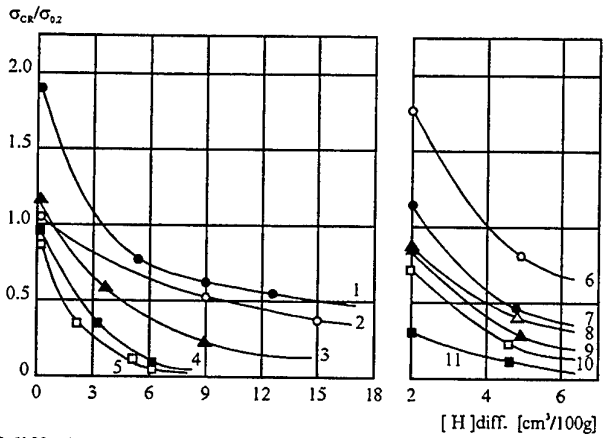

Fig. 19. Influence of diffusible hydrogen content on relative crack-resistance ($\sigma_{CR}/\sigma_{0.2}$) of the welds.

SMAW ($\tau_{8/1}$ = 15 min) (basic type coated electrodes):

1 - UONI-13/55, $\sigma_{0.2}$ = 500 MPa
2 - ANP-6P, $\sigma_{0.2}$ = 650 MPa
3 - ANP-2, $\sigma_{0.2}$ = 650 MPa
4 - ANP-7, $\sigma_{0.2}$ = 820 MPa
5 - 48N-13, $\sigma_{0.2}$ = 850 MPa

GMAW ($\tau_{8/1}$ = 19 min):

6 - [Mn-Si-Mo-Ti] wire + {CO_2} gas
7 - [Cr-Ni-Mn-Si-Mo-V-Ti-Al] wire + {Ar+CO_2} gas
8 - [Cr-Ni-Mn-Si-Mo-V-Ti-Al] wire + {CO_2} gas
9 - [Cr-Ni-Mn-Mo-Al] wire + {CO_2} gas
10 - [Cr-Ni-Mn-Mo-Al] wire + {Ar+CO_2} gas
11 - [Cr-Mn-Si-Ni-Mo-Cu-Al] wire + {CO_2} gas

Studies of the effect of diffusible hydrogen, preheating temperature and time of loading on the length of cracks and the value of critical tensile stresses were conducted on chrome-manganese-molybdenum high-strength steel 14Kh2GMR. Results of the studies are shown in Fig. 20.

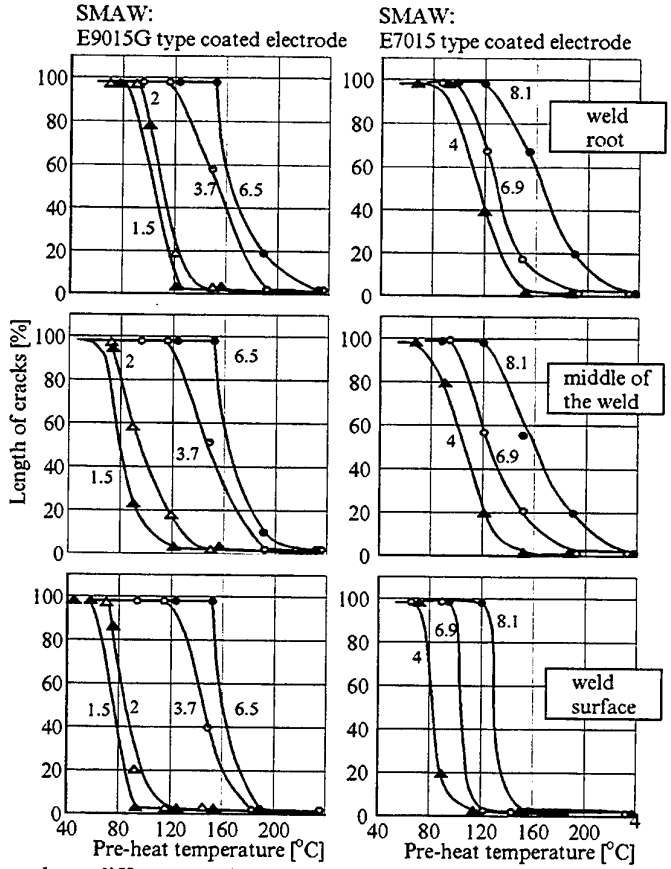

Fig. 20. The length of cracks at different pre-heat temperatures. The numbers on the plots represents content of diffusional hydrogen in $cm^3/100g$. Base metal type: 14Kh2GMR steel (element content: 0.15 wt.% C; 1.2 wt.% Mn; 0.3 wt.% Si; 1.45 wt.% Cr; 0.5 wt.% Mo; 0.004 wt.% B). Specimens of Lehigh University type, 150 x 200 x 20 mm in size. [H]diff. ≤ 2.0 $cm^3/100g$ for E9015G electrodes. [H]diff. ≤ 3.5 $cm^3/100g$ for E7015 electrodes.

It can be seen that the preheating temperature can be decreased and the crack-free welds at a comparatively high content of diffusible hydrogen can be made using electrodes which could provide weld metal with a comparatively low yield strength $\sigma_{0.2}$.

A decrease in the diffusible hydrogen content of weld metal from 6.5 cm^3/100 g to 1.8 cm^3/100 g allows the value of critical tensile stresses to be increased by 200 MPa (Fig. 21), other conditions being equal.

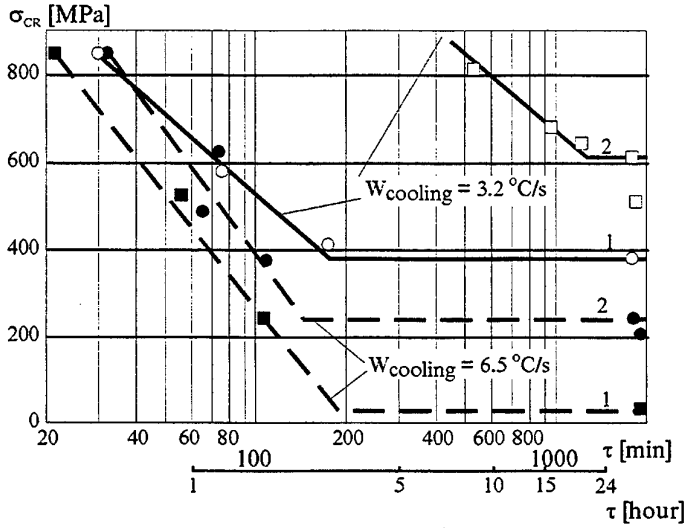

Fig. 21. The plot of critical tensile stresses (σ_{CR}) vs. duration (τ) of loading of the welded joint and diffusible hydrogen content in weld. Base metal type: 14Kh2GMR steel (element content: 0.15 wt.% C; 1.2 wt.% Mn; 0.3 wt.% Si; 1.45 wt.% Cr; 0.5 wt.% Mo; 0.004 wt.% B). 1- [H]diff. = 6.5 cm^3/100 g; 2 - [H]diff. = 1.8 cm^3/100 g.

The conducted studies resulted in finding the maximum permissible values of the diffusible hydrogen content of weld metal depending upon the level of strength of welds and cooling conditions, providing that $\sigma_{CR}/\sigma_{0.2} = 0.5$ (Fig. 22). Analysis of the given data shows an ambiguous effect of variation in the diffusible hydrogen content of weld metal and the cooling conditions on the delayed fracture resistance.

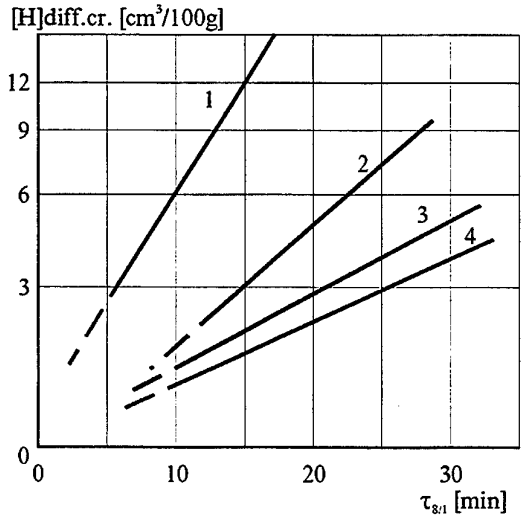

Fig. 22. Calculated plot of limiting values of hydrogen content in weld metal vs. time of cooling ($\tau_{8/1}$) at the different strength level of the metal for ($\sigma_{CR}/\sigma_{0.2}$) = 0.5.

1 - UONI-13/55 coated electrodes, $\sigma_{0.2}$ = 500 MPa
2 - ANP-2 coated electrodes, $\sigma_{0.2}$ = 650 MPa
3 - ANP-7 coated electrodes, $\sigma_{0.2}$ = 820 MPa
4 -48N-13 coated electrodes, $\sigma_{0.2}$ = 850 MPa

When developing consumables and technology for welding high-strength steels, it is necessary to take all measures of a metallurgy and technology character in order to minimize the diffusible hydrogen content and to set the preheating temperature depending upon the efficiency of these measures.

5. TECHNOLOGY AND METALLURGY METHODS FOR DECREASING DIFFUSIBLE HYDROGEN

Technology Methods

Sources of Hydrogen

- adsorbed moisture and organic materials in electrode coating, flux and flux-cored wire cores;
- water vapours in air and shielding gas;
- hydrogen in filler metal, wire, ferroalloys and parent metal;
- lubricant and rust at the wire surface;
- prime coat on parent metal.

Methods for Determination of Diffusible Hydrogen

Sampling and Analysis

Samples for determination of diffusible hydrogen can be made by 3 methods (Fig. 23)

(1) bead on composite steel sample (covered-electrode welding);
(2) bead on copper plate (submerged-arc welding);
(3) pouring of the welding pool into a copper mould (submerged-arc welding).

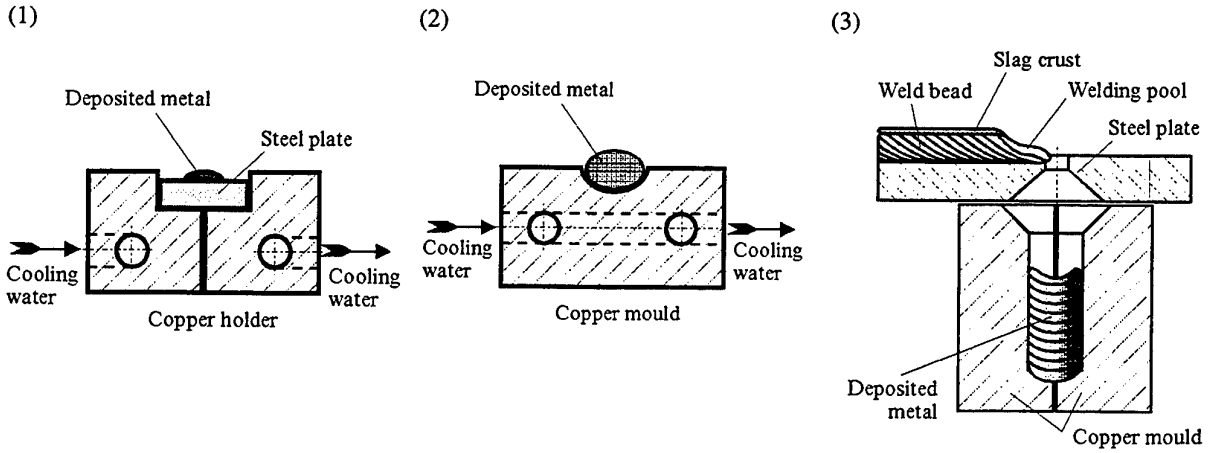

Fig. 23. Methods of metal sampling for the analysis of diffusible hydrogen content. Manual Metal Arc Welding.

Table 6

Hydrogen content [cm3/100g] in deposited metal.
Electrodes of E7018 type ∅ 5 mm. Welding current = 220 ... 230 A, DCRP

Method	[H] diffusible	[H] residual	[H] in total
(1)	6.0	0.87	6.87
(2)	4.7	0.83	5.53
(3)	5.0	1.1	6.1

Methods (2) and (3) are used in ship building.

Method (1) registers the higher rates of cooling a deposited metal than methods (2) and (3). Therefore, the diffusible hydrogen content of the samples is a bit higher. The measured amount of the diffusible hydrogen is related to a mass of the deposited metal (according to standard IIW-250). In our opinion, the diffusible hydrogen should be related to the mass of the molten metal.

Below some results of experiments are given. Fig. 24 shows the data on the effect of welding speed and current on [H] diff./depos. and [H] diff./molten. The share of mass of the deposited metal *md/mf* is decreased with an increase in current and welding speed. Therefore, the data on [H] diff./depos. do not reflect the actual picture of the hydrogen content of welds. Table 7 gives experimental data on four grades of the E7015 type electrodes which confirm the results of the previous experiments.

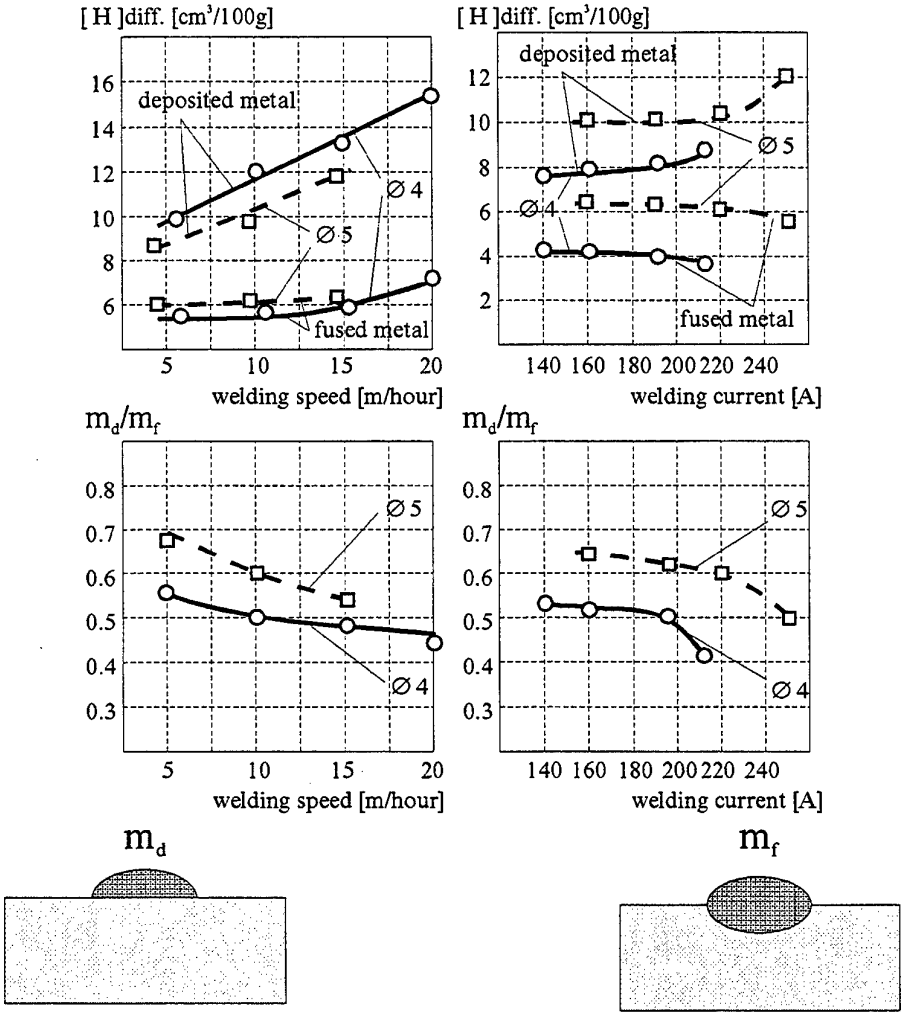

Fig. 24. Influence of welding conditions on diffusible hydrogen content in deposited and fused metal. Coated electrodes of E7015 type, DCRP. Welding current: for Ø 4 mm = 170 A; for Ø 5 mm = 220 A. Welding travel speed = 9 ... 9.5 m/hour.

Conclusion: For a correct evaluation of the amount of [H] diff. it is necessary to calculate the hydrogen content of weld metal (fused metal). Relating the hydrogen content to the deposited metal mass can lead to wrong conclusions.

Analysis of the amount of the evolved hydrogen is done using eudiometers. Mercury, glycerin or alcohol can serve as a sealing fluid (method IIW). When using glycerin or alcohol, the

measured amounts of hydrogen are by 20 ... 50 % lower. The alcohol sample is employed in ship building. Another options are the vacuum extraction and chromatographic methods.

Table 7

Electrode	Welding current [A]	Welding travel speed [m/hour]	[H]diff. deposited metal [cm^3/100 g]	[H]diff/ fused metal [cm^3/100 g]
1 (UONI 13/55)	190 ... 220	20.5	12.5	5.5
	165 ... 175	12.5	10.2	5.4
	135 ... 140	5.7	6.8	5.4
2 (NTS-46)	200 ... 210	21.0	8.3	3.7
	165 ... 175	12.5	7.2	4.0
	135 ... 140	5.7	5.4	3.7
3 (E1 38/50N)	200 ... 210	21.0	6.7	3.0
	165 ... 175	12.5	5.5	2.9
	135 ... 140	5.7	3.8	2.7
4 (ANO-9)	190 ... 200	20.5	7.5	3.3
	165 ... 175	12.5	6.4	3.6
	135 ... 140	5.7	4.8	3.5

The chromatographic method was originally developed and studied by the Paton Electric Welding Institute as early as in 1978. A portable analyzer was devised for this method, it provided measurements with the accuracy of ±7 %. The extraction temperature is 150°C. The residual hydrogen is determined by the chromatographic method. Temperature of heating a sample is 800°C.

A decrease in the potential hydrogen content of general-application welding consumables is done by the known methods. The basic methods among them are electrode and flux heat treatment and shielding gas drying. In the consumables intended for welding the high-strength steels the potential hydrogen content should be minimized. The electrode baking temperature is limited to 450°C. The further increase in temperature can lead to dissociation of the coating components, as in mixtures of minerals the dissociation beginning temperature can be lower than in the initial minerals (Fig. 25).

The attention should be drawn to the fact that minerals, impurities in them and slags can introduce a considerable amount of hydrogen. Fig. 26 shows the data on the effect of the heat treatment temperature on the hydrogen content of some minerals.

Hydrogen contained in them can be in the form of a solution in crystals and hydroxides, or in the form of an absorbed moisture. A substantial amount of hydrogen is evolved from minerals at temperatures which exceed the permissible points of baking electrodes and agglomerated fluxes.

Various slags can be used to manufacture electrodes, agglomerated fluxes and flux-cored wires. Investigation of a number of slags - fluxes showed that some of them contain a high amount of hydrogen. Table 8 gives data on the hydrogen content of flux ANF-6 (70 wt.% C + 30 wt.% Al_2O_3) in the process of its melting and after pelletizing.

Table 8

Hydrogen content in the flux (Flux ANF-6: 70 wt.% C + 30 wt.% Al_2O_3)

Temperature of the flux melt at outlet [°C]	Hydrogen content in the flux [cm^3/100g]	
	at outlet of furnace	after pelletizing and cooling
1520	74	46
1600	40	55
1640	20	26
1650	32	75
1700	23	95
1700	68	33

The hydrogen content of the flux melt varies within the wide ranges (from 20 to 74 cm^3/100 g) and does not depend upon the outlet temperature.

A number of metallurgy methods are used to decrease the hydrogen content of welds.

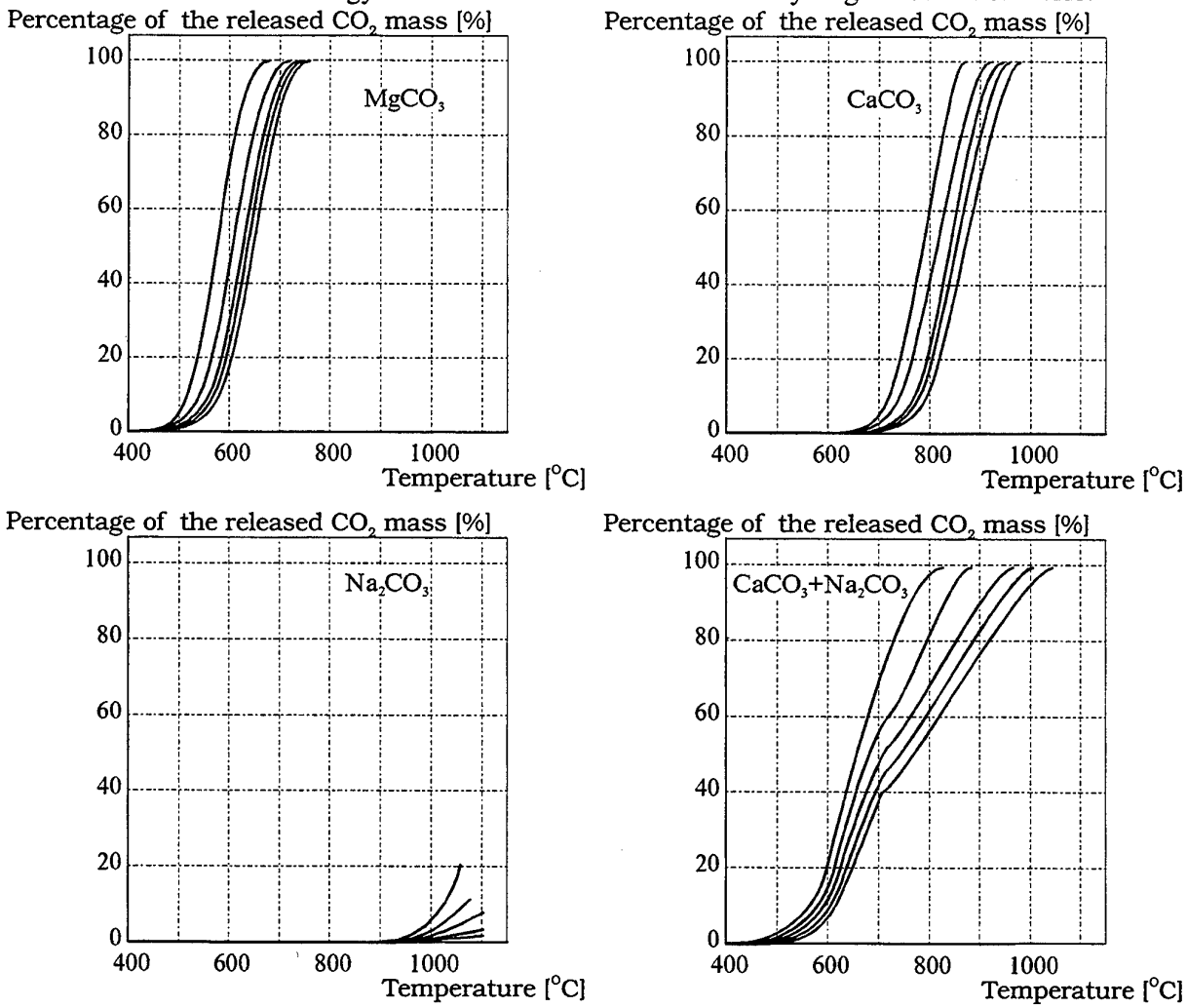

Fig. 25. Kinetics of carbon di-oxide gas evolution during thermal dissociation of some carbonates and their mixture used in the cores of FCW. Series of the curves represent heating rates 5, 10, 15, 20 and 25 °C/min correspondently.

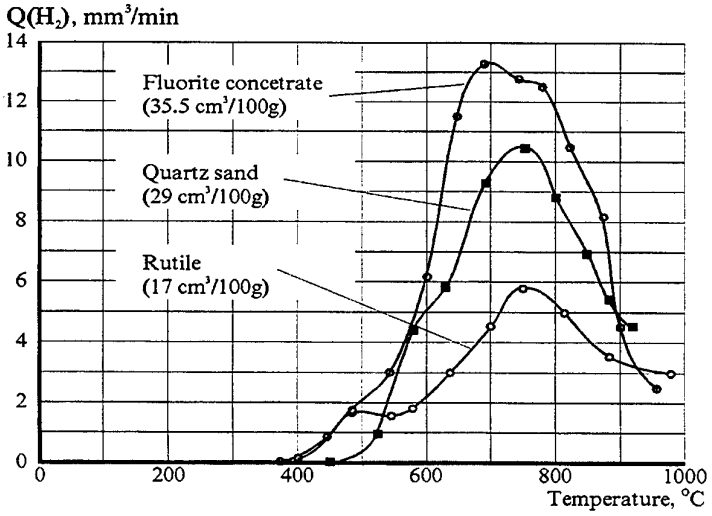

Fig. 26. Hydrogen evolution rate from raw materials at continuous heating. (Heating rate being 12 ... 14 °C/min).

Metallurgy Methods

Melts of the oxy-fluoride fluxes which are in contact with vapours of H_2O dissolve H_2O simultaneously with HF. Ratio of their concentrations in a molten flux is determined by the flux composition and temperature. In a general case, H_2O and HF dissolved in the flux can be assumed to be a generalized agent (H_2O + HF) where m is a coefficient which characterizes ratio of these gases in a particular melt.

The process of interaction of the hydrogen-containing gases dissolved in the molten flux with the most active oxidizing component of the metal pool (Me'') at the flux-metal interface can be described by such a diagram:

$$(H_2O + m\ HF)_{flux} + (1+m/2)\ [Me'']_{Me} = (MeO)_{flux} + m/2\ (MeF_2)_{flux} + (2 + m)\ H_{M/flux}$$

$$(2 + m)\ H_{M/flux} = (2 + m)\ [H]_{Me},$$

where: $H_{M/flux}$ is the atomic hydrogen formed at the metal-flux interface.

It is assumed that the reaction occurring at the flux-metal interface is a limiting stage of the kinetics of transfer of hydrogen from flux to metal. This reaction is reversible and allowing for a possibility in principle of additional hydrogenation of metal or removal of hydrogen into slag.

Thermodynamic analysis was conducted on the process of combining gaseous hydrogen present in the form of water vapours to form hydrogen fluoride insoluble in the molten iron.

Temperature in this case was from 2000 to 2500 K and pressure was $1 \cdot 10^5$ Pa. Calculations were done for the method of CO_2 flux-cored wire welding.

The initial phase composition was assumed to be as follows.

The gas phase was carbon monoxide with a small amount of water vapours, the metal phase was iron and the slag phase was CaF_2, SiO_2, Al_2O_3, TiO_2 and CaO in differing proportions. To create an oxidizing atmosphere, a certain amount of FeO was added to the calculated composition of the slag melt.

Various slag systems were analyzed, such as: SiO_2-CaO-CaF_2, TiO_2-CaO-CaF_2 and Al_2O_3-CaO-CaF_2. Besides, combining of hydrogen was investigated at different temperatures, different contents of water vapours and at the addition of SiF_4 and oxygen to the gas phase.

Fig. 27 shows calculated dependencies of the hydrogen content of molten metal upon the initial CaF_2 content of slag of the TiO_2-CaO-CaF_2 system. In the absence of CaO the optimal region is that where the CaF_2 content is 60 ... 75 wt.%. With an increase in the mass fraction of CaO in the slag, the region of the optimal composition is shifted towards a decrease in the CaF_2 content. However, the said region corresponds to a higher hydrogen content of metal. Similar dependencies were obtained also for the Al_2O_3-CaO-CaF_2 system. In general, system Al_2O_3-CaO-CaF_2 gives a higher hydrogen content than system TiO_2-CaO-CaF_2.

For system SiO_2-CaO-CaF_2 the mass fraction of CaO has no effect on the hydrogen content of molten metal, which decreases with a growth of CaF_2 in the slag.

Increasing the oxidation potential of the gas phase by adding the molecular oxygen caused an insignificant decrease in the hydrogen content of metal. Addition of SiF_4 to the gas phase was accompanied by a substantial decrease in the mass fraction of hydrogen in molten metal caused by its entering into the reaction with the free atoms of fluorine formed by dissociation of SiF_4 (Fig. 28). This method of decreasing the hydrogen content of molten metal appears to be more efficient than the addition of big amounts of SiO_2 and CaF into the slag composition because of occurrence of the

exchange reaction $2CaF_2 + SiO_2 = 2CaO + SiF_4$. The calculation results were confirmed experimentally. Fig. 29 shows data of the gravimetric analysis of mixture $CaF_2 + SiO_2$, as well as Na_2SiF_6 and $BaSiF_6$.

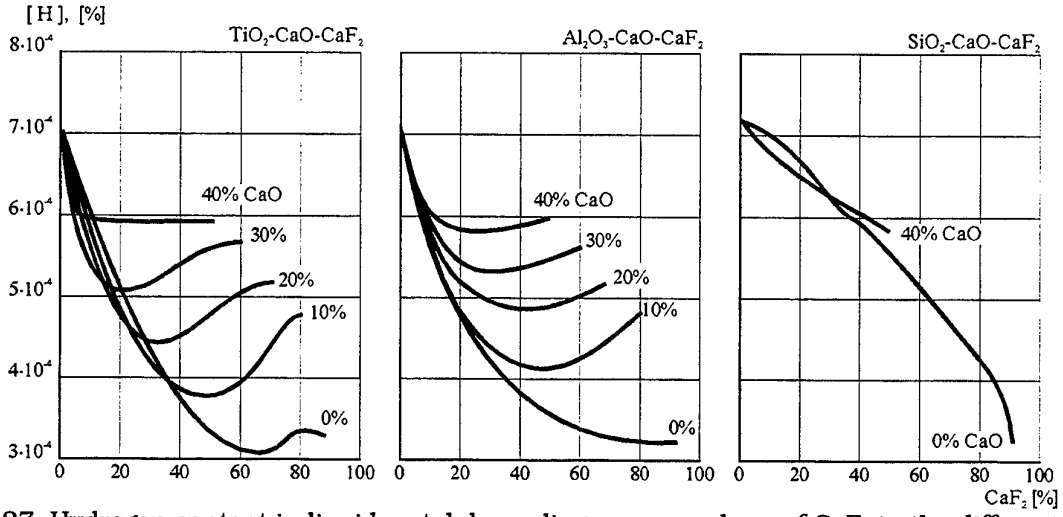

Fig. 27. Hydrogen content in liquid metal depending on mass share of CaF_2 in the different slag systems (calculated data).

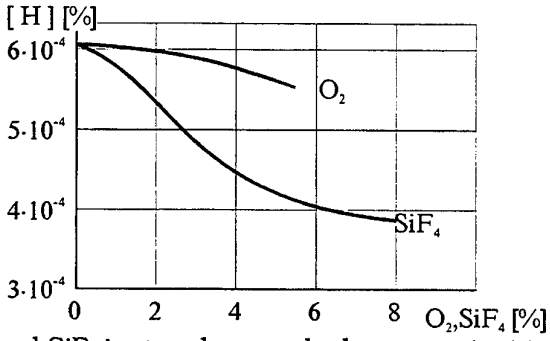

Fig. 28. Influence of O_2 and SiF_4 in gas phase on hydrogen content in liquid metal (calculated data). Slag composition: 45 wt.% SiO_2, 45 wt.% CaF_2, 10 wt.% FeO.

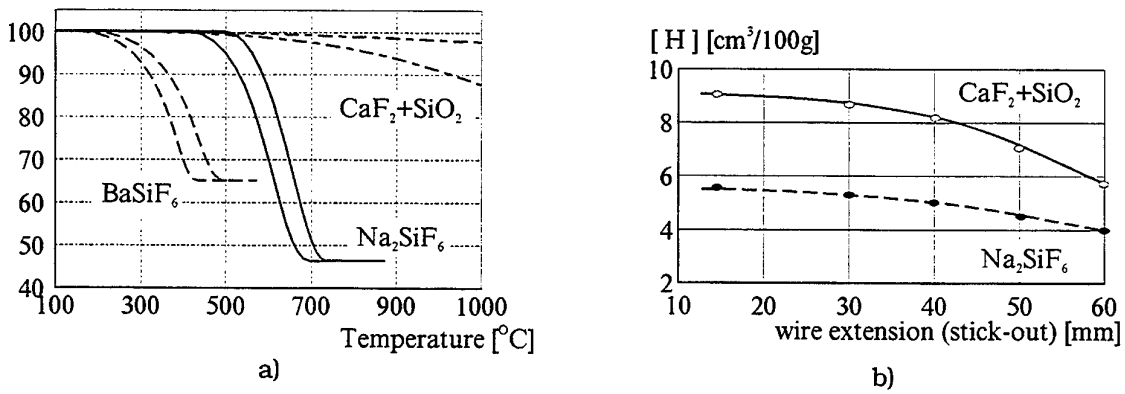

Fig. 29. Thermo-gravimetric analysis of dissociation of fluorides and silicon-fluorides (a) (curves represent the heating rates from 10 to 20°C/min) and diffusible hydrogen content in weld metal made with flux-cored wired with different fluorides in the core (b).

Interaction of CaF_2 with SiO_2 begins at temperature of 1100 K and higher. Dissociation of Na_2SiF_6 takes place at temperatures ~800 ... 900 K. Addition of silicon fluorides to the core of a flux-cored wire to decrease the hydrogen content of weld metal is more efficient than that of

mixtures CaF_2 + SiO_2. Fig. 30 shows the experimental results on the addition of different fluorides to the flux-cored wire core.

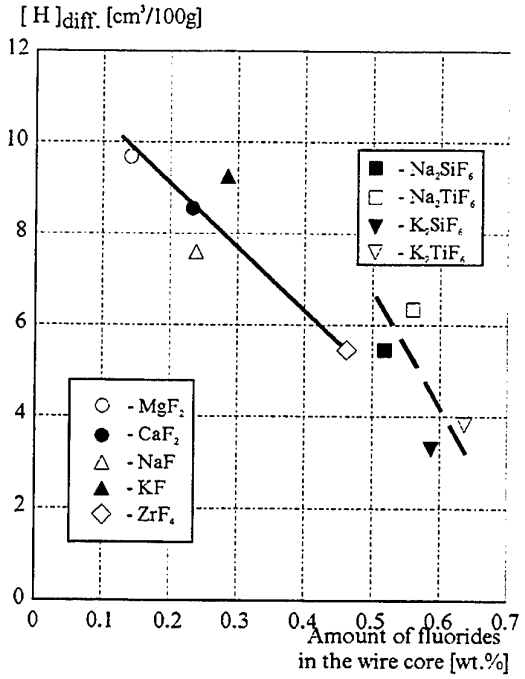

Fig. 30. Plot of diffusible hydrogen content in deposited metal vs. amount of fluorides in the wire core (content of fluorine being constant).

Addition of silicon fluorides is difficult to apply in practice of manufacture of electrodes and agglomerated fluxes, as this leads to degradation of ductility of coating materials. That is why the preference is given to the addition of CaF_2 and SiO_2 into a coating. Fig. 31 shows calculation of partial pressure P' SiF_4 for different concentrations of SiO_2 in the coating (4 wt.% and 11 wt.%) and the experimental data on the diffusible hydrogen content of weld metal. Noticeable is a decrease in [H]diff. with an increase in the content of SiO_2 and CaF_2 in the coating.

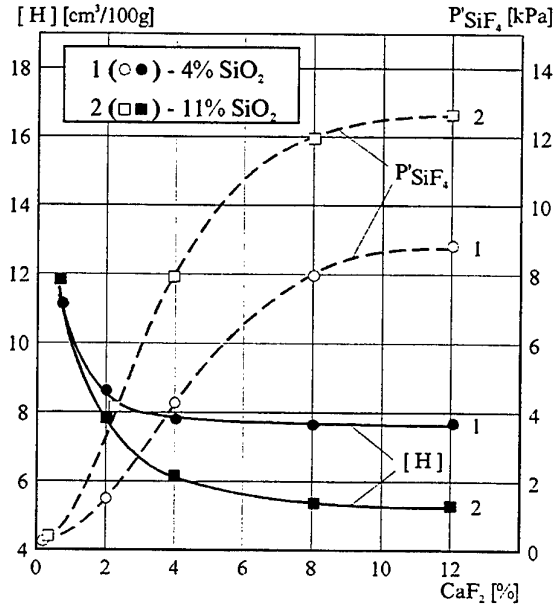

Fig. 31. Influence of CaF_2 and SiO_2 content in the coating on calculated values of partial pressure of tetra-fluorine-silicon in arc atmosphere and experimental values of hydrogen content in deposited metal.

The calculations indicated the probability of formation of iron fluorides in the arc atmosphere. Then this was proved experimentally by the mass-spectral analysis. The maximum yield of FeF_3 was observed at ratio $CaF_2 : Fe_2O_3 \sim 2 : 2.5$. The reaction to form FeF_3 allows the hydrogen content to be decreased by approximately 1 ... 1.5 $cm^3/100$ g.

Fluxes of high basicity (IB > 2.8) are used as a rule for welding of high-strength low-alloy steels. The slag base of such fluxes is made of the ternary system $CaO(MgO)-Al_2O_3-CaF_2$. Combining of hydrogen with fluorine cannot be efficiently utilized for submerged-arc welding using the high-basicity fluxes, as silica has low activity in such fluxes. The low level of hydrogen in this type of the fused high-basicity fluxes can be achieved by the high-temperature baking at temperature of 900°C. The addition of iron oxides to an electrode coating or a fused flux is also advantageous (Fig. 32).

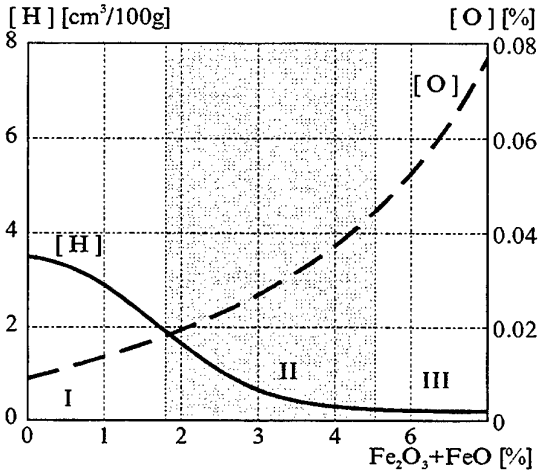

a) SMAW: Basic type coated electrode. Weld metal composition: 0.08 wt.% C; 1.1 wt.% Mn; 0.3 wt.% Si; 1 wt.% Cr; 1.5 wt.% Ni; 0.5 wt.% Mo.

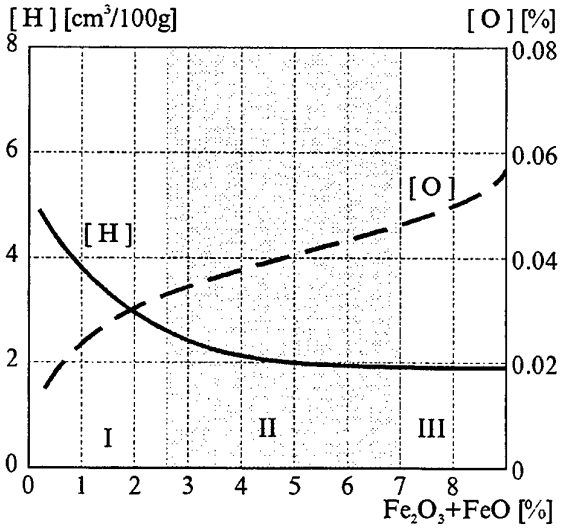

b) SAW: Solid wire (SW-08KhN2GMYu) + AN-17M flux. Wire composition: 0.08 wt.% C; 1.2 wt.% Mn; 0.35 wt.% Si; 0.9 wt.% Cr; 2.2 wt.% Ni; 0.5 wt.% Mo; 0.1 wt.% Al. Flux composition: SiO_2 18-22 wt.%; Al_2O_3 21-25 wt.%; MnO <3.0 wt.%; CaO 14-18 wt.%; MgO 9-12 wt.%; CaF_2 21-25 wt.%; FeO 3-5 wt.%.

Fig. 32. Influence of iron oxides in electrode coating and in flux on oxygen and diffusible hydrogen content in deposited metal. I - too many cold cracks; II - optimal properties of the welded joint; III - too low impact toughness.

Carbonates or higher oxides of iron or manganese are added to the agglomerated fluxes to decrease hydrogen.

Fig. 33 shows the results of experiments. Fe and Mn carbonates and higher oxides dissociate in the arc during heating. The partial pressure of hydrogen is decreased due to dilution of the arc atmosphere with carbon dioxide and oxygen and due to combining hydrogen to form hydroxides OH. It should be noted here that the carbonates added in large amounts cause a degradation of welding properties of the fluxes.

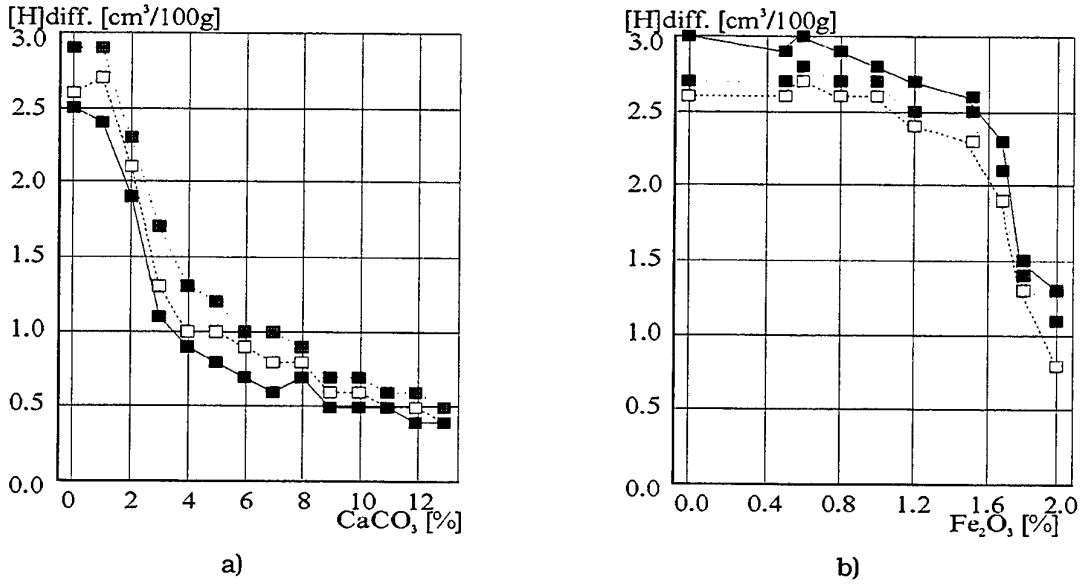

Fig. 33. Influence of marble and iron oxides in agglomerated flux on diffusible hydrogen content in weld metal

Submerged arc welding. Parent metal: Mn-Ni-Mo steel. Flux: agglomerated of the CaF_2-Al_2O_3-MgO-CaO system. Wire: Mn-Ni-Mo-Cu-Ti type. Method of [H]diff. determination: eudimeter, locking liquid is an alcohol.

The diffusible hydrogen content of weld metal can be decreased by microalloying it with rare-earth hydride-forming elements. The experimental results are shown in Fig. 34. The addition of rare-earth elements leads to redistribution of hydrogen in a weld, i.e., the content of [H]diff. is decreased and that of [H]res. is increased. This is attributed to dispersion of elements of a secondary structure of weld metal caused by the addition of rare-earth elements. The formed oxy-sulphides accumulate hydrogen, acting as traps.

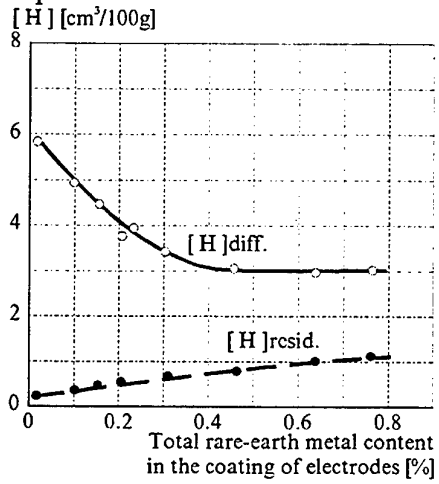

Alloying system of weld metal: Mn-Ni-Mo (1 ... 1.5 wt.% Mn; 1.5 ... 2.5 wt.% Ni; 0.3 ... 0.5 wt.% Mo) $\sigma_{0.2}$ = 700 ... 800 MPa.

Fig. 34. Influence of rare-earth metal content in electrode coating on diffusible and residual hydrogen content.

Modifying of non-metallic inclusions and refining of austenitic grains of weld metal lead to the 1.2 ... 1.5 times increase in the delayed fracture resistance of a welded joint. This is associated with a decrease in the diffusion rate and the amount of diffusible hydrogen. The possibilities of decreasing the content of [H]diff. in the high-strength weld metal by its metallurgical treatment with rare-earth elements are limited (1 ... 2 cm^3/100 g). Therefore, microalloying is advantageous at the content of [H]diff. in weld metal below 5 cm^3/100 g.

6. CONSUMABLES FOR WELDING LOW-ALLOY HIGH-STRENGTH STEELS

Low-alloy high-strength steels are used in heavy, transport and chemical engineering, ship building and other industries. New grades of wires, fluxes and electrodes were developed for fabrication of structures from such steels. It is worth to dwell now on characteristics of some of welding consumables devised for the Arctic ship building. Low-alloy high-strength Z-steel of grade 12KhN2MCuF is widely applied in construction of floating oil rigs (FOR). Average indices of mechanical characteristics of this steel are as follows:

σ_B 710 MPa
$\sigma_{0.2}$ 600 MPa
δ 21 %
ψ 60 %
ψ_Z 35 %
KCV at -50° C 78 J/cm^2

Microstructure of the steel in the initial condition is a temper sorbite.

We conducted comparison of weld metals obtained by welding using various low-silica fused fluxes and an experimental flux combined with the low-alloy welding wires.

Butt joints with the V-groove preparation were welded on commercial steel 12KhN2MCuF 40 mm thick. Welding conditions were as follows: I_{weld} = 550 ... 600 A, U_{arc} = 30 ... 34 V, V weld = 25 ... 30 m/h, the mean heat input was 24 kJ/cm.

Composition of metal of welds on steel 12KhN2MCuF made using different welding consumables is given in Table 9, and mechanical properties of weld metal in the as-welded condition are given in Table 10.

Analysis of the results indicates that the strength properties of weld metal are on the level of the requirements imposed on parent metal.

Impact energy of weld metal obtained using low-alloy welding wires and fused fluxes of all the grades is low (Table 10). Threshold of cold shortness is about -20°C. In this case the percentage of a fibre component in fracture of the Charpy specimens is not higher than 20 ... 25 % (Fig. 35).

Weld metal obtained using low-alloy welding wires combined with fused fluxes is heavily contaminated with non-metallic inclusions, this promoting an increase in brittleness at negative temperatures.

Along with the fused fluxes, we also tested an experimental agglomerated flux of the fluorite-basic type. Metal of the welds made using the agglomerated flux was less contaminated with non-metallic inclusions and had a structure of the finely dispersed acicular ferrite. This

provided > 60 % of the fibre component in fracture of the Charpy specimens that failed at -60°C (Fig. 35).

Table 9

Chemical composition of the weld metal

No	Wire grade	Flux grade and type	Flux system	Element content in the weld metal [wt.%]									
				C	Si	Mn	Cr	Ni	Mo	Ti	Cu	S	P
1	Sv-03KhGN3MCu	FIMS-20P Fused	SiO_2-Al_2O_3-CaO-MgO-CaF_2	0.02	0.46	0.39	0.69	2.63	0.49	0.014	0.80	0.013	0.016
2	Sv-03KhGN3MCu	AN-43 Fused	SiO_2-Al_2O_3-CaO-MgO-CaF_2-FeO	0.03	0.22	0.73	0.77	2.54	0.49	0.010	0.77	0.015	0.025
3	Sv-04KhGN3MCu	FIMS-20P Fused	SiO_2-Al_2O_3-CaO-MgO-CaF_2-	0.02	0.40	0.45	0.58	2.60	0.43	0.012	0.75	0.019	0.017
4	Sv-10GNMCuT	FIMS-20P Fused	SiO_2-Al_2O_3-CaO-MgO-CaF_2	0.07	0.30	0.80	0.25	1.10	0.30	0.020	0.63	0.014	0.025
5	Sv-10GNMCuT	Experimental Agglomerated	CaO-MgO-Al_2O_3-CaF_2-Fe_2O_3	0.07	0.20	1.30	0.25	1.20	0.30	0.010	0.50	0.010	0.021
6	Sv-04N3GMT	FIMS-20P Fused	SiO_2-Al_2O_3-CaO-MgO-CaF_2	0.07	0.52	0.51	0.12	2.43	0.10	0.015	0.16	0.014	0.025
7	Sv-04N3GMT	Experimental Agglomerated	CaO-MgO-Al_2O_3-CaF_2-Fe_2O_3	0.06	0.10	1.32	0.27	2.80	0.18	0.010	0.25	0.014	0.025

Table 10

Mechanical properties of the weld metal

No	Wire grade	Alloying system	Flux	σ_B MPa	$\sigma_{0.2}$ MPa	δ %	ψ %	Impact Energy [J] at the test temperature				
								+20°C	-20°C	-40°C	-50°C	-60°C
1	Sv-03KhGN3MD	Cr-Mn-Ni-Mo-Cu	FIMS-20P	724	625	18.4	61.3	55.9...62.8 58.8	24.3...40.2 33.3	15.7...21.6 18.6	19.6...23.5 21.6	11.8...20.6 15.7
2	Sv-03KhGN3MD	Cr-Mn-Ni-Mo-Cu	AN-43	794	705	14.1	52.8	36.3...43.1 39.2	24.5...28.4 25.5	18.6...24.5 20.6	20.4...24.5 22.6	16.7...21.6 19.6
3	Sv-04Kh3MD-VI	Cr-Ni-Mo-Cu	FIMS-20P	696	613	18.8	61.9	77.5...78.5 77.8	32.4...45.1 40.2	19.6...68.8 36.3	19.6...38.2 34.2	19.6...22.6 20.6
4	Sv-10GNMDTA	Mn-Ni-Cu-Ti	FIMS-20P	666.8	596	25.0	72.5	64.7...64.7 64.7	26.5...51.0 37.3	15.7...51.0 29.4	15.7...38.2 27.5	15.7...18.6 16.7
5	Sv-10GNMDTA	Mn-Ni-Cu-Ti	experimental agglomerated	698	610	23.0	66.2	106.0..157.0 124	120.6..151.0 136	96.0...114.0 110	74.5...94.1 80.4	76.0...82.0 77.7
6	Sv-04N3GMTA	Ni-Mn-Mo-Ti	FIMS-20P	594	513	25.2	66.5	117.8..129.4 118.7	68.6...79.4 74.5	42.2...54.9 51.0	14.7...53.0 34.3	17.7...37.3 28.4
7	Sv-04N3GMTA	Ni-Mn-Mo-Ti	experimental agglomerated	673.6	583	24.7	67.2	153.0..159.9 155.9	119.6..133.4 125.2	73.5...109.8 91.6	70.6...84.3 82.1	82.4...85.3 83.5

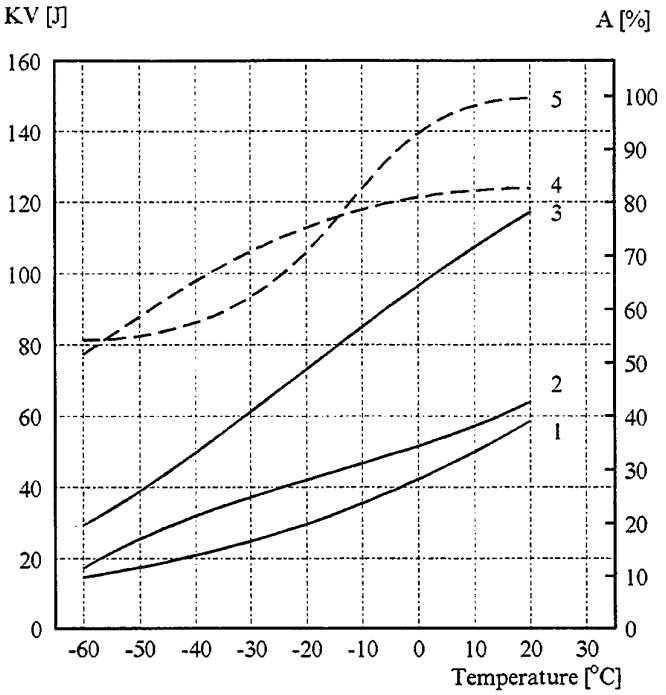

Fig. 35. Impact energy of weld metal (KV) and percentage of fibrous component (A) in the fracture of Charpy specimens at different test temperatures.

1 - Sv-03KhGN3MD solid wire + FIMS-20P fused flux
2 - Sv-10GNMDTA solid wire + FIMS-20P fused flux
3 - Sv-04N3GMTA solid wire + FIMS-20P fused flux
4 - Sv-10GNMDTA solid wire + experimental agglomerated flux
5 - Sv-04N3GMTA solid wire + experimental agglomerated flux

The diffusible hydrogen content of weld metal (determined by the alcohol test method) was not higher than 1 cm^3/100 g in case of welding using the experimental agglomerated flux of the fluorite-basic type, whereas when using the fused fluxes the mean content of the diffusible hydrogen was 1.5 ... 2.0 cm^3/100 g.

Under conditions of multipass welding the experimental flux combined with the said wires provides good weld formation, easily detachable slag crust and steady arc burning.

Table 11 gives data on resistance of weld to cold cracking. Several agglomerated fluxes of Ukrainian and foreign grades, combined with wire Union S3NCrMo2.5UP were tested. Parent metal was low-alloy high-strength steel 12KhN2MCuF 40 mm thick, alloyed with chromium, nickel, molybdenum, copper and vanadium.

Table 11

Weld metal resistance to cold crack formation (G-BOP test) when welding with the Union S3NiCrMo2.5UP wire

Flux	Area of cracks [%]			Preheat temperature [°C]
	min	max	middle	
OP121TT	0	3	1	60
UV421TT	3	8	5	60
48ANK-54	0	0	0	20
ANK-57	0	4	2	60

Chemical composition [wt.%] of welding wire Union S3NiCrMo2.5UP

C	Si	Mn	Cr	Ni	Mo	S	P
0.134	0.108	1.60	0.31	1.71	0.59	0.011	0.012

Welding conditions: Wire 4 mm in diameter, Welding current is 450 A, Arc voltage is 27 V, Welding travel speed is 23 m/hour

Flux 48-ANK-54 provides the low content of diffusible hydrogen [H]diff. and the crack-free bead-on-plate samples in welding without preheating (Table 11).

Table 12

Content of diffusible hydrogen [cm^3/100g]

Flux	[H]diff. in molten metal	[H]diff. in deposited metal
OP121TT	2.2	4.7
UV421TT	2.1	4.6
48ANK-54	1.2	2.6
ANK-57	2.0	4.2

Coated Electrodes

Electrodes 48KhN-4AN (type 360 acc. to GOST 9467-75) and 48KhN-5AN (type 370) were developed for welding cold-resistant low-alloy high-strength steels. Typical chemical compositions and mechanical properties of weld metal are given in Tables 13 and 14.

Table 13

Chemical composition of weld metal

Electrode grade	Element content [wt.%]							
	C	Mn	Si	Ni	Mo	Cr	S	P
48KhN-4AN	0.05	0.99	0.23	2.17	<0.03	0.10	0.009	0.012
48KhN-5AN	0.05	0.92	0.18	2.57	0.23	0.10	0.009	0.012
EA-981/15	-	2.45	0.30	22.0	5.5	16.5	0.015	0.016

Table 14

Mechanical properties of weld metal

Electrode grade	$\sigma_{0.2}$ MPa	σ_B MPa	δ %	ψ %	KCV [J/cm^2] at the test temperature [^oC]			
					+20	-20	-40	-60
48KhN-4AN	610	670	24	74	265	215	141	86
48KhN-5AN	712	762	22	71	212	148	102	76
EA-981/15	520	698	34	56	131	123	118	108

As can be seen from the data given, electrodes 48KhN-4AN and 48KhN-5AN provide impact toughness (Charpy) equal to not less than 50 J/cm^2 and the sufficiently high level of strength and ductility at temperature minus 60^oC. The new electrodes are somewhat inferior to the austenitic electrode EA-981/15 in cold resistance and are superior to it in strength.

The new electrodes ensure the low diffusible hydrogen content of the deposited metal (not more than 5 cm^3/100 g as determined by the chromatographic method).

The electrodes are characterized by small spattering of electrode metal, provide good formation of weld metal in all spatial positions and easily detachable slag crust. The deposition efficiency for electrodes 4 mm in diameter is 22 ... 27 g/min and that for electrodes 5 mm in diameter - 34 ... 39 g/min. The electrodes are intended for welding in all spatial positions, except for the vertical downward position.

Assessment of sanitary-hygienic characteristics of the electrodes indicated that the gross evolution and the intensity of evolution of the welding fume particulate matter (WFPM) during welding with the 48KhN-4AN and 48KhN-5AN electrodes were lower than during welding using the low-alloy electrodes of the known grades with the basic type of a coating and using the austenitic electrodes (Table 15). Besides, during welding using the new electrodes the WFPM hardly contains any of the most toxic elements, such as Cr^{6+} or Ni (in comparison with the austenitic electrode) (Table 16).

The electrodes were approved by the Register of the ex-USSR for welding the off-shore structures intended for operation under the North conditions.

Table 15

Gross evolution of welding fume particulate matter (WFPM)

Electrode grade	Electrode diameter [mm]	Welding conditions		Gross evolution of WFPM	
		Welding current [A]	Arc voltage [V]	g/min	g/kg
48KhN-4AN	4	150...160	22...24	0.28...0.30	7.2...7.8
48KhN-5AN	4	150...160	22...24	0.29...0.31	7.1...7.6
EA-981/15	4	140...150	22...24	0.58...0.68	11.8...16.3

Table 16

Chemical composition of WFPM

Electrode grade	Element content [wt.%]				
	Mn	Ni	F	Cr^{6+}	Cr^{3+}
48KhN-4AN	3.7	0.2	19.0	<0.02	<0.02
48KhN-5AN	3.8	0.2	18.4	<0.02	<0.02
EA-981/15	5.8	2.1	13.8	2.0	1.7

LINES OF THE FUTURE RESEARCH

To create a reliable technology for welding high-strength steels without preheating or with minimum preheating, we need to have a deeper insight in such problems as:

- effect of chemical composition of steel (C, Si, Mn, Cr, Ni, Mo, etc.), the possibility of further decreasing the carbon content in particular;
- effect of microalloying with rare-earth elements, Ti, B, V and other elements;
- effect of structural changes in welded joints caused by welding heat and heat treatment; mathematical modeling of such structures;
- effect of traps (pores, non-metallic inclusions, hydrides);
- finding ways for further decreasing the hydrogen content of welded joints;
- development of new welding consumables.

The E.O.Paton Welding Institute is open for cooperation with laboratories and research centers or companies been intesrested in.

In this presentation an attempt was made to give a brief review of the efforts made by the E.O.Paton Electric Welding Institute in the field of behaviour of hydrogen in welded joints and formation of cold cracks. A limited space given for the presentation did not allow to present a more detailed survey. To provide the more comprehensive idea of the problem, the list of references on the subject matter of my presentation is given below. Unfortunately, the majority of the papers in the references were published in Russian.

References

1. Bokstein S.Z., Ginzburg S.S. et al. Electron microscopic autoradiography in metals science. - M.: Metallurgiya, 1978. - 264 p. (in Russian).

2. Karpenko G.V., Litvin A.K., Tkachev V.I., Soshko A.I. On the problem of the hydrogen brittleness mechanism // FKhMM. - 1973. - No 4. - P. 6-12 (in Russian).

3. Kolachev B.A. Hydrogen brittleness of metals. - M.: Metallurgiya, 1985. - 216 p. (in Russian).

4. Pokhodnya I.K., Shvachko V.I. et al. On the mechanism of the effect of hydrogen on brittleness of metals // Doklady AN SSSR. - 1989. - 308, No 5. - P. 1131-1134 (in Russian).

5. Meshkov Yu.Ya., Pakharenko G.A. Structure of metal and brittleness of steel parts. - Kiev, Naukova Dumka, 1989. - 160 p. (in Russian).

6. Meshkov Yu.Ya, Serditova T.N. Ductile fracture criterion for uniaxial tension of low-carbon steels .- Physics of Metals.- 1985.- V. 5 (6).- P. 1180-1188 (in English).

7. Meshkov Yu.Ya, Pakharenko G.A., Serditova T.N. The relationship between brittle strength and resistance to ductile fracture for low-carbon steel in uniaxial tension.- Physics of Metals.- 1985.- V. 5 (4).- P. 728-733 (in English).

8. Meshkov Yu.Ya, Pakharenko G.A., Shevchenko A.V. Fracture of steel with globular cementite.- Physics of Metals.- 1985.- V. 5 (3).- P. 572-577 (in English).

List of some PWI's works on the problem of hydrogen and HICC in welds

1. Pokhodnya I.K. Gases in welds.- Moscow: Mashinostroenie, 1972.- 256 p. (in Russian).

2. Pokhodnya I.K. et al. On the mechanism of formation of pores in welded joints // Avtomaticheskaya Svarka (Automatic Welding). - 1978.- No 6.- P. 1 - 5 (in Russian).

3. Pokhodnya I.K. et al. Mathematical simulation of gas behaviour in welds // Doc. IIW XII-E -29-78 (in English).

4. Pokhodnya I.K., Paltsevich A.P. A chromatographic method for the determination of the amount of diffusible hydrogen in welded joints // Avtomaticheskaya Svarka. (Automatic Welding)- 1980.- No 1.- P. 37 - 39. (in Russian)

5. Pokhodnya I.K., Shvachko V.I. Mass-spectrometry of secondary ions and its application in the field of welding (Review) // Avtomaticheskaya Svarka (Automatic Welding). - 1987.- No 7.- P. 29 - 39 (in Russian).

6. Pokhodnya I.K., Paltsevich A.P., Yavdoshchin I.R. Effect of welding conditions on hydrogen content in welds made with basic electrodes // Avtomaticheskaya Svarka (Automatic Welding).- 1988.- No 3.- P. 19 - 22. (in Russian)

7. Pokhodnya I.K., Shvachko V.I. et al. Hydrogen influence mechanism on the embrittlement of metals // Doklady Academii Nauk USSR (Reports of the USSR's Academy of Sciences).- 1989.- 308, No 5. - P. 1131 - 1134 (in Russian).

8. Pokhodnya I.K., Shvachko V.I. et al. Effect of hydrogen on fragile of structural steels and their welded joints // Avtomaticheskaya Svarka (Automatic Welding). - 1989.- No 5.- P. 1 - 4 (in Russian).

9. Pokhodnya I.K. et al. Metallurgy of arc welding. Arc processes and electrode melting.- Kiev: Naukova Dumka, 1990. - 222 p. (in Russian).

10. Pokhodnya I.K. et al. Arc processes and electrode melting. - Cambridge, England: Riecansky Science Publishing Co., 1991. - 246 p. - (Metallurgy of arc welding. - vol. 1) (in English).

11. Pokhodnya I.K., Meshkov Yu.Ya., Shvachko V.I., Kotrechko S.A. et al. The method of qualitative determining of structural steels and welds hydrogen embrittlement degree // Russian patent department positive decision from 28.09.92 on the statement No. 5040067 (in Russian).

12. Pokhodnya I.K., Shvachko V.I. et al Mass-spectrometric method to quantitative hydrogen detection in solids// Author's Certificate No. 1711261 (USSR), Cl. H 01 J 49/26; G 01 N 33/10. - Publ. 07.02.92; Bull. No 5 (in Russian).

13. Determination of the diffusion coefficient of hydrogen in steel subjected to deformation and in weld deposits of basic and rutile coated electrodes / U.Dilthey, S. Trube, I.K. Pokhodnya, V.A.Pavlik // Welding and Cutting.- 1992. - No 12. - P. 668 - 671 (in German).

14. Pokhodnya I.K., Shvachko V.I. et al. Method to determination of the moisture contents in solids/ Author's Certificate No. 1793346 (USSR), Cl. G 01 N 25/14.-Publ. 07.02.93; Bull. No 5 (in Russian).

15. Pokhodnya I.K., Shvachko V.I. Effect of hydrogen on brittleness of structural steels and welds // Proc. Eighth Intern. Conf. on Fracture, Ukraine, Kiev, June 1993, Part II, p. 585 (in Russian).

16. Pokhodnya I.K., Shvachko V.I. Investigation of hydrogen embrittlement of welded joints of structural steels// Presented on Intern. Conf. "Welded Structures" (Ukraine, Kiev, Sept. 1995) (in Russian).

17. Pokhodnya I.K., Shvachko V.I. Effect of hydrogen on structure of steel welds. Presented on First Intern. Conf. "Hydrogen treatment of materials" (Ukraine, Donetsk, Sept. 1995) (to be publ. in "Intern. J. of Hydrogen Energy") (in Russian).

18. Pokhodnya I.K., Shvachko V.I. Hydrogen inducing mechanism of cold cracks in structural steels welded joints (Intern. Welding Conference (Slovakia, High Tatras Mountains, March 1996) (in English).

19. Makara A.M. Cracks in near-weld zone of alloyed steels // Jubilee collection of papers dedicated to E.O.Paton. - Kiev: Publ. Acad. Sc. UkrSSR.- 1951. - P. 340 - 356 (in Russian).

20. Kasatkin B.S., Musiyachenko V.F., Mikhodui L.I. Hydrogen influence on susceptibility of 14Kh2GMR to cold cracking // Avtomaticheskaya Svarka (Automatic Welding).-1975.- No 2.- P. 45 - 48 (in Russian).

21. Makhnenko V.I., Ryabchuk T.G. The calculation of pressure created by hydrogen in metal microcavities and heat-affected zone // Avtomaticheskaya Svarka (Automatic Welding).- 1985.- N4.- P.1 - 5 (in Russian).

22. Kasatkin B.S., Smiyan O.D. et al. Hydrogen effect on susceptibility to cracking in HAZ with stress concentrator // Avtomaticheskaya Svarka (Automatic Welding).- 1986.- No. 11. - P. 20-23 (in Russian).

23. Definition of thermodeformation dependences characterizing steel susceptibility to the cold cracking at welding / B.S. Kasatkin, V.I. Brednev, G.N. Strizjus et al. // Avtomaticheskaya Svarka (Automatic Welding).- 1988.- No. 3. - P. 1 - 5 (in Russian).

24. Grigorenko G.M., Pomarin Yu.M. Hydrogen and nitrogen in metals in plasma melting.- Kiev: Naukova dumka, 1989.- 200 p. (in Russian).

25. HAZ structure and cold cracks imitation at middle-alloyed steel welding / B.S. Kasatkin, G.N. Strizjus, A.K.Tsaryuk et al. // Avtomaticheskaya Svarka (Automatic Welding). - 1990.- No. 2.- P. 1 - 5. (in Russian)

26. Mikhodui L.I., Mel'nik I.S., Poznyakov V.D. Resistivity to delayed fracture of low alloyed welds during welding of higher strength steels with yield strength over 600 MPa // Avtomaticheskaya Svarka (Automatic Welding). - 1990. - No 2. - P. 14 - 20 (in Russian).

27. Musiyachenko V.F., Mikhodui L.I. Hydrogen during higher strength steel welding and its effect on resistivity of welded joints to cold cracking// Problems of welding and special electrical metallurgy. - Kiev: Naukova dumka, 1990.- P. 161 - 168 (in Russian).

28. Mikhodui L.I., Poznyakov V.D., Mel'nik I.S. Peculiarities of delayed fracture of steel 12GN2MFAYu with different concentration of impurities// Avtomaticheskaya Svarka (Automatic Welding).-1991.- No 12.- P.16-20 (in Russian).

29. Kasatkin B.S., Mikhodui L.I. Non-metallic inclusions and hydrogen effect on delayed fracture of alloyed steels welded joints// Avtomaticheskaya Svarka (Automatic Welding).-1991.- No. 8.- P. 1-6(in Russian).

30. Lakomsky V.I. Diatomic gases interaction with liquid metals at high temperatures. - Kiev: Naukova dumka, 1992.- 232 p. (in Russian).

31. Kasatkin B.S., Brednev V.I., Tsaryuk A.K., Zjuravlev Yu.M. Estimation of 15Kh2MFA steel welded joints resistment to cold cracks formation // Avtomaticheskaya Svarka (Automatic Welding).- 1993.- No. 5.- P. 3 - 7 (in Russian).

32. Kasatkin B.S., Strizjus G.N., Brednev V.I., Tsarjuk A.Š. Hydrogen embrittlement and cold cracks formation during the steel 25Kh2NMFA welding // Avtomaticheskaya Svarka. (Automatic Welding)- 1993.- No. 8.- P. 3 -10. (in Russian)

33. Gotal'sky Yu.N. The problem of quenching steels welding and known methods of its solution// Avtomaticheskaya Svarka (Automatic Welding).- 1994.- No.4. - P. 36 - 40 (in Russian).

34. Kasatkin O.G. Peculiarities of high-strength steel hydrogen embrittlement during welding (review) // Avtomaticheskaya Svarka (Automatic Welding).-1994.- No. 1.- P. 3-7 (in Russian).

Tsaryuk A.K., Brednev V.I. Problem of cold cracks preventing (review) // Avtomaticheskaya Svarka (Automatic Welding).-1996.- No.1.- P. 36-40 (in Russian).